Angiogenic and Metastatic Determinants of Malignant Melanoma

Asha M. Das

Angiogenic and Metastatic Determinants of Malignant Melanoma

Angiogene en Metastatische Determinanten van Maligne Melanoma

Thesis

to obtain the degree of Doctor from the Erasmus University Rotterdam
by command of the rector magnificus Prof.dr. H.A.P. Pols
and in accordance with the decision of the Doctorate Board

The public defense shall be held on
Wednesday 25 November 2015 at 11:30 hours

by

Asha Mooppilmadham Das
born in Cochin, Kerala, India

Erasmus University Rotterdam

DOCTORAL COMMITTEE

Promoter: Prof.dr. A.M.M. Eggermont

Other members: Prof.dr. S. Sleijfer
                       Prof.dr. D.S. Peeper
                       Prof.dr. D.F.E. Huylebroeck

Copromoter: Dr. T.L.M. ten Hagen

Lives of great men all remind us
    We can make our lives sublime,
And, departing, leave behind us
    Footprints on the sands of time;

Footprints, that perhaps another,
    Sailing o'er life's solemn main,
A forlorn and shipwrecked brother,
    Seeing, shall take heart again.

Let us, then, be up and doing,
    With a heart for any fate;
Still achieving, still pursuing,
    Learn to labor and to wait.

Excerpt from 'A PSALM OF LIFE'
Henry Wadsworth Longfellow

In loving memory of my Dad

TABLE OF CONTENTS

CHAPTER 1

General introduction

GENERAL INTRODUCTION

Cutaneous melanoma

Cutaneous melanoma or malignant melanoma of the skin is a malignancy resulting from the unregulated growth of melanocytes. Despite accounting for only 5-7% of skin cancers, it is responsible for the majority (75%) of skin cancer-related deaths. Importantly, the incidence of cutaneous melanoma is increasing faster than for any other human malignancy[1]. With a global incidence of 15-25 per 100,000 individuals and 48,000 deaths annually, melanoma represents a significant health burden. Melanomas are also one of the few cancers which tend to occur at a younger age and is one of the most common malignancies among young adults[1,2].

Localized melanomas (lesions restricted to the epidermis) or lesions with a thickness of less than one millimeter can be effectively treated by wide excision surgery at the primary site, and results in 5-year survival rates of greater than 95%[3]. However, melanomas are highly aggressive and tend to metastasize early. Upon dissemination to regional lymph nodes or distant organs, surgical intervention becomes problematic and survival rates dramatically decline. In patients presenting with positive sentinel lymph nodes, the 5-year survival rates drop to less than 50%. The presence of distant metastases indicates a dismal outcome, with 5-year survival rates of less than 10% and median life expectancy of 6-9 months[4].

The poor prognosis and high mortality rates associated with melanoma essentially result from the lack of effective treatments, particularly for advanced stage disease. Until recently, melanoma has remained largely untreatable with few approved therapies which have failed to impact the long-term prognosis of this disease. Recent research has thus focused on the identification of critical regulatory elements and signaling pathways in melanoma pathogenesis for the development of alternative therapeutic strategies.

Therapeutic approaches

Over the last several decades, a large variety of therapeutic modalities have been implemented in the treatment of malignant melanoma. These approaches have encompassed chemotherapy, bio-chemotherapy, radiation therapy, immunotherapy, cancer-specific vaccines, monoclonal antibodies, small molecule therapy and various combination therapies. None of these strategies have shown long term clinical benefits or durable response rates in a significant number of melanoma patients[5]. While the clinical staging and progression of melanoma is well defined, the molecular etiology of the disease is less well characterized. The focus has thus shifted to better defining molecular determinants of disease progression with an emphasis on genetic aberrations, signaling cascades and disease heterogeneity to identify potential targets which are amenable to therapeutic intervention. This approach has been successful and led to the Food and Drug Adminis-

tration (FDA) approval of two new drugs, ipilimumab and vemurafenib, in 2011. These are the first drugs in several decades to demonstrate a clinical benefit in the treatment of metastatic melanoma[6]. The following section describes previous and current therapeutic approaches used for the management of malignant melanoma.

Surgery

The American Joint Committee on Cancer's (AJCC) staging system adopted by the Union for International Cancer Control (UICC), is based on the evaluation of primary tumor (T), with Breslow's thickness and ulceration as the major prognostic factors; the presence or absence of regional lymphatic metastases (N), with number of involved lymph nodes as secondary prognostic factors; and distant metastases (M) with metastatic site and lactate dehydrogenase (LDH) levels as additional factors. For primary tumor evaluation, the most recent AJCC system from 2009 has also introduced mitotic activity in the pathology assessment of thin melanomas (≤ 1.00 mm)[4,7]. In the treatment of primary melanomas it has been demonstrated that extended surgical procedures, e.g. wide margins, elective lymph node dissection, prophylactic isolated perfusion or sentinel node staging have no significant impact on survival[8]. Sentinal node biopsy is the standard of care staging procedure to accurately classify patients with primary melanoma in the current AJCC/UICC system, and sentinal node status is currently the strongest prognostic factor in melanoma patients[9]. Recent reports indicate that the sentinel node positive patient population is very heterogeneous, and that, depending on tumor load, 5-year survival rates may vary from 91% to 64%[10-12]. For palpable node metastases full regional lymph node dissections remain standard of care. For oligometastatic disease, indicating few metastatic spots typically confined to one organ, surgery is the primary option. A new approach would be to induce a rapid tumor response in BRAF mutated tumors with a BRAF inhibitor followed by surgery at the time of maximal response. Oligometastatic visceral metastases, including brain metastases are increasingly treated by stereotactic radiotherapy, but a size larger than 3 cm usually demands surgery[13].

Chemotherapy

Melanoma has been historically refractory to cytotoxic chemotherapy and until 2011, dacarbazine (DTIC), temozolomide (TMZ) and fotemustine were the standard chemotherapeutic agents used for the palliative treatment of patients with advanced disease[14]. Although the exact mechanism of action is not known, all three drugs are thought to exert nonspecific antineoplastic activity by alkylating DNA which inhibits DNA synthesis and replication. DTIC is an intravenously administered prodrug that requires liver processing for activity. Clinical results indicate response rates ranging from 6-15% with a median response durability of 7-8 months[15]. TMZ is an imidazotetrazine derivative of DTIC and unlike DTIC, is orally administered and is activated systemically. Randomized

phase III clinical trials have indicated no significant survival advantages of TMZ over DTIC, with the median survival of patients treated with TMZ being 7.4 months[16]. Similarly, no significant survival benefit was observed between fotemustine (median survival 7.4 months) and DTIC when evaluated as first-line therapy[17]. Additionally, due to the non-specific nature of systemic chemotherapeutic regimens, such therapies are associated with high-grade toxicities and warrant alternative approaches for the treatment of malignant melanoma.

Immunotherapy

Interferon-alpha (IFN-α) and interleukin-2 (IL-2) received FDA approval in 1995 and 1998 respectively, and were the first immunological drugs approved for the treatment of metastatic melanoma. IFN-α as monotherapy shows modest antitumor activity in a subset of melanoma patients. IL-2 stimulates T-cell proliferation and enhances the cytotoxic activity of natural killer cells. Overall response rates associated with these cytokines range from 10-20%, with durable response rates observed in approximately 6% of patients[18,19]. However, due to the immunomodulatory nature of these treatment approaches, cumulative toxicities and severe side effects have been observed in patients. Thus treatments are limited to patients who are relatively healthy and more likely to respond[20].

Despite the limited success of initial immunological approaches, considerable advances have been made in both our understanding and implementation of immunotherapeutic modalities for the treatment of malignant melanoma. One such example is that of the anti-CTLA-4 (cytotoxic T lymphocyte-associated antigen 4) antibody, ipilimumab, which promotes sustained T-cell activation and functions as an immune checkpoint inhibitor. Clinical trials evaluating single agent use or in combination with chemotherapy have shown a clear survival benefit in advanced stage melanoma patients, leading to its FDA approval in 2011[21,22]. Since then two more immune checkpoint inhibitors, the anti-PD-1 (programmed cell death 1) antibodies nivolumab and pembrolizumab, have received FDA approval in 2014 for demonstrating superior response rates and durability of response[23,24]. Despite these exciting developments, several challenges remain to be addressed such as the high rate of severe grade immune related adverse events observed with ipilimumab treatment and acquisition of therapy resistance to the PD-1 antibodies[25].

Targeted therapy

A major development in the field of cancer therapy has been the recent advances in technologies such as next generation sequencing which enable the molecular and genomic characterization of the cancer genome. The identification of genetic alterations regulating disease progression has resulted in a paradigm shift in therapeutic approaches from standard conventional regimens to an individualized approach; a concept known as "personalized medicine". The BRAF (v-raf murine sarcoma viral oncogene homolog B1) inhibitor

story is one such example, which resulted from the discovery of the oncogenic V600E mutation (a valine to glutamate substitution at coding position 600) in approximately 50% of melanoma patients. This ultimately led to the FDA approval of the highly selective BRAF inhibitors, vemurafenib and dabrafenib, for the treatment of BRAF mutated unresectable melanoma. Clinical trials evaluating these inhibitors in comparison to the standard chemotherapeutic agent DTIC have shown a clear clinical benefit[26,27]. Although dramatic initial responses and tumor regression have been observed, the durability of responses have been relatively short with progression-free survival ranging from 5-7 months due to acquisition of drug resistance[27,28]. Targeted therapies thus continue to evolve with the application of combinatorial approaches[29] to combat transient responses and acquired drug resistance.

Melanoma development and biology

Melanoma initiation and development is depicted as a series of stages, based on clinical and histopathological features[30,31]. The five distinct steps include: 1) common acquired and congenital melanocytic nevus, which is a benign lesion with an increased number of structurally normal melanocytes; 2) dysplastic nevus, characterized by structural and architectural cytologic atypia and an increased risk of progressing to melanoma; 3) radial growth phase, non-malignant primary melanomas which remain confined to the epidermis; 4) vertical growth phase, primary melanomas which have the capacity to proliferate and invade the basement membrane; and 5) metastatic melanoma, where cells disseminate to other distant sites. The transition from one stage to the other is accompanied by several biological changes such as the escape of growth control from keratinocytes, acquisition of genetic aberrations, phenotypic plasticity and growth factor independence[32]. However, melanomas can also progress without identifiable intermediate lesions.

Although the clinical and histological staging of melanoma progression is well defined, the molecular alterations regulating these processes are yet unclear. Mutations in genes regulating cell cycle entry, such as the cyclin-dependent kinase (CDK)-N2A (p16INK) and CDK-4 have been identified in a subset of melanomas (familial melanoma, 5-12% of cases)[33,34]. The discovery of the missense mutation in BRAF (V600E), leading to the constitutive activation of the mitogen activated protein kinase (MAPK) pathway, in approximately 50% of melanoma patients has been a seminal finding[35]. However, recent advances in high throughput technologies such as next generation sequencing makes it abundantly clear that evolution of melanomas does not result from a single genetic defect, but rather is the outcome of cumulative alterations in multiple genes and signaling pathways. Identifying and understanding these molecular changes and their impact on the development of melanoma, is therefore crucial for the development of efficient therapeutic strategies.

An important outcome of years of melanoma research has been the realization that melanoma development is not solely a product of genetically altered melanocytes. The host stromal environment is integral to growth and progression and plays an active role in tumor development[36]. Studies have indicated that melanomas are infiltrated by multiple host cell types, including endothelial cells, fibroblasts and inflammatory cells. Melanomas can therefore be viewed as a complex, dynamic micro-ecosystem where neoplastic cells and host stromal cells communicate via direct cell-cell contacts, cytokines, chemokines, matrix proteins and other signaling factors. Based on our current understanding of the molecular and biological changes associated with melanoma development, tumorigenesis comprises the following critical steps: the acquisition of genetic instability, enhanced growth potential and insensitivity to anti-growth signals, induction and establishment of a neovasculature and the acquisition of an invasive phentotype with metastatic competence. Two of these critical regulatory cascades, the angiogenic and metastatic cascades, are further discussed below and has been the focus of the studies described in this thesis.

Angiogenic cascade in melanoma

Angiogenesis is a highly regulated, complex, physiological process, resulting in the elaboration of the pre-existing nascent host vasculature through generation of new capillary blood vessels. This multistep process is mediated through a defined cascade involving the loss of quiescence of endothelial cells and detachment from pre-existing vessels, followed by proliferation, survival and migration, ultimately resulting in structural reorganization and tube formation[37,38]. Physiological angiogenic events are restricted to defined circumstances such as embryonic development, endometrium cycling, chronic inflammation and wound repair. Such events are characterized by a tightly regulated transient neovascular response, achieved by a spatially and temporally organized interplay between angiogenic factors, which stimulate angiogenesis, and angiostatic factors, which restrain it. Pathological angiogenesis, on the other hand, is fundamentally mediated by the deregulation in the balance between angiogenic and angiostatic modulators, in favour of the former[39,40].

Neovasculature initiation and sustained angiogenesis are prominent features of melanoma development. Human melanoma cells produce an array of polypeptide cytokines including, but not limited to, vascular endothelial growth factor (VEGF), basic fibroblast growth factor (bFGF), platelet derived growth factor (PDGF), and interleukin-8 (IL-8)[41,42]. They exert a wide range of functions in the tumor microenvironment, either by acting directly on endothelial cells to promote neoangiogenesis, or indirectly by mobilizing host stromal and inflammatory cells[43]. Several observations highlight the importance of angiogenesis in disease progression, including the increased expression of these ligands and their receptors in melanomas as compared to benign nevi[44-46]. Elevated levels of proangiogenic modulators such as VEGF and bFGF have been detected in the serum

of melanoma patients and has been shown to correlate with disease progression and survival[47-49]. An increase in angiogenesis has been reported in the transition from the radial to the vertical growth phase of melanoma development and the degree of angiogenesis has been shown to correlate with tumor grade, risk of recurrence, metastatic potential and clinical outcome[50]. Additionally, the host stromal microenvironment actively participates in melanoma angiogenesis as evidenced by the increased presence of inflammatory cells such as macrophages which correlates with tumor stage, angiogenesis and prognosis[51-53]. Over the years, several *in vitro* and *in vivo* studies have demonstrated the contribution of various proangiogenic ligands to the angiogenic cascade of melanoma. However, clinical targeting of this cardinal hallmark of melanoma has remained challenging[43,54] and therefore requires further investigation.

Metastasic cascade in melanoma

Disseminated disease is the cause of the majority of melanoma-related mortalities[55]. Although the exact mechanisms responsible for the metastatic cascade remain to be elucidated, a series of complex sequential events comprising multiple tumor-host interactions are thought to be responsible for secondary tumor formation[56]. Under physiological conditions, melanocytes remain restricted to the epidermal layer. The acquisition of an invasive phenotype is characterized by multiple biological and phenotypic changes including the increased production of growth factors, loss of cell-cell contacts, downregulation of cell adhesion molecules, degradation of structural proteins of the basement membrane and extracellular matrix (ECM) and migration into the interstitial stroma. Subsequently, tumor cells gain access to hematogenous and lymphatic channels through the process of intravasation. Once in circulation, tumor cells evade immune surveillance and programmed cell death and eventually extravasate and arrest at secondary sites. Finally, the tumor cells must adapt to the microenvironment of the target organ, survive and proliferate in order to establish a distant metastatic colony[57]. In melanoma, the most frequent target sites for secondary tumor formation are the skin, lymph nodes, lung, liver, bone and brain[58].

The acquisition of the described invasive phenotypic traits is accompanied by several molecular changes. Altered expression of integrins, which are a family of heterodimeric receptors for ECM components, has been reported in melanoma. The vitronectin receptor αVβ3 has been identified as a melanoma progression marker with an increase in expression correlating with the transition from radial to vertical growth phase. Increased expression of the heterodimers α3β1, α4β1 and α5β1 has been reported in metastatic melanoma as compared to primary tumors, and has been implicated in cell migration, invasion and adhesion[59-62]. The expression of other adhesion molecules, such as cadherins, is also reported to be deregulated in melanomas. The loss of E-cadherin and gain of N-cadherin, also known as the cadherin switch, has been associated with several adverse

prognostic markers and predicts poor outcome[63]. Melanoma cells also overexpress matrix metalloproteinases (MMPs), which are serine proteases that degrade the ECM. Increased expression of MMP-2 and MMP-9 has been shown to correlate with melanoma invasion and metastasis[64-66].

Aberrations in several signaling pathways have also been implicated in the metastatic cascade of melanomas. Inactivation of the tumor suppressor phosphatase and tensin homolog (PTEN) leads to the constitutive activation of the PI3K/AKT pathway which regulates cell survival, growth, and proliferation. Higher levels of phosphoylated (active) AKT has been detected in metastatic tumors as compared to primary melanomas and nevi, and is associated with poor survival[67]. The BRAF[V600E] mutation causes a conformational change in the protein structure and leads to the constitutive activation of the MAPK pathway[68,69]. MAPK activation is predicted to modulate melanoma metastasis by regulating effectors of cell migration, survival and growth. Additionally, melanoma cells are thought to activate developmental programs such as the Wnt and Notch signaling pathways to maintain mesenchymal-like plasticity[25].

As an amendment to the classical view of the stepwise progression of melanoma, recent studies have indicated that melanoma cell populations exhibit considerable functional heterogeneity, and metastatic spread may occur in parallel with primary tumor development[70]. Although melanoma initiation is regarded as a clonal event[71], subsequent progression and secondary tumor formation is a consequence of various factors, including selective environmental pressures and the tumor initiating capacity of the melanoma cell, to name just a few. Thus while significant advances have been made in characterizing the metastatic process in melanomas, further elucidation of fundamental effectors of this complex cascade will be needed to provide new opportunities for therapeutic intervention.

Aims and scope of this thesis

Melanoma is a complex heterogeneous genetic disease with progression determined by several parallel pathways modulating cell growth, survival, migration and interactions with the host microenvironment. The main objective of this thesis was therefore to investigate the biological behavior and phenotypic traits of melanoma cells to identify intrinsic aspects which could be linked to genetic aberrations, and in extension, to the progression of the disease. Within this general framework, three main aspects of melanoma biology were investigated in this thesis. *Section I* of this thesis focuses on the angiogenic cascade of melanomas. *Section II* of this thesis focuses on the metastatic cascade of melanomas. *Section III* of this thesis describes tools to visualize early events in neovasulature development.

The acquisition of an angiogenic phenotype is crucial for tumor growth and progression.

Chapter 2 evaluates the angiogenic potential of melanoma cell lines, with respect to their ability to sustain endothelial cell survival under hypoxic conditions.

In **Chapter 3**, we investigated the ability of melanoma derived factors to promote directional endothelial cell migration, a crucial step in neovasculature formation. We were able to identify and functionally validate the role of TIMP3 as a negative modulator of melanoma-associated angiogenesis.

Chapter 4 is a follow-up to Chapter 3, where we extended our *in vitro* and *in vivo* observations of the role of TIMP3 in melanoma angiogenesis to a cohort of melanoma positive lymph node biopsies from stage III melanoma patients.

Melanomas exhibit a high migratory and invasive potential and disseminated disease is responsible for the majority of melanoma related mortalities. Thus delineating the modulators of the metastatic cascade is critical to effectively target this attribute of disease biology.

Chapter 5 describes the application of a novel migration assay to quantitatively evaluate several parameters of cell migration.

In **Chapter 6**, we used the novel migration assay to assess the migratory potential of melanoma cell lines and correlated this biological phenotypic trait with the genetic make-up of the cells. We were able to identify WNT5A as a crucial determinant of the metastatic cascade in melanomas.

In **Chapter 7**, we evaluated the role of TIMP3 as a tumor suppressor in melanoma progression. Using a cohort of matched Stage I/II, Stage III and Stage IV samples from melanoma patients, we observed that TIMP3 expression decreases during melanoma progression.

The ability to visualize tumor related events in real-time offers the possibility to better understand the spatiotemporal regulation of such events.

Chapter 8 describes the use of the transgenic eNOS-Tag-GFP mouse model as a platform for the *in vivo* and *ex vivo* study of sprouting angiogenic events.

In **Chapter 9**, the results of this thesis are discussed in a broader perspective with respect to our current understanding of melanoma biology, and future directions of research are proposed.

SECTION I

Angiogenic cascade in malignant melanoma

CHAPTER 2

Melanomas prevent endothelial cell death under restrictive culture conditions by signaling through AKT and p38 MAPK/ERK-1/2 cascades

Asha M. Das, Mario Pescatori, Cindy E. Vermeulen, Joost A.P. Rens, Ann L.B. Seynhaeve, Gerben A. Koning, Alexander M.M. Eggermont, Timo L.M. ten Hagen

ABSTRACT

Although melanoma progression and staging is clinically well characterized, a large variation is observed in pathogenesis, progression and therapeutic responses. Clearly, intrinsic characteristics of melanoma cells contribute to this variety. An important factor in both progression of the disease as well as response to therapy is the tumor associated vasculature. We postulate that melanoma cells communicate with endothelial cells (ECs) in order to establish a functional and supportive blood supply. Thus, further elucidation of the angiogenic process, along with the involved factors, could advance the understanding of the aggressive nature of this disease and assist in the development of new anti-angiogenic therapies. We investigated the angiogenic potential of human melanoma cell lines by monitoring survival of endothelial cells (ECs) upon exposure to melanoma-conditioned medium (MCM), under restrictive conditions. We observed long term (up to 72 h) EC survival under hypoxic conditions upon treatment with all MCMs. No such survival effect was observed with the CM of melanocytes. The CM of pancreatic and breast tumor cell lines did not show a long-term survival effect, suggesting that the survival factor is specific to melanoma cells. Further, all size fractions (up to < 1 kDa) of the MCM induced long-term survival of ECs. The survival effect observed by the < 1 kDa fraction eliminates known pro-angiogenic factors. Heat inactivation and enzymatic digestion of the MCM did not inactivate the survival factor. Global gene expression and pathway analysis suggests that this effect is mediated in part via the AKT and p38 MAPK/ ERK-1/2 signaling axis. Taken together, these data indicate the production of (a) survival factor/s (< 1 kDa) by melanoma cell lines, which enables long-term survival of ECs and promotes melanoma-induced angiogenesis.

INTRODUCTION

Malignant melanoma is a highly metastatic disease, with an increasing rate of incidence, poor prognosis and high resistance to therapeutic intervention[2]. While early diagnosis and surgical resection of the primary lesion could significantly improve survival, the high propensity of melanomas to disseminate through intradermal, haematogenous and lymphatic routes to regional and visceral sites leads to poor prognosis and high mortality rates[72,73]. Metastatic melanoma is by large refractory to conventional therapies and until recently, patients presenting with advanced disease had low life expectancies, with a median overall survival (OS) of 6 to 9 months and 5-year survival rates as low as 5-10%[2,4,25]. Promising recent therapeutic advances in the treatment of malignant melanoma, such as the use of targeted therapies[26,74,75] and immunological approaches[21,24,76,77], have demonstrated substantial clinical benefit and significantly improved survival in patients with advanced disease. These results, while encouraging, highlight the necessity to better characterize disease biology as a considerable fraction of melanoma patients still remain, or become, incurable.

Melanomas evolve through distinct sequential neoplastic transformations and tumor progression is intimately associated with a high degree of angiogenic activity, facilitated by the constitutive expression of multiple growth factors[41,42]. Angiogenesis is an imperative feature of melanoma development as evidenced by the correlation of degree of angiogenesis with aggressiveness, risk of recurrence and clinical outcome[50]. Further, increased expression of proangiogenic ligands and their receptors have been observed in melanomas compared to benign nevi[44-46] and elevated levels detected in the blood of melanoma patients[47-49]. The clinical relevance and therapeutic potential of targeting angiogenesis has led to the development of several targeting modalities. Despite promising preclinical results, clinical trials evaluating single antiangiogenic agent use as well as combinations with chemotherapy have thus far shown marginal response rates (reviewed in[43,54,78]). Translating the targeting of this pivotal pathophysiological feature of melanomas into a curative therapeutic modality has remained challenging, warranting a better insight into the angiogenic cascade of melanomas.

A critical component in eliciting and sustaining the angiogenic phenotype of tumors is hypoxia[79]. Heterogeneity in oxygenation is a constant feature of the tumor microenvironment as neoplastic vasculature development cannot keep up with the metabolic demands of proliferating tumor cells, resulting in an architecturally and functionally compromised vasculature. The hypoxic microenvironment of melanomas is associated with tumor progression and metastatic dissemination[80,81] and serves as a stimulus for the induction of several pro-angiogenic modulators. Endothelial cells are known to undergo cell death in response to adverse stimuli such as hypoxia[82]. As endothelial cell survival is a crucial step in the angiogenic cascade, we sought to evaluate the angiogenic potential of melanoma

cell lines, differing in their degree of aggressiveness and clinical staging[83], by investigating their ability to mediate endothelial cell survival under restrictive culture conditions.

MATERIALS AND METHODS

Reagents

Tissue culture reagents, unless otherwise specified, were obtained from Biowhittaker (Walkersville, MD). Human recombinant vascular endothelial growth factor (VEGF), basic fibroblast growth factor (bFGF) and epidermal growth factor (EGF) were purchased from PrepoTech (Rocky Hill, NJ). Sugen 5416 was obtained from Cayman Chemical Company (Ann Arbor, MI) and human VEGF neutralizing antibody was purchased from R&D Systems Europe (Abingdon, UK). Inhibitors LY294002, PD98059 and SB203580 were purchased from Cell Signaling Technology, Inc. (Bioke, Leiden, NL). Antibodies against Akt, Phospho-Akt (S473), p44/42 MAPK (ERK1/2), Phospho-p44/42 MAPK (ERK1/2), p38 MAPK and Phospho-p38 MAPK (Thr180/Tyr182) were from Cell Signaling and mouse anti-human beta actin monoclonal antibody was from Abcam (Cambridge, UK). Gelatin was obtained from Sigma-Aldrich and Fibronectin from Roche Diagnostics. SDS-PAGE reagents were obtained from BioRad (Hercules, CA). TaqMan Gene Expression assays were purchased from Applied Biosystems (Carlsbad, CA), TRIzol reagent and First Strand cDNA synthesis kits were purchased from Invitrogen (Carlsbad, CA). All other reagents were from Sigma-Aldrich Chemie B.V. (Zwijndrecht, NL), unless stated otherwise.

Cell lines and culture conditions

The five human melanoma cell lines BLM, M14, Mel57, 530, and 1F6 were kindly donated by Dr. van Muijen (Department of Pathology, University of Nijmegen, NL) and were maintained in Dulbecco's modified Eagle's medium (DMEM) with glutamine supplemented with 10% FBS. The modified human melanoma cell line, Mel57-VEGF165 was maintained in DMEM supplemented with 10% FBS and 1mg/ml G418. Normal human epidermal neonatal melanocytes (NHEM-neo) were maintained in MBM-4 medium supplemented with the MGM-4 Bulletkit (Clonetics Melanocyte Cell Systems, Lonza Benelux BV, Breda, NL). Immortalized human melanocytes (Hermes 1), a gift from Dr. Sviderskaya (Department of Basic Medical Sciences, St George's Hospital Medical School, London, UK) were grown in RPMI medium with glutamine supplemented with 10% FBS, 12-O-tetradecanoylphorbol-13-acetate (TPA, 200 nM), cholera toxin (200 pM), human stem cell factor (SCF, 10 ng/ml) and endothelin 1 (10 nM) and maintained under conditions of 10% CO_2, as previously described[84]. Human breast carcinoma cells (MCF-7, Cama-1 and SK-BR-3) were gifts from Dr. M. Schutte (Department of Medical Oncology, Josephine Nefkens Institute, Erasmus MC, NL) and were cultured in RPMI

2

medium with glutamine supplemented with 10% FBS. Pancreatic cancer cells (PANC-1, MIAPaCa-2 and BxPC-3) were donated by Dr. W. Dinjens (Department of Pathology, Josephine Nefkens Institute, Erasmus MC, NL) and were grown in RPMI 1640 medium with glutamine supplemented with 10% FBS.

Primary cultures of Human Umbilical Vein Endothelial Cells (HUVEC) were established by isolating endothelial cells (ECs) from umbilical cords with collagenase digestion, as described[85]. Primary EC cultures from eight separate donors were used for this study. Adult Human Microvascular Endothelial cells (HMVECs) were obtained from Clonetics (Lonza Benelux BV, Breda, NL). EC's were routinely cultured in Human Endothelial-SFM (Invitrogen) supplemented with 20% heat inactivated new born calf serum, 10% heat inactivated human serum, 20 ng/ml bFGF and 100 ng/ml EGF, on 0.1% gelatin coated flasks. All experiments and assays were performed on fibronectin (10 µg/mL) coated plates, with ECs between passages 3 and 6. NHEM-neo, ECs and tumor cells were routinely cultured in a well humidified incubator (20% O_2, 5% CO_2 37°C; referred throughout as normoxia) and passaged when confluent. To inflict profound cell death within 24–48 h, severe hypoxic treatments were conducted by placing cultures in a well humidified hypoxic chamber (Pro-ox-110, Biospherix, Redfield, NY) maintained at 1% O_2, 1% CO_2, 37°C (referred throughout as hypoxia).

Preparation and fractionation of melanoma conditioned medium (MCM)

Tumor cells and melanocytes were maintained in standard culture medium. Upon 70-80% confluency, the cells were washed twice and conditioned medium was prepared by incubation in either DMEM supplemented with 10% FBS or serum-free DMEM to generate MCM and SF-CM respectively, under normoxic or hypoxic conditions. For all experiments where MCM was used, DMEM + 10% FBS was used as the control and for experiments with SF-MCM, serum-free DMEM was used as the control. Controls are referred throughout as basal medium. The conditioned media were collected after 96 h, centrifuged at 1500 rpm for 5 min to remove cellular components and stored at −20°C. Where applicable, conditioned media were size fractionated using ultrafiltration devices with specific molecular weight cut-offs of 50,000 Da, 5,000 Da, 3,000 Da (Amicon Inc., Beverly, MA) and 1,000 Da (Microsep, Pall Corporation, Ann Harbor, MI) and stored at −20°C until use.

Cell survival assay

ECs were seeded at a density of 6×10^3 cells/well in 96-well cluster plates and grown to 60% confluence. After 24 h in endothelial culture medium, tumor conditioned medium was added to cultured cells, and incubations continued for 24–72 h under normoxic or hypoxic conditions. After 24–72 h, cells were fixed with 10% trichloroacetic acid, washed under tap water and stained with sulphophodamine B (SRB). After washing with 1%

acetic acid, plates were dried at 50°C and the dye was solubilized in 10mM Tris buffer. The absorbance was measured using a microplate reader (Victor 1420, Wallac, Turku, Finland) at 510 nm. All EC survival data were normalized to treatment with basal medium at 24 h under normoxic conditions, and is expressed as a percentage.

Cell morphology

ECs were seeded at a density of 3×10^4 cells/well in 24-well cluster plates and grown to 60% confluence. After 24 h in endothelial culture medium, conditioned medium was added to the ECs, and incubations continued for 24–72 h under normoxic or hypoxic conditions. After 24–72 h, cells were analyzed microscopically using an Axiovert 100M inverted microscope with a 10X/0.30 Plan-Neofluar objective (Carl Zeiss) and images were captured with an Axiocam MRC digital camera using AxioVision 4.5 software (Carl Zeiss B.V., Sliedrecht, NL).

Flow cytometry

ECs cultured under hypoxic conditions in the presence of MCM or basal medium were stained with FITC Annexin V/Dead Cell Apoptosis Kit (Molecular Probes, Carlsbad, CA), as per the manufacturer's instructions, and analyzed by flow cytometry (FACScan, Becton Dickinson, Palo Alto, CA). Data analysis was performed using the FlowJo software (TreeStar Inc, Ashland, OR).

Detection of adherent apoptotic cells

Yo-Pro-1 (Molecular Probes) staining was used for microscopic detection of adherent apoptotic cells. Endothelial culture medium supplemented with 25 µg/mL Etoposide was used as a positive control for apoptosis. Briefly, after 24 h of incubation with MCM or basal medium under hypoxia, detached cells were removed and ECs were incubated with 0.5 µM Yo-Pro-1 for 15 mins at 37°C. Fluorescence was visualized using an Axiovert 100M inverted microscope with a 10X/0.30 Plan-Neofluar objective (Carl Zeiss) and an ORCA II ER camera (Hamamatsu Photonics Systems).

Growth factors and inhibitors

Recombinant human VEGF (10 ng/ml) or bFGF (200 ng/ml) was added to ECs and survival under normoxia and hypoxia was monitored. Alternatively, VEGFR kinase inhibitor Sugen 5416 (5 µM) or VEGF-neutralizing antibody (0.3 µg/ml) was added to the melanoma conditioned medium. For pathway inhibition studies, ECs were treated with LY294002 (50 µM), PD98059 (20 µM) and SB203580 (10 µM) for 12 h in the presence of melanoma-conditioned medium and cell viability was analyzed by flow cytometry. Alternatively, EC survival was assayed up to 72 h.

ELISA

To determine the presence of VEGF in the melanoma-conditioned medium, a commercial ELISA kit for human VEGF165 (Quantikine, R&D Systems) was used, and assays were performed according to the manufacturer's specifications.

Heat inactivation of the melanoma conditioned media

Conditioned media were heat inactivated for 30 mins at 56, 80 and 100°C.

Trypsin and chymotrypsin digestion of the melanoma conditioned media

Conditioned media were subjected to trypsin (100, 200 µg/ml) and chymotrypsin (100, 200 µg/ml) treatments (Sigma-Aldrich). Digestions were carried out at 37°C for 30 min and the reaction was terminated by the addition of 1 mg/ml soybean trypsin inhibitor (Sigma-Aldrich) or L-1-Tosylamide-2-phenylethyl chloromethyl ketone (TPCK) treated inhibitor. Alternatively, for smaller size fractions (< 1 kDa) of CM treated with trypsin and chymotrypsin, the reaction was terminated by the removal of trypsin and chymotrypsin with a 3 kDa cutoff fractionation column (MW trypsin = 24 kDa, MW chymotrypsin = 25 kDa).

Acetone precipitation

In order to determine if the survival factor/s were present in the protein or non-protein phase, MCM were treated with ice-cold acetone in a 1:2 (v/v) ratio. The reaction was vortexed, incubated for 1 h at −20°C and pelleted by spinning at 14,000 rpm for 10 min at 4°C. The upper aqueous non-protein phase was collected and evaporated to a film in a rotary evaporator and subsequently dissolved in water. The air-dried protein pellet was reconstituted in serum-free basal medium. Both fractions were filter sterilized and assayed for their ability to promote endothelial cell survival under normoxic and hypoxic conditions.

BSA back exchange assay

Bovine serum albumin (BSA) back exchange assay was performed to separate the lipid and non-lipid components of the < 1 kDa SF-CM fraction. Briefly, the < 1 kD SF-CM fractions were treated with 1, 3 or 10% (w/v) fatty acid free BSA (Sigma-Aldrich) for 30 mins at 37°C. Treated samples were fractionated using a 30 kDa cut-off fractionation column (MW BSA = 66 kDa) to obtain the BSA rich fraction (retentate) and BSA poor fraction (flowthrough). Both fractions were filter sterilized and assayed for their ability to promote EC survival under normoxic and hypoxic conditions. Cell viability was measured using the XTT (2,3-Bis-(2-Methoxy-4-Nitro-5-Sulfophenyl)-2*H*-Tetrazolium-5-Carboxanilide) assay, as described elsewhere.

RNA isolation

Total RNA was extracted using TRIzol (Invitrogen) following manufacturer's instructions. Purified RNA was quantified by spectophotometric analysis using a NanoDrop 2000 (Thermo Fisher Scientific Inc., CA) and analyzed on an Agilent 2100 Bioanalyzer (Agilent Technologies, CA). Only RNA with RIN > 8.0 were used for the microarray experiment.

Affymetrix GeneChips

In this study we used the Affymetrix HG-U133-plus 2.0 GeneChip (Affymetrix Inc., Santa Clara, CA). Target synthesis was performed using 5 μg total RNA as template, as described in the Affymetrix Gene Expression Manual. GeneChips were washed and stained using the Affymetrix fluidic station 430 and analyzed using Affymetrix 3000 7G GeneChip scanner. Gene expression values were summarized from probesets using RMA as implemented in Affymetrix Gene Expression Console. The same software was used to quality control (QC) the GeneChips. Chips not meeting QC criteria were excluded from further analysis. RMA expression summaries were merged with the Affymetrix MAS 5.0 Presence calls into a single matrix, filtered in Excel and imported into BRB ArrayTools for further analysis[86]. Probesets were filtered out if called 'absent' in > 80% of the samples. Correlation among samples was assessed using the MDS and the hierarchical clustering tools in BRB ArrayTools. We identified genes that are differentially expressed among the two classes using a random variance t-test as implemented in the class comparison tool in BRB ArrayTools (developed by Dr. Richard Simon and BRB-ArrayTools Development Team). An estimate of the associated False Discovery Rate (FDR) was computed per gene using the method of Benjamini and Hochberg. Genes were considered significant if $p < 0.001$. A table reporting all the genes passing the test along with p-values, fold change and per gene FDR estimates is posted under supplementary materials. Gene clustering and visualization was performed using the BRB ArrayTools. Pathway analysis was performed using the GeneSet Class Comparison tool in BRB ArrayTools. For GeneSet enrichment, Gene Ontology, BioCarta and KEGG databases were independently queried. The microarray data from this publication has been submitted to the GEO database (http://www.ncbi.nlm.nih.gov/geo/) and assigned the identifier GSE33115.

Real-time RT-PCR

Microarray gene expression data were validated by measuring differential gene regulation in treated ECs, from three separate donors, using real time PCR. Briefly, total RNA extraction was performed with TRIzol Reagent (Invitrogen), according to the manufacturer's instructions. Reverse transcription was performed with 2 μg total RNA using the First-Strand cDNA Synthesis Kit (Invitrogen). 50 ng of cDNA was used for the qPCR reaction. Quantitative PCR was performed in duplicates, using the iCycler (Bio-Rad

Laboratories, Munich, Germany) with specific TaqMan Gene Expression assays (Applied Biosystems). The reactions were incubated in a 96-well optical plate at 50°C for 2 minutes (UDG incubation) and 95°C for 10 minutes, followed by 40 cycles of 95°C for 15 seconds and 60°C for 60 seconds.

Active caspases

Levels of active caspase-3/7 in treated ECs were assayed using the commercially available SensoLyte Homogeneous AnaRed Caspase-3/7 Assay Kit (AnaSpec Inc., Fremont, CA), according to manufacturer's instructions. Briefly endothelial cells were seeded at a density of 6×10^3 cells/well in 96-well black cluster plates and grown to 60% confluence. Various SF-CMs were added to cultured cells and incubated at 37°C under normoxic or hypoxic conditions. At 16 h and 24 h of treatment, caspase 3/7 substrate solution was added to the cells, and incubated in the dark for 1 min with gentle shaking. Fluorescence intensity was measured at 635 nm using a fluorescence microplate reader.

Western Blot analysis

To determine pathway effectors of the survival response, sodium dodecyl sulphate (SDS)-polyacrylamide gel electrophoresis was performed. Briefly, subconfluent EC cultures were washed twice and serum starved for 12 h in medium containing 0.5% serum, followed by treatment with fractionated or unfractionated conditioned media. Treated ECs were rinsed twice with ice-cold PBS, scraped and pelleted. Lysis was conducted in the presence of protease and phosphatase inhibitor cocktail tablets (Roche) and the protein concentration was measured with Coomassie Plus Reagent (Pierce). Equal amounts of proteins were loaded on 12% gels, electrophoresed and transferred to polyvinylidene difluoride (PVDF) membranes (BioRad). Membranes were blocked for 1 h at room temperature with 5% nonfat dried milk (BioRad) in PBS/0.05% Tween-20, followed by overnight incubations with primary antibodies against total AKT (rabbit polyclonal, 1:1000 dilution), phospho-AKT (Ser473) (mouse monoclonal, 1:1000 dilution), total ERK 1/2 (rabbit polyclonal, 1:1000 dilution), phospho-ERK (mouse monoclonal, 1:1000 dilution), total p38 MAPK (rabbit polyclonal, 1:1000 dilution) and Phospho-p38 MAPK (Thr180/Tyr182) (mouse monoclonal, 1:2000 dilution). Post washing, the membranes were incubated with IRDYE labeled secondary antibody (LI-COR) for 1 h at room temperature and scanned using the Odyssey Infrared Imaging System (LI-COR Biosciences).

RESULTS

Melanoma conditioned medium (MCM) prevents endothelial cell (EC) death under restrictive culture conditions

Conditioned medium derived from six melanoma cell lines, differing in angiogenic profiles[83,87], were tested for their ability to promote EC survival under normoxic and hypoxic conditions. All MCMs were capable of promoting long-term (up to 72 h) HU-VEC (Human Umbilical Vein Endothelial Cell) survival under hypoxia. Basal medium treatment did not prevent cell death as no viable population was observed at 48 and 72 h (Figure 1a). All MCMs and basal medium were capable of promoting HUVEC survival under normoxic conditions (Supplementary Figure 1a). To determine if the observed survival effect was restricted to an EC subtype, we tested the ability of MCMs to promote HMVEC (Human Dermal Microvascular Endothelial Cell) survival under hypoxia. As with HUVECs, all MCMs were capable of mediating HMVEC survival under normoxic and hypoxic conditions while basal medium only mediated survival under normoxic conditions (Figure 1b and Supplementary Figure 1b). These data suggest that the pro-survival effect induced by MCMs is not restricted to a specific EC subtype. Next, we sought to determine if MCM generated from melanoma cells cultured under hypoxic conditions were capable of inducing a similar pro-survival effect in ECs. Conditioned media derived from all melanoma cell lines under hypoxic conditions were capable of sustaining HUVEC (Figure 1c) and HMVEC (Figure 1d) survival under hypoxia. Survival of ECs under normoxic conditions are shown in Supplementary Figures 1c, d. Although the tested melanoma cell lines have been documented to vary in the expression of angiogenic factors and tumor vascular density in corresponding xenografts[83,88], we did not observe a clear correlation to the extent to which the MCMs promoted EC survival under hypoxia. Near confluent cultures of ECs treated with undiluted MCMs showed the classic cobblestone morphology under restrictive culture conditions (Figure 1e).

Melanoma conditioned medium prevents hypoxia induced apoptotic death

As non-physiological variances such as hypoxia are known to provoke cell death[82,89], we sought to determine if the observed survival effect was a result of inhibition of apoptotic or necrotic cell death. ECs treated with undiluted and diluted MCMs for 48 h under hypoxia were subjected to a bivariate FACS analysis using FITC-Annexin V and PI. This aided in the discrimination of viable cells (FITC$^-$PI$^-$), early apoptotic (FITC$^+$PI$^-$) and late apoptotic or necrotic cells (FITC$^+$PI$^+$). Representative dot-plots are shown in Figure 2a. Percentages of apoptotic and necrotic populations at 48 h hypoxia under various treatments are depicted in Figure 2b. While over 95% of the cells underwent apoptosis or became necrotic when cultured in basal medium under hypoxia, treatment with MCMs rendered the majority of the cells viable (85% for BLM CM and 83% for 1F6 CM) (Figures 2a, b). A
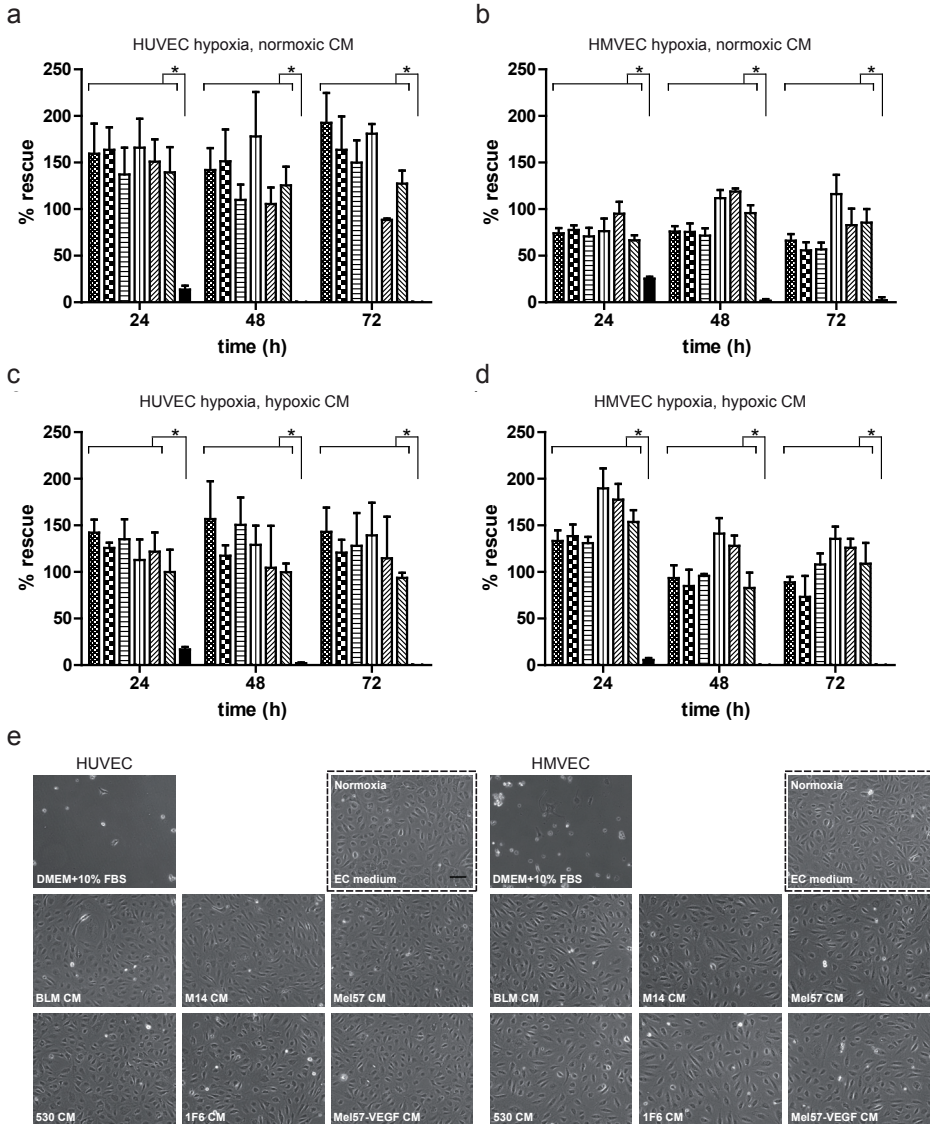
Figure 1. Melanoma conditioned medium (MCM) prevents endothelial cell (EC) death under severe hypoxia. (**a**) HUVEC and (**b**) HMVEC survival under hypoxia upon treatment with MCMs collected under normoxic conditions. (**c**) HUVEC and (**d**) HMVEC survival under hypoxia upon treatment with MCMs collected under hypoxic conditions. Subconfluent ECs were treated with various MCMs (BLM: ▨; M14: ▨; Mel57: ▤; 530: ▥; 1F6: ▨; Mel57-VEGF^{165}: ▧) and basal medium (■). Cells were fixed at 24, 48 and 72 h and the percentage of total surviving cells was determined. Cell survival (% rescue) data in (**a-d**) is expressed relative to treatment with basal medium (DMEM + 10% FBS) at 24 h normoxia and represent mean ± SEM of three independent experiments, conducted in triplicates. *$p < 0.05$. (**e**) Morphology of ECs under various treatments at 48 h hypoxia. Images in the dotted black box shows EC morphology with HUVEC culture medium under normoxic conditions. Scale bar, 100 μm.

a

b

c
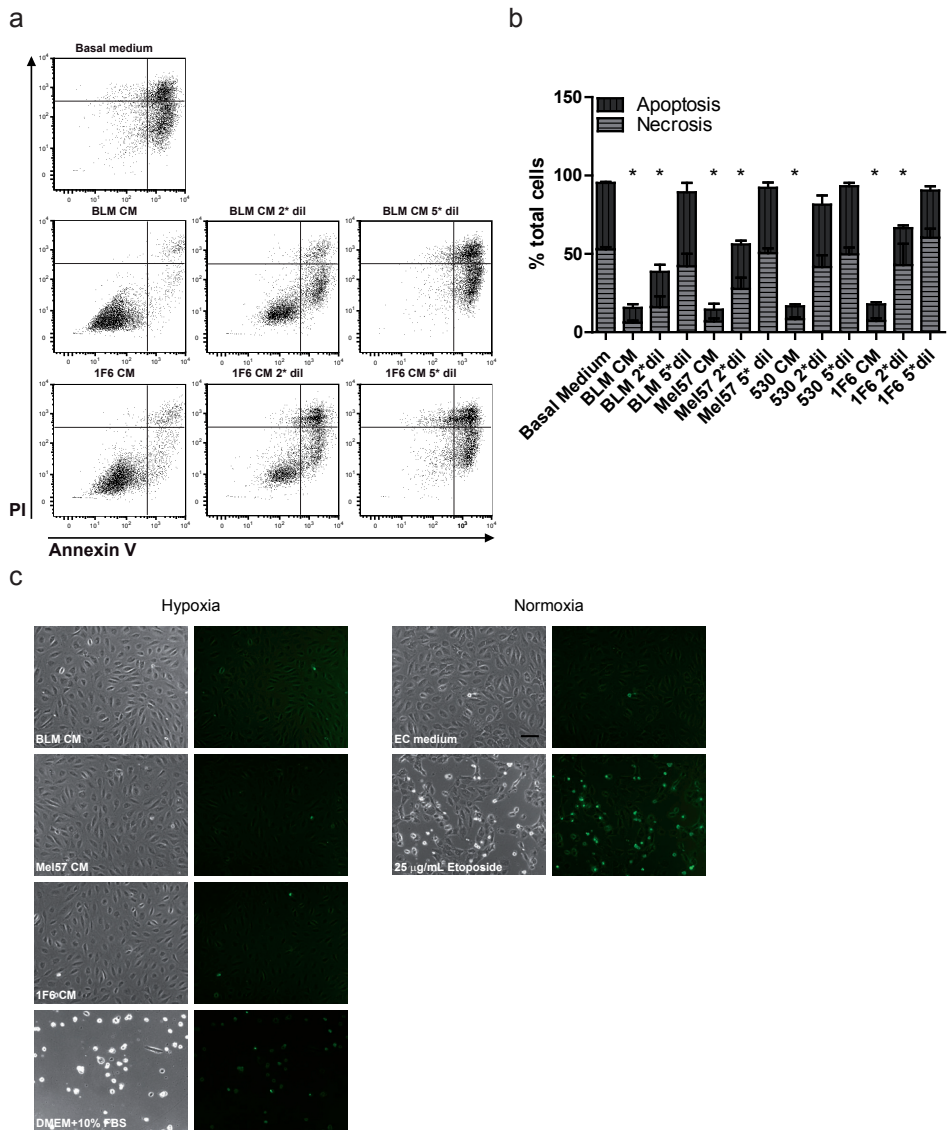
Figure 2. Melanoma conditioned medium (MCM) prevents hypoxia induced apoptosis of endothelial cells (EC). (**a,b**) Bivariate FACS analysis of MCM treated ECs (**a**) Representative dot plots of ECs treated with undiluted, twice diluted (2*dil) and five times diluted (5*dil) MCMs, and basal medium (DMEM + 10% FBS) at 48 h of hypoxia. Treated cells were stained with Annexin V (X-axis) and Propidium Iodide (PI, Y-axis) and subjected to flow cytometry analysis to determine percentages of apoptotic, necrotic and viable cells. (**b**) Relative percentages of apoptotic and necrotic ECs with different treatments at 48 h hypoxia. Treatment with diluted MCMs showed a gradual shift towards apoptotic cells. Data are derived from three independent experiments. *$p < 0.05$. (**c**) Visualization of apoptotic nuclei in ECs subjected to MCM or basal medium (DMEM+10% FBS) treatments at 48 h of hypoxia. As controls, ECs were treated with HUVEC medium with or without 25 µg/mL Etoposide (positive and negative control for apoptosis, respectively) under normoxic conditions. Scale bar, 100 µm.

shift towards apoptosis and necrosis was observed upon two-fold and five-fold dilutions of the MCMs. Further, the presence of apoptotic nuclei in treated ECs was visualized by staining with the nuclear dye, YOPRO-1 at 48 h of hypoxia treatment. MCM treated ECs under hypoxia did not show the presence of apoptotic nuclei, indicating viable ECs, while treatment with the cytotoxic agent Etoposide showed a marked increase in the presence of apoptotic nuclei. Basal medium treated ECs were not viable and showed fewer apoptotic nuclei indicating that cell detachment preceded cell death (Figure 2c).

Melanoma conditioned medium prevents endothelial cell death independent of the VEGF signaling pathway

The role of vascular endothelial growth factor (VEGF) and basic fibroblast growth factor (bFGF) as potent regulators of angiogenesis has been sturdily established in melanomas and other human tumors[90-92]. We therefore evaluated the ability of VEGF and bFGF in sustaining survival of ECs under restrictive culture conditions. Although both mitogens were capable of promoting EC growth under normoxia (Figure 3a), these factors were unable to rescue ECs from cell death when cultured under hypoxia (Figure 3b). Next, we evaluated the VEGF profile of melanoma cells by measuring the levels of VEGF in serum free melanoma conditioned medium. BLM produced the highest levels of VEGF (3.6 ng/10^6 cells) while Mel57 and 1F6 hardly produced any VEGF (Figure 3c). Additionally, we blocked VEGF signaling by the addition of either VEGF neutralizing antibody (Figure 3d) or VEGFR kinase inhibitor (Figure 3e) to undiluted and two-fold diluted MCM. Although EC proliferation was reduced upon VEGFR inhibition (Figure 3e), the ability of MCMs to promote EC survival under hypoxia was not hindered by blocking members of the VEGF signaling pathway, suggesting the involvement of alternate signaling pathways in mediating the observed survival effect.

Delineation and specificity of the melanoma induced survival effect

As the melanoma conditioned medium (MCM) has the presence of serum, we queried the contribution of serum to the observed survival effect. Additionally, as the growth rates of the tested melanoma cell lines used to generate the MCM varied, and therefore the consumption of serum components, we reasoned that the final concentration of serum might differ among the MCMs. Therefore, we prepared serum-free melanoma conditioned medium (SF-CM) and monitored long-term survival of ECs under hypoxic conditions. SF-CMs were capable of inducing a similar survival response in ECs as the MCMs, and likewise, this effect was lost upon dilution of the SF-CM (Figure 4a). In order to further characterize the melanoma induced survival effect, we size fractionated the SF-CMs with several molecular weight cut-offs. Interestingly, no long-term survival effect was induced by the > 50 kDa fraction, while all small molecule fractions tested (< 50 kDa, < 5 kDa, < 3 kDa, < 1 kDa) resulted in a survival effect comparable to that of the

a

b

c

d

e
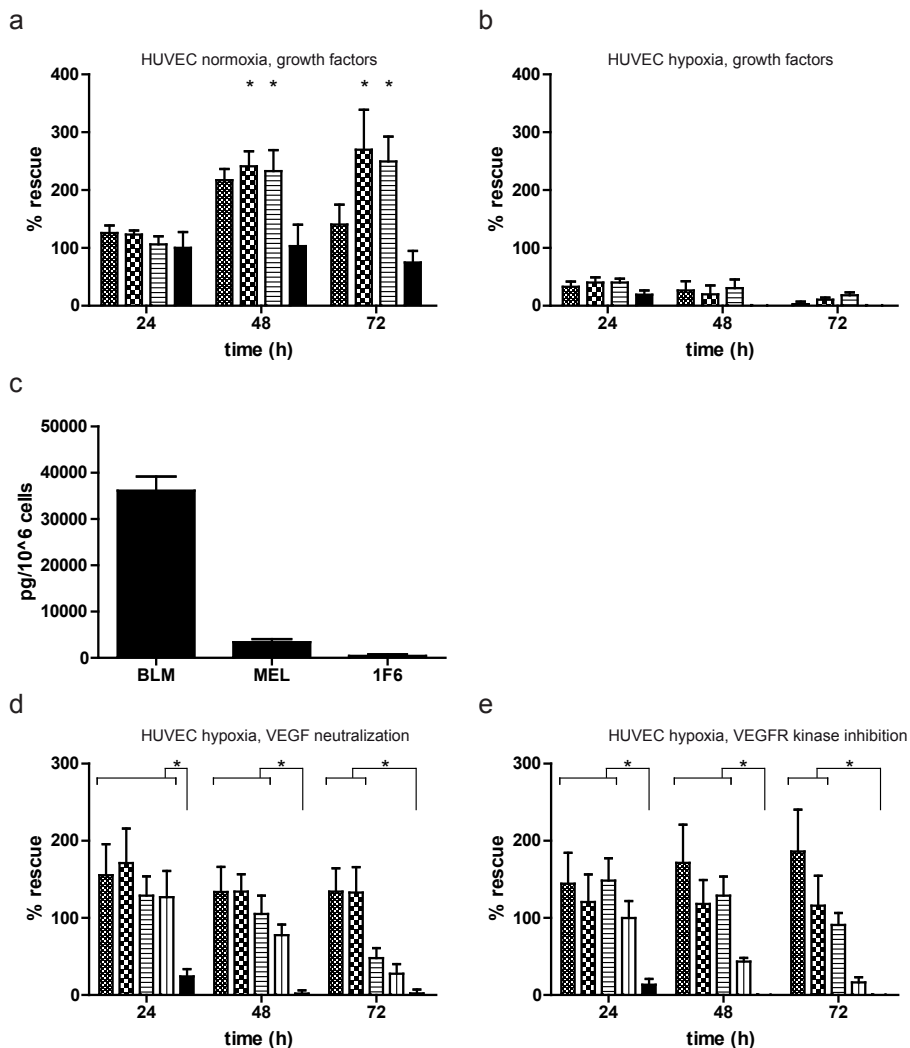
Figure 3. Melanomas mediate endothelial cell (EC) survival under hypoxia, independent of the VEGF signaling pathway. (**a,b**) ECs were treated with 10 ng/ml VEGF (▨) or 200 ng/ml bFGF (▨) alone, or in combination (▭). Cell survival was monitored under normoxia (**a**) and hypoxia (**b**) for up to 72 h. (**c**) Levels of VEGF (pg/ 1×10^6 cells) in serum-free conditioned medium (SF-CM) as detected by ELISA. Data were normalized to the number of cells used to generate the SF-CM and are expressed as mean ± SD of quadruplicate samples. (**d, e**) Effect of VEGF pathway inhibition on EC survival under hypoxia. ECs were treated with undiluted and twice diluted melanoma conditioned medium in the presence of (**d**) VEGF neutralizing antibody (0.3 µg/ml) or (**e**) VEGFR kinase inhibitor (0.3 µg/ml) (undiluted MCM: ▨; undiluted MCM with neutralizing antibody/inhibitor: ▨; twice diluted MCM: ▭; twice diluted MCM with neutralizing antibody/inhibitor: ▥; and basal medium: ■). Cell survival (% rescue) data in (**a,b,d,e**) is expressed relative to treatment with basal medium (DMEM + 10% FBS) at 24 h normoxia and represent mean ± SEM of three independent experiments, conducted in triplicates. *$p < 0.05$.

a

Serum free melanoma CM

b

Serum free melanoma CM fractions

2

c

Melanocyte SF-CM

d

Breast and Pancreatic SF-CM
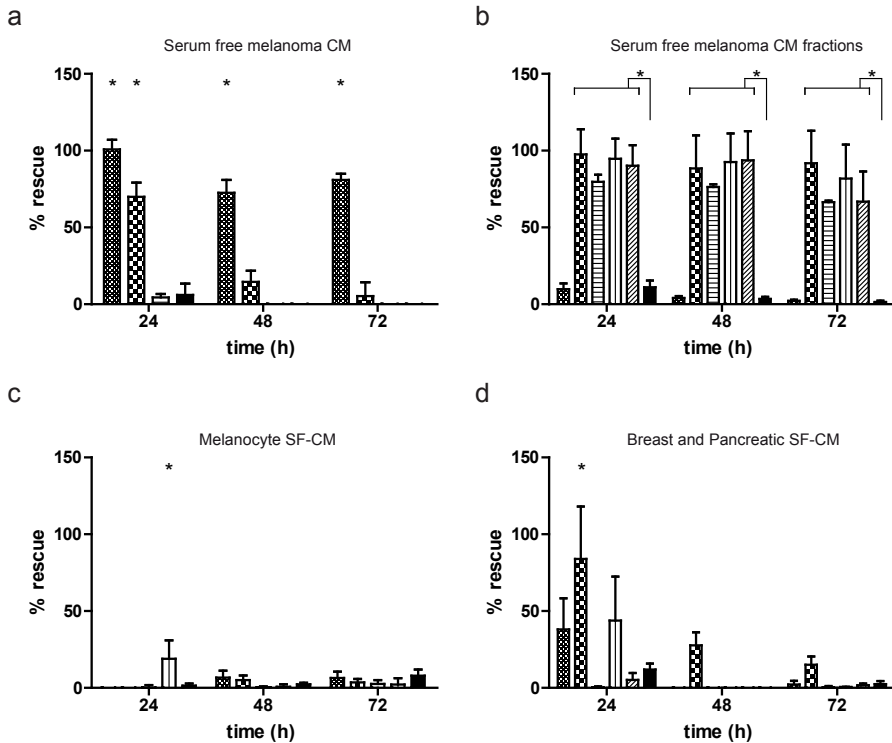
Figure 4. Delineation of melanoma induced survival effect. (**a**) Effect of serum on endothelial cell (EC) survival. ECs were grown to near confluence and treated with undiluted (▨), twice diluted (▨) and five times diluted (▭) serum-free melanoma conditioned medium (SF-CM) and basal medium (■) under hypoxia for up to 72 h. (**b**) Effect of SF-CM size fractionation on EC survival. SF-CMs were size fractionated and the various fractions (> 50 kDa: ▨; < 50 kDa: ▨; < 5 kDa: ▭; < 3 kDa: ▯; < 1 kDa: ▨; and basal medium: ■) were added to near confluent EC cultures. (**c**) Effect of melanocyte conditioned medium on EC survival. Unfractionated and fractionated serum-free melanocyte conditioned medium was added to near confluent EC cultures. Melanocyte conditioned medium was not capable of promoting EC survival under hypoxic conditions (unfractionated hMEL SF-CM: ▨; < 1 kDa hMEL SF-CM: ▨; unfractionated NHEM SF-CM: ▭; < 1 kDa NHEM SF-CM: ▯; and basal medium: ■). (**d**) Effect of breast and pancreatic cell conditioned medium on EC survival. Size fractionated < 1 kDa fractions of serum-free conditioned medium derived from breast cancer cell lines (MCF-7: ▨, SK-BR-3: ▨), pancreatic cancer cell lines (BxPC-3:▭, PANC-1:▯, MiaPaCa:▨) and basal medium (■) were added to near confluent EC cultures. Breast and pancreatic SF-CM were not capable of inducing long-term EC survival under hypoxia. Cell survival (% rescue) in (**a-d**) is expressed relative to treatment with basal medium (serum-free DMEM) at 24 h normoxia. Data represent mean ± SEM of four independent experiments, conducted in triplicates. *$p < 0.05$.
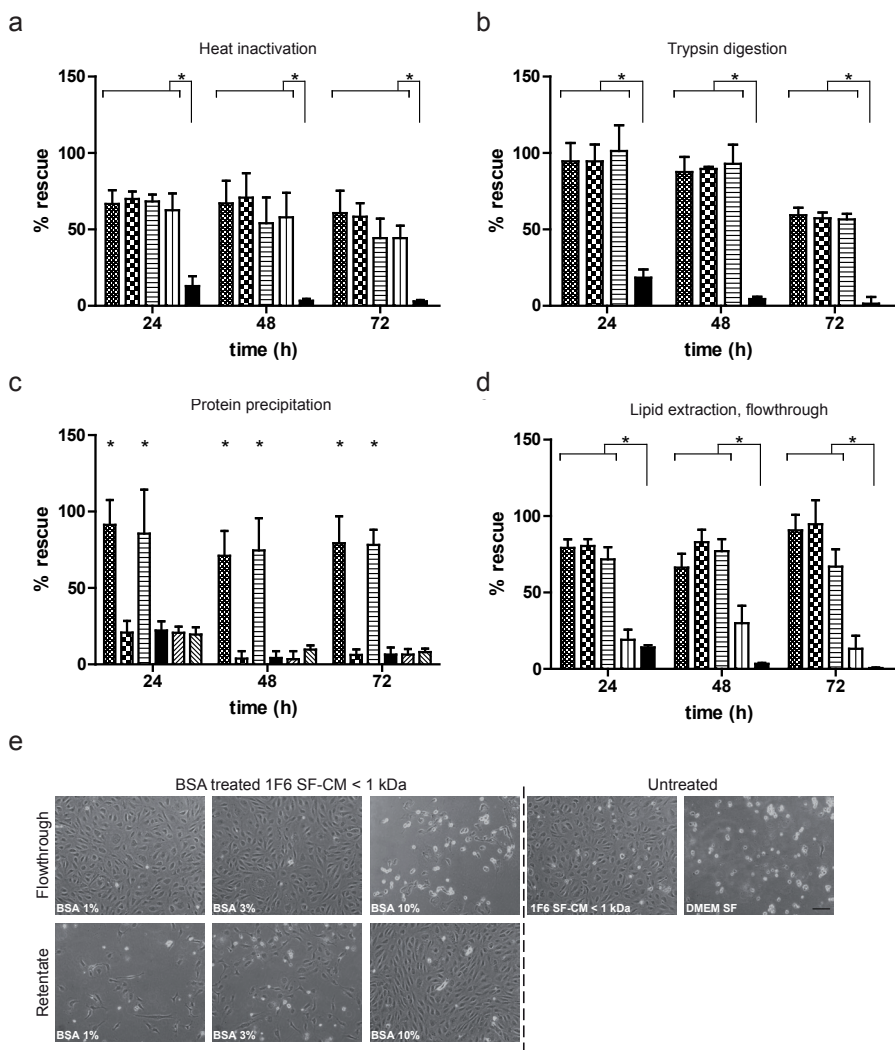
Figure 5. Characterization of the melanoma specific survival effect. (**a**) Effect of heat treatment on endothelial cell (EC) survival. Size fractionated < 1 kDa fraction of serum-free melanoma conditioned medium (SF-CM) was heat inactivated at 56℃, 80℃ and 100℃ respectively, for 30 min. Untreated (▨▨), heat-inactivated (56℃: ▨▨; 80℃: ▭; 100℃: ▥) media and basal medium (■) were added to near confluent EC cultures and long-term survival under hypoxia was monitored. (**b**) Effect of enzymatic digestion on EC survival. Size fractionated < 1 kDa fraction of melanoma SF-CM was treated with 100 and 200 μg/ml of trypsin for 30 min at 37℃. Untreated (▨▨), trypsin treated samples (100 μg/ml: ▨▨; 200 μg/ml: ▭) and basal medium (■) were added to near confluent EC cultures and monitored for long-term survival under hypoxia. (**c**) Effect of protein precipitation on EC survival. Size fractionated < 1 kDa fractions of melanoma SF-CM and basal medium were subjected to protein precipitation using acetone. Reconstituted protein and non-protein fractions were added to subconfluent EC cultures and survival under hypoxia was monitored (< 1 kDa SF-CM untreated: ▨▨; < 1 kDa SF-CM protein fraction: ▨▨; < 1 kDa SF-CM non-protein fraction: ▭; basal medium: ■; basal medium protein fraction: ▨; basal medium non-protein fraction: ▧). (**d,e**) Effect of lipid extraction on EC survival. Size fractionated < 1 kDa SF-CM fractions of

unfractionated SF-CM (Figure 4b). In order to determine if the observed pro-survival effect is an acquired trait during melanoma development, we assayed for the ability of primary and immortalized human melanocytes to promote EC survival under normoxic and hypoxic conditions. Both unfractionated and fractionated serum-free melanocyte conditioned media were not able to induce EC survival under hypoxia (Figure 4c). Under normoxic conditions, EC survival was observed upon treatment with melanocyte conditioned medium (Supplementary Figure 2a).

Further, we proceeded to determine if the survival effect mediated by the < 1 kDa fraction was specific to melanomas or a common feature among other tumor types. To this end we prepared serum-free conditioned medium from breast and pancreatic tumor cell lines, varying in their growth profiles and genomic abnormalities[93,94]. Unfractionated (data not shown) and fractionated (< 1 kDa) tumor conditioned media were tested for their ability to promote EC survival under hypoxia. Interestingly, although some cell lines were capable of inducing a short term survival response in ECs under hypoxia, no long-term survival was seen (Figure 4d). Thus the survival effect mediated by the < 1 kDa fraction seems to be specific for melanoma cells. Under normoxic conditions, EC survival was observed with all breast and pancreatic tumor conditioned medium tested (Supplementary Figure 2b).

Characterization of the melanoma specific survival effect

In order to further characterize the melanoma specific induction of survival responses in ECs under hypoxia, we subjected the SF-CM < 1 kDa fraction to heat inactivation (Figure 5a), trypsin (Figure 5b) and chymotrypsin digestion (data not shown). No difference was observed between pro-survival responses generated by treated and untreated < 1 kDa SF-CM fractions. Additionally, the protein and non-protein fractions of the < 1 kDa SF-CM were separated using acetone precipitation. We observed that while the reconstituted protein pellet was not able to mediate EC survival, the non-protein fraction sustained long-term EC survival under hypoxia. As a control, basal medium was subjected to the same treatment. No EC survival was observed (Figure 5c). We also performed a BSA back exchange assay, with increasing concentrations of fatty acid-free BSA, to separate the lipid

melanoma SF-CM were treated with 1%, 3% or 10% fatty-acid free BSA. BSA-poor (flowthrough) fractions were obtained as described under 'Materials and Methods'. (**d**) Untreated (▨), BSA treated flowthroughs (1%: ▨; 3%: ▭; 10%: ▯) and basal medium (■) were added to subconfluent ECs to monitor cell survival under hypoxia. (**e**) Morphology of ECs under various treatments at 48 h hypoxia. Scale bar, 100 µm. Cell survival (% rescue) in (**a-d**) is expressed relative to survival of basal medium (serum-free DMEM) treated ECs at 24 h normoxia and represent mean ± SEM of four independent experiments, conducted in triplicates. *$p < 0.05$.

and non-lipid components present in the < 1 kDa SF-CM fraction. Post treatment, samples were size fractionated to obtain BSA-rich (retentate) and BSA-poor (flowthrough) fractions. We observed EC survival under hypoxia when treated with the BSA-poor fractions (flowthrough) of the 1% and 3% BSA treated samples. Interestingly, treatment of the < 1 kDa SF-CM fraction with 10% BSA resulted in the removal of the observed survival effect from the flowthrough, suggesting that BSA selectively adsorbs the survival factor/s at a higher concentration (Figures 5d, e). This selective separation of the melanoma specific survival factor/s suggests that it might be a lipid/lipophilic molecule.

Global changes in gene expression upon treatment with melanoma conditioned medium

To characterize the molecular mechanisms underlying the survival effect, we performed a whole genome gene expression study and analyzed the changes in relative mRNA abundance induced by treating ECs with MCM or basal medium for 12 h under hypoxic and normoxic conditions. The 12 h time point was chosen, as basal medium treated ECs under hypoxia maintain substantial morphological integrity and cell viability; prolonging the treatment results in extensive cell death. Based on the confidence level of their expression measurements (Affymetrix presence calls), 27410 probe sets passed the set filtering threshold and were used for further statistical analysis. Unsupervised Multidimensional Scaling (MDS) analysis identifies hypoxic/normoxic growth conditions and MCM treatment as the main sources of variability in our dataset. Samples treated with MCM clustered apart from basal medium treated control samples, indicating that MCM treatment induces a consistent modification in the pattern of expressed genes. This modification appears to be minimally modified by the hypoxic/normoxic culturing condition, consistent with the observation that variations in cell morphology and viability is minimal at the 12 h time point (Figure 6a and Supplementary Figure 3). To identify the genes regulating the observed survival effect, we compared the gene expression profile of ECs treated with MCM to that of ECs grown in basal medium, under hypoxia. Using a random variance t-test, 694 probe sets were significantly modulated as a consequence of the MCM treatment. The 694 probe sets represent 524 individual transcripts, of which 296 were induced and 228 were repressed. A table reporting all the genes passing the test along with p-values, fold change and per gene FDR estimates is posted under Supplementary Information. Probe sets passing the test were clustered and displayed as a Heatmap using the clustering tool in BRB ArrayTools. Additionally, we visualized the expression values of the same probe sets in ECs treated for 12 h under normoxia (Supplementary Figure 3) and observed a similar pattern of gene expression modulation.

The gene expression changes identified appear consistent with the observed survival activity of MCM. Among the genes more differentially expressed, we observed increased expression of transcripts encoding cytokines and other gene products involved in cy-
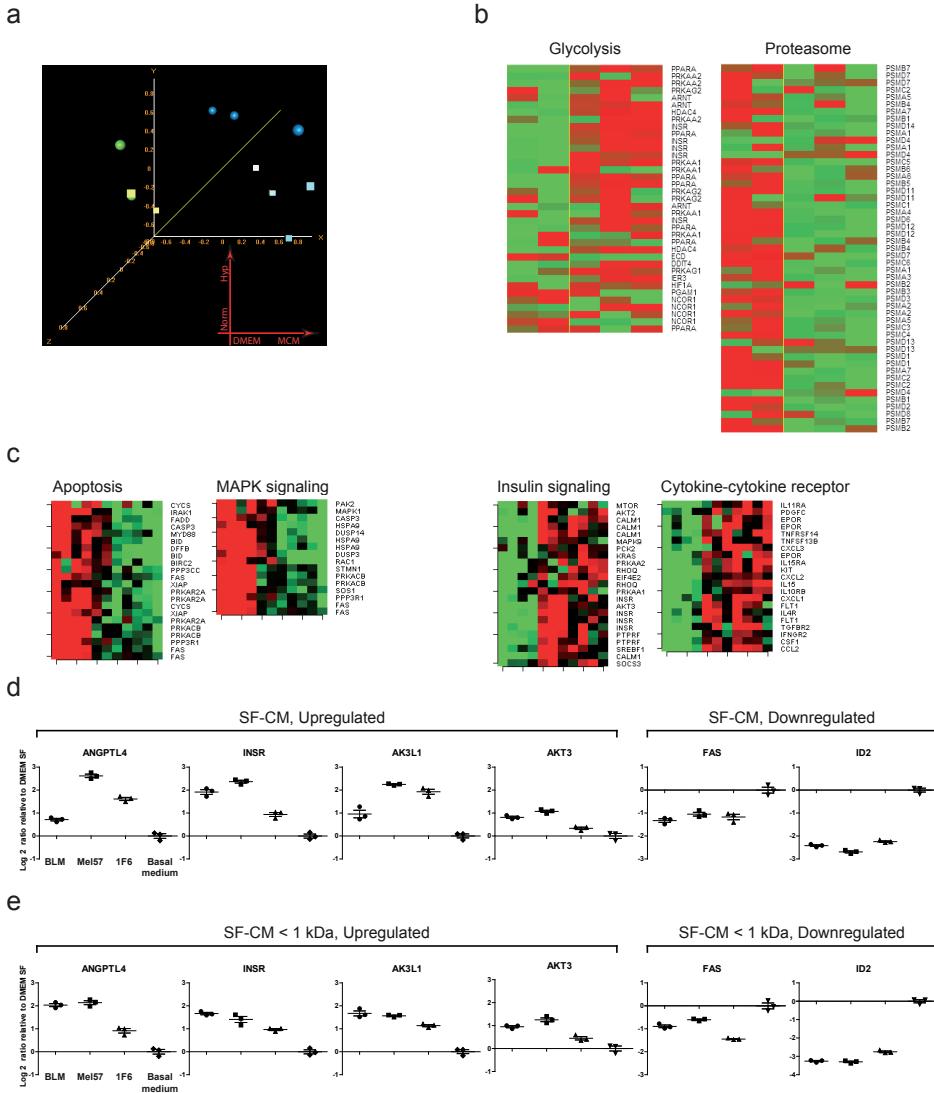
Figure 6. Global changes in gene expression upon treatment with melanoma conditioned medium.
(**a-c**) Changes in relative mRNA abundance induced by treating endothelial cells (EC) with MCM or basal medium for 12 h under hypoxic and normoxic conditions. (**a**) Unsupervised Multidimensional scaling analysis of the probesets passing Affymetrix presence calls (green sphere: basal medium, hypoxia; green cube: basal medium, normoxia; blue sphere: MCM hypoxia; blue cube: MCM, normoxia). (**b**) Heatmaps of pathways significantly altered as a consequence of MCM treatment at 12 h of hypoxia. (**c**) Heatmaps of genes constituting pro-apoptotic and pro-survival signaling pathways obtained from pathway analysis. A consistent downregulation of genes involved in pro-apoptotic signaling and an upregulation of genes involved in pro-survival signaling was observed with MCM treated ECs, as compared to basal medium treatment, both under hypoxic and normoxic conditions. (**d,e**) Differential expression of select genes from the microarray experiment were verified using real-time quantitative PCR. ECs were treated with (**d**) unfractionated or (**e**) fractionated (< 1 kDa) serum-free melanoma conditioned medium under hypoxia for 12 h. Changes in transcript abundance were normalized to B2M expression and are expressed as log2 ratio relative to basal medium (serum-free DMEM) treatment.

tokine signaling (CXCL2, CCL2, IL32, A2M, JAK3, STAT6, CXCR7, CASP1), cell metabolism, and survival (INSR, IGF1R, AKT3, MAP2K5, JUNB). A number of transcripts encoding proteins involved in apoptosis and inhibition of transcription (ID2, EID3, FAS) were among the most repressed ones. To gain further insight into the biological functions altered as a consequence of the gene expression changes induced by MCM treatment, we performed pathway analysis and interrogated different databases using the pathway analysis tool in BRB ArrayTools. Different pathways were significant under the test conditions used including KEGG "proteasome" (hsa03050) showing coordinated downregulation of multiple proteasome subunits, and GO "regulation of glycolysis" (GO:0006110) showing augmented expression of transcripts involved in glucose metabolism and energy production. Heatmaps displaying expression values of genes in relevant pathways are shown in Figure 6b. Further, we clustered and imaged the expression values of genes constituting the 'Apoptosis', 'MAPK kinase signaling', 'Insulin signaling' and 'Cytokine-cytokine receptor signaling' pathways of the KEGG database under hypoxic and normoxic conditions. We could clearly identify two main clusters of genes showing consistent modulation upon MCM treatment. Consistent with the observed survival effect induced by MCM, genes involved in the proapoptotic signaling cluster were downregulated in MCM treated group while genes involved in the pro-survival signaling cluster were upregulated (Figure 6c).

The gene expression changes observed in the microarray experiments were validated by real time PCR. For all the transcripts tested, the results of the real time PCR validation experiments were in good agreement with the microarray analysis. Of note, this validation experiment was performed with both unfractionated (Figure 6d) and fractionated < 1 kDa (Figure 6e) SF-CM to rule out the effect of growth factors and other large mass bioactive molecules present in unfractionated conditioned medium. Gene expression changes under normoxic conditions are provided in Supplementary Figure 4.

Melanoma conditioned medium induces a pro-survival signal transduction cascade in endothelial cells

As a robust survival response was generated in hypoxic ECs upon treatment with MCMs, we proceeded to investigate the signal transduction events mediating this effect. Caspases are a group of endoproteases that play a central role in the regulation of programmed cell death in response to environmental stresses such as hypoxia[95]. We therefore evaluated the levels of active caspases 3/7 in ECs treated with the < 1 kDa fraction of SF-CMs from a panel of cell lines. At 16 h of hypoxia treatment, levels of active caspases were 2.5 fold higher in melanocyte < 1 kDa SF-CM treated samples, and about 3 fold higher in breast and pancreatic tumor < 1 kDa SF-CM treated samples, as compared to the melanoma < 1 kDa SF-CM treatment (Figure 7a). Further, we evaluated the phosphorylation status of AKT, ERK-1/2 and p38 MAPK which are known to be central mediators of the survival signaling cascade in endothelial cells. We observed pronounced AKT and ERK-1/2 ac-

a

b
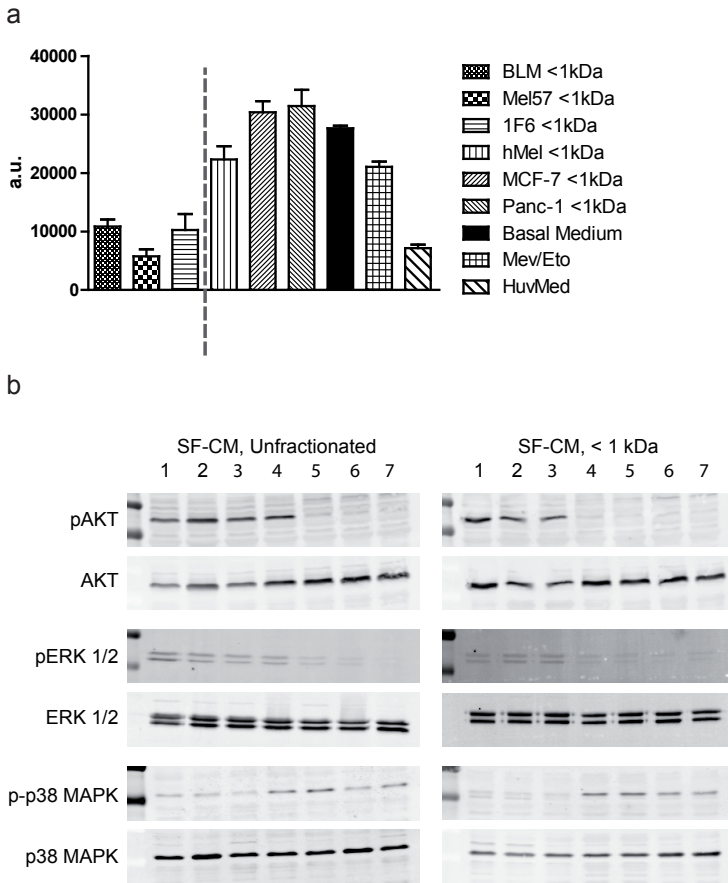
Figure 7. Melanoma conditioned medium induces a pro-survival signal transduction cascade. (a) Caspase induction in endothelial cells (ECs) under hypoxia. ECs were treated with < 1 kDa fractions of various serum-free melanoma conditioned media (SF-CM), under hypoxic conditions. ECs cultured with HUVEC medium under normoxic conditions were used as a negative control (NC) for apoptosis and the addition of Etoposide (25 µg/mL) served as the positive control (PC) for apoptosis induction. Levels of active caspase 3/7 were measured at 16 h of treatment. Data are represented as mean ± SD of three independent experiments, conducted in triplicates. **(b)** Serum starved ECs were treated with unfractionated or fractionated (< 1 kDa) SF-CM under hypoxic conditions. Cells were lysed and western blotting was performed to detect total and activated forms of AKT (MW, 60 kDa), ERK-1/2 (MW, 42,44 kDa) and p38 MAPK (MW, 43 kDa). SF-CM treatment lanes: 1- BLM, 2- Mel57, 3- 1F6, 4- PANC-1, 5- MCF-7, 6- hMEL, 7- Basal medium.
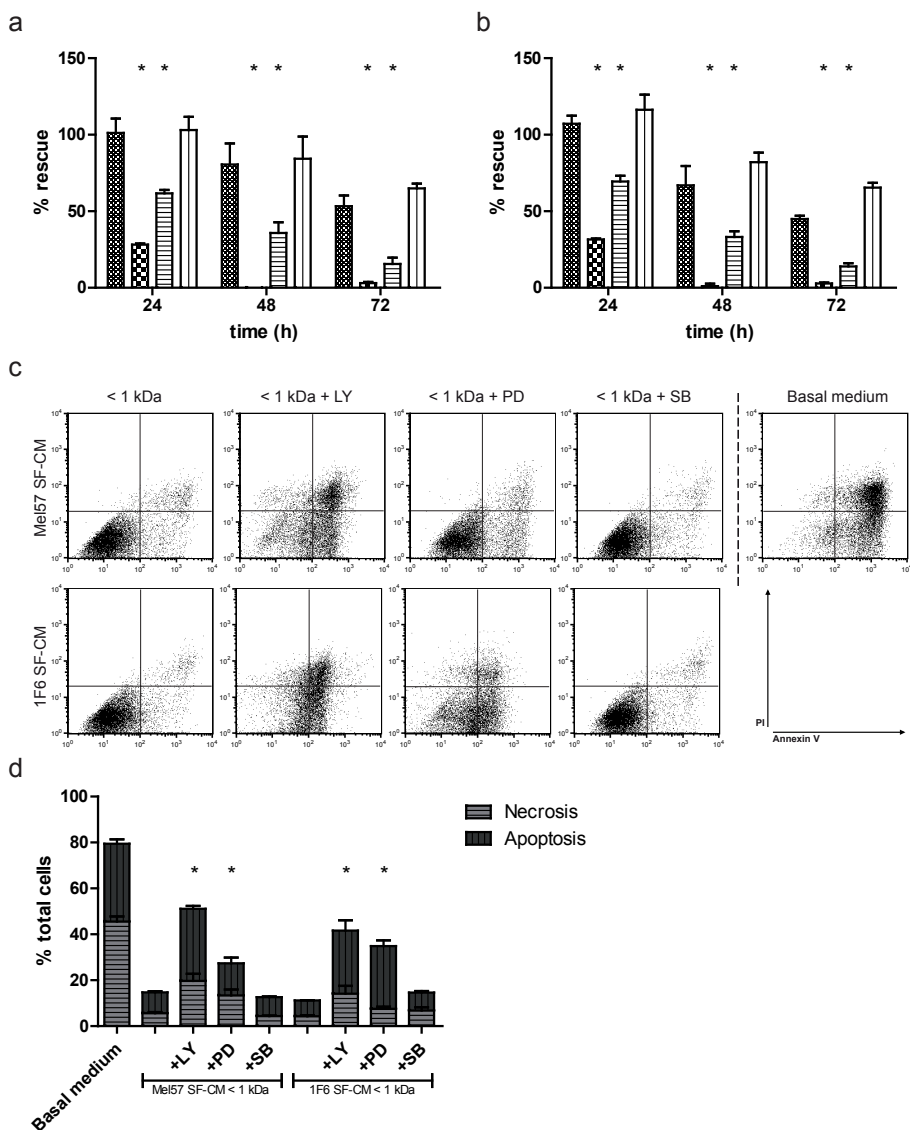
Figure 8. Inhibition of the melanoma specific survival effect. (**a,b**) Effect of pathway inhibitors on endothelial cell (EC) survival. ECs were treated with < 1 kDa fractions of (**a**) Mel57 or (**b**) 1F6 SF-CM, in the presence of PI3 kinase inhibitor (LY294002), MEK inhibitor (PD98059) or p38 MAPK inhibitor (SB203580) and long-term survival under hypoxia was monitored (< 1 kDa SF-CM: ▨; + LY294002, 50 µM: ▨; + PD98059, 20 µM: ▤; + SB203580, 10 µM: ▯). Cell survival (% rescue) in (**a,b**) is expressed relative to survival of basal medium (serum-free DMEM) treated ECs at 24 h normoxia and represent mean ± SEM of three independent experiments, conducted in triplicates. All inhibitor treated samples were compared to treatment with melanoma SF-CM < 1 kDa treatment. *$p < 0.05$. (**c,d**) Bivariate FACS analysis of ECs treated with pathway inhibitors (**c**) Representative dot plots of ECs treated with < 1 kDa melanoma SF-CM fraction with or without pathway inhibitors, and basal medium (serum-free DMEM) at 12 h of hypoxia. Treated cells were stained with Annexin V (X-axis) and Propidium Iodide (PI, Y-axis) and subjected to flow cytometry

tivation upon treatment with both fractionated and unfractionated melanoma SF-CM under hypoxia, as compared to other SF-CMs and basal medium. Consistent with the microarray observations, phosphorylated p38 MAPK levels were downregulated in both fractionated and unfractionated melanoma SF-CM treatments, indicating the induction of a pro-survival signaling cascade (Figure 7b).

Melanoma specific endothelial survival effect is mediated via the Akt/Erk/p38 MAPK signaling pathway

To corroborate our observation of activation of AKT and ERK-1/2 signaling when treated with the < 1 kDa fraction of the melanoma SF-CM, we blocked the respective signaling pathways using specific inhibitors. We observed that blocking AKT signaling, using the AKT inhibitor LY294002, reduced long term EC survival under hypoxic conditions. Alternatively, blocking ERK-1/2 signaling using the inhibitor PD98059 also reduced EC survival under hypoxia. In contrast, inhibiting p38 MAPK signaling with the inhibitor SB203580 resulted in viable ECs similar to untreated < 1 kDa SF-CM (Figures 8a, b). FACS analysis, performed at 12 h of hypoxia treatment, corroborated these results (Figures 8c, d). These results suggest that the survival specific factor produced by the melanoma cells induce a pro-survival effect in ECs under restrictive hypoxic conditions mediated by the AKT/ERK-1/2/p38 MAPK signaling pathway.

DISCUSSION

In this study we analyzed the angiogenic potential of a panel of human melanoma cell lines with respect to their ability to promote EC survival under tumor associated hypoxic conditions. Although the melanoma cell lines differed in their clinical staging, *in vitro* and *in vivo* growth properties[83], all tested melanoma conditioned supernatants were capable of eliciting a survival response in ECs under hypoxic conditions. Moreover the survival response was not EC subtype specific as melanoma conditioned medium (MCM) treated HMVECs were also capable of long-term survival under hypoxia. The survival response was determined to be regulated by prevention of apoptotic cell death. Interestingly, however, all diluted MCMs induced a shift in the EC populations to an apoptotic phenotype, suggesting dose dependency. We also observed that all size fractions (up to and including < 1 kDa) of the MCMs were capable of generating pro-survival responses in ECs. Further, this effect seemed to be an attribute specific to melanoma pathophysiology as neither

analysis to determine percentages of apoptotic, necrotic and viable cells. (**d**) Relative percentages of apoptotic and necrotic ECs with different treatments at 12 h hypoxia. Data are derived from three independent experiments. *$p < 0.05$.

melanocytes nor aggressive breast and pancreatic cell lines were capable of preventing EC apoptosis under hypoxia.

The clinical relevance and therapeutic potential of targeting angiogenesis has led to the development of several targeting modalities including neutralization of pro-angiogenic ligands using monoclonal antibodies, soluble decoy traps to inhibit receptor signaling, broad blocking with tyrosine kinase inhibitors and vascular disrupting agents which target the established tumor vasculature. Much of these efforts in melanoma have focussed on VEGF and bFGF[43,78]. The role of both mitogens in supporting melanoma growth *in vivo* has been established[83,88,96]. Graeven *et al.* demonstrated that bFGF is critical for melanoma growth *in vivo* while VEGF is dispensible[97]. Additionally, several *in vivo* studies report the role of these mitogens in promoting survival of tumor endothelium[98,99]. However, VEGF and bFGF were not capable of inducing EC survival under hypoxic conditions. Moreover, the melanoma cell lines tested vary in VEGF expression profile[88]. Thus while BLM produced the highest levels of VEGF, Mel57 and 1F6 cell lines recorded low VEGF production. Further, inhibition of the VEGF signaling axis, either by ligand neutralization or receptor blocking, in MCM treated ECs did not induce apoptosis under hypoxia. These data suggest that angiogenic events during melanoma development are not restricted to VEGF and bFGF signaling.

As the < 1 kDa melanoma specific fraction eliminates known angiogenic factors, we attempted to further characterize this factor/s. Heat inactivation, trypsin and chymotrypsin digestion did not alter the survival promoting attributes of the melanoma specific fraction. Global changes in endothelial gene expression were visualized by comparing MCM treatment and basal medium treatment. Of the transcripts most differentially regulated, proangiogenic modulators such as chemokine (C-C motif) ligand 2 (CCL2), angiopoetin-like-4 (ANGPTL4), v-akt murine thymoma viral oncogene homolog 3 (AKT3) and insulin receptor (INSR) were upregulated in the MCM treated samples. Further, genes involved in pro-apoptotic cascade such as Fas cell surface death receptor (FAS) and inhibitor of DNA binding 2 (ID2) were downregulated upon MCM treatment. The gene expression data were further verified with the small molecule fraction treatment, and similar changes in transcript abundance were observed.

The signal transduction pathways triggered by the melanoma specific fraction involved the AKT and p38 MAPK/Erk-1/2 signaling axis. Under hypoxic conditions, activation of AKT and ERK-1/2 was visible in all melanoma tumor conditioned medium treated samples. The levels of active caspases, the downstream effectors of apoptosis, were also lower in MCM treated samples as compared to other conditioned media treatments.

Taken together, our data demonstrate the presence of small molecule melanoma specific factor/s capable of promoting long-term EC survival under hypoxic conditions. This observation draws a parallel with a previous study where a small molecule fraction (< 3 kDa) of conditioned medium from malignant colon cancer cells was capable of pre-

venting EC apoptosis[100]. Elucidation and further characterization of the survival specific molecule/s could assist in the development of new anti-angiogenic therapies to target the aggressive attributes of malignant melanoma.

2

SUPPLEMENTAL FIGURES
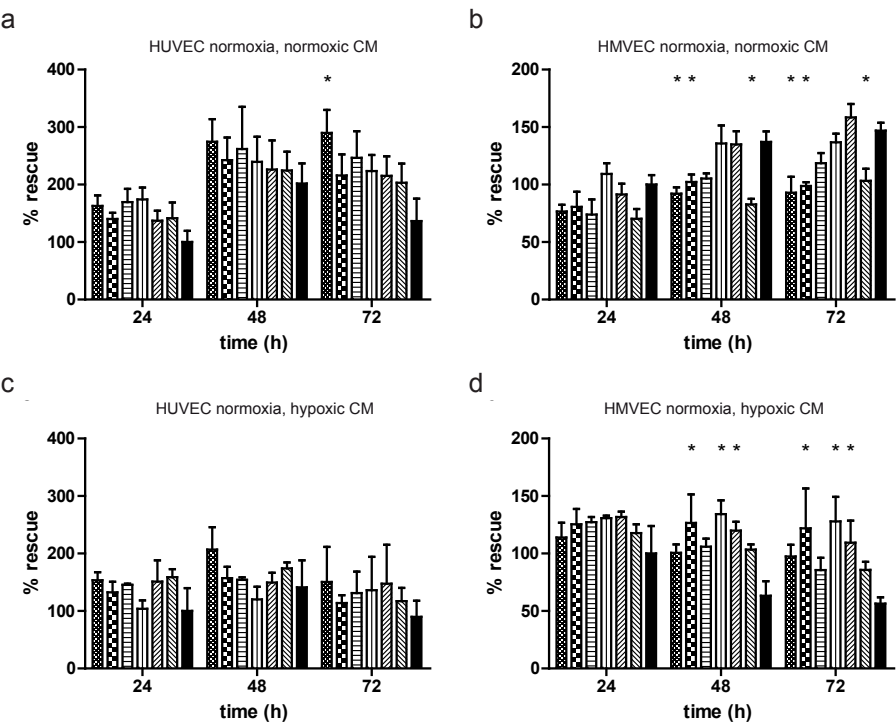
Supplementary Figure 1. Effect of melanoma conditioned medium (MCM) on endothelial cell (EC) survival under normoxia. (a) HUVEC and **(b)** HMVEC survival under normoxia upon treatment with MCMs collected under normoxic conditions. **(c)** HUVEC and **(d)** HMVEC survival under normoxia upon treatment with MCMs collected under hypoxic conditions. ECs were grown to near confluence and treated with various MCMs (BLM: ▨; M14: ▨; Mel57: ▭; 530: ▥; 1F6: ▨; Mel57-VEGF[165]: ▨) and basal medium (■). Cells were fixed at 24, 48 and 72 h and the percentage of total surviving cells was determined. Cell survival (% rescue) data in (**a-d**) is expressed relative to treatment with basal medium (DMEM + 10% FBS) at 24 h normoxia and represent mean ± SEM of three independent experiments, conducted in triplicates. *$p < 0.05$.

a

b
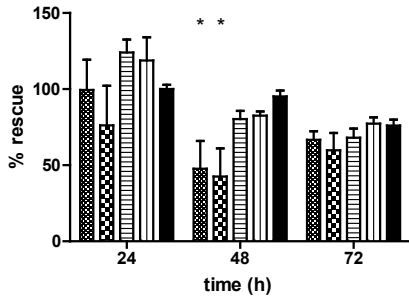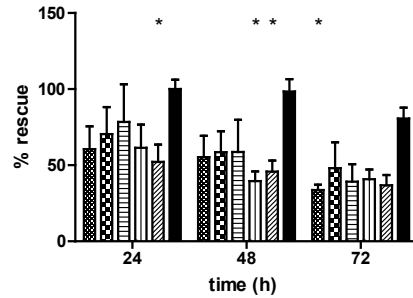
Supplementary Figure 2. Effect of non-melanoma conditioned medium on endothelial cell (EC) survival under normoxia. (a) Effect of melanocyte conditioned medium on EC survival. Unfractionated and fractionated serum-free melanocyte conditioned medium was added to subconfluent EC cultures and survival under normoxic conditions was monitored for up to 72 h (unfractionated hMEL SF-CM: ▨; < 1 kDa hMEL SF-CM: ▨; unfractionated NHEM SF-CM: ▤; < 1 kDa NHEM SF-CM: ⊞; and basal medium: ▮). **(b)** Effect of breast and pancreatic cell conditioned medium on EC survival. Size fractionated < 1 kDa fractions of serum-free conditioned medium derived from breast cancer cell lines (MCF-7: ▨, SK-BR-3: ▨), pancreatic cancer cell lines (BxPC-3: ▤, PANC-1: ⊞, MiaPaCa: ▨) and basal medium (▮) were added to subconfluent EC cultures and survival under normoxic conditions was monitored for up to 72 h. Cell survival (% rescue) in (**a,b**) is expressed relative to treatment with basal medium (serum-free DMEM) at 24 h normoxia. Data represent mean ± SEM of four independent experiments, conducted in triplicates. *$p < 0.05$.
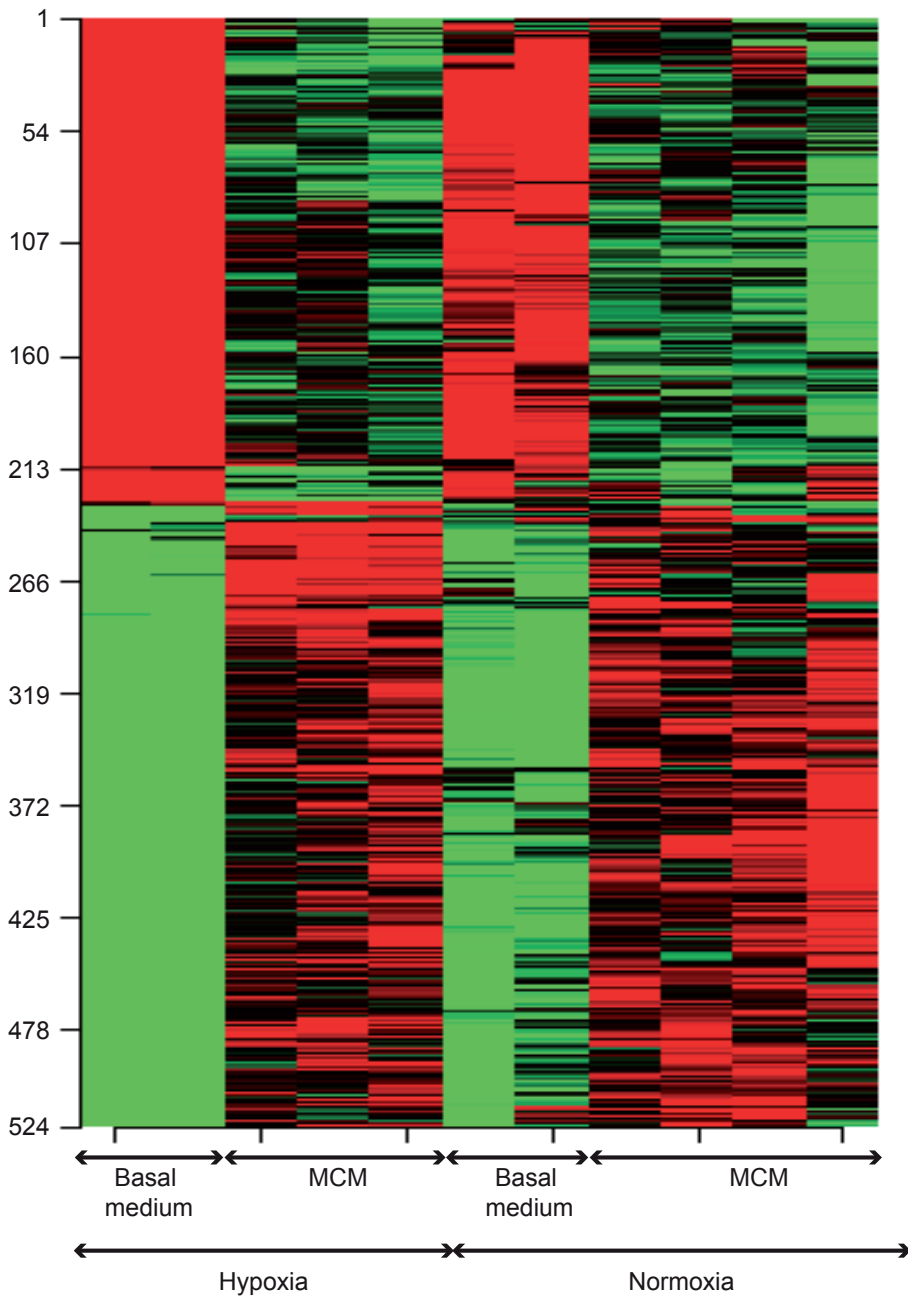
Supplementary Figure 3. Global changes in gene expression. Heatmap of differential gene expression in endothelial cells upon treatment with basal medium or melanoma conditioned medium for 12 h under hypoxia. 694 probesets, corresponding to 524 genes, were differentially regulated between the two groups. The expression of the same genes were visualized in samples treated with basal medium or MCM under normoxic conditions.

a

b
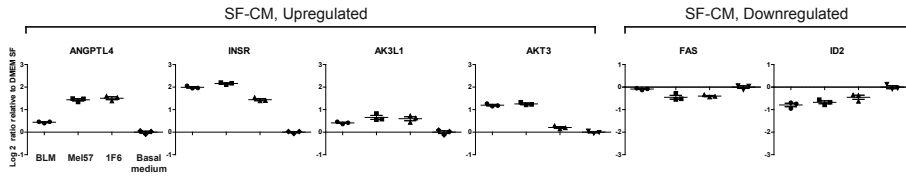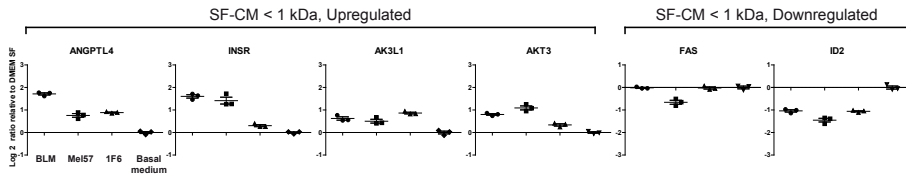
Supplementary Figure 4. Real-time PCR gene expression verification. Differential expression of select genes from the microarray experiment were verified using real-time quantitative PCR. ECs were treated with (**a**) unfractionated or (**b**) fractionated (< 1 kDa) serum-free melanoma conditioned medium (SF-CM) under normoxia for 12 h. Changes in transcript abundance were normalized to B2M expression and are expressed as log2 ratio relative to basal medium (serum-free DMEM) treatment.

CHAPTER 3

Differential TIMP3 expression affects tumor progression and angiogenesis in melanomas through regulation of directionally persistent endothelial cell migration

Asha M. Das, Ann L.B. Seynhaeve, Joost A.P. Rens, Cindy E. Vermeulen, Gerben A. Koning, Alexander M.M. Eggermont, Timo L.M. ten Hagen

ABSTRACT

The angiogenic potential of solid tumors, or the ability to initiate neovasculature development from pre-existing host vessels, is facilitated by soluble factors secreted by tumor cells and involves breaching of extracellular matrix barriers, endothelial cell (EC) proliferation, migration and reassembly. We evaluated the angiogenic potential of human melanoma cell lines differing in their degree of aggressiveness, based on their ability to regulate directionally persistent EC migration. We observed that conditioned medium (CM) of the aggressive melanoma cell line BLM induced a high effective migratory response in ECs, while CMs of Mel57 and 1F6 had an inhibitory effect. Further, the melanoma cell lines exhibited a varied expression profile of tissue inhibitor of metalloproteinase-3 (TIMP3), detectable in the CM. TIMP3 expression inversely correlated with aggressiveness of the melanoma cell line, and ability of the respective CMs to induce directed EC migration. Interestingly, TIMP3 expression was found to be silenced in the BLM cell line, concurrent with its role as a tumor suppressor. Treatment with recombinant human TIMP3 and CM of modified, TIMP3 expressing, BLM cells mitigated directional EC migration, while CM of TIMP3 silenced 1F6 cells induced directed EC migration. The functional implication of TIMP3 expression on tumor growth and angiogenic potential in melanoma was evaluated *in vivo*. We observed that TIMP3 expression reduced tumor growth, angiogenesis and macrophage infiltration of BLM tumors while silencing TIMP3 increased tumor growth and angiogenesis of 1F6 tumors. Taken together, our results demonstrate that TIMP3 expression impedes directionally persistent EC migration which adversely affects the angiogenic potential and growth of melanomas.

INTRODUCTION

Melanoma progression and metastatic dissemination is intimately associated with the process of angiogenesis[42]. Physiologically, the angiogenic process is comprised of a stringent cascade involving degradation of the vascular basement membrane (VBM), endothelial cell (EC) proliferation, survival, migration and reassembly, ultimately resulting in a new vessel[37]. Pathological (tumor) angiogenesis is cardinally mediated by tumor-associated modulators that arbitrate the multiple steps of the angiogenic cascade[39,101].

EC migration is an essential step in the sequence of the angiogenic cascade[38,102]. In response to favorable environmental cues, ECs polarize and acquire well defined leading and trailing ends. The sense of directional migration is derived from two driving attributes: the intrinsic migration directionality of the cell during chemokinesis (the inherent predilection to migrate in a single direction by activation of the cell motility machinery) and external regulation of migration or chemotaxis[103,104]. While regulation of chemotactic responses to graded extrinsic motogenic stimuli has been well documented[105-107], several fundamental processes during early development and tissue remodeling are mediated by the intrinsic property of a cell to undergo directionally persistent migration[103,108].

The TIMP family consists of four homologous, multifunctional proteins (TIMP1-4)[109], which are known to regulate an array of physiological effects including cell proliferation[110,111], pro-MMP activation, migration[112,113], invasion and apoptosis[114-116] via both MMP-dependent and MMP-independent pathways. TIMP3 shares only a 25% amino acid homology with its family members[117], and is unique among the TIMPs as it is sequestered to the ECM[118]. In addition to its MMP inhibitory activity[119], TIMP3 has been reported to induce apoptosis in normal and tumor cells *in vitro*[114-116], inhibit tumor growth[117,120], and inhibit angiogenesis by blocking the binding of VEGF to VEGFR-2[121]. Moreover, exogenous addition of recombinant TIMP3 has been shown to inhibit chemotactic EC migration and tubule formation *in vitro*[117,122], and functional capillary morphogenesis *in vivo*[117].

In the present study we evaluated the angiogenic potential of human melanoma cell lines differing in their degree of aggressiveness in nude mice[83,87], with respect to their ability to influence directionally persistent ECs migration. Using the ring-barrier based two-dimensional migration assay previously described[123], we assessed the migratory responses of ECs upon treatment with conditioned medium (CM) generated from highly invasive BLM cells, moderately invasive Mel57 cells and non-invasive 1F6 cells[87]. In consecutive experiments, we linked the observed differences in EC migration parameters to the varied expression profile of TIMP3 among the melanoma cell lines. *In vivo*, we observed that TIMP3 silencing favored angiogenesis and tumor growth in melanomas while enforced TIMP3 expression adversely affected angiogenic potential, macrophage infiltration and tumor growth. Our results implicate TIMP3 as a vital modulator of melanoma induced angiogenesis.

MATERIALS AND METHODS

Cell culture

Primary cultures of Human Umbilical Vein Endothelial Cells were established as previously described[85]. The human melanoma cells lines BLM, Mel57 and 1F6 were kindly donated by Dr. van Muijen (Department of Pathology, University of Nijmegen, NL). Culture conditions are provided in the Supplementary Information.

Preparation and fractionation of conditioned medium

Melanoma cells were cultured routinely and upon 70-80% confluency, the cells were washed and incubated in serum-free DMEM for 72 h. Serum-free melanoma conditioned medium, referred throughout as CM, was collected, centrifuged at 1500 rpm for 5 min, size fractionated using ultrafiltration devices (Amicon, Beverly, MA) with specific molecular weight cutoffs (50 kDa, 30 kDa, 10 kDa) and stored at −20°C. Prior to migration assays, all treatments were supplemented with 10% FCS to ensure consistent serum concentrations across assays.

Cell migration assay

Cell migration assays were performed using the ring-barrier migration assay previously described[123], with minor modifications. Briefly, a coverslip was inserted into an Attofluor incubation chamber (Molecular Probes) and subsequently sterilized. Coverslips were coated with fibronectin (10 µg/mL) and incubated for 1 h at 37°C, prior to cell seeding. A removable circular sterile migration barrier was inserted into the chamber, which averts cell growth in the center of the coated coverslip. 2×10^5 ECs were seeded around this barrier and the rings were incubated at 37°C for 24 h, thereby generating a confluent monolayer in the periphery and a cell-free area in the center of the coverslip. Post 24 h, the migration barrier was removed and the ECs were washed twice with DMEM serum-free medium, followed by incubation with the desired treatment. All migration assays were conducted in the presence of 10% FCS.

Time-lapse microscopy and analysis of cell migration

Time-lapse imaging was conducted on Axiovert 100 M inverted microscopes, equipped with AxioCam MRC digital cameras (Carl Zeiss B.V., Sliedrecht, NL). The cells were incubated with the desired treatment and migration was monitored for 24 h using time-lapse microscopy. The cells in the incubation chamber were maintained at 37°C in a constantly humidified atmosphere, with controlled and heated CO_2 flow. Images of migrating cells were captured every 12 min, for the duration of 24 h, using a 10X/0.30 Plan-Neofluar objective (Carl Zeiss). Time-lapse movies were used to quantify parameters of cell migration as previously described[123]. The net track movement of cells in 24 h was termed

'total distance of migration', while the directional movement of cells to the cell-free center of the coverslip was termed 'effective distance of migration'. Migration efficiency was determined as the percentage of directional movement over the total track distance. For each treatment, at least three independent migration assays were performed and 10 migrating cells, per assay, were tracked. All cell tracking measurements were conducted using AxioVision 4.5 software. Track diagram images were processed in Adobe Illustrator CS3 (Adobe Systems Inc., San Jose, CA). For quantification purposes, all 121 images were used. For videos compilations, every 4th image of the sequence was used and the resulting 31 images were set to a display rate of 5 frames/s, resulting in a 6 s video. Videos and video legends are listed as Supplementary Information, and are available online.

Real-time RT-PCR
Gene expression profiles of TIMP1, -2, -3 and -4 in the melanoma cell lines was determined using real-time quantitative PCR (qPCR) as described in detail in the Supplementary Information.

5-Aza-dC treatment
BLM cells were treated with 10 μM 5-Aza-dC (Sigma-Aldrich Chemie B.V. Zwijndrecht, NL) for 72 h and subjected to RNA extraction. Alternatively, post 72 h treatment, cells were washed and incubated in serum-free DMEM for 72 h to obtain CM.

Enzyme-linked immunosorbent assay (ELISA)
Presence of TIMP3 protein in melanoma CM was determined using the commercially available Human TIMP3 DuoSet ELISA kit (R&D systems), according to manufacturer's specifications.

Western blot analysis
TIMP3 protein content in CM of melanoma cells was detected using SDS-PAGE as detailed in the Supplementary Information.

Reverse zymography
Metalloproteinase inhibitory activity of TIMP3 in melanoma CMs was assessed with reverse zymography using protease-substrate gel electrophoresis. A detailed description is provided in the Supplementary Information.

TIMP3 shRNA transfection
TIMP3 was silenced in 1F6 cells using Neomycin SureSilencing shRNA Plasmids for human TIMP3 (SABiosciences, Fredrick, MD), following the manufacturer's instructions.

A detailed description is provided in the Supplementary Information. Gene knockdown was validated with qPCR.

Generation of TIMP3 constructs and transfection of BLM cells

TIMP3 pENTR221 (Ultimate ORF Clones, Invitrogen) was used as a template for the amplification of TIMP3 via standard PCR, using the primers Timp3 N2 XhoI UP (5′-CT-GAGCTCGAGGCAATGACCCCTTGGCTCGGGCTCATC-3′) and Timp3 N2 BamH1 DN (5′-CTGAGGGATCCCGGGGTCTGTGGCATTGATGATG-3′). The TIMP3 gene fragment was inserted into the pIRES2 DsRed-Express2 bicistronic expression vector (Clontech Laboratories, Palo Alto, CA). BLM cells were transfected using LipofectAMINE 2000 in OptiMEM-1 medium. Highly transfected BLM cell population was sorted based on DsRed expression using fluorescence-activated cell sorting (FACS, Becton Dickinson, Bedford, MA). Stable transfectants were expanded with G418 antibiotic selection, with DsRed expression being verified by fluorescence microscopy and TIMP3 gene and protein expression being verified by qPCR and ELISA, respectively.

Tumor cell inoculation

All animal studies were approved by the committee on Animal Research of the Erasmus MC (Rotterdam, NL). To assess the effect of TIMP3 on tumor growth, athymic nude mice (Harlan-CPB) were subcutaneously inoculated on the left flank with 1×10^6 tumor cells in PBS. Tumor growth was recorded and volumes were calculated using the formula $(A \times B \times C) \times 0.4$ where A, B and C represent the length, width and depth of the tumor respectively. At the end of the study, mice were sacrificed, tumors excised, snap frozen and cut into 5 μm sections along the largest diameter.

Immunohistochemical staining and image analysis

Tumor sections were fixed in acetone for 10 min at 4°C. Slides were dried for 10 min and rinsed thrice with PBS/0.05% Tween-20. Blocking was performed for 1 h at R.T. with 10% goat serum in PBS/1% BSA/0.5% Tween-20. The sections were incubated for 1 h at R.T. with rat anti-CD31 antibody (1:100, R&D Systems). Secondary antibody incubations were performed for 30 min at R.T. with Alexa Fluor 594 conjugated goat anti-rat antibody (1:500, Molecular Probes). Between all the steps of the staining procedure, slides were rinsed thrice. Stained tumor sections were mounted with Mowiol and tile scan images of the whole tumor section was acquired using a Zeiss LSM 510 Meta confocal microscope with a Plan-Neofluar 10× lens. Images were processed with ImageJ for quantification of vessel area. The RGB images were binarized, tumor area selected and CD31 coverage was measured. Vessel coverage is expressed as a percentage of the whole tumor section.

Statistics

Statistical analysis was performed using GraphPad Prism version 5.01 (GraphPad Software, San Diego, CA). Experimental groups were compared using the Kruskal-Wallis H test and considered significantly different when $p < 0.05$. Multiple groups were compared using the Dunn's multiple comparison post-test. For comparisons of less than three groups, the two-tailed Mann-Whitney test was used.

RESULTS

Conditioned media from melanoma cell lines induce distinct endothelial cell migratory profiles

Migratory profiles of ECs were evaluated in response to treatment with CM of melanoma cells. Basal migratory profiles of ECs were determined by treatment with basal medium (DMEM supplemented with 10% FCS). To discriminate between random and directional EC motility, we measured the total and effective migrated distances, respectively. Random or total migration quantitatively determines the exploratory profile of the cell in response to treatment but this does not necessarily translate to the capacity of the cell to effectively displace. The effective migration reflects the displacement of cells in response to a treatment over time.

We observed that although ECs exhibited the highest total migration in response to basal medium (833.7 ± 24.7 μm, Figure 1a), this movement did not translate to effective displacement (147.8 ± 10.1 μm, Figure 1b). All melanoma CM treatments resulted in reduced random motility of ECs when compared to that of basal medium (vs. BLM, $p < 0.05$; vs. Mel57, $p < 0.005$, vs. 1F6, $p < 0.005$) (Figure 1a). However, the effective migratory profiles revealed that ECs exhibited the highest displacement in response to BLM CM (vs. DMEM, $p < 0.005$; vs. Mel57, $p < 0.005$; vs. 1F6, $p < 0.005$) (Figure 1b). Mel57 and 1F6 CMs did not induce effective migratory profiles as no statistically significant differences were observed compared to basal medium. The efficiency of migration is expressed as the effective movement towards the center as a percentage of the total migrated distance (Figure 1c). BLM CM induced the most efficient migration. Migration efficiency was higher when treated with Mel57 CM as compared to 1F6 CM ($p < 0.005$). Higher migration efficiency with Mel57 CM can be attributed to the low total migration observed. Migration velocities of ECs were calculated by dividing the total track distance by the duration of migration (24 h). ECs showed a higher rate of random motility when treated with basal medium as compared to all melanoma CMs. Representative start and end positions of migrating ECs in response to various treatments are depicted in Figure 1d and Videos 1-3.

3
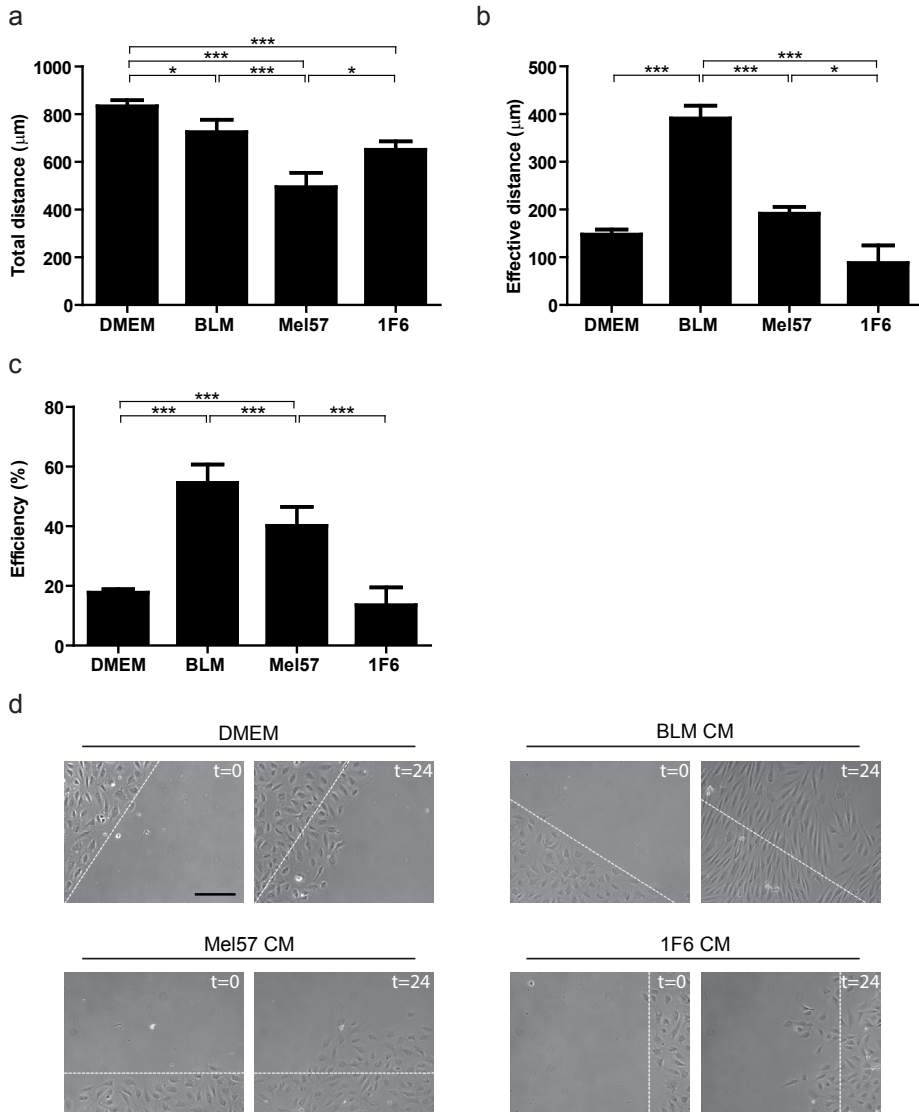
Figure 1. Effect of melanoma conditioned-medium (CM) on endothelial cell migration. Endothelial cells (ECs) were treated with basal medium (DMEM), BLM CM, Mel57 CM and 1F6 CM. All treatments were supplemented with 10% FCS. (**a**) Total distance of EC migration (μm) in 24 h. (**b**) Effective migrated distance (μm) per cell. Effective migration represents the directionality of cell movement (straight line path, perpendicular to the migration front, towards the cell free center). (**c**) Migration efficiency (%) induced by the different treatments. Migration efficiency was obtained by dividing the effective distance by the total distance, expressed as a percentage. Data in panels a-c represent mean ± SEM of at least 30 cells in at least three independent experiments. *$p < 0.05$, ***$p < 0.005$. (**d**) Representative pictures of migrating ECs at start (t = 0 h) and end (t = 24 h) positions of the migration assay for the respective treatments. Images were obtained from Videos 1 and 3-4. White dashed lines indicate the migration front at t = 0 h. Scale bar, 200 μm.

Inhibitory effect of Mel57 and 1F6 CM lies in the 10-30 kDa range

Next, we proceeded to determine whether CMs from Mel57 and 1F6 lacked the capacity to promote directional EC migration, or whether they had an inherent inhibitory effect as compared to BLM CM. In order to delineate the CM fraction responsible for the changes in the observed EC migratory capacity, CMs were size fractionated and designated as follows- < 50 kDa, < 30 kDa, < 10 kDa; fraction with factors in the range of 10 to 30 kDa: 10-30 kDa; fraction with factors greater than 30 kDa and smaller than 10 kDa (so that the 10-30 kDa range was excluded): > 30 + < 10 kDa. All CM fractions were tested for their ability to induce directional EC migration. All BLM CM fractions induced high effective migration compared to basal medium, indicative of the presence of several migration stimulatory molecules produced by BLM cells (Figure 2a). While the BLM size fractions showed a gradual reduction in inducing effective migration, all fractions were capable of inducing higher effective migration than basal medium, with the exception of the < 10 kDa and 10-30 kDa fractions (ns vs. Basal medium). Treatment with the < 10 kDa and 10-30 kDa fractions also resulted in significantly lower effective migration as compared to unfractionated BLM CM. This might be attributed to the successive removal of pro-angiogenic growth factors, with known migration stimulating capacities such as bFGF and VEGF, during the fractionation process. However, no significant difference was observed between the < 10 kDa and 10-30 kDa BLM CM fractions. Directional EC migration was significantly inhibited when treated with the < 30 kDa ($p < 0.05$) and 10-30 kDa ($p < 0.01$) fractions of Mel57 CM when compared to the basal medium (Figure 2b). Interestingly, although the < 10 kDa fraction did not induce effective EC migration when compared to basal medium treatment, a significantly higher migration was observed when compared to treatment with the 10-30 kDa fraction ($p < 0.005$), suggesting the presence of an inhibitory effect in the 10-30 kDa fraction. Fractionation of the 1F6 CM also indicated the presence of the inhibitory effect in the 10-30 kDa range as both < 10 kDa ($p < 0.005$) and > 30 + < 10 kDa ($p < 0.01$) fractions did not have an inhibitory effect when compared to unfractionated 1F6 CM and resulted in higher directed EC migration. Compared to basal medium, treatment with the < 30 kDa fraction showed a significant inhibition in directed EC migration ($p < 0.01$) while the < 10 kDa fraction showed a significant increase in directed EC migration ($p < 0.05$) (Figure 2c). The distinct migratory patterns adopted by ECs under the influence of the various CM size fractions are depicted in Figure 2d. All BLM CM size fractions indicate migration patterns directed from the migration front to the cell free area, while the inhibitory fractions of 1F6 and Mel57 CM indicate random migration with reduced net displacement of the ECs. Taken together, these results indicate the presence of a factor or factors with an inhibitory effect on directionally persistent EC migration, in the size range of 10-30 kDa in the CMs of Mel57 and 1F6.
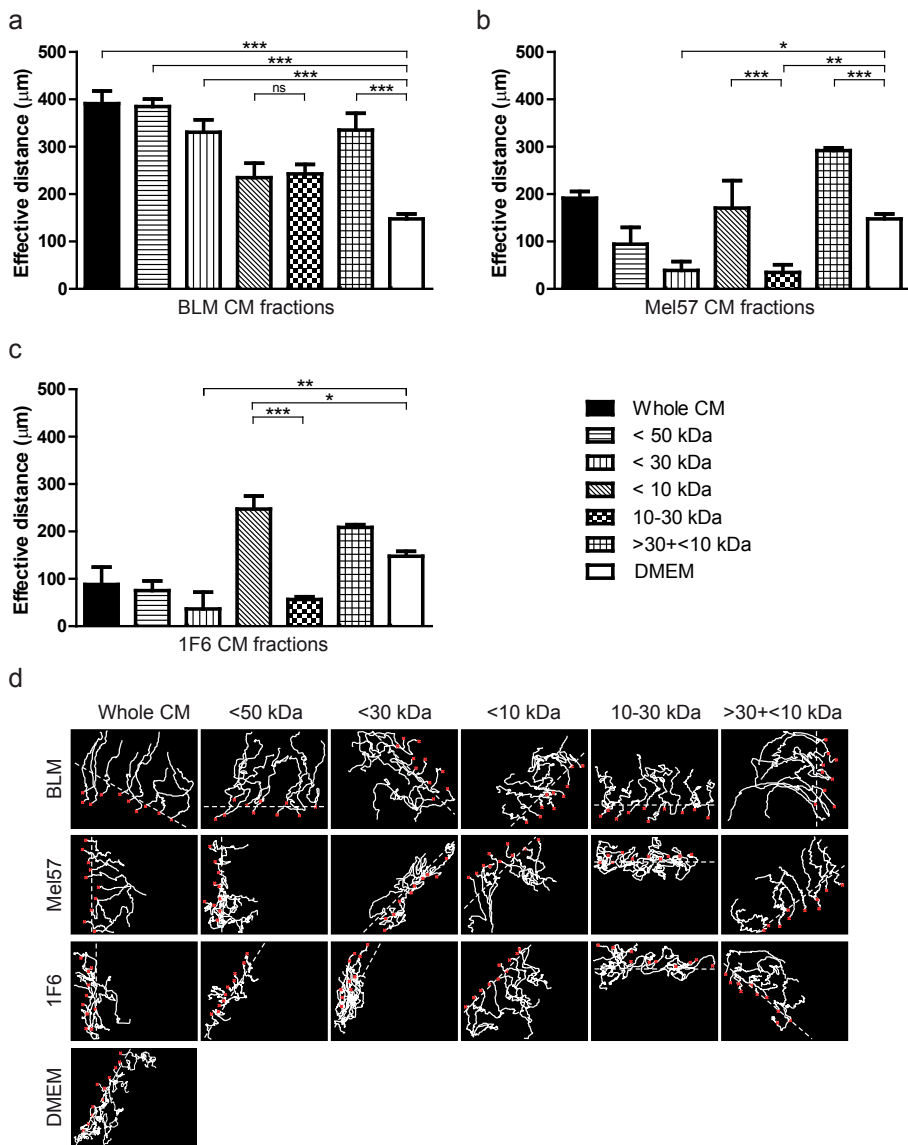
Figure 2. Effect of melanoma conditioned-medium (CM) fractions on endothelial cell migration. (a) Effective migrated distance (μm) per cell induced by BLM CM and fractions, compared to basal medium. **(b)** Effective migrated distance (μm) per cell induced by Mel57 CM and fractions, compared to basal medium. **(c)** Effective migrated distance (μm) per cell induced by 1F6 CM and fractions compared to basal medium. Data in panels a-c represent mean ± SEM of at least 30 cells in at least three independent experiments. ns= not significant, *$p < 0.05$, **$p < 0.01$, ***$p < 0.005$. **(d)** Representative migration track movements exhibited by endothelial cells upon treatment with the melanoma CM fractions described in panels a-c for 24 h. The white dashed line represents the migratory front upon removal of the barrier (t=0 h), the red crosses represent the tracked cells and the white lines represent the locomotion trajectories of individual cells during the course of 24 h.

3

Differential expression of TIMP3 by the melanoma cells

Previous studies have demonstrated that TIMP3 inhibits the chemotactic migration of ECs *in vitro*[117,122] and abrogates functional capillary morphogenesis during angiogenesis[117]. As the identified migration inhibitory factor has a molecular weight between 10 and 30 kDa, and all four TIMPs encode for proteins in the 20-30 kDa range[124], we evaluated the expression profile of TIMPs in our melanoma cell lines. We observed that the gene expression profile of TIMP1 and TIMP2 were high in all the melanoma cell lines, and did not show much variation across the cell lines. Interestingly, TIMP3 gene expression levels were strikingly different among the melanoma cell lines. Studies on human primary tumors and tumor cell lines have reported TIMP3 as a putative tumor suppressor gene and gene expression is frequently silenced due to hypermethylation of its promoter. The inactivation of TIMP3 due to aberrant methylation of promoter CpG islands has been reported in several human cancers[125-127]. Promoter methylation gene profiling studies in cutaneous melanomas have shown the silencing of TIMP3 in melanoma cell lines as well as tumor specimens from patients with stage III and stage IV melanoma[128]. We observed that Mel57 and 1F6 showed high TIMP3 expression, while no expression was detected in BLM (Figure 3a). Treatment with 5-Aza-dC restored TIMP3 expression in BLM cells confirming that decreased expression is a consequence of promoter methylation and gene silencing. TIMP4 was absent in all three cell lines (data not shown). To determine whether the differential gene expression profiles were also translated into different protein profiles, we analyzed TIMP3 protein levels in the CM of melanoma cells. ELISA measurements indicated that 1F6 cells secreted approximately 3.4 ng TIMP3/10^6 cells per 72 h while the Mel57 cells secreted approximately 2.2 ng TIMP3/10^6 cells per 72 h. No expression of TIMP3 was detectable in the CM of untreated BLM cells, while 5-Aza-dC treated BLM cells secreted approximately 1.1 ng TIMP3/10^6 cells per 72 h (Figure 3b). Western blot analysis confirmed the presence of the unglycosylated form of TIMP3 (~24 kDa) in melanoma CM (Figure 3c).

TIMP3 in melanoma conditioned medium exhibits MMP inhibitory activity

To determine whether the TIMP3 detected in the CM of melanoma cell lines exhibited MMP-2 inhibitory activity, reverse zymography was performed. MMP-2 inhibitory activity was observed at a molecular mass of about 24 kDa in the CM of both TIMP3 expressing cell lines (Mel57, 1F6), validating the functionality of the TIMP3 detected in melanoma CM (Figure 3d). In addition, MMP inhibitory activity of TIMP2 was observed at a molecular mass of about 21 kDa in all three cell lines. Band intensities, when normalized to cell numbers used to generate the CMs, revealed that TIMP3 activity was the highest in 1F6 CM. TIMP2 activity was similar in both BLM and 1F6 CM, when normalized for cell number.
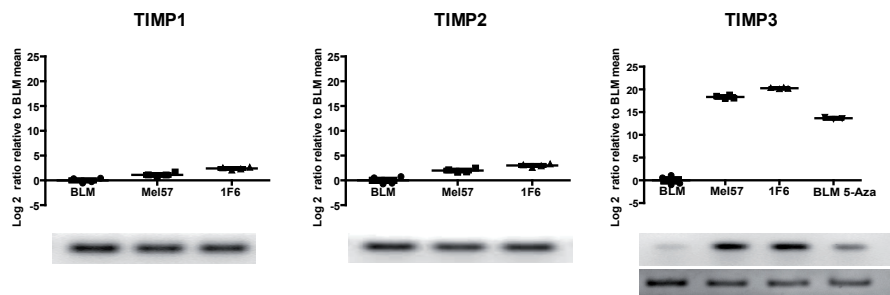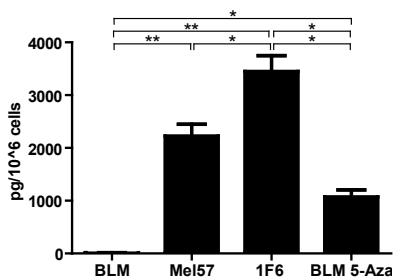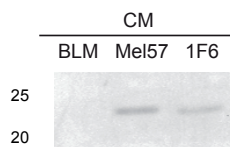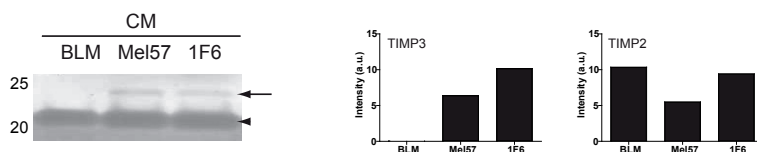
Figure 3. Differential TIMP3 expression in the melanoma cell lines. (**a**) Real-time RT-PCR gene expression levels of TIMP1, -2 and -3 in the melanoma cell lines BLM (●), Mel57 (■) and 1F6 (▲) and TIMP3 expression in 10 μM 5-Aza-dC treated BLM cells (▼), measured in quadruple samples. Changes in transcript abundance were normalized to HPRT expression and are expressed as log2 ratio relative to the corresponding BLM mean. Depicted below are qPCR products (TIMP3, 73 bp; HPRT, 192 bp) as visualized using gel electrophoresis. (**b**) Levels of TIMP3 (pg) in melanoma conditioned-medium as detected by ELISA. Data were normalized to the number of cells used to generate the CMs and are expressed as mean ± SEM of quadruplicate samples. *$p < 0.05$, **$p < 0.01$. (**c**) Western blot analysis of TIMP3 protein expression in melanoma CM. 2×10^5 melanoma cells were seeded in 6 well cluster plates and 24 h later the medium was replaced with serum free DMEM. CM was collected after 72 h, concentrated fivefold and 50 μL was loaded on gel. (**d**) Metalloproteinase inhibitory activity of TIMP3 produced by melanoma cells. Reverse zymography of the CMs showed an inhibitory activity at a molecular mass of 24 kDa (TIMP3, arrow) in Mel57 and 1F6, and 21 kDa (TIMP2, arrow head) in all CMs. Band intensities were quantified and normalized to cell numbers used to generate the CMs.
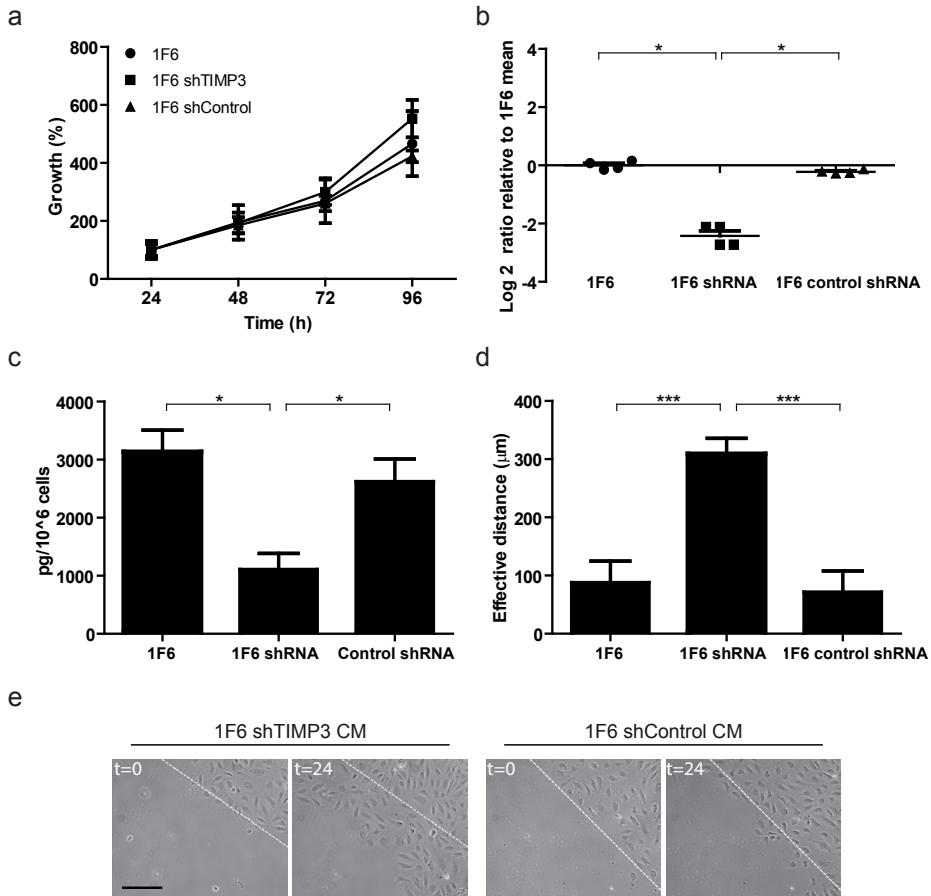
Figure 4. shRNA mediated silencing of TIMP3 in 1F6 cells. (**a**) *In vitro* growth rates of unmodified 1F6 (●), 1F6 shTIMP3 (■) and 1F6 shControl (▲) cell lines. (**b**) Real-time RT-PCR gene expression levels of TIMP3 in unmodified 1F6 (●), 1F6 shTIMP3 (■) and 1F6 shControl (▲) cells, measured in quadruple samples. Changes in transcript abundance were normalized to HPRT expression and are expressed as log2 ratio relative to 1F6 mean. *$p < 0.05$. (**c**) Levels of TIMP3 (pg) secreted by transfected and untransfected 1F6 cells into the CM as detected by ELISA. Data were normalized to the number of cells used to generate the CM and are expressed as mean ± SEM of quadruplicate samples. *$p < 0.05$. (**d**) Effective migrated distance (μm) per cell when treated with 1F6 CM, 1F6 shTIMP3 CM and 1F6 shControl CM. At least 30 cells from at least three separate experiments were tracked. ***$p < 0.005$. (**e**) Representative pictures of migrating ECs at start (t = 0 h) and end (t = 24 h) positions of the migration assay for the respective treatments. White dashed lines indicate the migration front at t = 0 h. Scale bar, 200 μm.

Conditioned medium of TIMP3 silenced 1F6 cells induces endothelial cell migration

To evaluate if the observed inhibition in directional migration of ECs upon treatment with 1F6 CM is indeed mediated by TIMP3, we silenced TIMP3 gene expression in 1F6 cells by stably transfecting short hairpin RNA plasmids. Transfections with either TIMP3 shRNA or control plasmids did not affect the growth properties of 1F6 cells (Figure 4a). Gene knockdown efficiency was determined using the RNAi Validation Data Analysis Template (SABiosciences) and found to be > 70%. TIMP3 gene expression levels were reduced in the specific shRNA transfectants (1F6 shTIMP3) compared to control shRNA transfectants (1F6 shControl) and unmodified 1F6 cells (Figure 4b). Reduction of gene expression in 1F6 shTIMP3 was accompanied by a decrease in the level of TIMP3 secreted into the CM. ELISA measurements detected 1.1 ng TIMP3/10^6 cells per 72 h in 1F6 shTIMP3 cells and was significantly reduced when compared to unmodified 1F6 cells ($p < 0.05$) and 1F6 shControl cells ($p < 0.05$) (Figure 4c). The reduced TIMP3 levels translated in an augmented capacity of the 1F6 CM to induce directed migration of the ECs (Figures 4d, e; Videos 4-5).

Recombinant human TIMP3 reduces directional endothelial cell migration

Although previous studies have reported inhibition of VEGF induced chemotactic migration of ECs upon addition of recombinant human TIMP3 (rhTIMP3) by engagement of the VEGF receptor 2[121], the effect of rhTIMP3 on the regulation of directionally persistent EC migration has not been evaluated. We observed that addition of rhTIMP3 almost completely abolished directed migration of ECs upon treatment with basal medium ($p < 0.05$), reduced effective migration induced by VEGF ($p < 0.005$), reduced directed migration induced by BLM CM ($p < 0.05$) and BLM CM fraction 10-30 kDa ($p < 0.01$) (Figure 5a). These data suggest that the involvement of TIMP3 in angiogenic inhibition is at least in part regulated by the inhibition of directionally persistent EC migration. Panel tracks (Figure 5b) represent the migratory trajectories of ECs under various treatments, with and without rhTIMP3. An interesting observation is that BLM CM induces a higher effective migratory response as compared to VEGF alone, suggesting the presence of other proangiogenic molecules produced by this melanoma cell line. This observation is further supported by the fact that the 10-30 kDa fraction (which does not contain VEGF, VEGF Mw ~42 kDa) of BLM CM induces a similar migratory response as VEGF alone (Figure 5a).

Expression of TIMP3 by transfected BLM cells

To determine if the CM of modified, TIMP3 expressing, BLM cells (BLM-TIMP3) could affect directional EC migration, BLM cells were transfected with the recombinant plasmid encoding for TIMP3 and DsRed fluorescent marker protein. qPCR confirmed the expres-

a
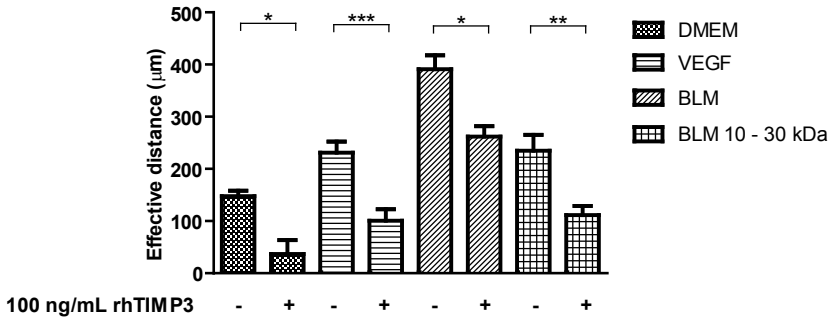
b
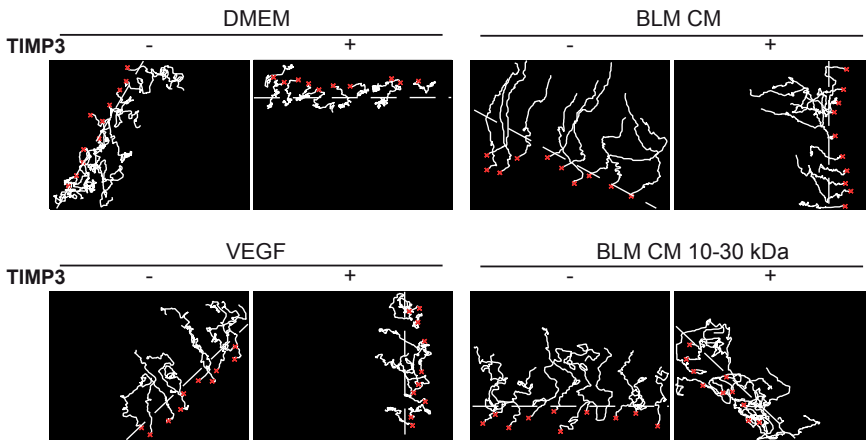
Figure 5. Effect of rhTIMP3 on endothelial cell migration. (**a**) Effective migrated distance (μm) per cell with various treatments in the absence (−) and presence (+) of 100 ng/mL rhTIMP3. At least 30 cells from at least three independent experiments were tracked. *$p < 0.05$, **$p < 0.01$, ***$p < 0.005$. (**b**) Representative migration track movements exhibited by endothelial cells under treatments mentioned in panel A. The white dashed line represents the migratory front upon removal of the barrier (t = 0 h), the red crosses represent the tracked cells and the white line represents the locomotion of the individual cells during the course of 24 h.

sion of TIMP3 mRNA transcripts in BLM-TIMP3 cells (Figure 6a). ELISA measurements showed that BLM-TIMP3 cells produced approximately 2 ng TIMP3/10[6] cells per 72 h (vs. unmodified BLM cells, $p < 0.05$; vs. BLM-EV cells, $p < 0.05$) (Figure 6b).

Overexpression of TIMP3 does not inhibit the growth properties of the melanoma cells

Previous studies have indicated that adenoviral mediated TIMP3 overexpression induces apoptotic cell death in some melanoma[115] and other tumor cell lines[114]. To address whether TIMP3 overexpression had a direct effect on the growth of the highly proliferative BLM

a

b

c

d

e
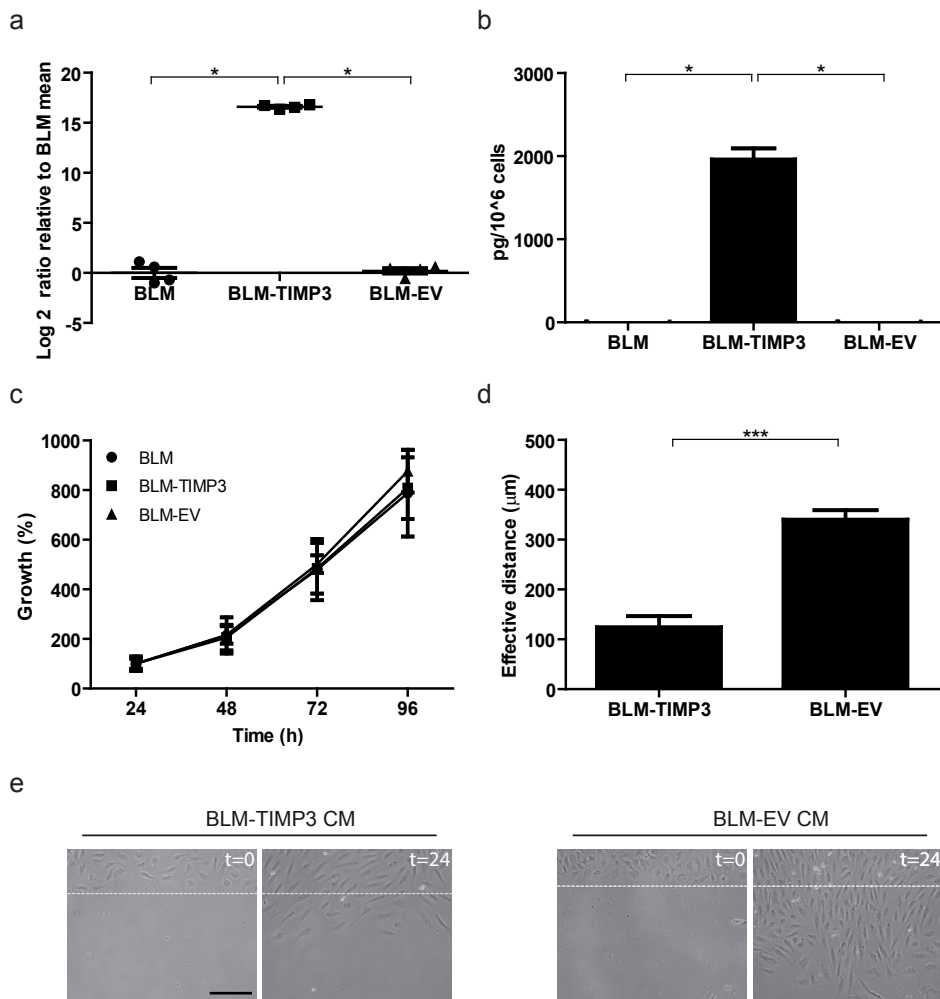
Figure 6. Enforced expression of TIMP3 in BLM melanoma cells. (**a**) Real-time RT-PCR gene expression levels of TIMP3 in unmodified (●), BLM-TIMP3 (■) and BLM-EV (▲) cells, measured in quadruple samples. Changes in transcript abundance were normalized to HPRT expression and are expressed as log2 ratio relative to BLM mean. *$p < 0.05$. (**b**) Levels of TIMP3 (pg) secreted by transfected and untransfected BLM cells into the CM as detected by ELISA. Data were normalized to the number of cells used to generate the CM and are expressed as mean ± SEM of quadruplicate samples. *$p < 0.05$. (**c**) *In vitro* growth rates of unmodified parental BLM (●) cell line compared to BLM-TIMP3 (■) and BLM-EV (▲) transfected cell lines. (**d**) Effective migrated distance (μm) per cell induced by the treatments. At least 30 cells from at least three separate experiments were tracked. ***$p < 0.005$. (**e**) Representative pictures of migrating ECs at start (t = 0 h) and end (t = 24 h) positions of the migration assay for the respective treatments. White dashed lines indicate the migration front at t = 0 h. Scale bar, 200 μm.

cell line, we evaluated the growth rates of unmodified BLM cells with that of transfected BLM-TIMP3 and BLM-EV cells. Transfected cell lines showed similar growth rates as compared to the unmodified cell line (Figure 6c). These results are in concordance with a previous study where TIMP3 was overexpressed in a murine melanoma cell line and did not alter the growth properties of the parental cell line[117]. These results suggest that the restraining effects of TIMP3 on tumor growth are, at least in part, mediated by negative regulation of factors in the tumor microenvironment.

Transfected BLM-TIMP3 conditioned medium inhibits directional endothelial cell migration

The ability of the CM of BLM-TIMP3 cells to regulate directed EC migration was reduced compared to that of BLM-EV cells. The effective distance of EC migration was reduced to 124.4 ± 22 μm when treated with CM of BLM-TIMP3 cells as compared to the CM of BLM-EV cells (340.3 ± 18 μm, $p < 0.005$) (Figures 6d, e; Videos 6-7). A corresponding decrease in migration efficiency was also observed ($p < 0.005$, data not shown). To determine if the inhibitory effect of TIMP3 was regulated through MMP-dependent or MMP-independent pathways, we performed migrations with BLM-EV and BLM-TIMP3 CMs in the presence of the MMP inhibitor, GM6001 (Supplementary Figures 1a, b, c). A detailed description of the results is provided in the Supplementary Results section. Our data suggests that TIMP3 inhibits EC migration, at least in part, via MMP independent pathways.

TIMP3 in melanoma conditioned medium does not affect endothelial cell (EC) proliferation but affects EC adhesion and invasion

We analyzed the effect of melanoma derived TIMP3 on the proliferative, adhesive and invasive properties of ECs. We observed that while the presence of TIMP3 did not affect EC proliferation in the BLM and 1F6 CM sets or in basal medium (Supplementary Figures 2a, b, c), it did increase both the adhesion (Supplementary Figures 2d, e, f, g) and invasion (Supplementary Figures 3a, b) of ECs. A detailed description of the results is provided in the Supplementary Results section.

Effect of TIMP3 modulation on tumor growth and angiogenesis

In order to assess the *in vivo* effect of TIMP3 knockdown on tumor growth, NMRI nu/nu mice were subcutaneously inoculated with either 1F6 shTIMP3 or 1F6 shControl cells. Tumor take was observed in 8/10 mice injected with 1F6 shTIMP3 cells and 6/10 mice injected with 1F6 shControl cells. 1F6 shTIMP3 tumors grew significantly faster than 1F6 shControl tumors. The mean volume of 1F6 shTIMP3 tumors was 0.45 ± 0.2 cm^3 while that of 1F6 shControl tumors was 0.04 ± 0.02 cm^3 on day 26 after tumor cell inoculation ($p < 0.005$) (Figure 7a). Histopathological analysis of excised tumor sections stained with
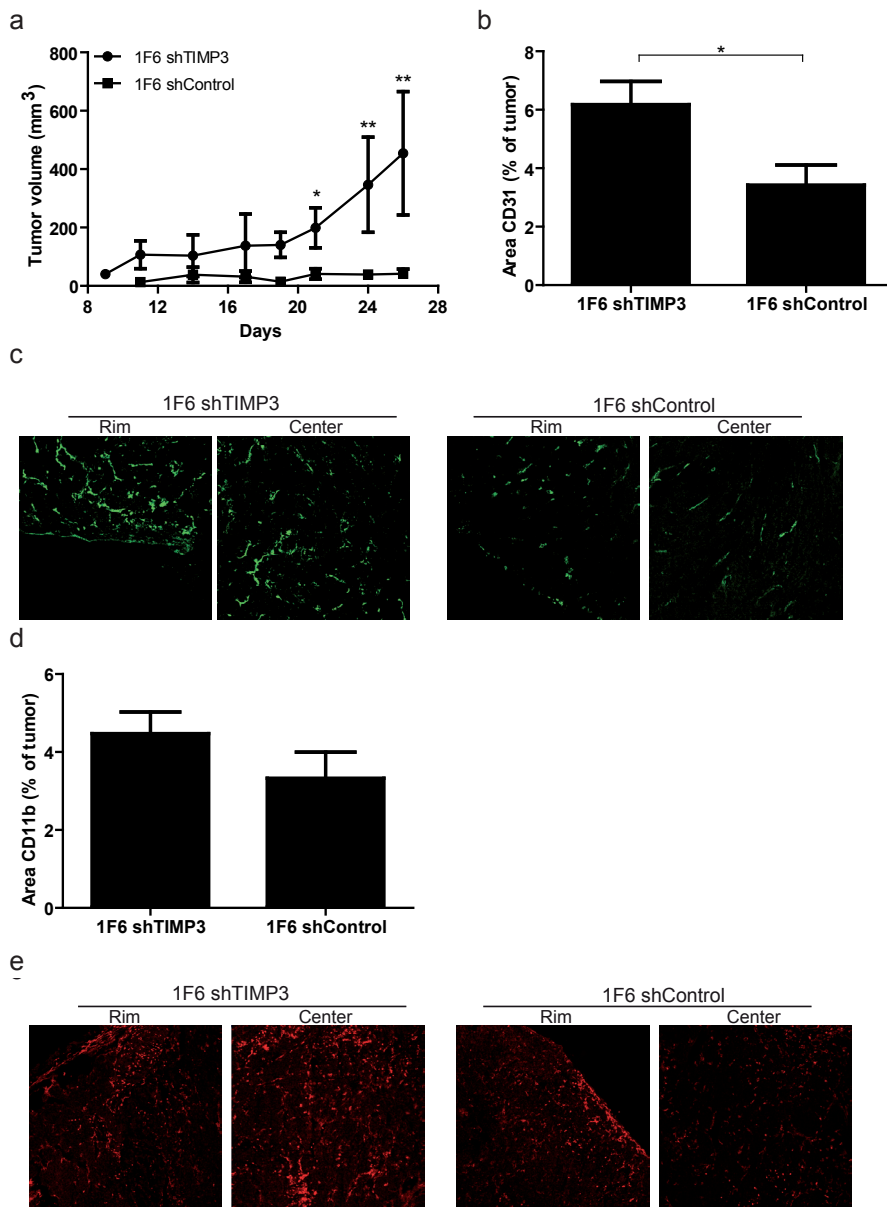
Figure 7. *In vivo* tumor growth following inoculation of modified 1F6 melanoma cells. (**a**) *In vivo* growth of 1F6 shTIMP3 (●) and 1F6 shControl (■) tumor cells in NMRI nu/nu mice (n = 10 mice/group). *$p < 0.05$, **$p < 0.005$. (**b**) Vascular coverage is expressed as the mean value of CD31 positive area as percentage of the total tumor section in 1F6 shTIMP3 and 1F6 shControl tumors. (**c**) Representative sections showing vessel coverage as indicated by CD31 staining in the rim and center of 1F6 shTIMP3 and 1F6 shControl tumors. (**d**) Macrophage infiltration is expressed as the mean value of CD11b positive staining in 1F6 shTIMP3 and 1F6 shControl tumor sections. (**e**) Representative sections showing macrophage infiltration as indicated by CD11b staining in the rim and center of 1F6 shTIMP3 and 1F6 shControl tumors. All immunohistochemical analyses were performed on a tile scan of the whole tumor section.

3
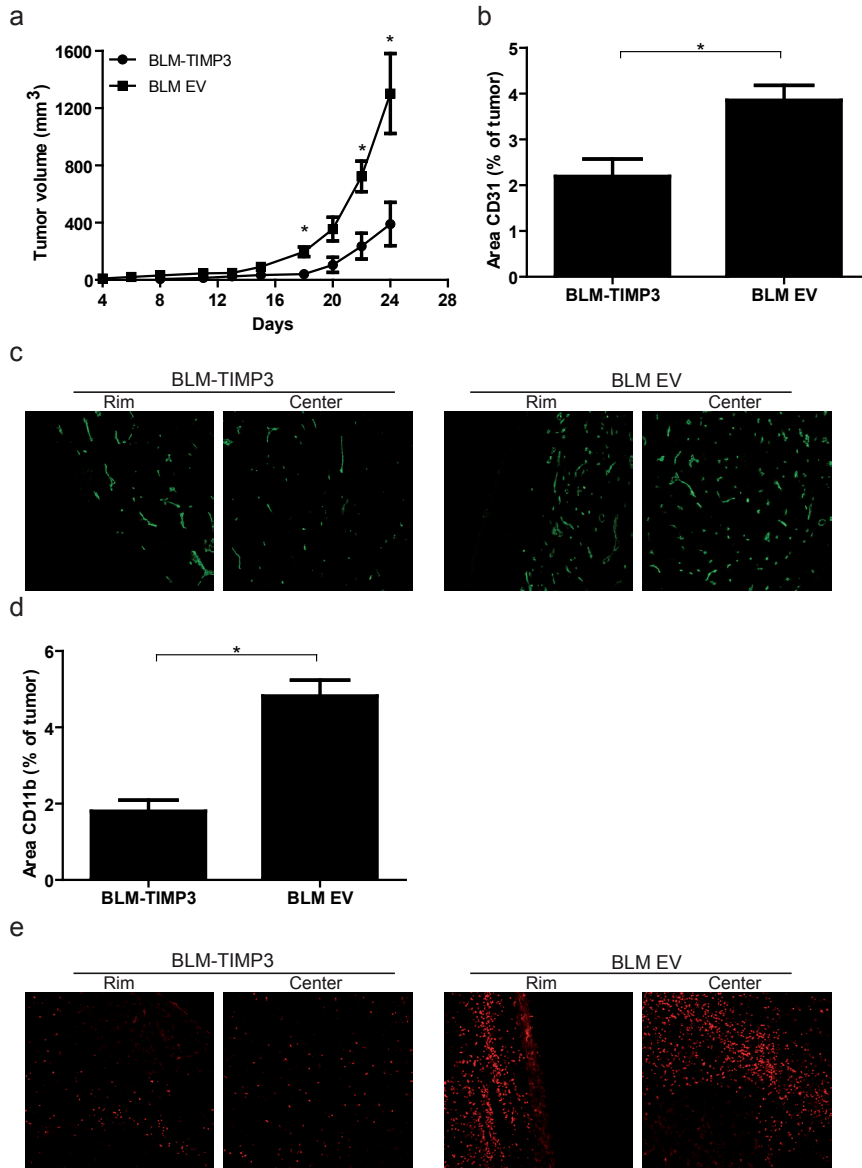
Figure 8. *In vivo* **tumor growth following inoculation of modified BLM melanoma cells.** (**a**) *In vivo* growth of BLM-TIMP3 (■) and BLM-EV (▲) tumor cells in NMRI nu/nu mice (n = 6 mice/group). *$p < 0.05$. (**b**) Vascular coverage is expressed as the mean value of CD31 positive area as percentage of the total tumor section in BLM-TIMP3 and BLM-EV tumors. (**c**) Representative sections showing vessel coverage as indicated by CD31 staining in the rim and center of BLM-TIMP3 and BLM-EV tumors. (**d**) Macrophage infiltration is expressed as the mean value of CD11b positive staining in BLM-TIMP3 and BLM-EV tumor sections. (**e**) Representative sections showing macrophage infiltration as indicated by CD11b staining in the rim and center of BLM-TIMP3 and BLM-EV tumors. All immunohistochemical analyses were performed on a tile scan of the whole tumor section

CD31 antibody revealed that the vessel coverage of 1F6 shTIMP3 tumors was significantly higher than that of 1F6 shControl tumors ($p < 0.05$) (Figure 7b). Silencing TIMP3 in 1F6 cells increased tumor associated angiogenesis and the difference in vessel coverage between the two groups was evident both at the rim and center of the tumor section (Figure 7c). Studies in human malignant melanomas have reported a correlation between angiogenesis, tumor progression and macrophage infiltration[51,129]. Although the number of positive CD11b stained cells was higher in the center of 1F6 shTIMP3 compared to 1F6 shControl tumors, no significant difference was observed when the whole tumor section was analyzed (Figures 7d, e). Further, to examine the effect of TIMP3 restoration on tumor growth *in vivo*, NMRI nu/nu mice were subcutaneously injected with BLM-TIMP3 or BLM-EV cells. Tumor take was observed in 5/5 mice in both cases. However, the growth of BLM-TIMP3 tumors was significantly inhibited compared to that of BLM-EV tumors. The mean volume of BLM-TIMP3 tumors was 0.2 ± 0.09 cm^3 and 0.39 ± 0.15 cm^3 as compared to that of BLM-EV 0.7 ± 0.10 cm^3 and 1.3 ± 0.2 cm^3, on days 22 and 24 respectively ($p < 0.05$) (Figure 8a). Staining for CD31 revealed that blood vessel coverage of BLM-TIMP3 tumors was significantly lower than that of BLM-EV tumors ($p < 0.05$) (Figure 8b). This was also evident in the decreased mean vessel density observed both at the rim and center of BLM-TIMP3 tumors as compared to BLM-EV tumors (Figure 8c). Analysis of CD11b staining showed extensive macrophage infiltration in BLM-EV tumors as compared to BLM-TIMP3 tumors ($p < 0.05$) (Figure 8d). This was evidenced both at the periphery and the center of the tumor (Figure 8e).

DISCUSSION

Angiogenesis is an imperative component of cutaneous melanomas and is most prominent during the vertical growth phase of neoplastic transformation[91]. The melanoma cell lines described in this study vary in their *in vivo* growth profiles, mean vessel density (MVD) and the ability to generate spontaneous metastasis. Thus, while BLM is highly aggressive and exhibits a high MVD, Mel57 and 1F6 are less aggressive and exhibit low MVD[83,87,130]. In the present study, we evaluated the angiogenic potential of the human melanoma cell lines based on their ability to regulate directionally persistent EC migration.

We used the 2D ring-barrier migration assay previously described[123] to quantify the parameters of EC migration in response to factors secreted by melanoma cells. We observed that ECs exhibited high persistent directional migration in response to CM of highly aggressive BLM cells, while CMs of Mel57 and 1F6 did not induce such an effect and was comparable to that of basal medium. The latter observation was unexpected as melanomas are known to produce high levels of proangiogenic factors which arbitrate the multiple steps of the tumor associated angiogenic cascade[42]. Further confirmation of this inhibitory effect is the observed reduced directional EC migration upon treatment

with the 10-30 kDa fraction of Mel57 and 1F6 CM, while no inhibition was observed upon treatment with the complementary fraction (> 30 + < 10 kDa). Successive size fractions of BLM CM also showed a gradual reduction in the ability to induce directional EC migration. However, all BLM CM fractions were capable of inducing higher directed migration as compared to basal medium and hence the gradual reduction observed is most likely due to the successive removal of proangiogenic molecules during CM size fractionation, as opposed to the inhibitory effects observed with the Mel57 and 1F6 fractions. In addition, stimulation of directional migration by the melanoma CMs seems to be independent of their reported differential MMP profiles[65], as BLM CM and BLM CM fractions < 50 kDa and < 30 kDa induce similar migratory profiles in ECs (the fractions being devoid of MMP activity; active MMP-2 Mw ~66 kDa, active MMP-3 Mw ~57 kDa). Of interest is the observation that the small molecule fraction (< 10 kDa) of all melanoma CMs induce directionally persistent EC migration, suggestive of the involvement of several small molecule proangiogenic factors during melanoma angiogenesis.

TIMPs are a family of endogenous matrix metalloproteinase inhibitors which regulate several physiological effects including, but not limited to, ECM turnover and angiogenesis[124,131]. We detected a striking difference in the gene expression profile of TIMP3, but not TIMP1 or -2, among the melanoma cell lines, and the expression pattern inversely correlated with the degree of aggressiveness of melanomas. Promoter methylation gene profiling in melanoma cell lines have shown the silencing of TIMP3 in cutaneous melanomas[128]. We observed that demethylation treatment of BLM cells restored TIMP3 expression, corroborating the tumor suppressor role of TIMP3 during melanoma pathogenesis. Another interesting observation is the presence of TIMP3 protein in melanoma CM. TIMP3 is often reported to be unique among the TIMPs in that it is matrix bound and hence undetectable in the CM generated from normal[113,132] and tumor[115] cells overexpressing TIMP3. Other studies have shown detectable levels of TIMP3 in the conditioned medium generated from tumor cells[117,127]. Here we show that high levels of TIMP3 were detectable in the CMs of the endogenous TIMP3 expressing melanoma cell lines, Mel57 and 1F6. Moreover, enforced expression of TIMP3 in BLM cells led to the production and accumulation of TIMP3 in the CM. We hypothesize that it is the amount of TIMP3 produced by the cells which determines the detectability in tumor CM. As shown earlier, the Mel57 and 1F6 cell lines produce a considerable amount of TIMP3 and although a fraction of the total TIMP3 produced might remain bound to the ECM, detectable levels are secreted into the medium. It is the secreted version of TIMP3 which mediate the inhibitory effects on directional EC migration described herein, as the tumor cells are not in contact with ECs during migration. It is important to note that the inhibitory effects mediated by TIMP3 on the angiogenic cascade *in vivo* might be a concerted effect of the sequestered and secreted fractions. The MMP inhibitory activity profile of TIMPs in melanoma CMs revealed that all melanoma cells produced high and similar levels of

active TIMP2, dismissing TIMP2 as a possible inhibitor in our study, while only Mel57 and 1F6 cell lines produced active TIMP3.

Several studies have reported the inhibition of primary tumor growth upon enforced expression of TIMP3 in tumor cells[117,120]. These effects have been shown to be mediated by inhibition of angiogenesis[117,122], inhibition of tumor cell invasion and induction of tumor cell apoptosis[114,115]. However, we observed that BLM-TIMP3 cells did not show any difference in proliferation rates compared to both BLM-EV and the unmodified BLM cells, suggesting that the inhibitory effect of TIMP3 is exerted by its effect on angiogenesis and not by the direct effect on the tumor cell itself. In accordance with studies reporting the inhibition of angiogenesis by TIMP3[117,121,122], we observe a striking reduction in the directional migration of ECs in the presence of rhTIMP3 and TIMP3 produced by transfected (BLM-TIMP3) cells. This observation was corroborated *in vivo* as vascular coverage, macrophage infiltration and tumor growth of BLM-TIMP3 tumors was significantly reduced as compared to BLM-EV tumors. Conversely, the loss of TIMP3 expression enhanced the angiogenic potential, vascular coverage and tumor growth of 1F6 shTIMP3 tumors. The traditional paradigm of ECM remodeling implicates the proteolytic nature of MMPs and the inhibitory nature of TIMPs. However, pharmacological targeting of MMPs in clinical trials, as a treatment modality for cancers, yielded disappointing results[133]. Recent studies have highlighted the role of TIMPs as multifunctional molecules, regulating the angiogenic cascade via both MMP-dependent and MMP-independent mechanisms[121,134-137]. Interestingly, in this study, we observe that although MMP inhibition inhibited total and directional EC migration induced by BLM-EV CM, no additive inhibitory effect was observed when MMPs were inhibited in the presence of BLM-TIMP3 CM. Moreover, treatment with BLM-TIMP3 CM showed significantly reduced migration as compared to BLM-EV CM treatment in the presence of the MMP inhibitor suggesting, at least in part, the involvement of MMP-independent pathways in TIMP3 mediated angiogenesis regulation.

It is interesting to note the reduction of tumor infiltrating macrophages in TIMP3-expressing melanomas, as macrophage infiltration is known to correlate with melanoma growth, progression and angiogenesis[51,129]. Moreover, studies in breast and pancreatic tumors have reported a reduction in infiltrating macrophages upon inhibition of VEGF-VEGFR-2 signaling[138,139]. We hypothesize that TIMP3 inhibits tumor infiltration of macrophages, either through inhibition of matrix breakdown which affects the liberation and presence of chemotactic factors and/or possibly through the inhibition of VEGFA-VEGFR-2 signaling. Additional studies are required to validate this aspect of TIMP3 signaling in melanoma pathophysiology.

Taken together, our data clearly implicate TIMP3 as a dominant intrinsic negative regulator of melanoma induced angiogenesis, suggesting possible therapeutic applications of TIMP3. It is important to bear in mind that melanoma cells produce a plethora of angiogenic modulators and while TIMP3 has a dominating effect, other factors produced by the

melanoma cells may also modulate the angiogenic cascade. Next to the effect of TIMP3, which is consistent between the cell lines studied and seems to supersede other factors, deciphering additional alterations and mutations present in melanomas may contribute to a better understanding of the multiple aspects of melanoma induced angiogenesis.

ACKNOWLEDGEMENTS

The online version of this article contains supplementary material, which is available to authorized users.

3

SUPPLEMENTAL FIGURES

a

b

☐ +GM6001
■ +GM6001 Negative Control

c
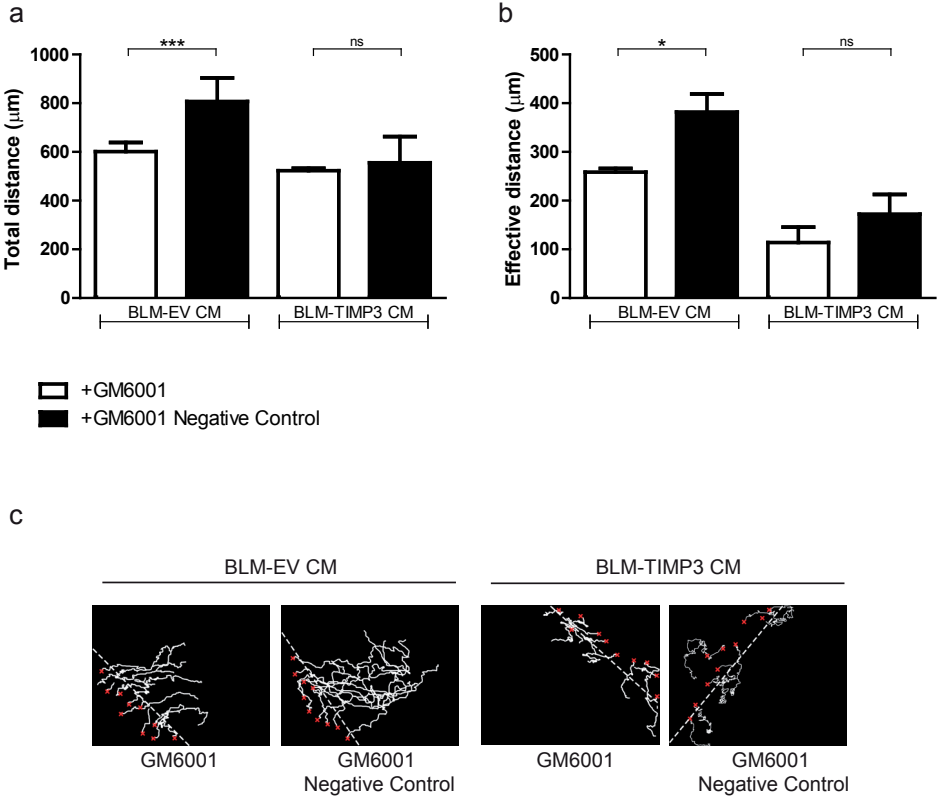
Supplementary Figure 1. Effect of MMP inhibition on endothelial cell migration. Endothelial cells (ECs) were treated with BLM-EV CM or BLM-TIMP3 CM in the presence of the synthetic broad spectrum MMP inhibitor GM6001 (10μM, white bars) or the mock inhibitor GM6001 Negative control (10 μM, black bars). All treatments were supplemented with 10% FCS. At least 30 cells in at least 3 independent experiments were tracked. (**a**) Total distance of EC migration (μm) in 24 h. (**b**) Effective migrated distance (μm) per cell. Effective migration represents the directionality of cell movement (straight line path, perpendicular to the migration front, towards the cell free center). Data in panels a, b represent mean ± SEM of at least three independent experiments. *$p < 0.05$, ***$p < 0.005$. (**c**) Representative migration track movements exhibited by ECs with the treatments described in panels a, b for 24 h. The white dashed line represents the migratory front upon removal of the barrier (t = 0 h), the red crosses represent the tracked cells and the white lines represent the locomotion trajectories of individual cells during the course of 24 h.
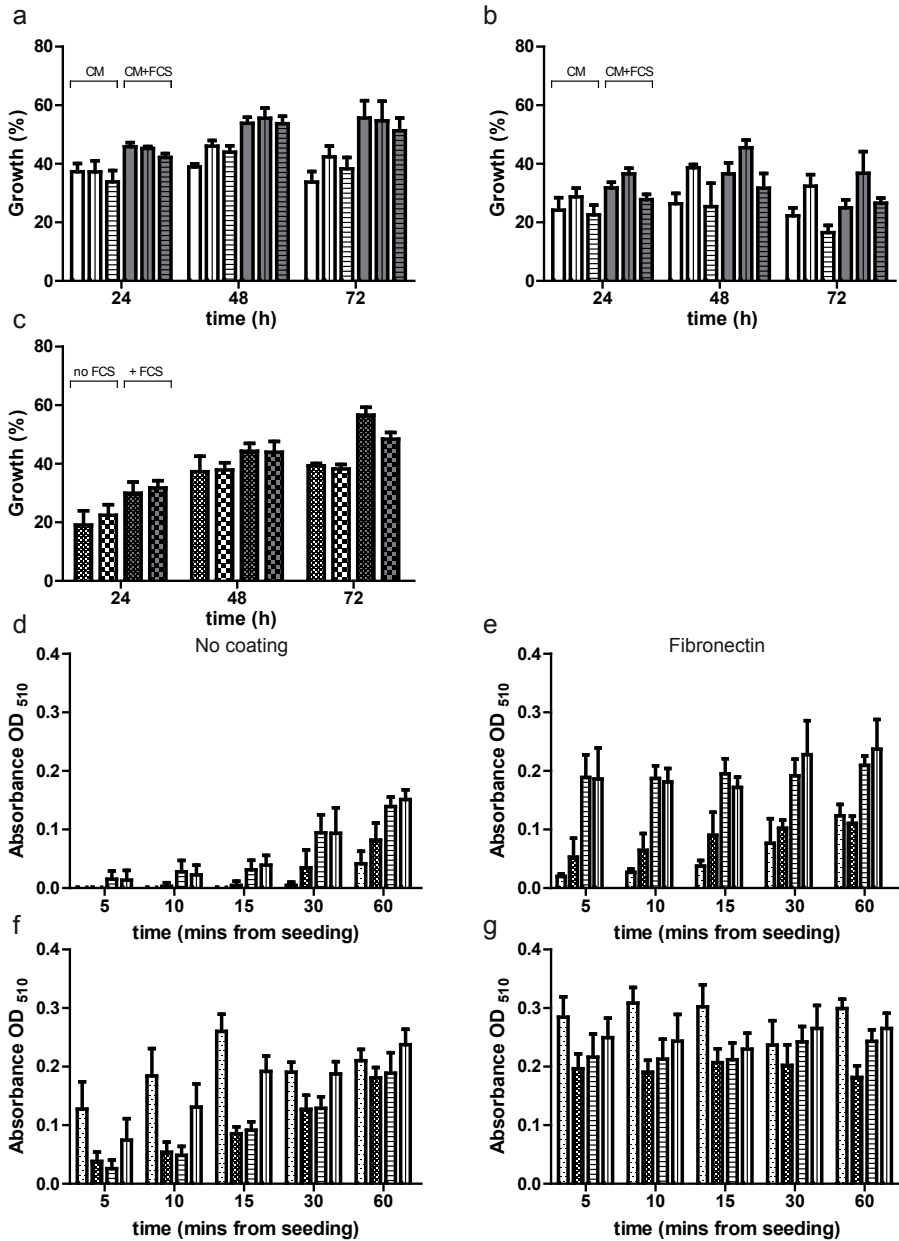
Supplementary Figure 2. TIMP3 in melanoma conditioned-medium does not affect endothelial cell proliferation but affects endothelial cell adhesion. (**a,b,c**) Endothelial cell proliferation in the presence of melanoma CMs. ECs were grown to near confluence and treated with various melanoma CMs supplemented with or without 10% FCS. White bars indicate absence of serum and grey bars indicate serum supplementation. (**a**) EC proliferation with BLM (☐), BLM-TIMP3 (☐) and BLM-EV (☐) CM. (**b**) EC proliferation with 1F6 (☐), 1F6 shTIMP3 (☐) and 1F6 shControl (☐) CM. (**c**) EC proliferation with basal medium in the absence (▨) and presence (▨) of rhTIMP3. Cells were fixed at 24, 48 and 72 h

and growth was determined by normalizing the data to the 0 h time point (time of treatment addition), and is expressed as a percentage. (**d,e,f,g**) Endothelial cell adhesion in the presence of melanoma CMs. EC adhesion with CMs of BLM (⬚), BLM-EV (▨), BLM-EV supplemented with rhTIMP3 (▱) and BLM-TIMP3 (▱) cells on non-coated (**d**) and fibronectin coated (**e**) cluster plates. EC adhesion with CMs of 1F6 (⬚), 1F6 shTIMP3 (▨),1F6 shTIMP3 supplemented with rhTIMP3 (▱) and 1F6 shControl (▱) cells on non-coated (**f**) and fibronectin coated (**g**) cluster plates. Cells were fixed at the indicated time points after seeding, stained and the absorbance was measured at 510 nm.
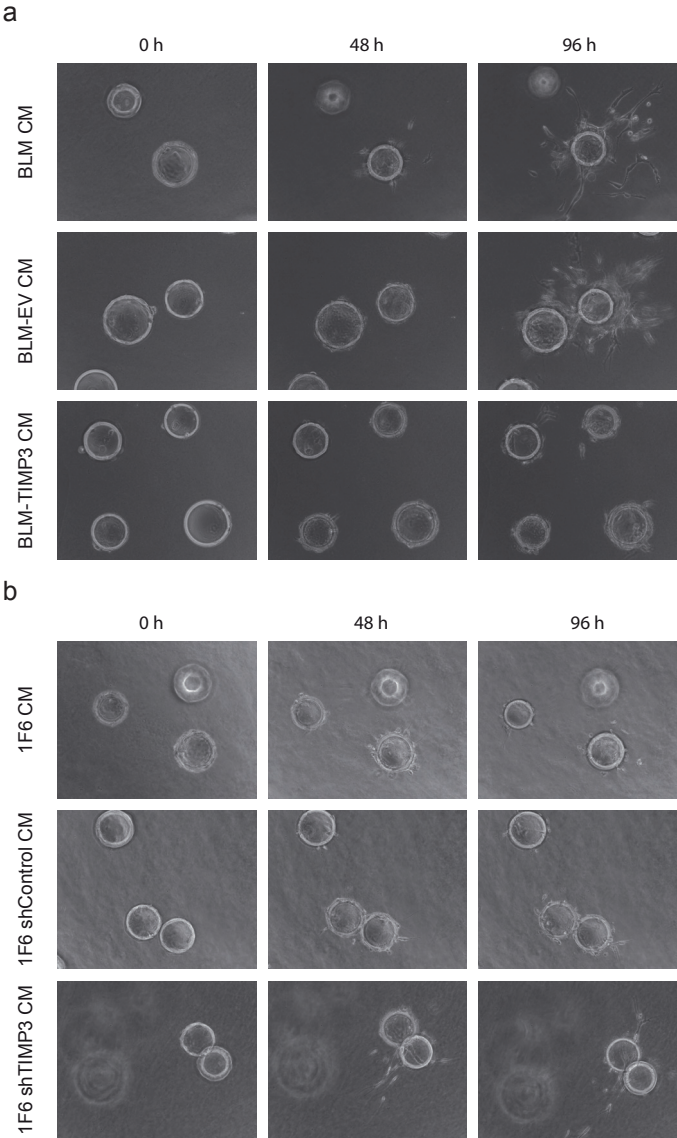
Supplementary Figure 3. TIMP3 in melanoma conditioned-medium inhibits the invasive capacity of endothelial cells. (**a**) Endothelial cell invasion in the presence of CM from modified and unmodified BLM cells. (**b**) Endothelial cell invasion in the presence of CM from modified and unmodified 1F6 cells.

a

100 ng/mL bFGF, no serum

100 ng/mL EGF, no serum

10 ng/mL VEGF, no serum

b

c

bFGF

EGF

VEGF
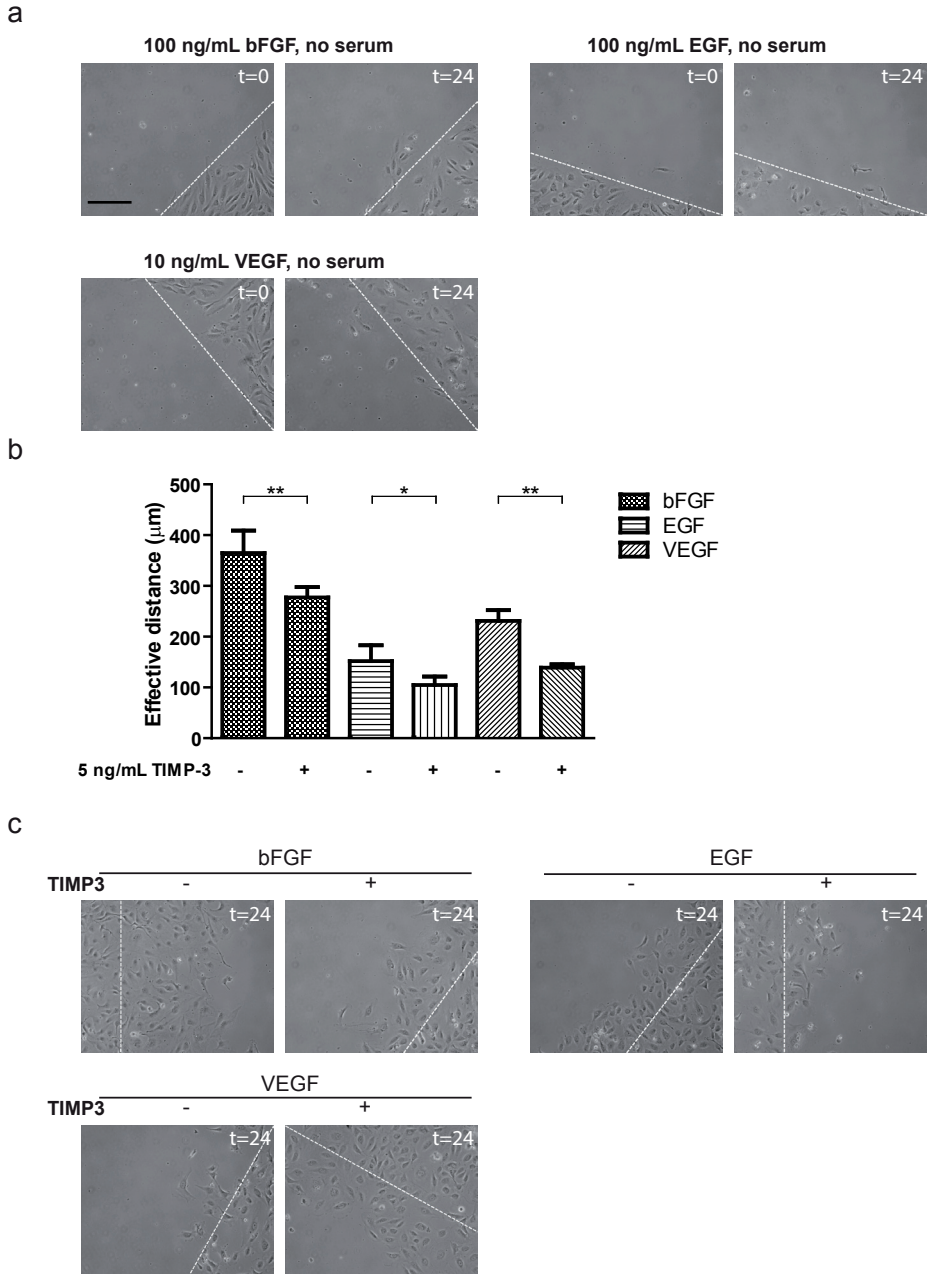
Supplementary Figure 4. Effect of serum supplementation on endothelial cell migration in the 2D ring-barrier assay. Endothelial cells (ECs) were treated with chemotactic agents known to promote migration, in the absence of serum supplementation. (**a**) Representative pictures of migrating ECs at start (t = 0 h) and end (t = 24 h) positions in the presence of 100 ng/mL bFGF, 100 ng/mL EGF and 10 ng/mL VEGF. White dashed lines indicate the migration front at t = 0 h. Scale bar, 200 μm. (**b,c**) Effect of rhTIMP3 on EC migration

induced by known chemotactic agents, with serum supplementation. (**b**) Effective migrated distance (µm) per cell when treated with 100 ng/mL bFGF, 100 ng/mL EGF and 10 ng/mL VEGF, with or without rhTIMP3, in the presence of 10% FCS. At least 30 cells from at least three separate experiments were tracked. Data represents mean ± SEM of at least three independent experiments. $*p < 0.05$, $**p < 0.01$. (**c**) Representative pictures of migrating ECs at start (t = 0 h) and end (t = 24 h) positions of the migration assay for the respective treatments. White dashed lines indicate the migration front at t = 0 h. Scale bar, 200 µm.

a

b
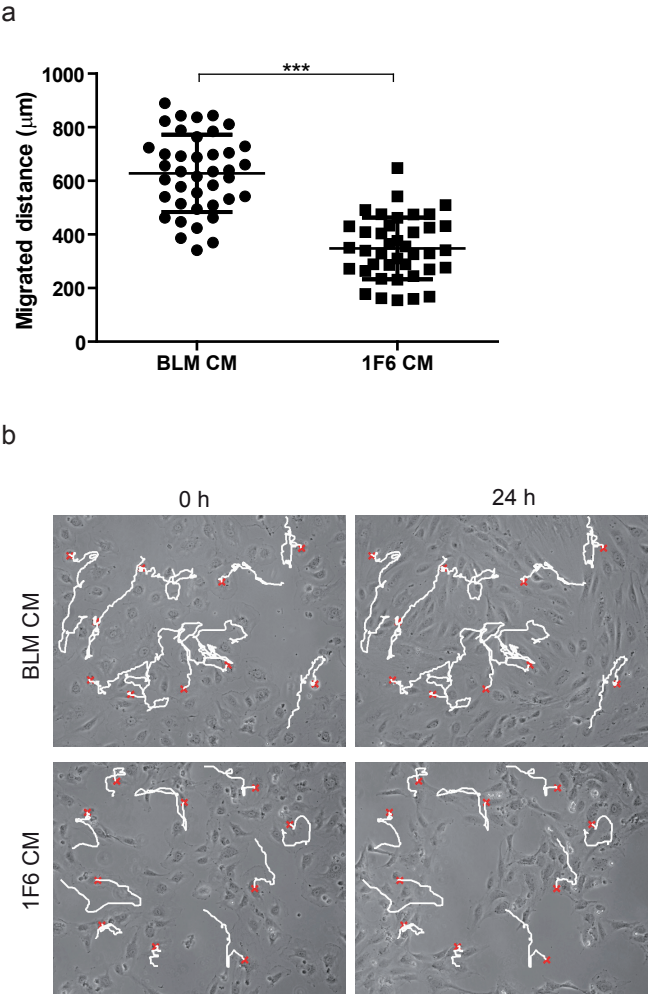
Supplementary Figure 5. Melanoma conditioned-media induce distinct migration trajectories in sub-confluent cultures of ECs. Sub-confluent cultures of ECs, seeded in migration rings in the absence of a barrier, were treated with BLM CM and 1F6 CM. Treatments were supplemented with 10% FCS. At least 40 cells in at least 4 independent experiments were tracked. (**a**) Total distance of EC migration (µm) in 24 h. $***p < 0.005$. (**b**) Overlay of net trajectories of subconfluent ECs on the start (t = 0 h) and end (t = 24 h) positions with the treatments described in panel a. The red crosses represent the tracked cells and the white lines represent the locomotion trajectories of individual cells during the course of 24 h.

CHAPTER 4

Association of TIMP3 expression with vessel density, macrophage infiltration and prognosis in human malignant melanoma

Asha M. Das, Senada Koljenović, Charlotte M.C. Oude Ophuis, Thom van der Klok, Boris Galjart, Alex L. Nigg, Wiggert A. van Cappellen, Vincent Noordhoek Hegt, Winand N.M Dinjens, Peggy N. Atmodimedjo, Cindy E. Vermeulen, Cornelis Verhoef, Alexander M.M. Eggermont, Timo L.M. ten Hagen

ABSTRACT

Several antitumor properties have been ascribed to the tissue inhibitor of matrix metalloproteinases-3 (*TIMP3*) gene, including inhibition of neovascularization in tumor xenografts. Reduced protein expression has been linked to promoter hypermethylation and allelic loss of heterozygosity in various human malignancies. In melanoma positive lymph nodes from patients, we evaluated the association between TIMP3 expression, vessel density, macrophage infiltration and potential correlations with disease-free survival (DFS) and overall survival (OS).

TIMP3 expression was analyzed by immunohistochemistry (IHC) in melanoma lymph node biopsies of stage III melanoma patients (n = 43). Blood vessel density and macrophage infiltration were quantitatively assessed and correlation with TIMP3 expression was investigated. Methylation status of the gene promoter was determined using methylation specific PCR (MSP). Protein expression and promoter methylation status were investigated for associations with DFS and OS.

Reduced expression of TIMP3, as determined by IHC, was observed in 74% of the cases (32/43). A significant inverse correlation was observed between TIMP3 expression and vessel density ($p = 0.031$). Correlation between TIMP3 expression and macrophage infiltration was not statistically significant ($p = 0.369$). MSP analysis revealed methylation of the gene promoter in 18% (7/38) of the analyzed cases. No differences in OS and DFS were observed between cases with high and low TIMP3 expression. Gene promoter methylation was significantly associated with both poor 5-year DFS ($p = 0.024$) and OS ($p = 0.034$).

Our data indicate that TIMP3 is a dominant negative regulator of angiogenesis in cutaneous melanoma and gene silencing by promoter methylation is associated with poor outcome.

INTRODUCTION

Extracellular matrix (ECM) remodeling is crucial to neovasculature initiation and development and is orchestrated by an interplay between matrix metalloproteinases (MMPs) and their endogenous inhibitors, tissue inhibitor of matrix metalloproteinases (TIMPs)[124]. The *TIMP3* gene located at 22q12.3, codes for a 24 kDa glycoprotein with broad inhibitory effects. TIMP3 has been described as a tumor suppressor in a number of human malignancies, including breast[140], colorectal[141] and prostate cancers[142], with decreased expression correlating with poor prognosis and outcome. Reduced TIMP3 expression has been attributed to aberrant promoter hypermethylation[125,143-145] and allelic loss of heterozygosity[146,147] in several tumor types. Concurrent with its role as a tumor suppressor, TIMP3 has been documented to exert antitumor effects via both MMP-dependent and MMP-independent pathways. Overexpression of TIMP3 has been reported to induce apoptosis[114,115] and inhibit tumor growth[117,120,148] and metastasis[149] in several tumor cell lines. Additionally, TIMP3 is a dominant negative regulator of angiogenesis, and has been shown to block the binding of VEGF to its receptor[121], and suppress neovascularization in several tumor xenografts[127,150].

Human malignant melanoma is an aggressive disease, with the highest increase in incidence in the western world of all malignancies, and accounts for the majority of skin cancer related deaths[2,41]. Melanomas are highly vascular tumors and the angiogenic element is crucial for disease progression and subsequent metastatic dissemination[78,151]. We have previously shown that TIMP3 inhibits directionally persistent endothelial cell migration and impairs angiogenesis and macrophage infiltration in melanomas in a xenograft model[152]. However, the clinical association between TIMP3 expression and angiogenesis in melanoma is not known. In the present study we evaluated TIMP3 expression and correlation to mean vessel density and macrophage infiltration in a cohort of melanoma positive lymph node biopsies from stage III melanoma patients using immunohistochemistry. We also assessed the methylation status of the TIMP3 gene promoter CpG island using methylation-specific PCR (MSP) analysis. Finally, the association of protein expression and gene promoter methylation to clinicopathological variables were analyzed.

MATERIALS AND METHODS

Patient samples

43 cases of stage III melanoma lymph node biopsies were obtained from the pathology archives of the Erasmus Medical Center, with the approval of the research ethics committee. The tumor specimens used in this study were obtained between 2008 and 2009 and verified by pathological diagnosis. Tumor staging was based on the American Joint

Committee on Cancer (AJCC) TNM staging system[4]. All patient data for the present study were collected from medical records according to local Institutional Review Committee guidelines and national legislation.

Immunohistochemistry

5 µm serial tissue sections were cut from the FFPE melanoma blocks using a Microm HM325 microtome (Thermo Fisher Scientific, Waltham, MA) and mounted on Objectglas Superfrost Plus slides (VWR). One tissue section was used for H&E staining and tumor areas were demarcated. Serial tissue sections were immunohistochemically stained for TIMP3 (rabbit polyclonal, Abcam ab2169, 1:100), CD31 (mouse monoclonal, Abcam, clone JC/7A, ab9498, 1:50) and CD68K (mouse monoclonal, DAKO, clone KP1, M0814, 1:1600) using the Ventana Benchmark Ultra stainer (Ventana Medical Systems, Tucson, AZ). The staining procedure included pretreatment with CC1 (cell conditioner 1, pH 8) for 64 min followed by primary antibody incubations at 36°C for 32 min. Stainings for TIMP3, CD31 and CD68K were visualized using the Ventana ultraView Universal Alkaline Phosphatase Red Detection Kit (760-501). For all antibodies, the Ventana Amplification Kit (760-080) was used. Nuclei were counter stained with hematoxylin. Human placenta tissue was used as a positive control for TIMP3 staining.

TIMP3 staining evaluation

Evaluation of TIMP3 immunohistochemical staining was performed by two experienced pathologists (S.K. and V.N.H.) who were blinded toward patient characteristics, patient outcome, and results of promoter methylation status. TIMP3 staining was graded semiquantitatively as previously described[153], with modifications. Staining intensity was graded as 1 (no staining), 2 (weak stain), 3 (clear stain), or 4 (strong stain). To account for intratumoral heterogeneity, the percentage of cells exhibiting the various intensities was recorded. The intensity and abundance (expressed as a fraction) scores were multiplied to obtain a total immunoreactivity score which ranged from a maximum total score of 4 (intensity score 4, abundance 100%) to a minimum total score of 1 (intensity score 1, abundance 100%). For correlation analysis and survival analysis, samples with an immunoreactivity score of > 2.4 were classified as high and ≤ 2.4 were classified as low. Differences in scoring was evaluated by Kappa test and discrepant scores were resolved by consensus.

CD31 and CD68K density evaluation

To quantitatively determine vessel density and macrophage infiltration, whole slide scanning was performed on serial sections immunohistochemically stained for CD31 and CD68K. Stained slides were scanned using the Hamamatsu NDP slide scanner (Hamamatsu Nanozoomer 2.0HT) and digitally converted into virtual slides[154]. Depend-

ing on the size of the tumor tissue, 6-12 tumor areas were randomly annotated at an ×20 magnification using the NDP.View analysis platform. Images of annotated areas were exported as .jpg and analyzed with a self-written plugin for the Image J software to obtain percentages of blood vessel density and macrophage infiltration.

Methylation Specific PCR

Two to three 10 μm FFPE tissue sections were macrodissected with reference to the hematoxylin-eosin stained sections to include areas with > 80% tumor cells. Genomic DNA was isolated using the QIAmp DNA FFPE tissue kit (Qiagen Benelux B.V., Venlo, NL) and quantified using the Qubit® 2.0 fluorometer (Life Technologies, CA, USA). 500 ng DNA was bisulfite modified using the EpiTect Bisulfite kit (Qiagen). 50 ng of modified DNA was amplified by PCR in 24 μL reactions, using AmpliTaq Gold® DNA Polymerase (Life Technologies) and 0.25 μM of each primer per reaction. Primer sequences for TIMP3 MSP have been described before[125]. Primers specific for unmethylated DNA were 5′-TTTTGTTTTGTTATTTTTTGTTTTTGGTTTT-3′ (sense) and 5′-CCCCCAAAAACCCCACCTCA-3′ (antisense), yielding a 122 bp product. Primers specific for methylated DNA were 5′-CGTTTCGTTATTTTTTGTTTTCGGTTTC-3′ (sense) and 5′-CCGAAAACCCCGCCTCG-3′ (antisense), yielding a 116 bp product. The PCR reactions were performed with an annealing temperature of 59°C. 10 μL of each PCR sample was resolved by electrophoresis on 2% agarose gels. Epitect Control DNA set (Qiagen) was used as controls for MSP.

Statistical Analysis

Statistics were performed with Statistical Package for the Social Sciences version 22.0 (SPSS Inc., Chicago, IL). Disease-free survival (DFS) was defined as the number of months from the date of surgery to the date of first recurrence (locally or distant), to death without relapse or to last follow up. Overall survival (OS) was defined as the number of months from the date of surgery to death of any cause as registered by the social security death index (SSDI) or to last follow up. Univariate analysis of the clinicopathologic characteristics was performed using χ^2 test for nominal variables, Kendall's tau for ordinal variables and Mann-Whitney-U test for non-parametric continuous variables. Survival curves were plotted using the Kaplan-Meier method, and comparison of survival times was performed with the log-rank test. All tests were two-sided, and $p < 0.05$ was considered statistically significant.

RESULTS

Patient population

Baseline characteristics of the patient population are provided in Table 1. All 43 patients had stage III disease at the time of surgery. Surgery consisted of either a sentinel node biopsy, a diagnostic lymph node biopsy, or a therapeutic lymph node dissection. Only histologically confirmed metastatic lymph node samples were used for this study.

Median age was 54 years (interquartile range, IQR, 46–66 years), and median follow-up was 29 months (IQR, 11–63 months). Median Breslow thickness was 3.00 mm (IQR, 1.80-7.00 mm). Most primary melanomas were situated on the lower extremity (n = 19, 44%), 14 melanomas (33%) were situated at the trunk, eight melanomas (19%) were situated in the head and neck area and there was one melanoma (2%) of unknown primary origin.

Table 1. Baseline characteristics

Characteristic	All (n = 43)	TIMP3 High (n = 11)	TIMP3 Low (n = 32)	p value
Gender				
Male	22 (50)	4 (36)	18 (56)	
Female	21 (50)	7 (64)	14 (44)	0.255
Breslow thickness				
T1 (≤ 1.0 mm)	1 (2)	0	1 (3)	
T2 (1.1 - 2.0 mm)	14 (33)	3 (27)	11 (34)	
T3 (2.1 - 4.0 mm)	12 (28)	2 (18)	10 (31)	
T4 (> 4.0 mm)	11 (26)	4 (36)	7 (22)	
Missing	5 (11)	2 (18)	3 (9)	0.244
Ulceration				
Present	13 (30)	3 (27)	10 (31)	
Absent	16 (37)	5 (46)	11 (34)	
Missing	14 (33)	3 (27)	11 (34)	0.531
Tumor burden				
Microscopic	5 (12)	1 (9)	4 (13)	
Macroscopic	38 (88)	10 (91)	28 (87)	0.761
Nr. excised lymph nodes				
Total (median, IQR)	12 (5 - 17)	9 (2 - 16)	14 (5 - 18)	0.288
Positive (median, IQR)	2 (1 - 5)	2 (1 - 5)	2 (1 - 5)	0.501
Nr. positive lymph nodes				
1	16 (37)	5 (46)	11 (34)	
2 to 3	11 (26)	3 (27)	8 (25)	
> 3	16 (37)	3 (27)	13 (41)	0.410
LNR (median, IQR)	0.33 (0.14 - 0.67)	0.38 (0.10 - 1.00)	0.33 (0.14 - 0.65)	0.555
Extranodal growth				
No	29 (67)	9 (82)	20 (63)	
Yes	14 (33)	2 (18)	12 (37)	0.238

Data are expressed as n (%) unless otherwise specified
Abbreviations: IQR, interquartile range; LNR, lymph node ratio
Significant at $p < 0.05$, calculated using χ^2 test, Mann-Whitney-U test

Immunohistochemical analysis of TIMP3 protein expression

TIMP3 was graded semiquantitatively and staining intensity was scored on a scale of 1-4 as illustrated in Figure 1a. TIMP3 protein was expressed heterogeneously between and within the tumor samples (Figure 1b) and expression was predominantly cytoplasmic and membranous. The median TIMP3 score was 2.0 (IQR, 1.9-2.5). Based on the total immunoreactivity scoring cutoff criteria of 2.4, 11 cases (26%) were classified as high and 32 cases (74%) were classified as low.

a

b
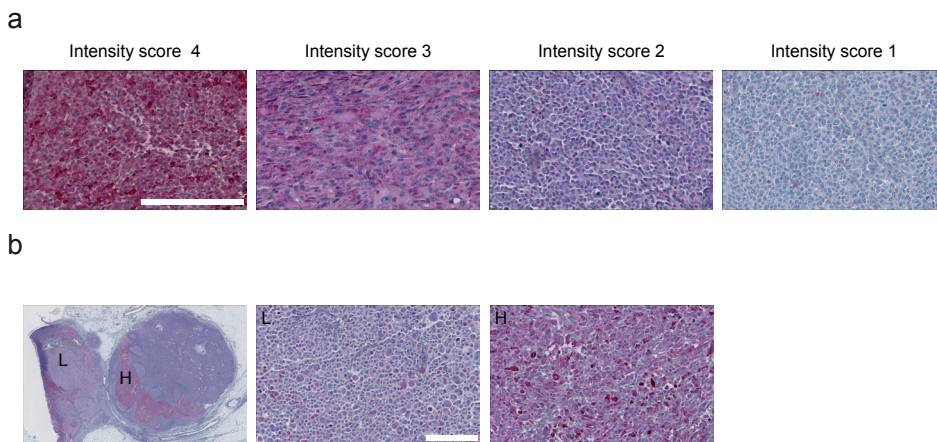
Figure 1. Immunohistochemical staining and scoring of TIMP3 expression. (**a**) Melanoma lymph node biopsies were immunohistochemically stained with polyclonal TIMP3 antibody. Staining intensity was graded semiquantitatively on a scale of 1 to 4, where score 4 represents a strong stain, score 3 represents a clear stain, score 2 represents a weak stain and score 1 represents no staining. Representative images of the intensity scores are shown. Magnification, ×40. (**b**) Overview (×1.25) and magnification (×20) of a tumor showing heterogeneous expression of TIMP3. L, low TIMP3 expression; H, high TIMP3 expression. Scale bars, 200 μm.

Correlation between TIMP3 expression, vessel density and macrophage infiltration

Vessel density and presence of infiltrating macrophages were visualized by staining with CD31 (Figure 2a) and CD68K (Figure 2b) antibodies, respectively. The median CD31 score was 2.5 (IQR, 1.4-3.6) and CD68K score was 2.8 (IQR, 1.7-4.9). Tumors with a high total TIMP3 immunoreactivity score had a lower vessel density (median 1.5; IQR, 1.2-2.2) as compared to cases with a low TIMP3 score (median 2.7; IQR, 1.7-4.0). CD68K abundance did not differ between TIMP3 high (median 2.8; IQR, 1.7-3.4) and TIMP3 low (median 2.9; IQR, 1.7-5.3) samples. Associations between these parameters were evaluated using Spearman's correlation analysis (Figures 2c, d, e and Table 2). We observed a significant inverse correlation between TIMP3 expression and vessel density (correlation coefficient −0.330, $p = 0.031$). A positive correlation was observed between vessel
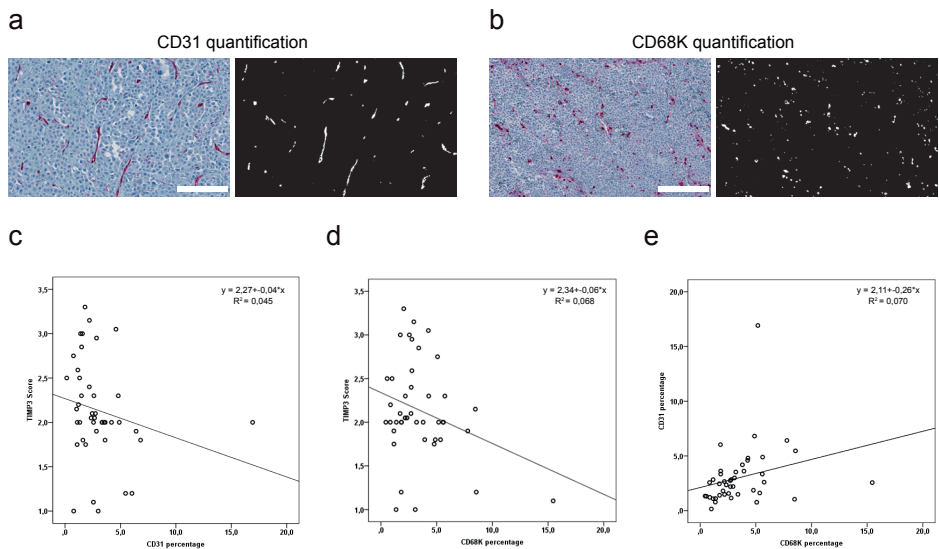
Figure 2. Analysis of blood vessel density and macrophage infiltration. Quantitative analysis of blood vessel density and macrophage infiltration was performed using the Nanozoomer digital pathology platform and Image J as specified in the Materials and Methods section. (**a**) Representative annotated image of CD31 staining and quantification analysis. (**b**) Representative annotated image of CD68K staining and quantification analysis. Scale bars, 200 μm. Correlation analysis of (**c**) TIMP3 expression and vessel density, (**d**) TIMP3 expression and macrophage infiltration, and (**e**) vessel density and macrophage infiltration.

density and macrophage infiltration (correlation coefficient 0.438, $p = 0.003$). However, no significant association was observed between TIMP3 expression and macrophage infiltration (correlation coefficient -0.140, $p = 0.369$).

Table 2. Correlation analysis

		CD31 %	CD68K %	TIMP3 score
TIMP3 score	Correlation Coefficient	−0.330*	−0.140	1.000
	p value	0.031	0.369	
CD31 %	Correlation Coefficient	1.000	0.438*	−0.330*
	p value		0.003	0.031
CD68K %	Correlation Coefficient	0.438*	1.000	−0.140
	p value	0.003		0.369

* Correlation is significant at the 0.05 level (two-tailed)
Statistical test: nonparametric, Spearman's rho test

TIMP3 promoter methylation analysis

The frequency of TIMP3 promoter methylation in the tumor samples was detected by MSP. Adequate DNA was available for 38 cases and the methylation status of TIMP3

promoter was evaluated (Figures 3 a, b). TIMP3 promoter methylation was detected in 18% (n = 7/38) of the cases.

a

b
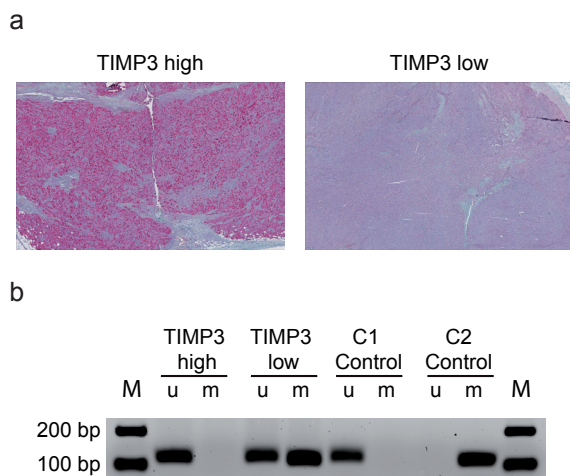
Figure 3. Methylation-specific PCR (MSP). (**a**) Overview images (×2.5) of tumors with low and high TIMP3 expression. (**b**) MSP was performed on DNA isolated from the tumor samples to evaluate promoter methylation status of TIMP3 and PCR products were resolved on 2% agarose gels. M, EZ Load 100 bp Molecular Ruler; u, unmethylation amplification fragment (122 bp); m, methylation amplification fragment (116 bp). Bisulfite converted unmethylated (C1) and methylated (C2) human control DNA were used as controls for MSP.

Clinical correlations

Lymph node positive melanoma (stage III) is extremely heterogeneous and 5-year survival rates can vary depending on the three most important prognostic factors for stage III melanoma which are: (i) microscopic versus macroscopic (palpable) nodal involvement, (ii) the number of involved nodes (1 vs. 2-3 vs. ≥ 4 positive nodes), and (iii) absence vs. presence of ulceration of the primary tumor[4,155]. For microscopic disease only the tumor load in the sentinel node according to the Rotterdam criteria further demonstrates the important spread of 5-year survival rates (50-90%)[10,11,156]. In the current cohort there were no significant differences in any of these prognostic factors (Table 1). Kaplan-Meyer estimated 5-year OS and 5-year DFS did not differ significantly between high and low TIMP3 score: 5-year OS was 36% (SE 1.5%) vs. 25% (SE 7.7%), and 5-year DFS was 30% (SE 1.5%) vs. 25% (SE 7.7%) (Figures 4a, b). A significant difference in OS and DFS was seen for patients with TIMP3 promoter methylation vs. those without methylation; 5-year OS was 0% vs. 32% (SE 8.4%) ($p = 0.034$), and 5-year DFS was 0% vs. 30% (SE 8.4%) ($p = 0.024$) (Figures 4c, d).

a
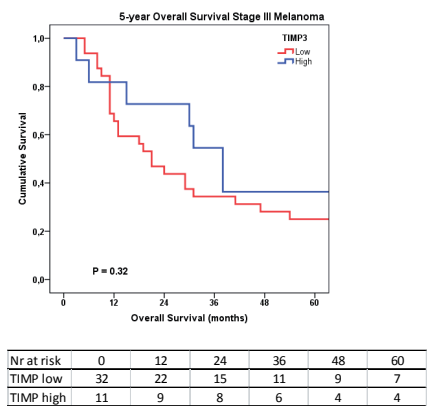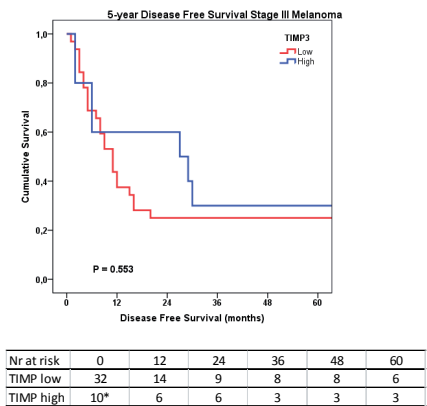
5-year Overall Survival Stage III Melanoma

Nr at risk	0	12	24	36	48	60
TIMP low	32	22	15	11	9	7
TIMP high	11	9	8	6	4	4

b

5-year Disease Free Survival Stage III Melanoma

Nr at risk	0	12	24	36	48	60
TIMP low	32	14	9	8	8	6
TIMP high	10*	6	6	3	3	3

* One patient with missing date of first recurrence

c

5-year Overall Survival Stage III Melanoma

Nr at risk	0	12	24	36	48	60
Meth -	31	22	17	14	11	9
Meth +	7	5	3	0	0	0

d

5-year Disease Free Survival Stage III Melanoma

Nr at risk	0	12	24	36	48	60
Meth -	30*	14	11	9	9	7
Meth +	7	2	0	0	0	0
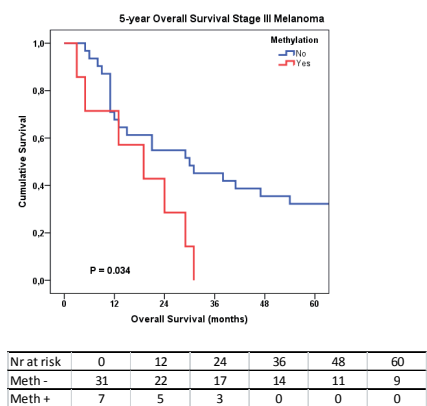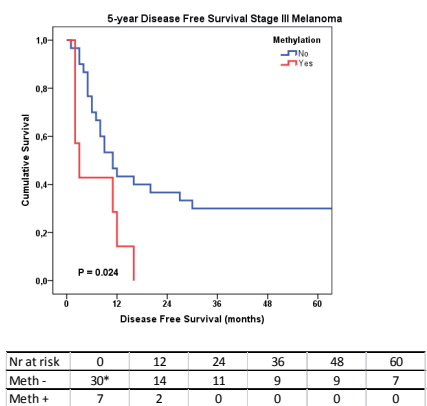
* One patient with missing date of first recurrence

Figure 4. TIMP3 expression and promoter methylation in the prognosis of malignant melanoma. Kaplan Meier curves of overall survival and disease-free survival of patients with tumors expressing (**a,b**) high or low TIMP3 and (**c,d**) methylated or unmethylated gene promoter.

DISCUSSION

Malignant melanomas arise from the neoplastic transformation of melanocytes, and disease progression and metastatic dissemination relies on the angiogenic cascade. Several lines of evidence indicate the importance of angiogenesis in melanoma development, including increased expression of proangiogenic modulators[42] and correlation of angiogenesis to aggressiveness and poor clinical outcome[50]. In addition to tumor secreted angiogenic factors, the tumor stromal environment facilitates tumor growth by functioning as a reservoir of angiogenic ligands. In particular, inflammatory cells such as macrophages have been shown to contribute to tumor angiogenesis and have been linked to disease progression and poor prognosis in several tumor types[157], including melanomas[51-53]. Despite the fundamental role of angiogenesis in melanoma pathophysiology, strategies to combat this attribute have remained relatively unsuccessful with marginal clinical benefits (reviewed in [54,78]). Thus the further identification of relevant molecular targets mediating this vital cascade is essential for the development of successful therapies. This may be of particular importance to prevent progression of micrometastatic residual disease in the adjuvant setting, as would be the case for stage III patients after lymph node dissection.

TIMP3, a member of the TIMP family of endogenous MMP inhibitors, is known to exert tumor-suppressive functions in several human malignancies. These effects are mediated via both MMP-dependent and MMP-independent mechanisms and include inhibition of tumor growth, angiogenesis and invasion. We extended our observations of the inhibitory effect of TIMP3 on the angiogenic cascade in melanoma xenografts[152] to a cohort of lymph node biopsies from stage III melanoma patients. We first evaluated TIMP3 protein expression in our dataset using immunohistochemistry. Intratumoral heterogeneity in TIMP3 expression was observed in the biopsies and this was taken into account for the scoring system. Based on our cut-off criteria, the majority of the lymph node biopsies scored low (74%) on the total immunoreactivity score. These results are in accordance with the reduced expression of TIMP3 reported in in other human malignancies with high-grade tumor phenotype[146,153,158] and suggest that the loss of TIMP3 expression is an important event in melanoma progression and pathogenesis.

Several reports indicate that TIMP3 functions as a dominant negative regulator of angiogenesis and these effects are thought to be mediated by the ability to inhibit VEGF-VEGFR2 signaling[121]. We and others have shown that TIMP3 inhibits endothelial cell migration and tube formation, and enforced expression or viral delivery reduces neovascularization and macrophage infiltration in various tumor xenografts[117,120-122,127,150,152]. We analyzed blood vessel density in our patient set and observed a significant inverse correlation with TIMP3 expression. The presence of infiltrating macrophages has previously been described to correlate with blood vessel density in melanomas[51,52], and we observed

a significant correlation in our cohort. As TIMP3 has been shown to inversely correlate with infiltrating macrophages in xenograft models[127,152], we also explored the possible correlations between these parameters. In our dataset we did not observe a significant correlation between tumor infiltrating macrophages and TIMP3 expression. Of note, in this study we used the pan-monocyte/ macrophage marker CD68K which does not discriminate between pro-inflammatory M1 macrophages and anti-inflammatory M2 macrophages. It might be of interest to evaluate potential associations between infiltrating macrophage subsets and TIMP3 expression.

As loss of expression of TIMP3 has been attributed to gene promoter hypermethylation in several tumor types, we evaluated the methylation status of the TIMP3 promoter in our dataset. Our results show that methylation associated silencing of TIMP3 is a low frequency event in melanomas (7/38; 18%). These results are in accordance with a previous study where promoter methylation gene profiling analysis of melanoma cells and tumors revealed TIMP3 promoter methylation to be a low frequency event[128]. As promoter methylation alone does not explain the low levels of TIMP3 protein expression, alternate mechanisms of loss of expression have been suggested, such as the post-transcriptional regulation by miRNAs. A recent study by Martin del Campo et al. reports reduced TIMP3 expression upon overexpression of miRNA-21 in melanoma cell lines, suggesting an alternate mode of TIMP3 expression regulation[159].

Finally, we explored the clinical relevance of reduced TIMP3 expression in melanomas. TIMP3 expression did not show any association with the analyzed clinicopathological variables for Stage III melanoma. We did not observe differences in 5-year DFS or OS between high and low expression samples. Interestingly, when classified based on promoter methylation status we found that patients with methylated TIMP3 promoter experienced significantly shorter 5-year DFS and OS compared to patients without methylation. Although these results suggest that promoter methylation status of TIMP3 could have value as a prognostic marker in cutaneous melanomas, it is important to bear in mind that the total number of patients at risk in the current study is very low. Thus larger studies need to be conducted to ascertain TIMP3 promoter methylation as a truly significant prognostic factor in melanoma.

Collectively, our results suggest a tumor suppressor role of TIMP3 in melanoma pathogenesis. Reduced TIMP3 expression was observed in the majority of stage III melanoma cases studied and protein expression inversely correlated with mean vessel density. Although promoter methylation was detected in only 18% of the samples analyzed, this epigenetic regulation seemed to impact outcome. Our results suggest that promoter methylation may not be the only mechanism responsible for reduced protein expression and thus other modes of gene inactivation, such as post-transcriptional regulation by microRNAs, need to be investigated.

ACKNOWLEDGEMENTS

4

SECTION II

Metastatic cascade in malignant melanoma

CHAPTER 5

A ring barrier-based migration assay to assess cell migration *in vitro*

Asha M. Das, Alexander M.M. Eggermont, Timo L.M. ten Hagen

ABSTRACT

Cell migration is a key feature of virtually every biological process and can be studied in a variety of ways. Here we outline a protocol for the in vitro study of cell migration using a ring barrier-based assay. A 'barrier' is inserted in the culture chamber, which prevents cells from entering a defined area. Cells of interest are seeded around this barrier, and after the formation of a peripheral monolayer the barrier is removed and migration into the cell-free area is monitored. This assay is highly reproducible, convenient to perform and allows deduction of several parameters of migration, including total and effective migration, velocity and cell polarization. An advantage of this assay over the conventional scratch assay is that the cells move over an unaltered and virgin surface and thus the effect of matrix components on cell migration can be studied. In addition, the cells are not harmed at the onset of the assay. Through computer automation 4 individual barrier assays can be monitored at the same time. The procedure can be used in a 12-well standard plate allowing higher throughput, or modified to perform invasion assays. The basic procedure takes 2-3 days to complete.

INTRODUCTION

Cell migration is indispensable to a wide variety of biological processes and is key to the regulation of embryogenesis as well as physiological and pathological conditions in the adult organism[160]. It is a multi-step process orchestrated by complex interactions involving soluble guidance cues, the microenvironment and the genetic composition of the cell. Under favorable conditions, cells polarize asymmetrically to generate well-defined leading and trailing ends. Migration ensues, aided by the formation of membrane protrusions, adhesive interactions and accompanying cytoskeletal changes[161,162]. Fundamentally, cell motility can be attributed to intrinsic directionality of migration or the inherent propensity of cells to migrate in a single direction upon uniform application of a motogenic stimuli (chemokinesis), or chemotaxis, which is motility in response to a chemical gradient[104]. Cells can polarize in the absence of graded stimuli and undergo directionally persistent migration. Such events are observed during development[163], tissue remodeling[108] and metastatic dissemination of tumor cells and indicate interactions with the surrounding matrix.

Commonly used cell migration assays

Traditionally, cell migration (intrinsic directionality) has been evaluated using the scratch assay or wound healing assay which involves the application of a wound to a monolayer of cells and subsequent monitoring of the duration it takes to fill up the wound. Although inexpensive, convenient to perform and relevant in studying regeneration and wound healing, the scratch assay is obscured by cell proliferation, omits the capacity of the cell to follow other cells, ignores the modifications cells make to the matrix or surface, and in most settings provides only start and endpoint monitoring[164,165]. A number of cell migration assays have been developed which use a bio-compatible gel or agarose droplet[166,167], a Teflon ring[168] or a Flexiperm-Disc[169]. Commercially available cell migration assays employ the use of solid stoppers or biocompatible gels which generate a cell-free area but might modify the matrix. Most such assays also require live cell compatible dyes or labels and quantification is based on relative fluorescence. Additionally assays such as the Boyden chamber, despite generating a gradient for chemotactic migration, cannot be used to visualize the migratory process in real time[170]. Taking these restraints into account, we developed a ring-barrier based migration assay which implemented a number of improvements[123].

Overview of the ring-barrier based migration assay

The migration assay we employ is based on a so called 'barrier' (inserted in an Attofluor cell chamber or a 12-well cluster plate) which prevents cells from entering a defined area. This area can be provided with an extracellular matrix (ECM) coating which is not af-
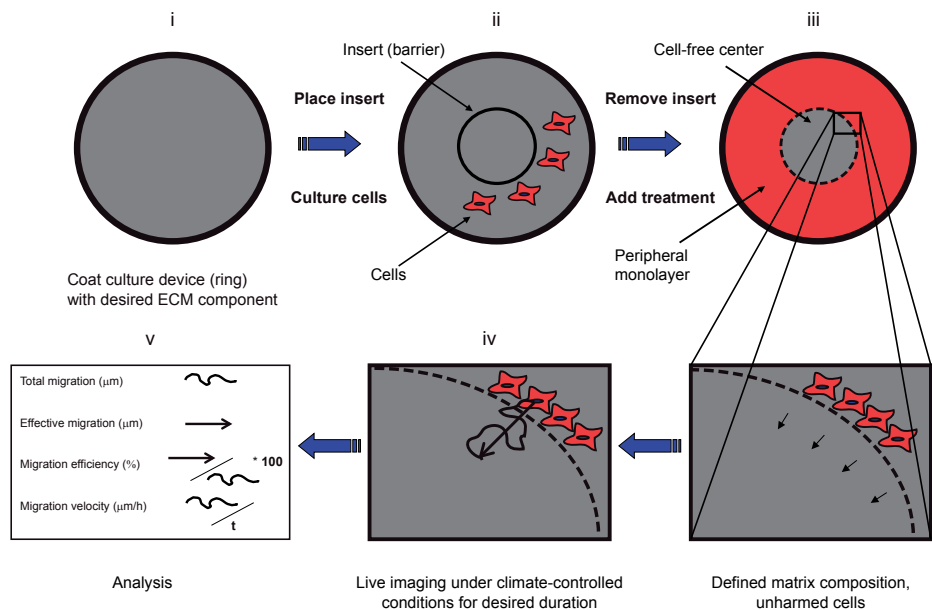
Figure 1. Ring barrier-based migration assay. Schematic overview of the ring-barrier based two dimensional migration assay; (i) the migration chamber is coated with the extracellular matrix (ECM) to be tested, (ii) the barrier is placed and cells are seeded around this area, (iii) upon confluency, the barrier is removed which results in a peripheral monolayer and a cell-free center. The desired treatment is added and (iv) live imaging commenced under climate controlled conditions for desired durations. (v) Parameters of migration can be calculated from the acquired images.
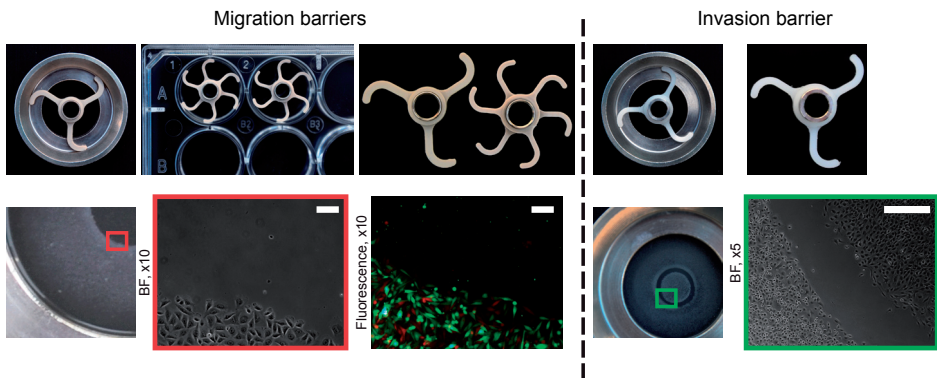
Figure 2. Ring barrier configurations. Images of ring-barrier configurations to monitor single population, co-culture migrations or invasion assays. Migration barriers, top panel: Migration barrier in an Attofluor cell chamber or 12-well plate and individual migration barriers for Attofluor cell chamber or 12-well plate; bottom panel: cell monolayer in migration ring after removal of barrier, zoomed in detail of cell monolayer with the border indicated by the red box and fluorescent image of a co-culture assay with a mixed population of red and green fluorescent cells. Invasion barrier, top panel: Invasion barrier in an Attofluor cell chamber and individual invasion barrier; bottom panel: cell monolayer after removal of the invasion barrier and zoomed in detail showing the cell free area with the border indicated by the green box. Scale bars indicated are 100 μm. BF, Bright-field.

fected by cells prior to the onset of migration, is native and precisely controlled. Cells of interest are seeded around this barrier and following the formation of a peripheral mono-layer, the barrier is removed and migration into the cell-free area is monitored (Figures 1 and 2, Supplementary Video 1, Supplementary Figures 1 and 2, Supplementary Manuals 1 and 2, and Supplementary Data 1-4). The general procedure for the ring-barrier based migration assay is listed in Figure 3 and takes 2-3 days to complete. Integration of the climate-controlled migration chamber with a computer-controlled microscope, equipped with a camera and a motorized stage, enables continuous monitoring of migration under multiple treatment conditions per experiment and multiple positions within a treatment for any desired duration (Figure 4 and Supplementary Figure 3).

The assay can be used to visualize morphological changes such as polarity of individual cells and interaction between cells in response to treatment (Figure 5). Importantly, the cells and the matrix are unharmed which is not the case with the scratch assay (Figure 6). The barrier configuration in conjunction with time-lapse imaging enables the quantitative assessment of several parameters with relative ease. From the acquired sequence, cells at the migration front can be tracked individually and the following parameters, in response to ECM substrates or treatments, can be deduced: total migration, which is the whole track movement of individual cells including possible detours; effective migration, which is the straight line between start and end positions showing net displacement; migration efficiency, which is the ratio of effective and total distance; migration velocity and cell polarization (Figures 5 and 6, and Supplementary Videos 2 and 3). The set-up can be modified to include live acquisition of fluorescence, thus expanding the applicability to include visualization of tagged proteins and mixed (co-culture) migrations with different cell populations (Figure 7a). The assay has also been expanded to a 12-well system for higher throughput. Additionally, the barrier insert has been modified (thickness, 1 mm) to monitor heterotypic interactions in 2D invasion assays, such as the invasion of tumor cells into a fibroblast culture. In this application cells are seeded outside as well as inside of the barrier (Figure 7b). Alternatively or in addition, cells can be fixed at any point during migration for subsequent immunofluorescent assessment of cytoskeletal components (Figure 8).

Applications of the ring-barrier migration assay

Cell migration is a key feature of virtually every biological process and the ring-barrier assay offers the possibility to quantitatively assess the migratory profile of any adherent cell line in the context of development, immune surveillance, gap closure, vascular disease, chronic inflammatory diseases, and tumor formation and metastasis, among others. This assay can be easily adapted to different applications, such as testing the contribution of different genes to the migratory process[171] (genetic manipulation such as transient, inducible and stable gene silencing/overexpression), deciphering stimulators

Day 0:
Steps 1-2

Preparation of migration
chambers

ECM coating

Cell chamber format
12-well format

Day 0:
Steps 3-7

Seeding cells

Single population
Dual population
Invasion

Day 1:
Steps 8-10

Adding treatments

Growth factors, inhibitors, drugs

Day 1:
Steps 11-14

Time-lapse imaging

Brightfield
Fluorescence
Confocal

Day 2-3:
Steps 15, 16

Immunofluorescence staining
and imaging

Fixed, fluorescence

Steps 17-19

Cleaning and sterilization

Step 20

Quantification

Total migration
Effective migration
Migration efficiency
Migration velocity
Cell polarization

Figure 3. Flow diagram of the general protocol with the time course, the main steps in solid boxes and the options in dotted boxes.
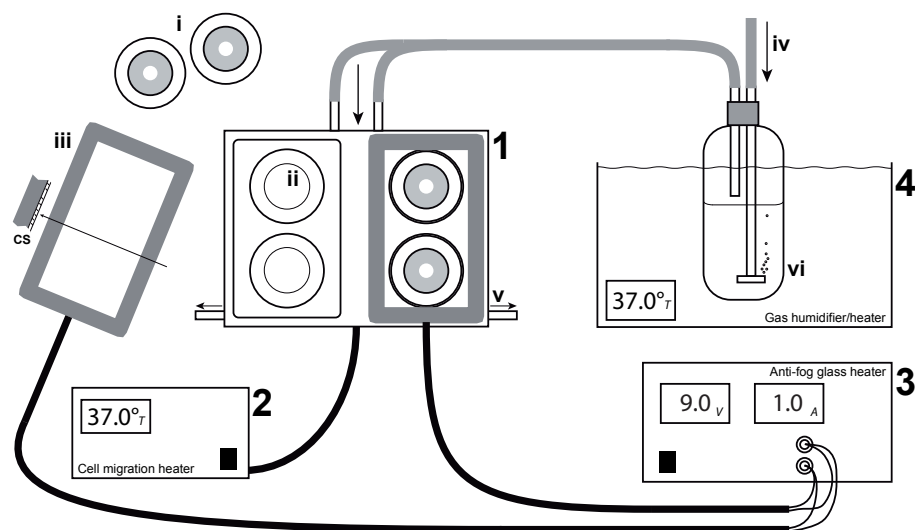
Figure 4. Cell migration unit and configuration. Schematic overview of the cell migration unit (1) which maximally holds four cell chambers (i). On the right side of the unit two cell chambers are shown in place. The grey area represents chambers with a central free space. On the left side (ii) two cell chambers need to be inserted. The migration unit is electrically heated with the Cell migration heater (2) which can be set to a desired temperature. After the migration chambers are placed, the migration unit is closed with the two glass windows (iii) which are fixed to a heating frame. See cross section (CS) showing the heating frame in grey attached to the glass window. The temperature of the frames can be controlled with the Anti-fog glass heater (3) which prevents condensation. After the unit is closed it is connected to the Gas humidifier/heater (4). A proper mixture of gas (generally 5% CO_2 / 95% air) is used which is humidified and heated (iv). The gas enters the Cell migration unit at the arrow and is vented through the exit ports (v). The flow should be adjusted based on the air bubbles observed (vi). A relatively slow bubble rate is often enough to maintain proper air mixture above the cells.

and inhibitors of migration[152,172], molecular regulation of migration[173-176] and the effect of small-molecule drugs.

Limitations of the ring-barrier migration assay

The primary limitations of the ring-barrier based assay include the inability to monitor chemotaxis, as a chemical gradient cannot be applied under this setting, and the inapplicability to non-adherent cells. While under a number of physiological conditions cells migrate along two dimensional surfaces comparable to the migration assay, the assay is not suitable for evaluating physiological cell dispersion events under the influence of complex microenvironments, such as the amoeboid movement demonstrated by cells while invading through a matrix.
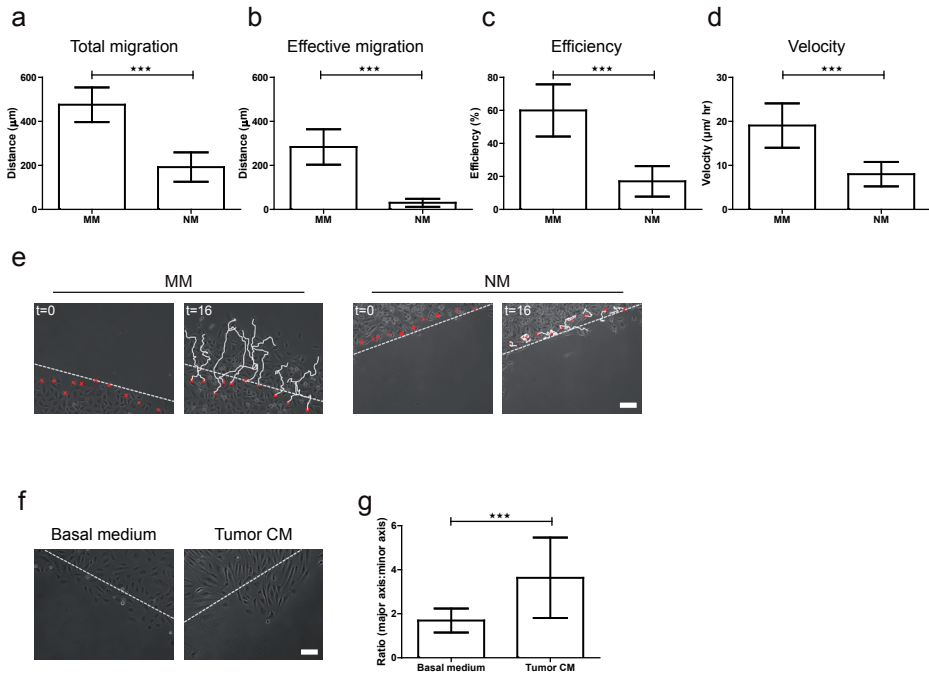
Figure 5. Migratory parameters. (**a-e**) Metastatic (MM) and non-metastatic (NM) melanoma cells (2×10^5) were cultured in migration chambers coated with fibronectin. Upon barrier removal, cells were supplemented with fresh culture medium. Migration was monitored for 16 h using time-lapse microscopy and 3 independent experiments were performed. 10 cells were tracked in each individual experiment. (**a**) Total distance of cell migration (μm) in 16 h. (**b**) Effective migrated distance (μm) per cell in 16 h. Effective migration represents the directionality of cell movement (straight line path, perpendicular to the migration front, towards the cell free center). (**c**) Migration efficiency (%) was obtained by dividing the effective distance by the total distance. (**d**) Migration velocity (μm/h) was calculated by dividing the total distance of migration by the duration of the migration assay (16 h). Data in panels a-d were analyzed using non-parametric two-tailed Mann-Whitney test and represent mean ± SD of three independent experiments. ***$p < 0.0001$. (**e**) Representative pictures of migrating cells at start (t = 0 h) and end (t = 16 h) positions of the migration assay with track overlay. Dotted white lines indicate the migration front at t = 0 h, the red crosses represent the cells used for quantification and the white lines represent the trajectories assumed by individual cells during the course of 16 h. Images were obtained from Supplementary Videos 2 and 3. Scale bar, 100 μm. (**f**) Images of endothelial cells (ECs) in response to treatment with basal medium or tumor conditioned medium (CM) at 12 h of migration. Note polarized morphology of cells treated with tumor conditioned medium. Scale bar, 100 μm. Cell polarity (**g**) is expressed as a ratio of the length of the major axis to the minor axis of individual cells at the migration front. 10 cells each from three different experiments were used for analysis and data are expressed as mean ± SD ***$p < 0.0001$.
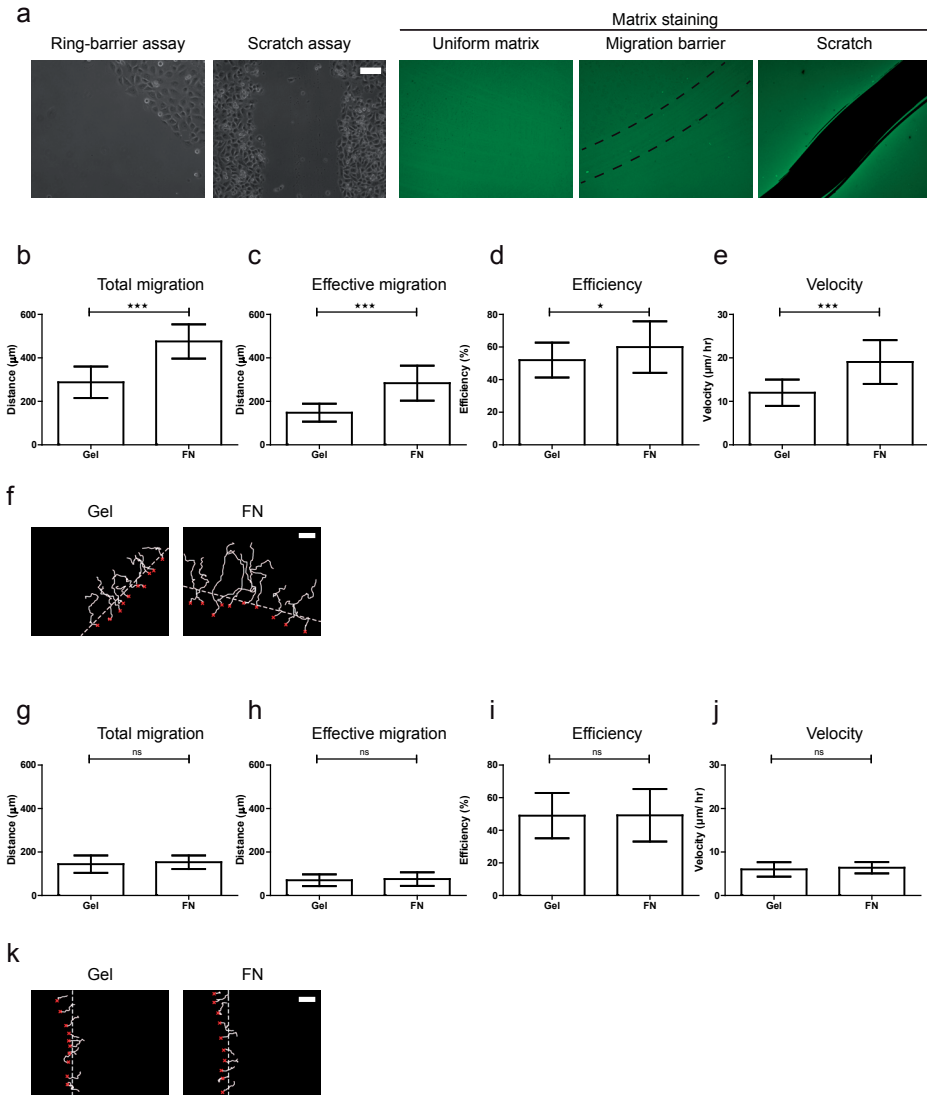
Figure 6. Migratory responses to ECM coatings. Metastatic melanoma (MM) cells (2×10^5) were cultured in migration chambers with a migration barrier or grown to confluence for a scratch assay. Coverslips were coated with gelatin (Gel; 1 mg/mL) or fibronectin (10 μg/mL). Migration and scratch assays were performed for 16 h and cells were tracked for quantitative parameters. (**a**) Images of the migration front in the respective migration assays. Representative matrix stainings of coverslips coated with fibronectin illustrate an unharmed matrix upon removal of the migration barrier while significant damage is observed upon introducing a scratch wound. Dotted black lines indicate the region where the migration barrier was placed. Migratory parameters and representative track diagrams derived from a ring-barrier migration assay (**b-f**) and a scratch assay (**g-k**). Dotted white lines indicate migration front at t = 0 h, the red crosses represent tracked cells and the white lines represent migratory trajectories. Data in panels (b-e and g-j) were analyzed using non-parametric two-tailed Mann-Whitney test and represent mean ± SD of three independent experiments. 10 cells were tracked in each individual experiment. ***$p < 0.0001$, *$p < 0.05$, ns= not significant. Scale bars, 100 μm.

EXPERIMENTAL DESIGN

Choice of migration chambers and migration set up. Depending on the experimental question, the ring-barrier assay can be performed using the single or the 12-well chamber format to monitor cell migration or invasion (Figure 2). The migration unit (Figure 4 and Supplementary Figure 3) is relatively easy to setup. For standard migration experiments, with the benefits of the ring-barrier assay, the 4 position cell migration unit is a good choice. It is important to always run a control cell chamber to check that all conditions are optimal: temperature stability during the experiment, and minimal evaporation or condensation of medium. We routinely use a ×10 objective lens and bright field phase contrast for imaging cell migration which are analyzed manually. When labelled cells are used with a bright and localized fluorescent marker, either the whole cell or the fluorescent component can be tracked. Software capable of tracking individual cells can subsequently be applied.

Choice of matrix. As a starting point any adherent cell line can be used with its usual growth conditions. The optimal seeding densities should be determined prior to commencing large scale experiments. It is important to check the compatibility of the chosen cells with the matrix substrate being used. As the ring-barrier migration assays will detect the impact of matrix coating (Figure 6), the choice of coating is crucial. Select the coating which fits the experimental question or try different coatings for the optimal result.

Image acquisition. If detailed imaging at high magnification is required, the best option is to use the single migration unit. When oil immersion lenses are used, changing between cell chambers is not advised. The objective lens will function as a heat sink generally resulting in lower temperature in the focus area and consequently poor migration performance. This type of imaging is particularly used when looking for instance at cytoskeletal activities. Because of the high magnification, the cell will quickly move out of focus and the imaging area. Determine the migration speed of the cells and accordingly adjust the time span of imaging. In principal the ring-barrier migration setup can be applied to any inverted microscope; bright field, white light fluorescence, or confocal. In every setting it is crucial to determine whether continuous imaging affects cell behavior. The energy from the light source might adversely affect cellular responses. When continuous imaging is performed in a fluorescence setting, check for phototoxicity and bleaching. It is advised to first run a number of control cell chambers and image cell migration at low magnifications before moving to more demanding settings.

Basic immunofluorescence stainings. In general it is recommended to perform immunofluorensense stainings in the 12-well migration chamber format as several treatments can be processed simultaneously and staining with the Parafilm method requires smaller quantities of reagents and is more economical. However, if the cells being analyzed are limited, stainings can be performed in cell chambers.

Controls. Experimental variables must be considered and controlled for to minimize inter-assay variations.

- Cell proliferation. Long durations of time lapse imaging will inevitably result in cell proliferation. Where treatment affects proliferation significantly, image migration for shorter durations. Record growth profiles of tested cells using cell proliferation assays.
- Serum concentration. Serum concentrations in culture medium during migration will affect cell proliferation. Reduce serum concentrations if necessary.
- Vehicle controls. For all treatments added to culture medium for migration assays, appropriate mock or vehicle controls should be performed.

Materials

Reagents

- Primary or tumor cells of interest, e.g. endothelial cells (ECs), fibroblasts, human breast cancer cells
- Medium usually used to grow cells of interest, e.g. Dulbecco's modified Eagle's medium with 4,5 g/L glucose and L-glutamine (Sigma, cat.no. D0819)
- Trypsin EDTA (200 mg/mL Versene, 170,000 U/L Trypsin; Lonza, cat. no. BE-17-161E)
- Penicillin-streptomycin (10,000 U/mL penicillin, 10,000 U/mL streptomycin; Lonza, cat. no. DE-17-602E)
- PBS (Dulbecco's Phosphate Buffered Saline, suitable for cell culture; Sigma, cat. no. D8537)
- FBS (EU approved fetal bovine serum; Sigma, cat. no. F7524)
- Fibronectin (Roche, cat. no. 10838039001)
  ▲ CRITICAL This and the other ECM substrates (gelatin, collagen and laminin) are optional.
- Gelatin Type B from bovine skin (Sigma, cat. no. G9391)
- Collagen type I, tat tail (Millipore, cat. no. 08-115)
- Laminin from human placenta (Sigma, cat. no. L6274)
- Paraformaldehyde (Sigma, cat. no. P6148)
  ! CAUTION Toxic; flammable solid
- Methanol (Sigma, cat. no. 32213)
  ! CAUTION Toxic; highly flammable liquid and vapor
- Ethanol absolute (Sigma, cat. no. 24102)
  ! CAUTION Highly flammable liquid and vapor
- NaOH, ACS reagent (Sigma, cat. no. **30620**)
  ! CAUTION Corrosive
- EGTA (Ethylene glycol-bis(2-aminoethylether)-*N,N,N',N'*-tetraacetic acid; Sigma, cat. no. E4378)

- Phosphate Buffered Saline Dulbecco 'A' Tablets (Oxoid, cat. no. BR 00144)
- Triton X-100 solution, Bioultra for molecular biology (10% in H_2O; Sigma, cat. no. P93443)
- Tween 20, for molecular biology (Sigma, cat. no. P9416)
- Bovine Serum Albumin (BSA; Sigma, cat. no. A9418)
- Alexa Fluor® 568 Phalloidin (Life Technologies, cat. no. A12380)
- Primary antibody against cytoskeletal component of interest, e.g. anti-vinculin, anti-tubulin
- Species specific conjugated secondary antibody, e.g. Donkey anti-Mouse Alexa Flour® 488
- DAPI (4′,6-Diamidino-2-Phenylindole, Dilactate; Molecular Probes®, Life Technologies, cat. no. D3571)
- Fluoromount G (Southern Biotech, cat. no. 0100-01)
- Immersol™ Immersion oil (Carl Zeiss, cat. no. 12-070-397)

Equipment

- Attofluor® Cell Chamber, for microscopy (Molecular Probes®, Life Technologies, cat. no. A-7816)
- Migration barrier inserts
- Decker glass 25 mm round coverslips #1 (thickness 0.13-0.16 mm; Menzel-Glaser cat. no. CB00250RA1)
- Decker glass 18 mm round coverslips #1 (thickness 0.13-0.16 mm; Menzel-Glaser cat. no. CB00180RA1)
- Decker glass 55 mm round coverslips #1 (thickness 0.13-0.16 mm; Menzel-Glaser cat. no. CB00550RA1)
- Cell star dish, 100×20 mm (Greiner bio-one cat. no. 664160)
- 12-well cluster plates (Greiner bio-one cat. no. 665180)
- Steriking R-flat sterilization roll (Wipak Oy cat. no. R42)
- Parafilm M (Sigma, cat. no. P7793)
- Pointed forceps
- Glass slides
- Laminar flow tissue culture hood
- Falcon tube
- Eppendorf tube
- Hemocytometer
- Inverted microscope with electronic table (Phase-contrast, fluorescence with electronic table e.g. AxioVert 100M or similar)
- Camera (AxioCam or similar)
- Stage incubator

- Water bath with gas wash bottle
- CO_2 supply
- Image analysis software (AxioVision image analysis module or similar)

Reagent setup

Fibronectin, 10 µg/mL Prepare a stock solution of 1 mg/mL with sterile water (see manufacturers' instructions) and store reconstituted solution in aliquots at −20°C until the expiry date. Avoid repeated freeze-thaw cycles. For coating migration chambers, dilute with sterile PBS to a working concentration of 10 µg/mL. Working concentration solutions can be stored at 4°C for 2 weeks.

Gelatin, 1 mg/mL Dissolve 500 mg gelatin in 500 mL PBS overnight at 37°C. Filter sterilize using Stericup vacuum filtration systems and store at 4°C for up to 1 year.

Collagen, 50 µg/mL Freshly dilute collagen stock solution with sterile PBS to a working concentration of 50 µg/mL.

Laminin, 10 µg/mL Slowly thaw laminin at 4°C and freshly dilute with sterile PBS to the working concentration. Undiluted laminin can be stored in aliquots at −70°C until the expiry date. Avoid repeated freeze-thaw cycles.

PBS, 1× Dissolve 10 tablets in 1 L of distilled water and sterilize by autoclaving at 115°C for 15 min. Store indefinitely at room temperature (22-25°C).

PFA, 4% w/vol Warm 500 mL 1× PBS in the microwave and add 200 µl of 5 M NaOH to the PBS. Pour the PBS onto 20 g of PFA in a conical flask . Stir vigorously to dissolve and upon cooling add 75 µl concentrated HCl (37%). The pH should be 7.4; check and adjust if necessary. Store in aliquots at −20°C for up to 3 months. Defrost before use and refreeze leftover PFA only once.

! CAUTION Wear face mask, gloves and work in a fume cabinet

Methanol/1 mM EGTA Prepare 0.5 M EGTA in water and adjust the pH to 8.0. Chill methanol at −20°C for 20 min and immediately before use add EGTA to a working concentration of 1 mM.

Tween-20, 10% vol/vol Dilute Tween-20 with 1× PBS and leave on a rotary shaker overnight to dissolve. Store indefinitely at room temperature (22-25°C).

PBT buffer, 1% BSA w/vol Freshly dissolve 100 mg BSA in 10 mL 1× PBS and add 0.05% Triton X-100 (vol/vol).

Equipment setup

Migration barriers and chambers: The barrier is a cylinder made of surgical stainless steel and is kept in position by a three legged spacer made of polyether ether ketone (PEEK). The cylinder and spacer are fitted together as one part. The dimensions of the cylinder for the migration barrier are: outer diameter of 6 mm, thickness of 0.5 mm and length of 12 mm. The cylinder wall is tapered resulting in a thickness of 0.15 mm at the

end (Supplementary Figure 1 and Supplementary Manual 1). The 12-well plate barrier has the same dimensions but is 17 mm long. The invasion barriers have similar dimensions except the outer diameter of the cylinder is 7 mm, thickness is 1 mm and the ends are 0.8 mm (Supplementary Figure 2 and Supplementary Manual 2). Supplementary Data 1-4 are STEP and IGS files of the migration and invasion barriers which can be used with any compatible CAD (computer-aided design) software package such as SolidWorks and AutoCAD and facilitate automated construction. If resources/facilities are not available to produce the barrier on site, barriers will be provided on request. The barriers fit tightly in the appropriate migration chamber. The Attofluor cell chamber consists of two parts. Place a coverslip glass (~0.16 mm thick, 25 mm diameter) in the lower part and subsequently assemble with the top part. After a migration experiment, clean the barriers and cell chambers with warm water and ethanol and autoclave for reuse.

Cell migration unit: This unit is electrically heated and connected to a temperature controller. The unit is made of black coated aluminum. Switch on the heating of the cell migration unit and set it to the right temperature. Check with a control cell chamber if the target temperature (generally 37°C) is reached. Adjust if necessary. Transport the prepared migration chambers from the incubator to the microscope in the sterile Petri dish. Insert the migration chambers in the slots. It is crucial that cell chambers fit tightly to allow heat transfer and to prevent shifting of the cell chamber during movement. Cover the cell chambers with glass plates which are heated independently to prevent condensation. This anti-fog system is crucial, as bright-field imaging is negatively affected by water droplets in the light path.

Climate control: Connect the cell migration unit to the temperature unit. Switch this unit on and set it to 37°C well before the experiment. When possible, leave the system running and only switch it off when it is not used for longer periods. Set the flow of air/CO_2 mixture by using a water bath with a gas wash bottle connected to a cylinder with 5% CO_2/air mixture. The flow rate can be adjusted based on the formation of air bubbles in the gas wash bottle. The flow rate should be set to low, i.e. minimum rate of air bubble formation, to prevent evaporation of medium in migration chambers.

Inverted microscope: A standard inverted microscope is enough for single migration. Set up the microscope and migration experiment in a space with minimum temperature changes, prevent activities and movements around the setup and use a sturdy or (air) stabilized table. When multiple migrations are done at the same time and/or multiple spots in the cell chamber need to be monitored, the microscope needs an electronic table with x, y and z adjustment controlled by software. Use a ×10 (or if needed ×20) dry objective lens. Image one chamber (one position) at a time when an oil immersion objective lens is used. When an oil or water immersion objective lens is used, the objective lens needs to be heated as well. Set the software to adjust per location for z (i.e. let the microscope focus at every location). Some software packages provide autofocus or focus correction

modules. Check your system with control cell chambers to determine whether the focus plane shifts during heating. It is advised to leave the system on for two-three hours for acclimatization prior to starting image acquisition.

Fluorescence microscopy: Fluorescence provide additional opportunities and possibilities. Insert the cell migration unit and connect heating and air-flow as described above. Either use an automated shutter to cut off the light in between images or move the cell migration unit to a position where the cells are not exposed to the light.

Imaging: When using bright field set the camera to gray scale. Set the halogen light on the microscope low (i.e. 2 V) to prevent heat emitted from the light source from affecting the temperature in the cell migration unit. This is possible as only little light is needed when imaging in the grey scale mode. Apply a heat filter in the light path if available.

Imaging software: We routinely use the AxioVision Image Acquisition software which generates images in ZVI format and the AxioVision Image Analysis module for quantification of cell migration. Other comparable software packages may be used.

Procedure

Preparation of migration chambers (day 0) ● TIMING 5 min for 8 cell chambers

1. Prepare chambers for migration or invasion studies by placing a sterile 25 mm coverslip within the bottom section of a sterile Attofluor cell chamber. Subsequently, fasten the top section of the cell chamber to generate a sealed cell incubation ring. Alternatively, for high throughput studies, place a sterile 18 mm coverslip in each well of a 12-well cluster plate.

Coating of migration chambers with ECM substrates (optional) (day 0) ● TIMING 1 h

2. Coat the coverslip with 500 μL of the chosen ECM substrate (gelatin/collagen/laminin/fibronectin) under study and incubate the migration chambers for 1 h at 37°C.

▲ CRITICAL STEP Concentration of matrix components can influence migration and must be evaluated prior to large scale experiments.

Preparation of cell suspensions (day 0) ● TIMING 15-30 min

3. Culture adherent cells routinely with appropriate tissue culture medium. Harvest subconfluent cells by trypsinization and determine cell count using a hemocytometer. Pellet cells and prepare optimal dilutions for single population cell migration (option A), dual population cell migration (option B) or invasion (option C) studies.

▲ CRITICAL STEP The amount of cells required to obtain a confluent monolayer in the migration ring varies from cell line to cell line. For comparisons among cells lines and treatments within the same cell line, it is important to seed the same number of cells for the assay.

▲ CRITICAL STEP Cell numbers in the range of $2–4 \times 10^5$ per migration chamber usually generates a peripheral monolayer in 24 h. A quick and reliable way to optimize

concentrations for a cell line is to seed a range of cell numbers ($1–5 \times 10^5$ cells) onto 18 mm coverslips coated with the ECM component of interest, in a 12-well cluster plate (growth area of 18 mm coverslips = 2.54 cm^2; effective growth area of the assembled migration ring with a cover slip = 2.68 cm^2; growth area of the barrier = 0.19 cm^2). The concentration that yields a confluent peripheral monolayer in the desired duration can be chosen for migration assays. For invasion studies, cell numbers in the inner chamber usually range from $1–2 \times 10^4$ cells and must be optimized.

(A) Cell suspensions for single population migration assays

(i) Resuspend harvested and pelleted cells to a concentration of 1×10^6 cells/mL in culture medium.

(ii) Add 700 μL of fresh culture medium to a sterile 1.5 mL Eppendorf tube.

(iii) To this tube, add 400 μL of cell suspension (1×10^6 cells/mL) as prepared above. The tube thus has a total amount of 4×10^5 cells in a final volume of 1100 μL and can subsequently be used to seed two migration chambers.

(B) Cell suspensions for dual population migration assays

(i) Separately resuspend both harvested cell lines to a concentration of 1×10^6 cells/mL in culture medium.

(ii) Add 700 μL of fresh culture medium to a sterile 1.5 mL Eppendorf tube.

(iii) Add 200 μL of each cell suspension (1×10^6 cells/mL) as prepared above. The tube thus has a total amount of 4×10^5 cells in a final volume of 1100 μL and can subsequently be used to seed two migration chambers.

(C) Cell suspensions for invasion assays

(i) Harvest and pellet both cell lines of interest for the invasion assay.

(ii) Resuspend the cells to be seeded in the area peripheral to the barrier to a concentration of 1×10^6 cells/mL in culture medium.

(iii) Add 700 μL of fresh culture medium to a sterile 1.5 mL Eppendorf tube.

(iv) To this, add 400 μL of the cells to be seeded peripheral to the barrier (1×10^6 cells/mL). The tube thus has a total amount of 4×10^5 cells in a final volume of 1100 μL and can subsequently be used to seed two migration chambers.

(v) Resuspend the cells to be seeded within the barrier to a concentration of 1×10^5 cells/mL in culture medium.

Placing migration barriers and cell seeding (day 0) ● TIMING 20 min for 8 cell chambers

4. Remove the coating substrate by suction and if applicable, air dry the migration rings followed by two washes in sterile PBS.

5. Gently insert a sterile migration barrier corresponding to the configuration of the migration chamber in use, ensuring the barrier makes contact with the coverslip tightly without breaking the glass.

▲ CRITICAL STEP Forcefully pressing down the barrier may cause the coverslip to break and/or damage the ECM coating. Gently press down the barrier using two spacers at a time to establish contact with the coverslip. Invert the ring chamber and check for optimal barrier placement.

6. Seed the cell suspensions prepared in step 3 for migration (option A) or invasion assays (option B).

(A) Seeding cells for migration assays

(i) Simultaneously, suspend 530 μL of the cell suspension in the area peripheral to the barrier and 200 μL of tissue culture medium in the center of the barrier. If the suspension is prepared as described in steps 3A(iii) and B(iii), 550 μL of the suspension will contain 2×10^5 cells; 530 μL is used to account for dead volume.

(B) Seeding cells for invasion assays

(i) Simultaneously, suspend 530 μL of the cell suspension prepared in step 3C(iv) in the area peripheral to the barrier and 200 μL of the cell suspension prepared in step 3C(v) in the center of the barrier. The invasion chamber will thus contain 2×10^5 cells peripheral to the barrier and 2×10^4 cells within the barrier.

7. Incubate the migration chambers for 24 h at 37°C in a humidified incubator.

Removing migration barriers and adding treatments (day 1) ● TIMING 15-20 min for 8 cell chambers plus time for treatment preparation

8. Post 24 h of incubation, gently remove the migration barrier.

▲ CRITICAL STEP This step should be performed slowly as moving around the barrier in the ring will damage the cells. Firmly hold down the migration chamber and gently grasp the top cylindrical end of the barrier and ease it out in a vertically upward motion.

? TROUBLESHOOTING

9. Aspirate the medium and wash the cells once with 800 μL PBS or serum-free medium to remove any detached cells.

? TROUBLESHOOTING

10. Fill the migration chamber with 1200 μL (maximum volume for the Attofluor cell chamber) of fresh medium or the desired treatment.

▲ CRITICAL STEP To assay the effect of test compounds on migration, include the soluble factors in the media before adding to the cells.

Imaging cell migration (day 1) ● TIMING variable

11. Mount the migration chambers on the climate-controlled stage of the microscope (maintained at 37°C in a constantly humidified atmosphere, with controlled and heated CO_2 flow) and incubate for 30 min to allow acclimatization.

? TROUBLESHOOTING

? TROUBLESHOOTING

12. Depending on the microscope set-up and available imaging software, choose positions to be imaged at the migration front. We routinely use the AxioVision Image Acquisition software which in conjunction with a motorized stage, enables multi-dimensional acquisition. This enables simultaneous image acquisition at multiple positions within a migration chamber. In the absence of a motorized stage, choose a single position to be imaged at the migration front.

▲ CRITICAL STEP For the 12-well high throughput format, a climate control chamber and a motorized stage are required.

? TROUBLESHOOTING

13. Set the desired duration and interval for acquisition using time-lapse imaging. Usually migration is monitored for 12–24 h with images being captured every 12 minutes, with a 10X/0.30 PLAN-NEOFLUAR objective lens. Shorter movies of 8 or 12 h can also be performed and the interval between images can be reduced.

14. Start acquisition using bright-field or fluorescence settings for fluorescently labelled cells.

? TROUBLESHOOTING

Staining and imaging (optional) ● TIMING 4 h; imaging variable

15. To determine the distribution of cytoskeletal components involved in motility in response to either ECM substrates or treatments, cells in migration chambers can be fixed at the end of the experiment for immunofluorescent stainings. Stainings can be performed in both the cell chamber format (option A) or the 12-well format (option B).

(A) **Immunofluorescense protocol for staining cells in cell chambers**

(i) Aspirate culture medium from the cell chamber and wash with 1 mL of PBS.

(ii) Fix cells with 1 mL of the appropriate fixative for the cytoskeletal component of interest.

▲ CRITICAL STEP It is crucial to choose the appropriate fixative for maintaining morphological integrity of the cytoskeletal component under study. For example, for visualization of actin filaments use 4% PFA for 15 min at room temperature and for microtubules fix with chilled methanol/1 mM EGTA for 15 min at −20°C.

(iii) Aspirate the fixative and wash twice for 5 min each with 1mL of 1× PBS + 0.1% Tween-20 (vol/vol).

(iv) Permeabilize cells with 1 mL of 1× PBS + 0.15% Triton-X (vol/vol) for 10 min at room temperature.

(v) Block with 1 mL PBT buffer for 1 h at room temperature.

(vi) Prepare primary antibodies in PBT buffer at the dilutions recommended by the manufacturer and incubate cell chambers with 500 μL antibody solution for 1 h at room temperature. If using fluorescently labelled primary antibodies, perform this and the following steps in a dark box. If multiple antibodies are used, include conjugated antibodies in the secondary antibody incubation step.

(vii) Remove the antibody solution and wash 3 × 10 min with 1mL of 1× PBS + 0.1% Tween-20 (vol/vol).

(viii) If unconjugated primary antibodies are used in step (vi), incubate in the dark with 500 μL of fluorescently labelled secondary antibody diluted in PBT buffer for 30 min at room temperature. To counterstain cell nuclei, add DAPI at 1/1000 dilution.

(ix) Aspirate the secondary antibody solution and wash 3 × 10 min with 1 mL of 1× PBS + 0.1% Tween-20 (vol/vol).

(x) Aspirate the wash solution and gently disassemble the cell chamber by unscrewing the top and bottom parts. The coverslip will be attached to the rubber ring in the upper chamber.

(xi) Invert the upper chamber and gently insert the tip of a pointed forceps between the rubber ring and the coverslip. Gently separate the coverslip from the rubber ring.

(xii) Blot the edge of the coverslip on a tissue paper and mount inverted on a glass slide with a drop of Fluoromount-G. Store covered at room temperature for 30 min followed by 4°C overnight. When the mounting medium has set, seal around the coverslips with nail polish to prevent coverslips from drying out.

■ PAUSE POINT Stained coverslips can be stored dry and protected from light at 4°C until imaging.

(B) Immunofluorescense protocol for staining cells in 12-well plates

(i) Fix and permeabilize cells on coverslips in the 12-well plate as in Step 15A (i-iv). All further staining steps are performed by placing coverslips face-down on a piece of Parafilm in a humid chamber. Between all staining steps, handle coverslips with fine forceps and drain excess solution by blotting the edge of the coverslip on a tissue paper.

(ii) Invert each coverslip and block for 1 h at room temperature with 150 μL of PBT buffer on Parafilm in a humid chamber.

(iii) Prepare primary antibody dilutions as in Step 15A(vi) and apply to an unused part of the Parafilm. Transfer the coverslips to the primary antibody and incubate for 1 h at room temperature.

(iv) Remove the antibody solution and wash 3 × 5 min with 1× PBS + 0.1% Tween-20 (vol/vol).

(v) Prepare secondary antibody dilutions as in Step 15A(viii) and apply to an unused part of the Parafilm. Transfer the coverslips and incubate for 30 min at room temperature.

(vi) Remove the antibody solution and wash 3 × 5 min with 1× PBS + 0.1% Tween-20 (vol/vol).

(vii) Blot the edge of the coverslip on a tissue paper and mount inverted on a glass slide with a drop of Fluoromount-G. Store covered at room temperature for 30 min followed by 4°C overnight. When the mounting medium has set, seal around the coverslips with nail polish to prevent coverslips from drying out.

■ PAUSE POINT Stained coverslips can be stored dry and protected from light at 4°C until imaging.

16. Image using epifluorescense or confocal microscopy to visualize cytoskeletal organization in response to test conditions.

Cleaning and sterilization ● TIMING 1 h

17. Upon completion of the experiment, clean the Attofluor cell chambers and migration barriers with warm water.

18. Spray with 70% (vol/vol) ethanol and air-dry on a clean surface.

19. Pack the migration rings and barriers in sterilization wrap and sterilize by autoclaving for 30 min at 121°C for reuse.

Quantification of migratory parameters and analysis ● TIMING variable

20. If image acquisition is conducted as described in Step 13, data can be used to manually quantify migratory parameters using the AxioVision Image Analysis module, as described in Box 1. Alternatively, other automated quantifications can be performed[177-180].

Box 1. Quantification of time lapse sequence of migrating cells using AxioVision v 4.5 or higher

Quantifications can be performed manually by tracking individual cells using the AxioVision Image Analysis module with the method described here. Alternatively, algorithms employing image correlation techniques or commercially available tracking software can be used. When performing manual quantifications, it is crucial to preclude selection bias. As a general rule, preselect 10 cells at the migration front (first row of cells) for quantification. During quantification if the cell being tracked moves out of frame or undergoes cell death, replace it with a cell from the second row of cells.

1. Open the time-lapse sequence which is saved in a .zvi format.

2. From the 'Measure' drop down menu, choose 'Scalings'.
3. Choose the scaling appropriate for the image format and objective used. This information can be viewed under the 'Info View' tab. Load the scaling by clicking 'Apply selection to image'.
4. Using the 'Line' tool, draw a straight line in front of the cells; this is the migration front.
5. Use the 'Marker' tool to choose ten cells to be quantified at the migration front.
6. Set the player interval to a delay of 400 ms.
7. Select the 'Curve tool'.
8. Click on the cell to be quantified and press play. The sequential frames will play out depending on the set player interval.
9. Track cells till the last frame of the sequence. Right click to stop tracking. This will provide distance in μm and is the 'Total migration'.
10. Use the 'Length' tool to measure the straight-line distance between the marker and the end point of the migration trajectory. This is the 'Effective migration'. Other parameters of migration such as cell polarity, number of proliferation events etc. can be measured from the above sequence.
11. Track at least 10 cells individually, per migration chamber, per treatment. Repeat the experiment thrice.

Troubleshooting

Troubleshooting advice is provided in Table 1.

Timing

The entire procedure takes 2-3 d to complete, depending on the duration of imaging conducted and the optional steps undertaken. Approximate timings are provided below.

Step 1, Preparation of migration chambers: 5 min for 8 cell chambers

Step 2, Coating of migration chambers with ECM substrates (optional): 1 h

Step 3, Preparation of cell suspensions: 15-30 min

Steps 4-7, Placing migration barriers and cell seeding: 20 min for 8 cell chambers

Steps 8-10, Removing migration barriers and adding treatments: 15-20 min for 8 cell chambers

Steps 11-14, Imaging cell migration: variable, up to 24 h

Steps 15-16, Staining and imaging: 4 h; imaging variable

Steps 17-19, Cleaning and sterilization: 1 h

Step 20, Quantification of migratory parameters and analysis: variable

Box 1, quantification of time-lapse sequence of migrating cells using AxioVision v.4.5 or higher: 30-45 min per migration sequence

Table 1. Troubleshooting

Step	Problem	Possible reason	Solution
8	Cell chamber leaks	When cell chambers are autoclaved repeatedly, the rubber ring wears out. Also it may be more difficult to close the chamber	Replace the rubber ring if needed. Clean the cell chamber parts thoroughly and make sure any residue is removed from the thread. Close the cell chamber tightly to prevent leakage.
9	Cells detach	Some cells adhere to glass only lightly and easily detach	Check compatibility of used cell line with glass. Remove the migration barrier carefully. Also different coatings can be tested which provide optimal cell attachment. Be aware that the coating influences migration.
11	Medium evaporates	Air flow too high or air too dry	When the air flow through the cell chamber is too high, medium evaporates fast. Set the inflow as low as possible. Make sure the humidification of the air is good. To prevent condensation in the air tube, insulate this tube up to the cell migration unit.
11	Temperature in cell chamber too high during imaging	Anti-fog or illumination too high	The heating of the glass covers on the cell migration unit may influence the overall temperature of the unit. Prevent direct contact of the anti-fog system with the unit or set the temperature lower. Also, set the illumination as low as possible and use an automated shutter to block the light between images.
12	Cells not in focus	Due to expansion and shrinkage during temperature changes, focal drift occurs	Preheat and precondition the whole system. It is advised when possible to leave the system running and only switch it off when not used for longer periods.
14	Image becomes blurred during the experiment	When condensation occurs on the cover glass of the cell migration unit this negatively affects bright field imaging	Apply an anti-fog or anti-condensation system as used here. Check before to see what temperature of the cover glass is needed to prevent condensation without influencing the temperature of the cell migration unit.

ANTICIPATED RESULTS

Using the ring-barrier migration assay, migration profiles of adherent cells can be monitored, quantified and analyzed. Typical results are shown in Figures 5a-e where the migratory potential of a metastatic melanoma cell line (MM) and a non-metastatic melanoma cell line (NM) were assessed. MM cells were found to be highly motile as is evident by the high total and effective migrations observed. Note that the NM cells do demonstrate some motility but are unable to displace far from their starting point (Supplementary Videos 2 and 3).

Responses to treatments can also be monitored by quantifying cell polarity, which is measured as the ratio of the major axis to the minor axis. Endothelial cells treated

with basal medium or tumor conditioned medium show marked differences in polarity (Figures 5f, g).

Importantly, the impact of matrix components, applied as coating, can be measured. Figure 6a shows the cell migration front after removal of the barrier or inducing the scratch wound. Note the presence of detached and damaged cells in the scratch assay. Additionally, staining of fibronectin coated coverslips to view the matrix composition revealed that placing a migration barrier did not damage the underlying matrix while application of a scratch wound resulted in severe damage to the ECM substrate (Figure 6a). Quantification revealed that fibronectin significantly promoted motility as compared to gelatin, in the ring-barrier assay (Figures 6b-e). No significant differences were observed in the same experiment carried out with the scratch assay (Figures 6g-j). Cells migrated less in the scratch assay, possibly due to the damage inflicted, as can be seen in the migration trajectories (Figures 6f, k).

The system can be expanded to monitor heterotypic interactions during co-culture experiments (Figure 7a) and cell invasion studies (Figure 7b). When scaling up to fluorescence microscopy, additional specific staining procedures enable visualization of

5
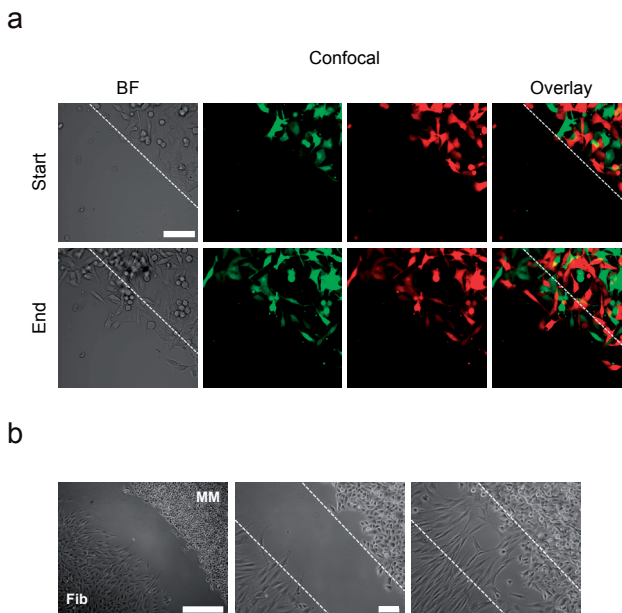
Figure 7. Co-culture assay and invasion assay. (**a**) Green and red fluorescently labelled cells were seeded at a 1:1 ratio in a migration chamber and images were acquired by confocal microscopy with a ×20 objective. Dotted white lines indicate the migration front at $t = 0$ h. BF, Bright-field. (**b**) Representative overview (×5) and start-end positions (×10) of an invasion assay with metastatic melanoma (MM) cells (2×10^5) seeded peripheral to the invasion barrier and human dermal fibroblasts (Fib, 1×10^4) seeded within the barrier. Scale bars indicated are 100 μm.

F-actin	β-tubulin	Vinculin+F-actin
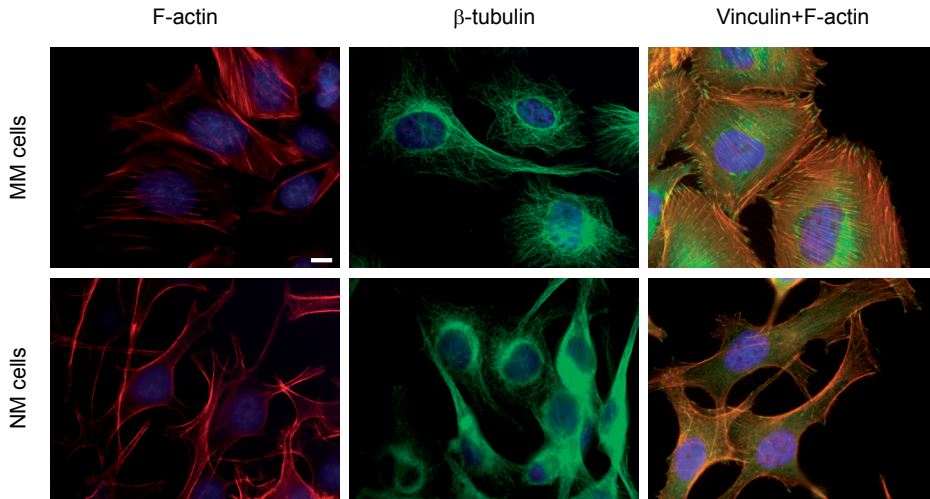
Figure 8. Immunofluorescense stainings. Metastatic (MM) and non-metastatic (NM) melanoma cells were fixed at the end of a migration experiment and immunofluorescently stained to visualize F-actin and β-Tubulin. Vinculin (green) was co-stained with F-actin (red). Primary antibodies used were β-Tubulin (9F3) Rabbit mAb (Cell Signaling Technology, cat. no. 2128) and Mouse Anti-Vinculin Monoclonal Antibody, purified clone 7F9 (Millipore, cat. no. MAB3574). Nuclei were visualized by counterstaining with DAPI (blue). Images were acquired with an Axiovert 100M microscope with ×63 Oil-FLUAR lens (Carl Zeiss) and an ORCA II ER camera (Hamamatsu Photonics Systems). Scale bar, 10 μm.

the organization of cytoskeletal components. Figure 8 shows the morphology of some cytoskeletal components in motile MM and less motile NM cells. Note the presence of several actin stress fibers in the MM cells while they are arranged as peripheral bundles in the NM cells.

ACKNOWLEDGEMENTS

SUPPLEMENTAL FIGURES
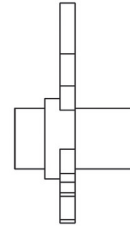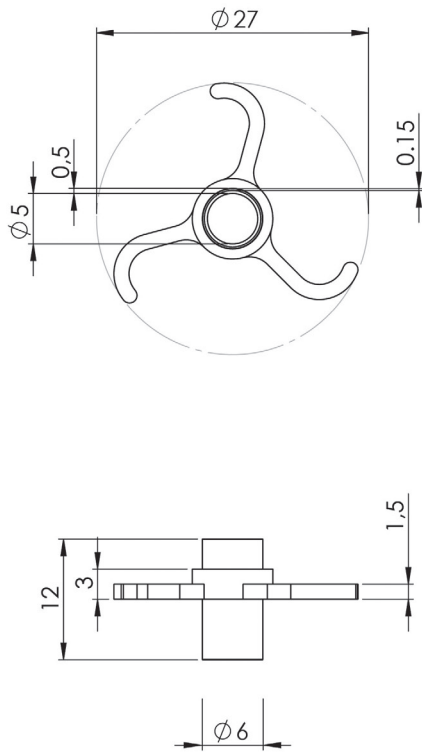
Supplementary Figure 1. Cell migration barrier. The cell migration barrier consists of a surgical stainless steel cylinder and a three legged spacer made of polyether ether ketone (PEEK). The basic dimensions of the cell migration barrier are provided.
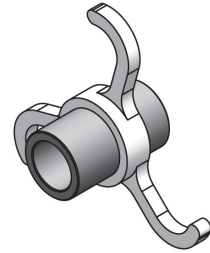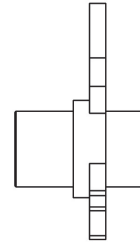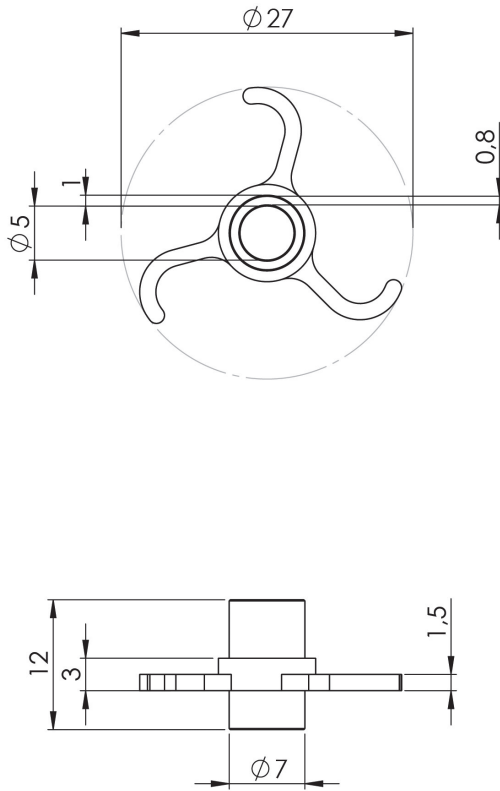
Supplementary Figure 2. Cell invasion barrier. The cell invasion barrier consists of a surgical stainless steel cylinder and a three legged spacer made of polyether ether ketone (PEEK). The basic dimensions of the cell invasion barrier are provided.

a
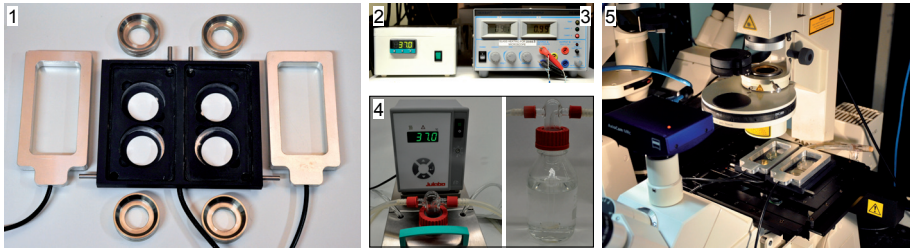
b

c
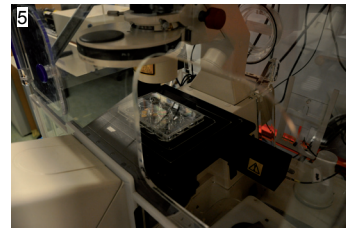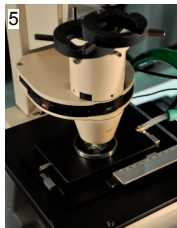
Supplementary Figure 3. Cell migration unit configurations. Images of cell migration unit configurations for imaging (**a**) multiple cell chambers (**b**) single cell chamber and (**c**) 12-well plates with the unit components: Cell migration units (1), Cell migration heater (2), Anti-fog glass heater (3), Gas humidifier/heater (4) and suitable microscopes (5).

5

CHAPTER 6

Biological profiling of the migratory phenotype of melanoma identifies WNT5A as a metastasis determinant

Asha M. Das, Michiel Bolkestein, Mario Pescatori, Joost A.P. Rens,
Cindy E. Vermeulen, Alexander M.M. Eggermont, Ron Smits, Timo L.M. ten Hagen

INTRODUCTION

The metastatic cascade is a highly complex, multistep process which involves local invasion and subsequent dissemination of neoplastic cells from the primary tumor to regional and anatomically distant sites[181]. Although the exact mechanisms remain to be elucidated, genetic and epigenetic alterations are thought to initiate the process, manifesting in several biological changes including increased growth factor production, constitutive activation of cell survival pathways, loss of cell-cell contacts, increased motility, and degradation of structural components of the extracellular matrix (ECM), facilitating entry into lymphatic and hematogenous circulation. Disseminated disease is responsible for > 90% of cancer-related mortalities[182], and as such there is a pressing need to identify effectors and mediators of this process.

Malignant melanoma is the most aggressive form of skin cancer and is responsible for greater than 75% of skin cancer-related mortalities[25]. In contrast to the classical view of stepwise progression, recent studies have indicated that metastatic spread may occur in parallel with primary tumor development[70]. Additionally, the high mutational load[183,184], and clonal and functional heterogeneity demonstrated by melanoma cell populations[185], compounds to the challenge of identifying core mediators of the metastatic cascade. Therefore, we postulated that linking the biological phenotypic traits of melanoma cells to their genetic composition might be a useful approach to identify crucial mediators regulating varied aspects of pathogenesis. As the acquisition of a motile and invasive behavior is a critical step in the metastatic cascade, we determined the migratory profile of a well characterized panel of melanoma cell lines, with known metastatic competence in nude mice[83,87]. Through correlation analysis of the evaluated migratory behavior with the genetic make-up of these cells, we identified WNT5A as a crucial regulator of melanoma metastasis. Further, using i*n vitro* and *in vivo* studies, we were able to validate the role of WNT5A in the metastatic cascade of melanomas. Our results indicate that characterizing biological behavior to obtain insights into genetic alterations is a powerful approach to identify effectors of disease biology.

MATERIALS AND METHODS

Cell lines and culture conditions

Human melanoma cell lines BLM, M14, Mel57 and 1F6 were kindly donated by Dr. van Muijen (Department of Pathology, University of Nijmegen, NL) and routinely cultured in Dulbecco's modified Eagle's medium (DMEM) with glutamine supplemented with 10% FBS. Immortalized human melanocytes (Hermes 1), kindly donated by Dr. Sviderskaya (Department of Basic Medical Sciences, St George's Hospital Medical School, London, UK) were grown in RPMI medium with glutamine supplemented with 10% FBS, 12-O-

tetradecanoylphorbol-13-acetate (TPA, 200 nM), cholera toxin (200 pM), human stem cell factor (SCF, 10 ng/ml) and endothelin 1 (10 nM) and maintained under conditions of 10% CO_2, as previously described[84].

Ring-barrier migration assay

Cell migration was evaluated using the ring barrier-based assay previously described[186]. Briefly, 2×10^5 melanoma cells were seeded on fibronectin (10 μg/mL), gelatin (1 mg/mL), collagen (50 μg/mL) coated or uncoated coverslips and migration was monitored for 24 h using time-lapse microscopy. Images were captured every 12 min. Parameters of cell migration were obtained from the acquired sequence using AxioVision SE64 Rel. 4.9.1 software (Carl Zeiss B.V., Sliedrecht, NL). Track diagram images were processed in Adobe Illustrator CS6 (Adobe Systems Inc, San Jose, CA).

Cell dispersion assay

The invasive potential of the melanoma cell lines was evaluated using a previously described cell dispersion assay[171,187]. Briefly, 5×10^5 melanoma cells were mixed with sterile Cytodex-3 microcarrier beads (Sigma-Aldrich Chemie B.V., Zwijndrecht, NL) in a falcon tube considering a ratio of 40 cells per bead. The suspension was incubated at 37°C for 6 h with gentle mixing to ensure complete coating of the beads. Next, the suspension was transferred to a 25 cm² culture flask and incubated overnight to remove unattached cells. The coated microcarrier beads were embedded in 1.6 mg/mL collagen gel in a 24-well cluster, such that each well had 150 beads. The plates were incubated at 37°C for 2 h for the beads to settle in the gel and the polymerized gels were covered with 500 μL of medium, supplemented with 20% FBS. Cell dispersion was followed for up to 96 h with a 10X/0.30 PLAN-NEOFLUAR objective lens (Carl Zeiss). Images were acquired using AxioVision Image Acquisition software (Carl Zeiss) and processed using the AxioVision Image Analysis module (Carl Zeiss). For each cell line, three independent experiments were performed in triplicate.

Immunocytochemistry-fluorescence (ICC-F)

2×10^5 melanoma cells were cultured on 18 mm glass coverslips, coated with various ECM components, in 12-well cluster plates. Cells were fixed for 15 min at RT in 4% paraformaldehyde in PBS, washed thrice with PBS/0.1% Tween-20, permeabilized for 15 min with 0.15% Triton-X100 in PBS and blocked with 1% BSA, 0.05% Triton-X100 in PBS. Primary antibody incubations were performed overnight at 4°C followed by incubation with secondary antibodies for 1 h at RT. Coverslips were mounted using Fluoromount mounting medium (Southern Biotech, Birmingham, AL). Immunofluorescent images were acquired using an Axiovert 100M inverted microscope with ×63 Oil-FLUAR lens (Carl Zeiss) and an ORCA II ER camera (Hamamatsu Photonics Systems).

RNA isolation

Total RNA was extracted using TRIzol (Invitrogen, Carlsbad, CA) following manufacturer's instructions. The quality and quantity of purified RNA was analyzed using the Agilent 2100 Bioanalyzer (Agilent Technologies, Santa Clara, CA). Only RNA with RIN > 8.0 was used for the microarray experiment.

Gene expression profiling

We used the Affymetrix HG-U133-plus 2.0 GeneChip (Affymetrix Inc., Santa Clara, CA) for gene expression profiling of the melanoma cells. Target synthesis was performed using 5 μg total RNA as template, as described in the Affymetrix Gene Expression Manual. GeneChips were washed and stained using the Affymetrix fluidic station 430 and analyzed using Affymetrix 3000 7G GeneChip scanner. Gene expression values were summarized from probe sets using RMA as implemented in Affymetrix Gene Expression Console. The same software was used to quality control (QC) the GeneChips. Chips not meeting the QC criteria were excluded from further analysis. RMA expression summaries were merged with the Affymetrix MAS 5.0 Presence calls into a single matrix, filtered in Excel and imported into BRB ArrayTools for further analysis[86]. Probe sets were filtered out if called 'absent' in > 80% of the samples. To identify genes significantly associated with the migratory phenotype, we ranked the cell lines in an ascending order based on the exhibited migratory capacity. We performed Pearson correlation analysis implemented in BRB ArrayTools and genes passing the set threshold of $p < 0.0001$ were considered significantly associated with the assayed phenotypic trait.

cDNA synthesis and qPCR

Reverse transcription was performed with 2 μg total RNA using the Superscript III First-Strand Synthesis System for RT-PCR kit (Invitrogen). Quantitative PCR was performed in duplicates, using the iCycler iQ5 platform (Bio-Rad Laboratories, Munich, Germany). 100 ng cDNA was used per reaction with Taqman Gene expression Master mix and specific TaqMan Gene Expression assays (Applied Biosystems). The reactions were incubated in a 96-well optical plate at 50°C for 2 minutes (UDG incubation) and 95°C for 10 minutes, followed by 40 cycles of 95°C for 15 seconds and 60°C for 60 seconds. Gene expression values were normalized to the housekeeping gene B2M. Differences in transcript abundance are plotted as log2 ratios relative to a selected mean expression.

Western blotting

Semi-confluent cell cultures were washed twice with ice-cold PBS and lysed in lysis buffer (50mM Tris-HCL pH 7.4, 150 mM NaCl, 1 mM EDTA, 1% NP-40, protease inhibitor cocktail and phosphatase inhibitor cocktail) for 30 min on ice. Lysates were cleared by centrifugation at 12,000 g for 10 min at 4°C. Protein concentration of cell lysates was

determined with Coomassie Plus Reagent (Pierce, Rockford, IL). Samples were denatured by boiling in Laemmli buffer and equal amounts of protein were electrophoresed on 12% SDS-polyacrylamide gels and transferred to polyvinylidene difluoride (PVDF) membranes. Membranes were blocked in 50% Odyssey blocking buffer (LI-COR Biosciences, Lincoln, NE) in PBS for 1 h at room temperature, followed by incubation with diluted primary antibodies overnight at 4°C. Membranes were further incubated with IRDye labeled secondary antibodies (LI-COR) for 1 h at room temperature and scanned using the Odyssey Infrared Imaging System (LI-COR Biosciences).

Cell proliferation assay

Melanoma cells were seeded at a density of 5×10^3 cells/well in 96-well cluster plates. At 24, 48, 72 and 96 h, cells were fixed with 10% trichloroacetic acid, washed under tap water and stained with sulphophodamine B (SRB) as previously described[152]. The absorbance was measured using a microplate reader (Victor 1420, Wallac, Turku, Finland) at 510 nm. All proliferation data were normalized to the 24 h time point, and is expressed as a percentage.

shRNA vectors and lentiviral transduction

Lentiviral short hairpin pLKO.1-puro vectors for WNT5A and Non-Target shRNA Control (SHC016) were obtained from the Erasmus Center for Biomics (Sigma-Aldrich TRC library). Lentiviruses were generated using the Lenti-X HTX Packaging System (Takara Bio Europe, Westburg BV, Leusden, NL) according to manufacturer's instructions. BLM cells were transduced with lentiviral particles and selected with Puromycin (Takara Bio Europe, 1 µg/mL) from the first passage onwards.

Generation of WNT5A constructs and overexpression

WNT5A was amplified by PCR from the human WNT5A ORF clone IOH39817 (Ultimate ORF Clones, Invitrogen) template, using the primers WNT5A XhoI UP (5′-GCGCTCGAGATGAAGAAGTCCATTGGAATATTAAGC-3′) and WNT5a XbaI DN (5′-GCATCTAGACTACTTGCACACAAACTGGTCCACG-3′). The WNT5A gene fragment was inserted into the pLVX-IRES-ZsGreen1 bicistronic expression vector (Clontech Laboratories, Palo Alto, CA). Lentiviruses were produced as described above for transduction of 1F6 cells. Stably transduced cells were sorted based on ZsGreen1 expression using fluorescence-activated cell sorting (FACS, Becton-Dickinson, Bedford, MA).

Tumor growth curves

All animal studies were approved by the committee on Animal Research of the Erasmus MC (Rotterdam, NL). For tumor growth assessment, athymic nude mice (Harlan-CPB)

were subcutaneously inoculated on the left flank with $1-4 \times 10^6$ tumor cells in PBS. Tumors were measured every alternate day and volumes were calculated using the formula $(A \times B \times C) \times 0.4$, where A, B and C represent the length, width and depth of the tumor respectively.

Computed Tomography (CT)

Small animal imaging was performed with the Quantum FX µCT system (PerkinElmer, Waltham, MA) to follow tumor development in the lungs. Lungs were scanned weekly with respiratory gating, field-of-view of 20 mm and an acquisition time of 4.5 min, 90 kV, 160 µA.

Fluorescent Activated Cell Sorting (FACS) analysis

Tumor bearing mice were sacrificed at the end of the experiment and the lungs and tumors were isolated. Collagenase digestion was used to obtain a single cell suspension and subjected to flow cytometry analysis to detect the presence of metastatic tumor load in the lungs.

Statistical Analysis

Statistical analysis was performed using GraphPad Prism version 5 (GraphPad Software, San Diego, CA). Multiple groups were compared using the non-parametric Kruskal-Wallis H-test and Dunn's multiple comparison post-test. For comparisons of less than three groups, the two-tailed Mann-Whitney test was used. Results were considered significantly different when $p < 0.05$.

6

RESULTS AND DISCUSSION

Migratory phenotype correlates with the metastatic potential

The acquisition of metastatic competence is associated with an increase in the migratory and invasive potential of genetically altered melanocytes. The human melanoma cell lines used in this study show marked differences in their propensity to generate lung metastases when grown as xenografts in nude mice[87]. Thus while the BLM cell line frequently generates lung metastases, the M14 and Mel57 cell lines are sporadically metastatic. The 1F6 cell line is reported to be non-metastatic in nude mice. To evaluate if the migratory capacity reflected the metastatic potential, we used the previously described 'ring barrier-based migration assay'[186]. This assay enables detailed evaluation of the migratory process and helps to quantitatively distinguish features such as random movement and directional migration. We also included the immortalized melanocyte cell line Hermes 1 (hMEL) in our study. Quantitative analysis of migratory parameters on the extracellular matrix (ECM) component, fibronectin, revealed a clear association between the migra-

tory and reported metastatic potential of the melanoma cell lines (Figures 1a-d). Thus while BLM demonstrated the highest total (766.25 ± 48.07 μm) and effective migration (396.80 + 39.04 μm), 1F6 cells demonstrated low motility. Additionally, this did not translate into the ability to effectively displace (effective migration, 49.66 ± 7.31 μm). M14 and Mel57 cells demonstrated intermediate total and effective migration. The immortalized melanocytes also exhibited low motility. ECM components are known to contribute to migratory behavior[123]. Therefore to ascertain whether the tested cell lines exhibit a similar migratory response with other ECM components, we also performed migration assays with gelatin, collagen and laminin (data not shown). Although differences in migratory parameters were detected with various ECM components, similar trends of migratory behavior were observed.

In addition to enhanced motility, tumor cells are also required to invade the underlying basement membrane and ECM for successful dissemination[188]. To determine if the observed migratory patterns also reflected the ability of these cells to invade a matrix,
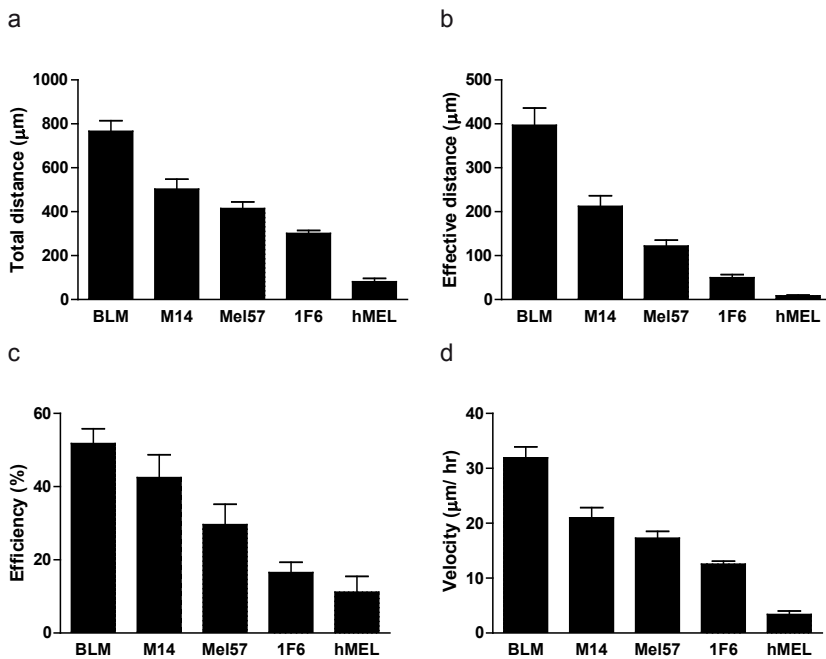
Figure 1. Migratory parameters of melanoma cell lines. Melanoma cells were cultured in migration chambers on fibronectin coated coverslips. Migration was monitored for 24 h using time-lapse microscopy. A total of 30 cells from three independent experiments were tracked. (**a**) Total distance of cell migration (μm). (**b**) Effective migrated distance (μm). (**c**) Migration efficiency (%) was obtained by dividing the effective distance by the total distance. (**d**) Migration velocity (μm/h) was calculated by dividing the total distance of migration by the duration of the migration assay (24 h). Data in panels a-d were derived from tracking at least 30 cells from three independent experiments.

we performed a cell dispersion assay. Cell coated microcarrier beads were embedded in a collagen matrix and cell dispersion into the surrounding matrix was investigated. Corroborating the 2D migration assay results, BLM showed a high invasion capacity, followed by M14 and Mel57 cells. The non-metastatic 1F6 cells and melanocytes were unable to invade the collagen matrix (Figure 2).

Cell migration is accompanied by changes in intracellular distribution of cytoskeletal components[162]. An assessment of the actin cytoskeletal organization of fixed melanoma cells revealed marked differences in morphology. Highly motile cells indicated the presence of several stress fibers and membrane ruffles, while actin filaments were organized in peripheral bundles in cells exhibiting low motility (Figure 3).

Genetic modulators correlating with phenotypic trait

As a clear trend was observed between the *in vitro* migratory phenotype and the reported *in vivo* metastatic potential of the melanoma cells, we postulated that linking these phenotypic aspects to gene expression profiles might reveal potential mediators of the metastatic cascade. To this end, we performed a correlation analysis (Pearson
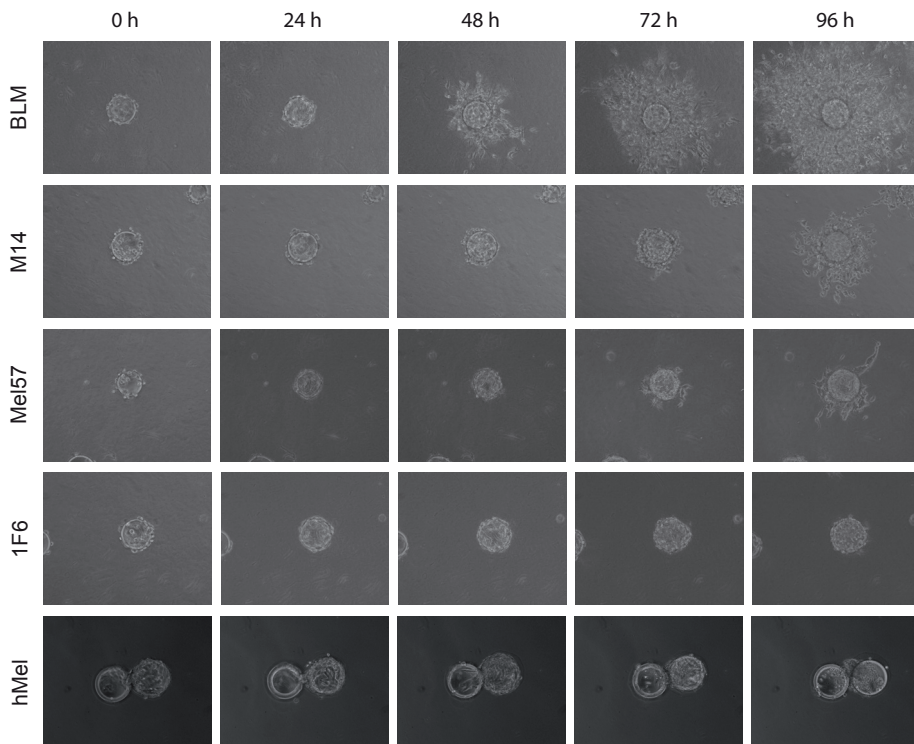
Figure 2. Cell dispersion assay. Invasive capacity of the melanoma cell lines was evaluated by monitoring their dispersion into a collagen matrix. Images were acquired at 0, 24, 48 and 72 h after embedding.
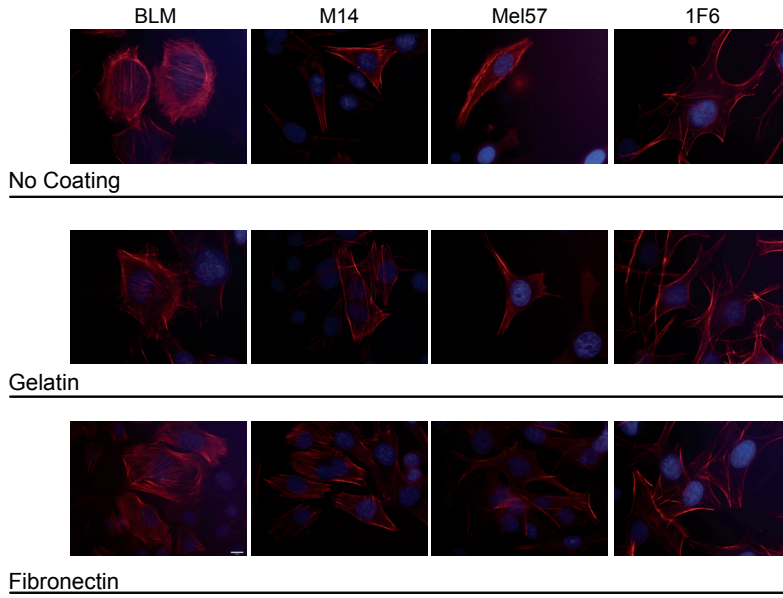
Figure 3. Actin organization. Cytoskeletal organization of actin filamets in the melanoma cells were visualized by staining fixed cells with F-actin plus the additional nuclear stain, DAPI. Scale bar, 100 μm.

correlation test, $p < 0.0001$) by ranking the melanoma cells in ascending order of the migratory phenotype, and comparing this to the genetic make-up of the melanoma cells as determined by microarray gene expression analysis. Based on the confidence level of their expression measurements (Affymetrix presence calls), 27642 probe sets passed the set filtering threshold and were used for further statistical analysis. We identified 735 probe sets significantly correlated with the assayed biological trait, among which 305 showed a positive correlation and 430 showed a negative correlation. Probe sets passing the correlation test were clustered and displayed as a heat map using the clustering tool in BRB ArrayTools (Figure 4). To obtain further insights into the biological functions regulated by the differentially expressed genes, we performed Ingenuity Pathway analysis. We identified Rho signaling, Wnt signaling and integrin signaling as the top canonical pathways associated with the migratory phenotype.

WNT5A and cell migration

Among the transcripts showing differential expression, we identified several genes implicated in cell migration such as WNT5A, E-cadherin and integrin subunits. WNT5A is a secreted molecule and a member of the non-canonical Wnt pathway[189]. WNT5A has been reported to exert an oncogenic role in several human malignancies, including melanoma, lung, prostate, breast and gastric cancers[190-195]. Conversely, a tumor suppressor role
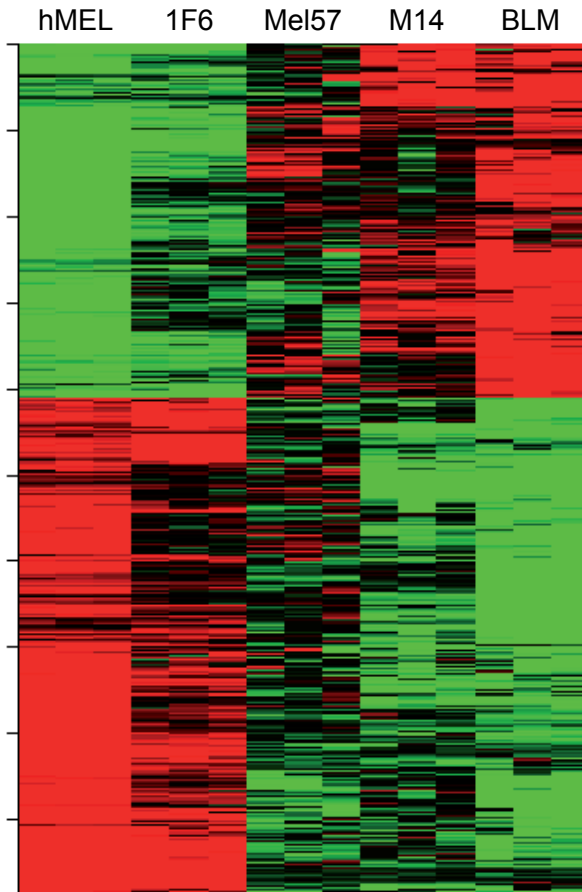
Figure 4. Heatmap of genes significantly correlated with the migratory phenotype, as determined by Pearson correlation analysis at $p < 0.0001$. A total of 735 genes passed the set significant threshold.

has been described in neuroblastoma and leukemia[196,197]. The observed differences in signaling activity suggest a lineage-specific effect. In melanoma, increased expression of WNT5A and signaling has been shown to mediate cell motility and invasion[198-200]. Additionally, WNT5A expression has been reported to increase with melanoma progression and is an independent risk factor for reduced disease-free and overall survival[190]. We further verified the observed gene expression changes on the protein level (Figure 5). Wnt5a protein expression was detected in both cell lysates and conditioned medium of the melanoma cells and correlated with the observed migratory behavior. Additionally, differential expression of several molecules implicated in the changes associated with epithelial to mesenchymal transition (EMT) was also observed at the protein level.

To evaluate the functional implications of WNT5A expression in our set of melanoma cell lines, gene modulation experiments were performed. Lentiviral shRNA vector medi-
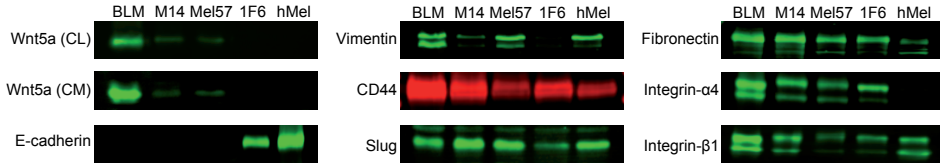
Figure 5. Protein expression of various molecules derived from pathway analysis.
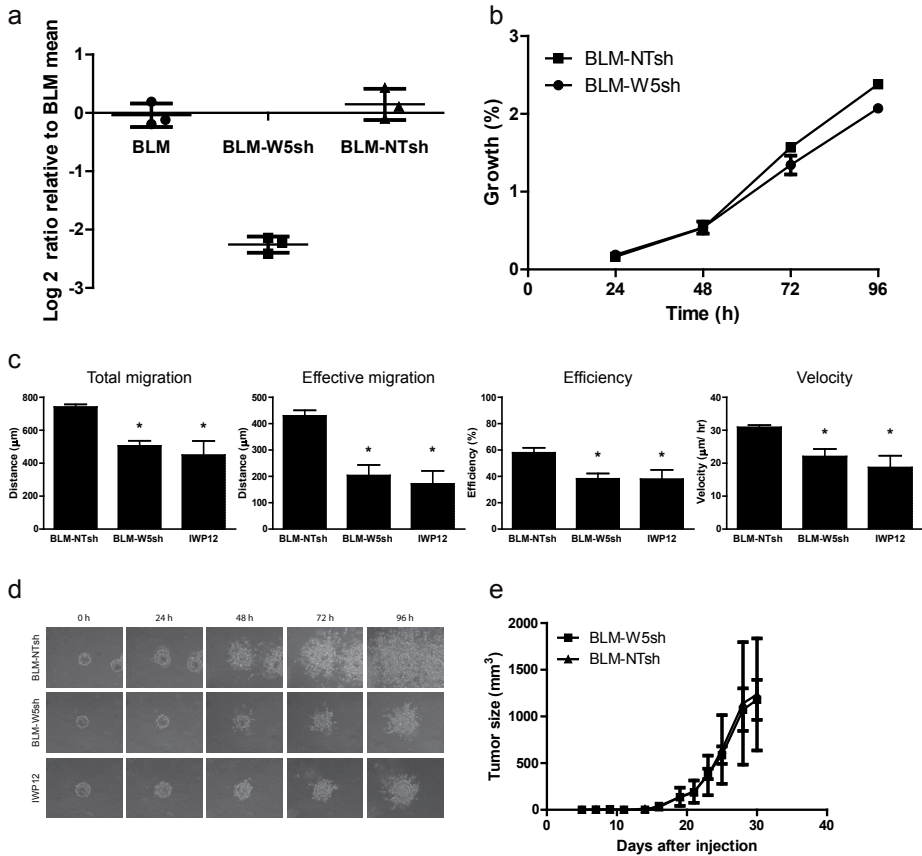
Figure 6. Effect of WNT5A knockdown in melanoma cells. (**a**) Quantitative PCR gene expression levels of WNT5A in BLM, BLM-W5sh and BLM-NTsh cells. Changes in transcript abundance were normalized to B2M expression and are expressed as log2 ratio relative to the BLM mean. Protein expression as determined by western blot of cell lysates. (**b**) *In vitro* growth rate of the transduced cell lines. Data are derived from three independent experiments conducted in duplicate. (**c**) Migratory parameters derived using the ring barrier-based migration assay. At least 30 cells from at least three separate experiments were tracked. *$p < 0.05$. (**d**) Invasive capacity of the transduced cell lines was evaluated by monitoring their dispersion into a collagen matrix. Images were acquired at 0, 24, 48 and 72 h after embedding. (**e**) *In vivo* growth of BLM-W5sh (●), BLM-NTsh (■) tumor cells in NMRI nu/nu mice (n = 6 mice/group).

ated stable gene knockdown of WNT5A in BLM cells (BLM-W5sh) showed a marked reduction in motility as compared to the non-targeted knockdown cells (BLM-NT) (Figures 6a,c). BLM-W5sh cells also showed decreased invasive potential in the cell dispersion assay (Figure 6d). Further, inhibition of Wnt signaling using the pan Wnt inhibitor IWP12 also resulted in a similar reduction in the migratory and invasive potential of treated, non-targeted knockdown cells. Conversely, we overexpressed WNT5A in the otherwise negative 1F6 cell line (Figure 8a) and assayed for differences in the migratory phenotype. We did not observe an increase in total migration but a significant increase in directional migration was observed upon WNT5A overexpression (Figure 8c). This consequently translated into an increase in migration efficiency. Enforced expression also conferred an invasive phenotype as 1F6-W5 cells were able to invade the collagen matrix in contrast to the 1F6-EV cells (empty vector transfection) (Figure 8d). Further, analysis of several pathway mediators showed that overexpression of WNT5A induced an EMT response (Figure 8e).

The role of WNT5A in regulating tumor cell proliferation has been suggested to be cell-context dependant[201]. Thus while several studies have reported WNT5A mediated modulation of cell proliferation in glioma, leukemia, lung cancer and esophageal cancer cells[202-204], among others, no differences in the *in vitro* or *in vivo* growth rates were observed in gastric and prostate cancer cells[191-193]. In melanoma, a previous study indicated that expression of the canonical Wnt ligand WNT3A reduced human and murine melanoma
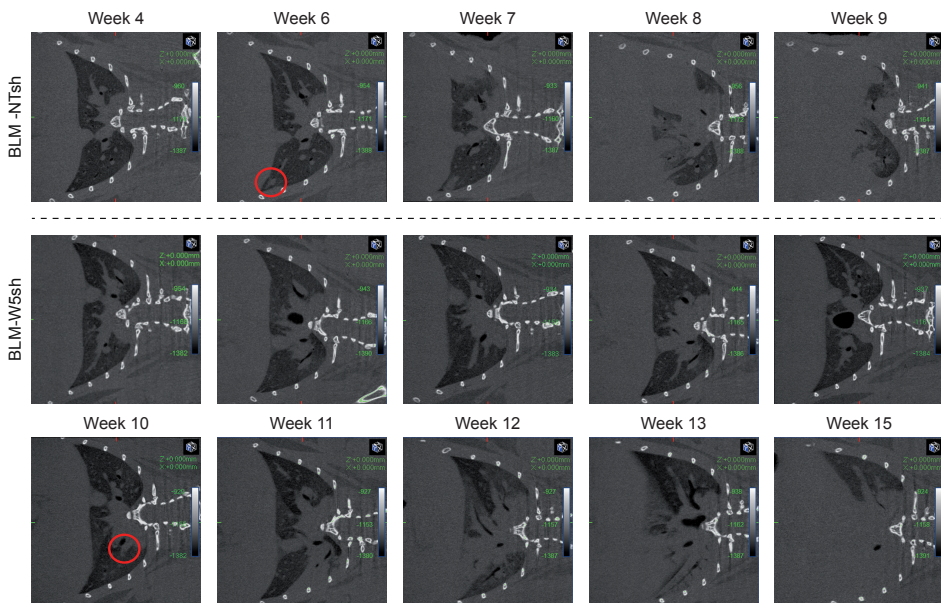
Figure 7. Experimental lung metastasis assay. 1×10^6 BLM-W5sh or BLM-NTsh cells were injected i.v. via the tail vein. Lungs were imaged weekly to observe metastasis formation.

a

b

c

d

e
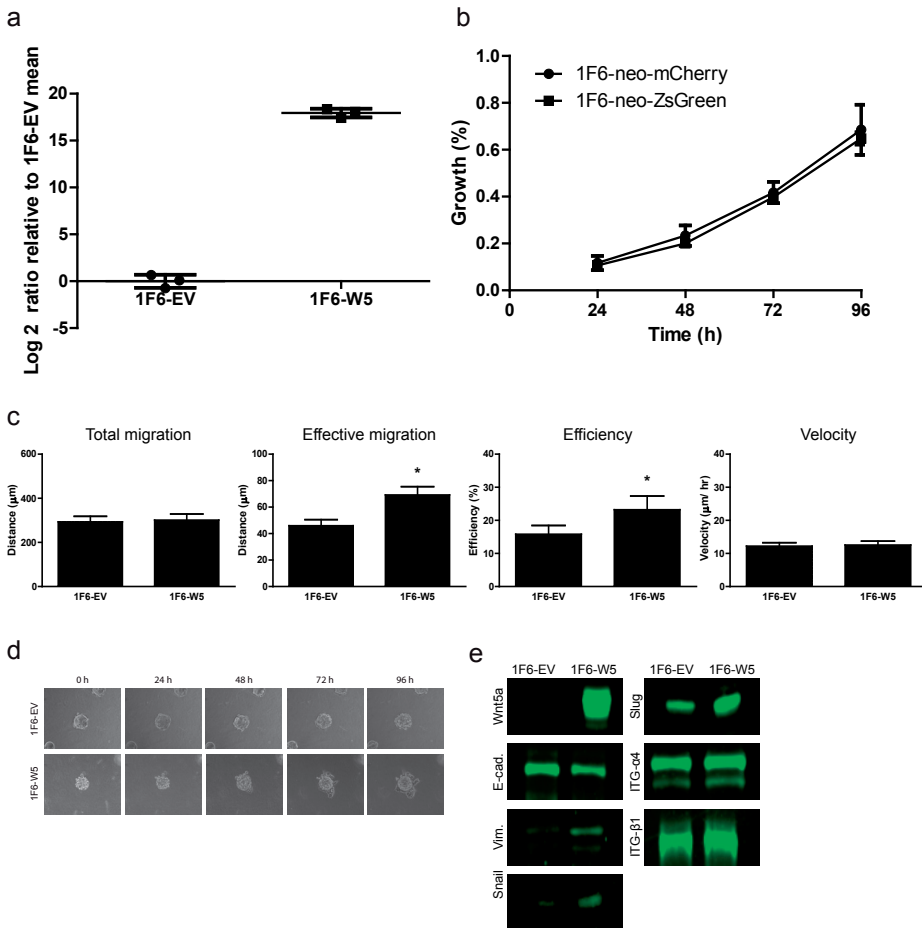
Figure 8. Effect of WNT5A overexpression in melanoma cells. (**a**) Quantitative PCR gene expression levels of WNT5A in 1F6-EV and 1F6-W5 cells. Changes in transcript abundance were normalized to B2M expression and are expressed as log2 ratio relative to the 1F6-EV mean. Protein expression as determined by western blot of cell lysates. (**b**) *In vitro* growth rate of the transduced cell lines. Data are derived from three independent experiments conducted in duplicate. (**c**) Migratory parameters derived using the ring barrier-based migration assay. At least 30 cells from at least three separate experiments were tracked. *$p < 0.05$. (**d**) Invasive capacity of the transduced cell lines was evaluated by monitoring their dispersion into a collagen matrix. Images were acquired at 0, 24, 48 and 72 h after embedding. (**e**) Western blots showing differential expression of pathway effectors upon Wnt5a overexpression.

cell proliferation, while WNT5A overexpression had no effect on proliferation rates[205]. In contrast, a recent study reported reduced melanoma cell proliferation upon siRNA mediated gene knockdown of WNT5A[206]. We did not observe differences in cell proliferation upon gene knockdown (BLM-W5sh vs. BLM-NTsh cells) (Figure 6b) or overexpression (IF6-W5 vs 1F6-EV cells) (Figure 8b). Further no differences were observed in the *in*

vivo growth rates of BLM-W5sh and BLM-NTsh xenografts (Figure 6e). Interestingly, 1F6-W5 xenografts showed increased growth compared to 1F6-EV cells (Figure 9a). This
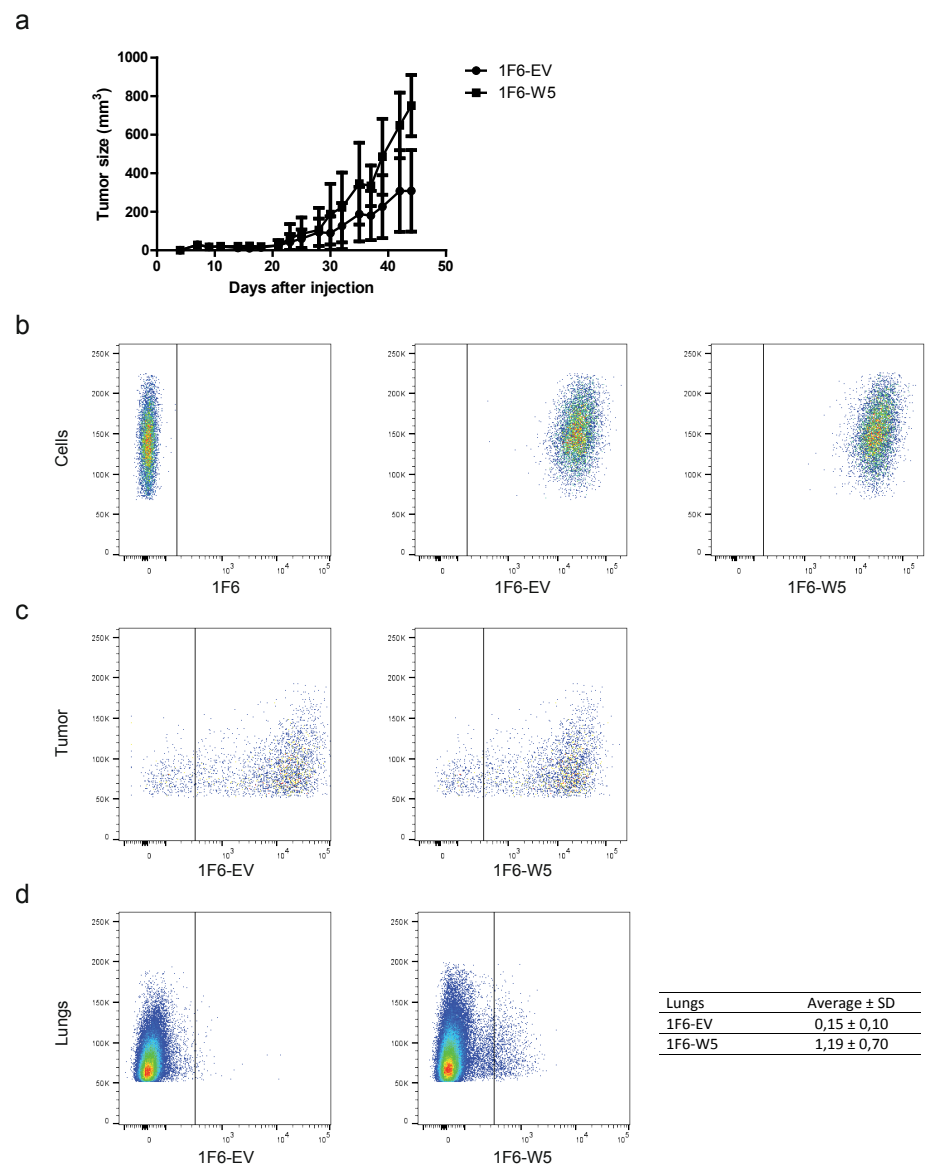
Figure 9. Effect of WNT5A overexpression on tumor growth and metastasis. (**a**) *In vivo* growth of 1F6-EV (●) and 1F6-W5 (■) tumor cells in NMRI nu/nu mice (n = 4 mice/group). (**b**) FACS analysis showing Zs-Green expression in transduced cell lines. FACS analysis of the (**c**) tumor and (**d**) lungs of mice bearing xenografts of the transduced cells.

Lungs	Average ± SD
1F6-EV	0,15 ± 0,10
1F6-W5	1,19 ± 0,70

observation suggests the involvement of the stromal compartment and is currently being investigated.

WNT5A and melanoma metastasis

Finally, the impact of WNT5A expression on the metastatic cascade *in vivo* was assessed. As the BLM xenografts exhibit a high growth rate, tumor bearing mice are usually sacrificed four weeks after tumor take. Therefore to observe the formation of lung metastasis longitudinally, we used an experimental lung metastasis assay (Figure 7). BLM-W5sh and BLM-NTsh cells were injected i.v. via the tail vein and lungs were imaged weekly using breath-hold gated micro-CT imaging. In the three mice injected with BLM-NTsh cells, we detected metastatic colonies as early as 6-7 weeks post inoculation. By week 9-10, the mice had to be sacrificed on account of extensive tumor colonization of the lungs. In the BLM-W5sh group (n = 3), metastatic nodules were detected at 10 weeks post inoculation in one mouse. Extensive lung colonization was observed over time and the mouse was sacrificed at week 15. No metastatic colonies were detected in the other two mice in this group (imaged up to 20 weeks).

Further, to investigate if overexpression of WNT5A could confer metastatic competence to the reportedly non-metastatic 1F6 cells, lungs of xenograft bearing 1F6-EV and 1F6-W5 cells were harvested 6 weeks after tumor inoculation and subjected to a FACS analysis to detect ZsGreen expressing tumor cells (Figure 9). In the 1F6-EV group (n = 4), few tumor cells were detected in the lungs of two mice (0.15 ± 0.10%), while, strikingly, we detected an increase in tumor cells in the lungs of 1F6-W5 xenograft bearing mice (1.19 ± 0.70%).

Taken together, our results suggest that WNT5A is an important mediator of the metastatic cascade in melanoma. Moreover the use of biological profiling, i.e the linking of biological behavior to the genetic make-up of tumor cells, might be an effective approach to identify crucial modulators of pathogenesis.

CHAPTER 7

TIMP3 expression decreases during melanoma progression and inhibits melanoma cell migration

Asha M. Das, Michiel Bolkestein, Thom van der Klok, Charlotte M.C. Oude Ophuis,
Cindy E. Vermeulen, Joost A.P Rens, Winand N.M Dinjens, Peggy N. Atmodimedjo,
Cornelis Verhoef, Senada Koljenović, Ron Smits, Timo L.M. ten Hagen,
Alexander M.M. Eggermont

INTRODUCTION

The global incidence of malignant melanoma is rising faster than for any other solid tumor with an estimated 160,000 cases and 48,000 deaths annually[2,3]. Although early diagnosis and surgical management of primary melanomas increases the chance of cure in patients, melanomas have a high invasive potential and tend to metastasize early[2,4]. Until recently, metastatic melanoma in its disseminated form was a uniformly fatal disease. Recent years have seen the successful implementation of a wide variety of therapeutic approaches, including immunotherapy and targeted therapy, which have demonstrated substantial clinical benefit[1,207]. However, several challenges, such as transient responses and the development of drug resistance remain to be addressed[208], warranting the elucidation of crucial mediators of melanoma metastasis.

Tissue inhibitor of metalloteinases-3 (TIMP3) is a member of the TIMP family of endogenous metalloproteinase inhibitors and has been described as a tumor suppressor in several malignancies, with loss of expression correlating with poor prognosis[140-142]. In a recent study by our group, we observed reduced expression of TIMP3 in the majority of stage III melanoma lymph node biopsies. We postulated that loss of TIMP3 might be an important event during melanoma pathogenesis. To this end we used sequential archived tumor material from each stage, i.e., stage I/II, stage III and stage IV samples from melanoma patients to investigate changes in TIMP3 expression during disease progression. TIMP3 protein and gene expression was evaluated using immunohistochemistry and quantitative PCR, respectively. Association of protein expression with clinical outcome was evaluated and methylation status of the gene promoter was assessed using methylation specific PCR. Finally, the functional consequences of TIMP3 expression on behavioral aspects of melanoma cells were investigated.

MATERIALS AND METHODS

Patient samples

Thirty-three cases of primary cutaneous melanomas with matched lymph node or in transit (Stage III) and distant metastasis (Stage IV) specimens were selected from the pathology archives of the Erasmus Medical Center, with the approval of the research ethics committee. All patients were diagnosed with a primary melanoma between 1989–2010.

Immunohistochemistry

4 μm serial tissue sections were cut from the FFPE tissue blocks using a Microm HM325 microtome (Thermo Fisher Scientific, Waltham, USA) and mounted on Objectglas Superfrost Plus slides (VWR). H&E stained slides were used to demarcate tumor areas. Tissue sections were immunohistochemically stained for TIMP3 (rabbit polyclonal, Abcam ab2169, 1:100)

using the Ventana Benchmark Ultra stainer and visualized using the Ventana ultraView Universal Alkaline Phosphatase Red Detection Kit (760-501) (Ventana Medical Systems, Tucson, AZ). Nuclei were counter stained with hematoxylin. Paraffin embedded cytoblocks of melanoma cells were prepared using the Cellient™ automated cell block system (Hologic Corporation, Marlborough, MA) and used as controls for TIMP3 staining.

Staining Evaluation

Evaluation of TIMP3 immunohistochemical staining was performed by two experienced pathologists (T.K. and S.K) who were blinded toward patient characteristics, patient outcome, transcript abundance and promoter methylation status. TIMP3 staining was graded semiquantitatively and staining intensity was scored on a scale of 1 to 4, as follows: 1 (no staining), 2 (weak stain), 3 (clear stain), or 4 (strong stain). Intratumoral heterogeneity was taken into account by recording the abundance of the various staining intensities observed. The product of intensity and abundance scores (expressed as a fraction) was used to attain a total immunoreactivity score. This ranged from a maximum total score of 4 (intensity score 4, abundance 100%) to a minimum total score of 1 (intensity score 1, abundance 100%). For all clinical analyses, samples with a total score of > 2.4 were classified as high and ≤ 2.4 were classified as low. Differences in scoring were evaluated by Kappa test and discrepant scores were resolved by consensus.

Statistical Analysis

Statistics were performed with Statistical Package for the Social Sciences version 22.0 (SPSS 141 Inc., Chicago, IL). Disease-free survival (DFS) was defined as the number of months from the date of primary excision to the date of first recurrence (locally or distant), to death without relapse or to last follow up. Overall survival (OS) was defined as the number of months from the date of primary excision to death of any cause as registered by the social security death index (SSDI) or to last follow up. Univariate analysis of the clinicopathologic characteristics was performed using $\chi 2$-test for nominal variables, Kendall's tau for ordinal variables and Mann-Whitney-U test for non-parametric continuous variables. Survival curves were plotted using the Kaplan-Meier method, and comparison of survival times was performed with the log-rank test. All tests were two-sided, and p-value < 0.05 was considered statistically significant. Time to progression was calculated for 1) progression to stage III: i.e. date of primary excision till first metastasis in transit/regional lymph node in months, and 2) progression to stage IV: i.e. date of first metastasis in transit/regional lymph node till first distant metastasis. Time from stage IV till death or last follow-up was also recorded in months.

DNA isolation, bisulfite conversion and Methylation Specific PCR (MSP)

Two to three 10 μm FFPE tissue sections were macrodissected with reference to the

H&E stained sections to include areas with > 80% tumor cells. Genomic DNA was isolated using the QIAmp DNA FFPE tissue kit (Qiagen Benelux B.V., Venlo, NL) and quantified using the Qubit DNA Broad-Range assay kit and Qubit® 2.0 fluorometer (Life Technologies, CA, USA). 250 ng DNA was bisulfite modified using the EpiTect Bisulfite kit (Qiagen) and eluted in 10 µL elution buffer. 50 ng of converted DNA was amplified by PCR, using AmpliTaq Gold® DNA Polymerase (Life Technologies). Primer sequences specific for unmethylated DNA were 5′-TTTTGTTTTGTTATTTTTTGTTTTTG-GTTTT-3′ (sense) and 5′-CCCCCAAAAACCCCACCTCA-3′ (antisense), (122 bp) and methylated DNA were 5′-CGTTTCGTTATTTTTTGTTTTCGGTTTC-3′ (sense), and 5′-CCGAAAACCCCGCCTCG-3′ (antisense), (116 bp) and have been previously described[125]. PCR reactions were performed in 24 µL reactions with an annealing temperature of 59°C and products were visualized on 2% agarose gels. As controls, converted methylated and unmethylated genomic DNA from the Epitect Control DNA set (Qiagen) and unmethylated genomic DNA treated with CpG Methyltransferase (M.SssI) were used.

Cell lines and culture conditions

Human melanoma cell lines BLM, M14, Mel57, 530 and 1F6 used in this study have been described previously[83]. Cells were routinely cultured in Dulbecco's modified Eagle's medium (DMEM) with glutamine supplemented with 10% FBS and maintained in a well humidified incubator under conditions of 5% CO_2.

shRNA vectors and lentiviral transduction

Lentiviral short hairpin pLKO.1-puro vectors for TIMP3 and Non-Target shRNA Control (SHC016) were obtained from the Erasmus Center for Biomics (Sigma-Aldrich TRC library, Zwijndrecht, NL). Lentiviruses were generated using the Lenti-X HTX Packaging System (Takara Bio Europe, Westburg BV, Leusden, NL) according to manufacturer's instructions. 1F6 cells were transduced with lentiviral particles and selected with Puromycin (Takara Bio Europe, 1 µg/mL) from the first passage onwards.

Generation of TIMP3 constructs and overexpression

TIMP3 was amplified by PCR from the TIMP3 pENTR221 (Ultimate ORF Clones, Invitrogen) template, using the primers TIMP3 XhoI UP (5′-CTGAGCTCGA GCCGC-CACCATGACCCCCTTGGCTCGGGCTCATC-3′) and TIMP3 BamH1 DN (5′-CT-GAGGGATCCTAGGGGTCTGTGGCATTGATGATG-3′). The TIMP3 gene fragment was inserted into the pLVX-IRES-tdTomato bicistronic expression vector (Clontech Laboratories, Palo Alto, CA). Lentiviruses were produced as described above for transduction. Stably transduced cells were sorted based on TdTomato expression using fluorescence-activated cell sorting (FACS, Becton-Dickinson, Bedford, MA).

5-Aza-dC Treatment

3×10^5 melanoma cells were treated with 5 µM 5-Aza-dC (Sigma-Aldrich) for 72 h and subjected to DNA and RNA extraction.

RNA isolation, cDNA synthesis and Quantitative PCR (qPCR)

Total RNA from cells was isolated using TRIzol reagent (Invitrogen, Carlsbad, CA). Reverse transcription was performed with 4 µg total RNA using the Superscript III First-Strand Synthesis System for RT-PCR kit (Invitrogen). Quantitative PCR was performed in duplicates, using the iCycler iQ5 platform (Bio-Rad Laboratories, Munich, Germany). 50 ng cDNA was used per reaction with Taqman Gene expression Master mix and Taq-Man Gene Expression assays (Applied Biosystems, Carlsbad, CA). The reactions were incubated in a 96-well optical plate at 50°C for 2 minutes (UDG incubation) and 95°C for 10 min, followed by 40 cycles of 95°C for 15 seconds and 60°C for 60 seconds. Gene expression values were normalized to the expression of the housekeeping gene B2M. Differences in transcript abundance were plotted as log2 ratio relative to a selected mean expression. qPCR products were visualized on 2% agarose gels.

RNA isolation from FFPE samples

Two to three 10 µm FFPE tissue sections were macrodissected with reference to the hematoxylin-eosin stained sections to include areas with > 80% tumor cells. Total RNA was isolated using the PureLink FFPE RNA Isolation Kit (Invitrogen, CA, USA), as per manufacturer's instructions, and eluted in 20-30 µl of RT-PCR grade water (Ambion, CA, USA). Total RNA was treated with DNase I to eliminate the presence of any contaminating genomic DNA. RNA yields were quantified using the Qubit RNA Broad-Range assay kit and Qubit® 2.0 fluorometer (Life Technologies, CA, USA).

cDNA synthesis and Quantitative PCR (qPCR)

Reverse transcription was performed with 500 ng total RNA, as described above, with minor modifications. Transcription was performed in 20 µL reactions with a mixture of Oligo dT (1.25 µM) and Random Hexamers (1.25 ng/uL), using Superscript III Reverse Transcriptase. 25 ng cDNA was used per qPCR reaction with Taqman Gene expression Master mix and specific TaqMan Gene Expression assays (Applied Biosystems) for human TIMP3 (Hs00165949_m1), human B2M (Hs99999907_m1), and human HPRT1 (Hs99999909_m1). TIMP3 gene expression values in the samples were normalized to the housekeeping genes B2M and HPRT. qPCR products were further visualized on 2% agarose gels (TIMP3: 59 bp, B2M: 75 bp).

Western blotting

Semi-confluent cell cultures were washed twice with ice-cold PBS and lysed in lysis buffer

(50mM Tris-HCL pH 7.4, 150 mM NaCl, 1 mM EDTA, 1% NP-40, protease inhibitor cocktail and phosphatase inhibitor cocktail) for 30 min on ice. Lysates were cleared by centrifugation at 14,000 g for 10 min at 4°C. Protein concentration was determined with Coomassie Plus Reagent (Pierce, Rockford, IL). Samples were denatured by boiling in Laemmli buffer and equal amounts of protein were resolved on 12% SDS-polyacrylamide gels and transferred to polyvinylidene difluoride (PVDF) membranes. Membranes were blocked in 50% Odyssey blocking buffer (LI-COR Biosciences, Lincoln, NE) in PBS for 1 h at room temperature, followed by incubation with diluted primary antibodies overnight at 4°C. After washing, membranes were incubated with IRDye secondary antibodies (LI-COR Biosciences) for 1 h at room temperature and scanned using the Odyssey Infrared Imaging System (LI-COR Biosciences).

Colony formation assay

Melanoma cells were trypsinized and plated at a low density (250 cells per well of a 6-well cluster plate) and cultured in DMEM with 10% FBS. After 7 days, the colonies were fixed with ethanol and stained with hematoxylin and eosin, and the colony count was determined, as described previously[209].

Anoikis assay

The effect of TIMP3 on the anchorage independent growth capacity of melanoma cell lines was evaluated with the anoikis assay. Briefly, 5,000 cells per well were added to standard 96-well cluster plates or Ultra-Low attachment plates (Corning). After 24 h, viable cells were detected using the XTT (2,3-Bis-(2-Methoxy-4-Nitro-5-Sulfophenyl)-2H-Tetrazolium-473 5-Carboxanilide) assay as described elsewhere. Cell viability (%) is expressed relative to the growth in standard cluster plates.

Ring-barrier migration assay

Cell migration was evaluated using the ring-barrier based assay previously described[186]. 2×10^5 melanoma cells were seeded on fibronectin (10 μg/mL) coated coverslips and migration was monitored for 16 h using time-lapse microscopy, with images being captured every 12 min. Where appropriate, recombinant human TIMP3 was added at a concentration of 100 ng/mL. Parameters of cell migration were obtained from the acquired sequence using AxioVision SE64 Rel. 4.9.1 software (Carl Zeiss B.V., Sliedrecht, NL). Track diagram images were processed in Adobe Illustrator CS6 (Adobe Systems Inc, San Jose, CA). All migration assays were conducted in the presence of 10% FBS.

Cell dispersion assay

The invasive potential of the melanoma cells was evaluated using a cell dispersion assay[171] with Cytodex-3 microcarrier beads (Sigma-Aldrich). The microcarrier beads were pre-

pared according to the manufacturer's instructions. 5×10^5 melanoma cells were mixed with the sterile microcarrier beads in a falcon tube considering a ratio of 40 cells per bead. The suspension was incubated at 37°C for 6 h with gentle mixing to ensure complete coating of the beads. Next, the suspension was transferred to a 25 cm^2 culture flask and kept overnight to remove unattached cells. The coated microcarrier beads were embedded in 1.6 mg/mL collagen gel in a 24-well cluster plate, such that each well had approximately 150 beads. The plates were incubated at 37°C for 2 h for the beads to settle in the gel and the polymerized gels were covered with 500 µL of medium, supplemented with 20% FBS. Where appropriate, recombinant human TIMP3 was added at a concentration of 100 ng/mL. Cell dispersion was followed for up to 96 h with a 10X/0.30 PLAN-NEOFLUAR objective lens (Carl Zeiss). Images were acquired using AxioVision Image Acquisition software (Carl Zeiss) and dispersion measurements were performed using the AxioVision Image Analysis module (Carl Zeiss). Cell dispersion for each time point was measured as the maximum migrated distance from the surface of the bead into the collagen gel. For each treatment, three independent experiments were performed in triplicate.

RESULTS

Baseline characteristics

Matched primary, stage III and stage IV samples from 33 patients with a primary cutaneous melanoma were investigated. Baseline characteristics of the study population are described in Table 1. The primary melanoma samples had a median Breslow depth of 2.35 mm, (interquartile range (IQR), 1.65–3.55 mm), and 10 cases (30%) were ulcerated. Most primary melanomas were located on extremities (22 cases, 67%), 7 cases (21%) were located on the trunk and 4 cases (12%) were located in the head and neck area. The majority of matched stage III tumor samples were from lymph nodes: 25 cases (76%). The matched stage IV samples were from the gastrointestinal tract (27%), brain (18%), lungs (12%), subcutaneous (24%), distant lymph node metastasis (9%) and other sites (bone/scrotum, 9%).

TIMP3 expression during melanoma progression

TIMP3 expression was graded semiquantitatively as described in the 'Materials and Methods' section. Staining intensity was scored on a scale of 1-4 as illustrated in Figure 1a. Intratumoral heterogeneity in TIMP3 expression was observed and taken into account to obtain the total immunoreactivity score (Figures 1b, c). TIMP3 expression varied over time in most patients, with a general trend to decrease at progression to stage III and stage IV (Figures 1d, e and Table 2). A decrease was seen in 16 stage III samples, and a stable expression in 9 samples. Of the 16 samples with decreased expression, 7 decreased further, and 9 increased. Of the 9 samples with stable expression, 4 decreased and 5 increased. An increase in TIMP3 expression was seen in 8 stage III samples. Fur-

Table 1. Baseline characteristics (n = 33)

Characteristic	N	%
Gender		
Female	16	49
Male	17	51
Age		
≤ 49 years	17	51
> 49 years	16	48
Location primary		
Extremity	22	67
Trunk	7	21
Head and neck	4	12
Histology		
SSM	14	43
NM	9	27
ALM	3	9
Other	7	21
Breslow thickness		
T1 ≤ 1.00mm	3	9
T2 1.01–2.00mm	11	33
T3 2.01–4.00mm	12	37
T4 > 4.00 mm	7	21
Ulceration		
Absent	23	70
Present	10	30

Table 2. TIMP3 Expression Per Melanoma Stage (n = 33)

	Stage I-II	Stage III	Stage IV
TIMP3 High, n (%)	25 (76)	14 (42)	12 (36)
TIMP3 Low, n (%)	8 (24)	19 (58)	21 (64)
Median TIMP3 score (IQR)	3.0 (2.5–3.1)	2.3 (2.0–3.0)	2.2 (1.8–2.9)

ther increase of TIMP3 expression in stage IV samples was seen in 2/8; in 6/8 TIMP3 expression had decreased.

Time to progression did not differ based on TIMP3 expression: median time to progression to stage III was 29 months (IQR, 7–71 months) for patients with high TIMP3 expression versus 30 months (IQR, 12–49 months) for patients with low expression in the primary melanoma ($p = 0.758$); median time from stage III to stage IV progression was 14 months (IQR, 8–51 months) vs. 14 months (IQR, 10–21 months) for high TIMP3 vs. low TIMP3 in stage III samples ($p = 0.839$); and median time from stage IV to death was 10 months (IQR, 7–25 months) vs. 11 months (IQR, 8–27 months) for high vs. low TIMP3 expression in stage IV samples ($p = 0.974$) respectively. The 8 patients with an increased TIMP3 expression in their stage III sample had similar median time to progression to stage III (29 months, IQR, 11–55 months), but a longer median time to progression to stage IV (25 months, IQR, 7–64 months) and a longer median time from stage IV to

a

b

Intensity 4 (20%), Intensity 3 (80%)

c

Intensity 2 (100%)

d

e
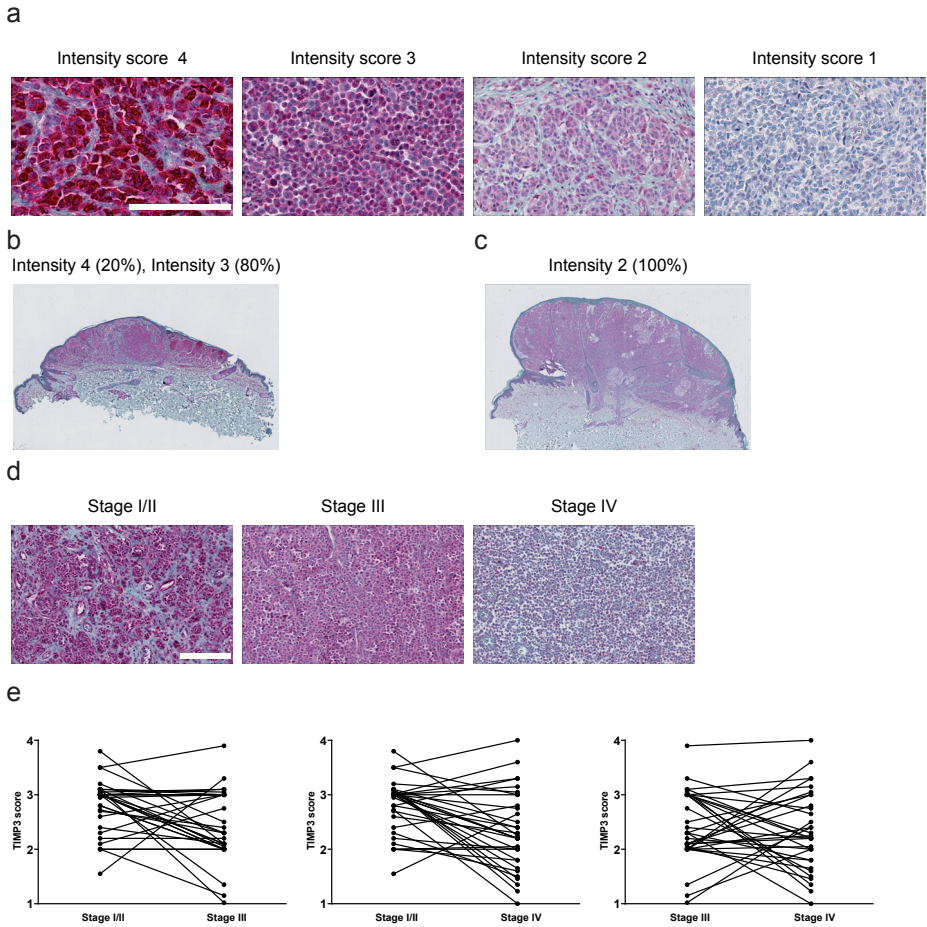
Figure 1. Immunohistochemical staining and scoring of TIMP3 expression. (**a**) Melanoma biopsies were immunohistochemically stained with polyclonal TIMP3 antibody. Staining intensity was graded semi-quantitatively on a scale of 1 to 4, where score 4 represents a strong stain, score 3 represents a clear stain, score 2 represents a weak stain and score 1 represents no staining. Representative images of the intensity scores are shown. Magnification, ×40. (**b,c**) Panoramic images of tumors with (**b**) heterogeneous and (**c**) homogenous TIMP3 expression, as illustrative examples for obtaining the total immunoreactivity score. (**d**) TIMP3 expression in three stages of melanoma from the same patient. Magnification, ×20. (**e**) Changes in total TIMP3 immunoreactivity scores between the various stages of disease. Scale bars, 200 μm.

death (28 months, IQR, 9–50 months). None of these time intervals reached significance when compared to patients without an increase in TIMP3 expression.

TIMP3 expression and outcome

Figure 2 shows the survival curves for estimated 5-year OS and DFS for high vs. low TIMP3 expression in the primary melanoma sample, stage III sample, and stage IV sample, respectively. As all deceased patients passed away due to melanoma, melanoma

a

b

c

d

e

f
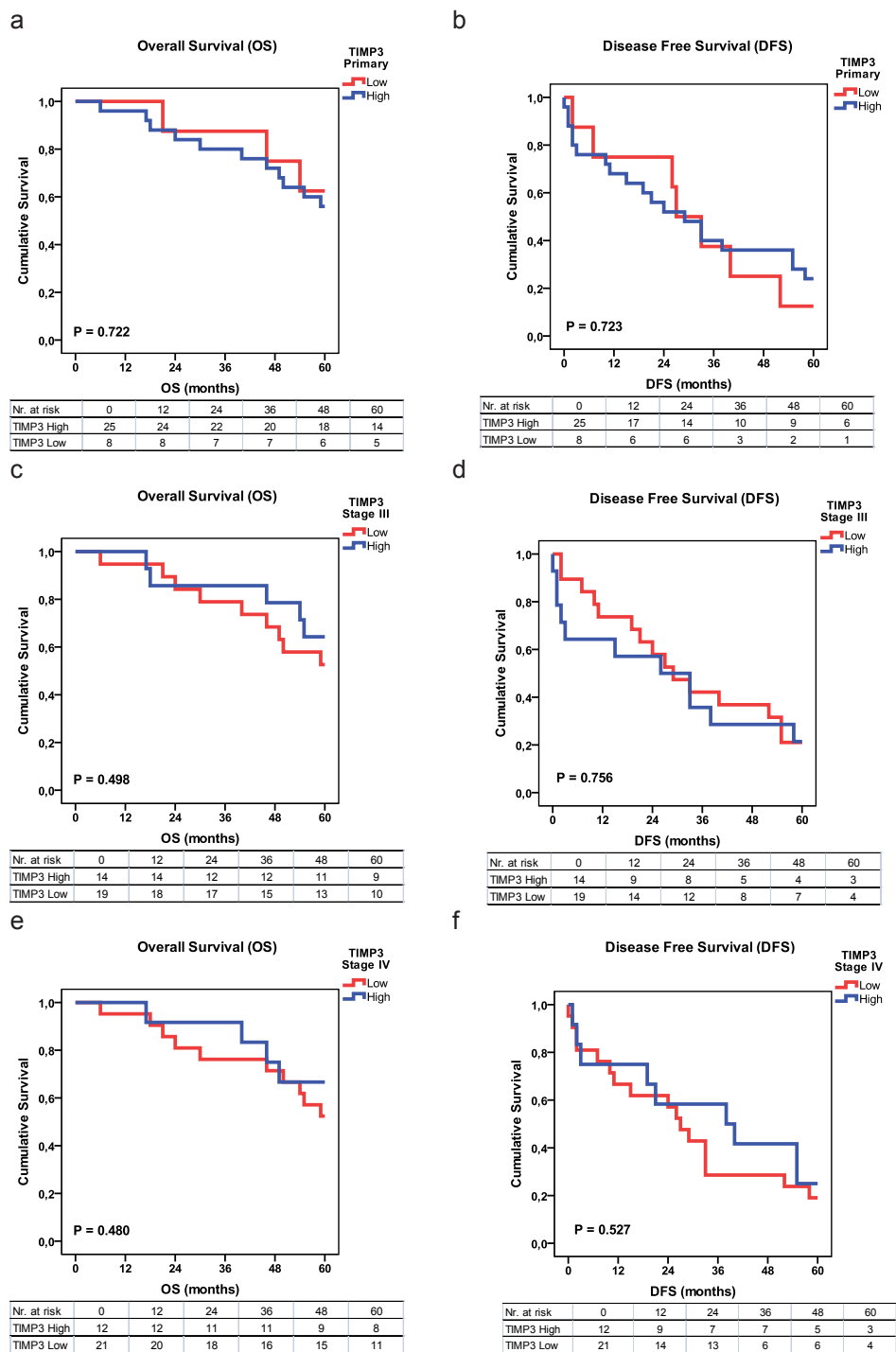
Figure 2. TIMP3 expression and outcome. Kaplan Meier curves of overall survival and disease-free survival of patients expressing high or low TIMP3 in (**a,b**) stage I/II, (**c,d**) stage III and (**e,f**) stage IV.

specific survival equals OS, hence only OS is shown. Five-year estimated OS was 63% ± 17% for high primary TIMP3 expression, and 56% ± 10% for low TIMP3 expression ($p = 0.722$). Five-year estimated DFS was 24% ± 8.5% for high TIMP3 expression vs. 13% ± 12% for low primary TIMP3 expression ($p = 0.723$). Survival for high vs. low TIMP3 expression at stage III and stage IV did not reach statistical significance.

Methylation associated gene silencing

The frequency of TIMP3 promoter methylation was evaluated in the stage III and stage IV samples using MSP (Figures 3a, b). Adequate DNA was available for 31 stage III cases and 30 stage IV cases. Gene promoter methylation was detected in one stage III sample,
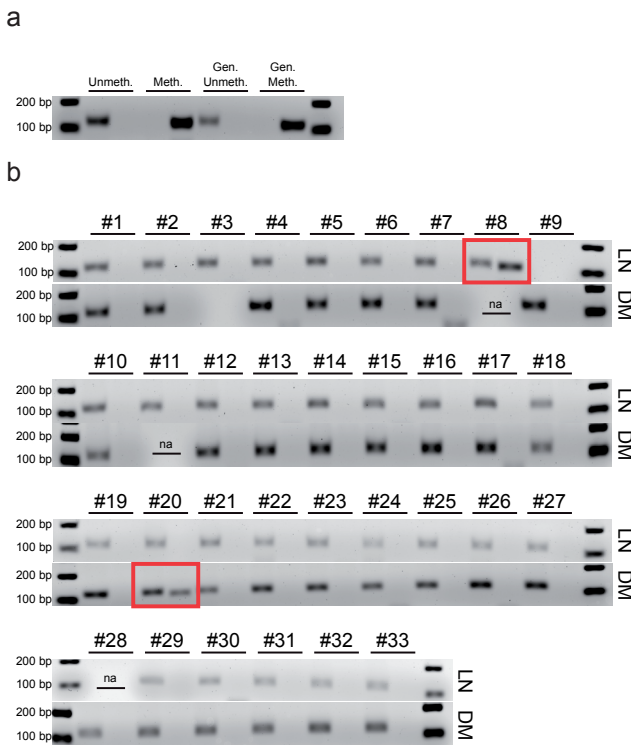
Figure 3. Methylation-specific PCR (MSP). (a) MSP with Epitect control DNA set. C1, unmethylated converted DNA; C2, methylated converted DNA; C3, unmethylated control human DNA bisulfite converted with the Epitect Bisulfite kit; C4, unmethylated control human DNA treated with M.SssI followed by bisulfite conversion. (**b**) MSP was performed with DNA isolated from matched stage III and stage IV samples. NA, indicates DNA was not available for analysis. PCR products were resolved on 2% agarose gels. M, EZ Load 100 bp Molecular Ruler; u, unmethylation amplification fragment (122 bp); m, methylation amplification fragment (116 bp).

where the corresponding stage IV sample could not be analyzed; and one stage IV sample where the corresponding stage III sample did not show promoter methylation.

TIMP3 expression in melanoma cells

Next, we analyzed TIMP3 expression in a well described panel of melanoma cell lines which vary in their aggressiveness and metastatic potential[83,87]. Evaluation of protein expression using immunohistochemistry on paraffin embedded cytoblocks (Figure 4a) and western blot (Figure 4b) revealed an inverse correlation between TIMP3 expression and the metastatic potential of these cell lines. MSP analysis showed promoter methyla-
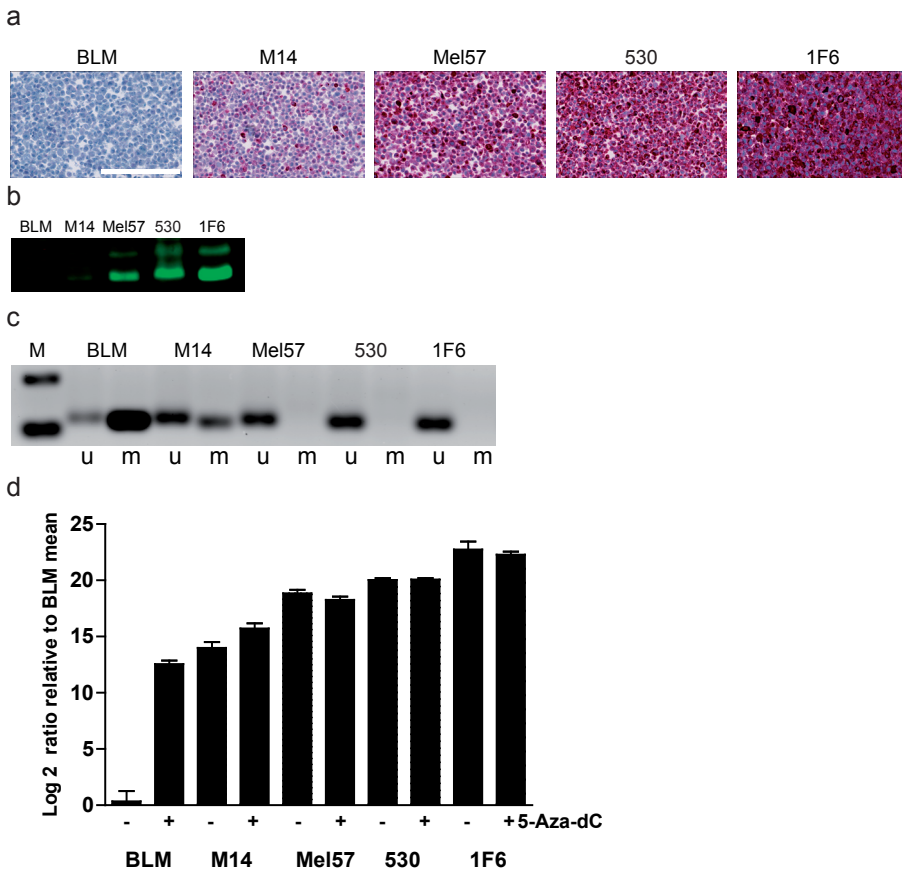
Figure 4. TIMP3 expression of melanoma cells. TIMP3 protein expression in melanoma cells as detected by (**a**) immunohistochemistry of formalin fixed paraffin embedded cytoblocks, magnification, ×40, scale bar, 200 µm, and (**b**) western blot of cell lysates. (**c**) MSP analysis of TIMP3 promoter methylation in melanoma cells with DNA isolated from cytoblocks. PCR products were resolved on 2% agarose gels. M, EZ Load 100 bp Molecular Ruler; u, unmethylation amplification fragment (122 bp); m, methylation amplification fragment (116 bp). (**d**) Quantitative PCR gene expression levels of TIMP3 in the melanoma cell lines without (−) or with (+) 5-Aza-dC (10 µM) treatment. Changes in transcript abundance were normalized to B2M expression and are expressed as log2 ratio relative to BLM mean.
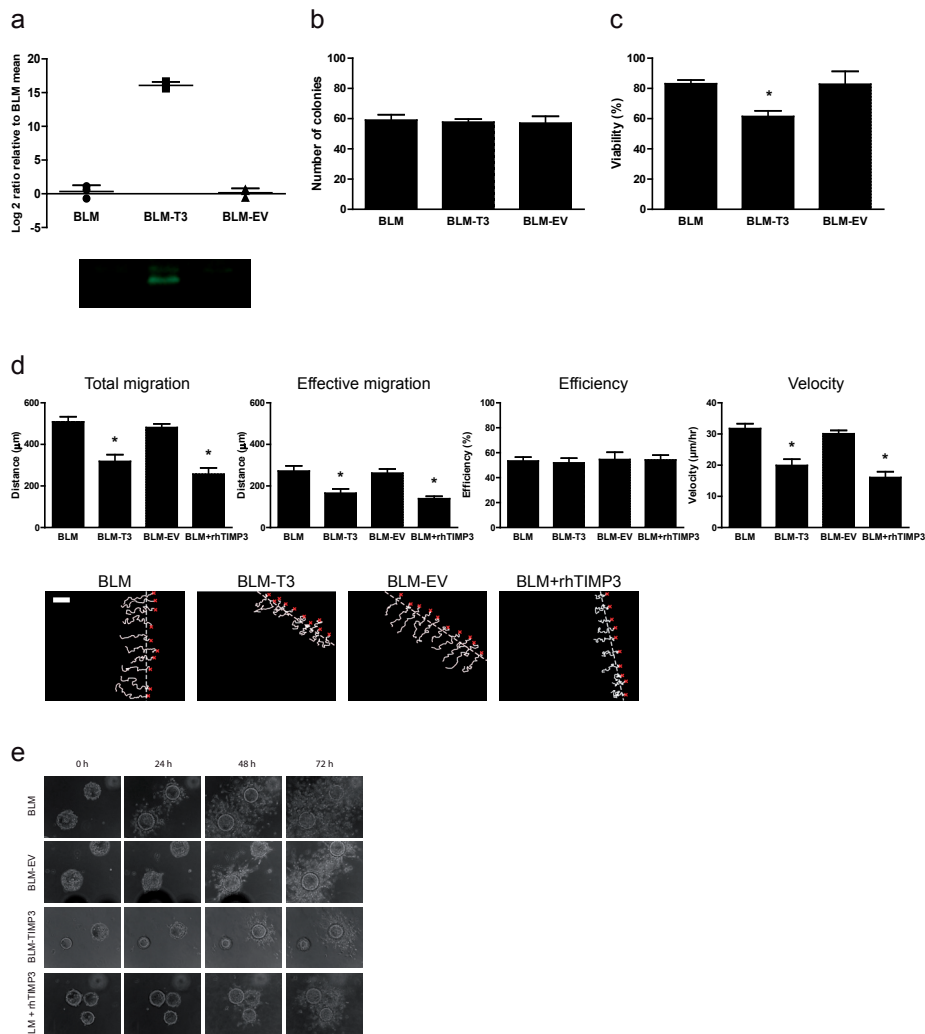
Figure 5. Effect of TIMP3 overexpression in melanoma cells. (**a**) Quantitative PCR gene expression levels of TIMP3 in BLM, BLM-T3 and BLM-EV cells. Changes in transcript abundance were normalized to B2M expression and are expressed as log2 ratio relative to BLM mean. Protein expression as determined by western blot of cell lysates. (**b**) Cell proliferation as determined by the colony formation assay. Data are derived from three independent experiments conducted in duplicate. (**c**) Anchorage independent growth as determined by the anoikis assay. Cell viability (%) is expressed relative to growth on standard culture plates. Data are derived from three independent experiments conducted in duplicate. *$p < 0.05$ (**d**) Migratory parameters and representative track diagrams as evaluated using the ring barrier-based migration assay. A minimum of 20 cells from at least three separate experiments were tracked. Scale bar, 100 μm. *$p < 0.05$. (**e**) Invasive capacity of the melanoma cell lines were evaluated by monitoring their dispersion into a collagen matrix. Images were acquired at 0, 24, 48 and 72 h after embedding.
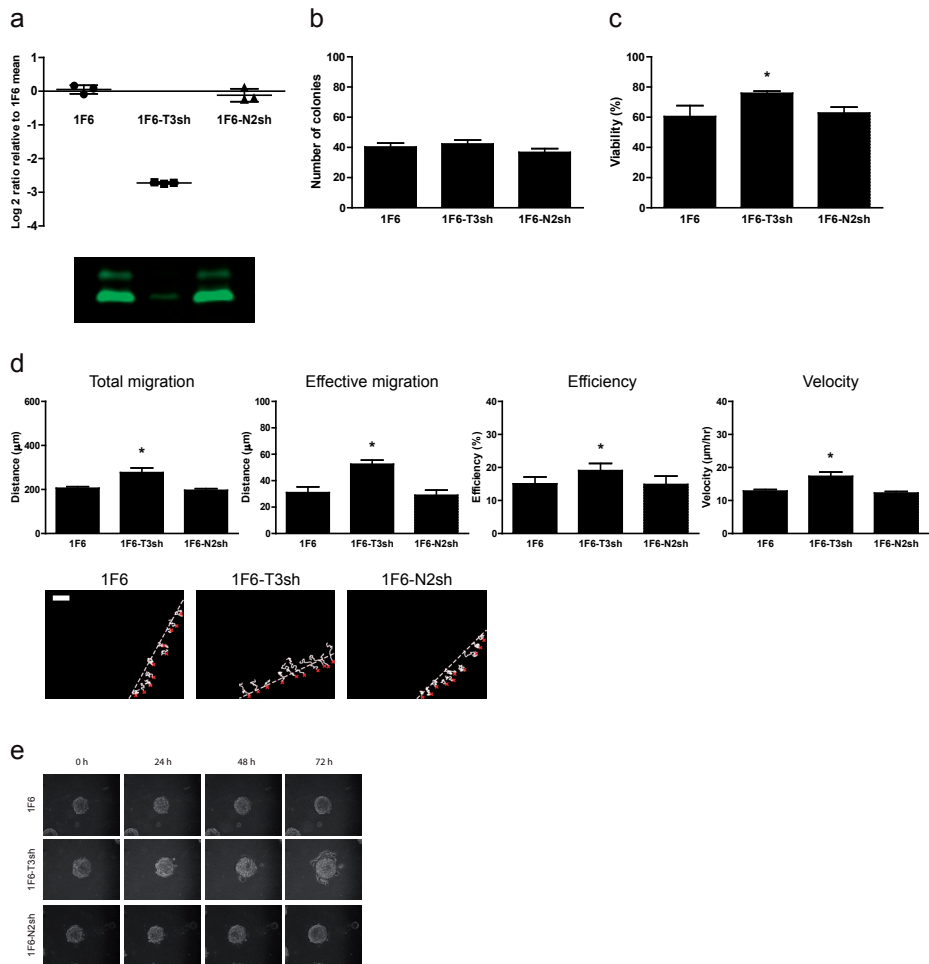
Figure 6. Effect of TIMP3 knockdown in melanoma cells. (**a**) Quantitative PCR gene expression levels of TIMP3 in 1F6, 1F6-T3sh and 1F6-N2sh cells. Changes in transcript abundance were normalized to B2M expression and are expressed as log2 ratio relative to 1F6 mean. Protein expression as determined by western blot of cell lysates. (**b**) Cell proliferation as determined by the colony formation assay. Data are derived from three independent experiments conducted in duplicate. (**c**) Anchorage independent growth as determined by the anoikis assay. Cell viability (%) is expressed relative to growth on standard culture plates. Data are derived from three independent experiments conducted in duplicate. *$P < 0.05$. (**d**) Migratory parameters and representative track diagrams as evaluated using the ring barrier-based migration assay. At least 20 cells from at least three separate experiments were tracked. Scale bar, 100 μm. *$p < 0.05$. (**e**) Invasive capacity of the melanoma cell lines were evaluated by monitoring their dispersion into a collagen matrix. Images were acquired at 0, 24, 48 and 72 h after embedding.

tion in the highly metastatic BLM cells. The metastatic M14 cells also indicated promoter methylation, however the detection of the unmethylated product indicated heterogeneity in cell populations. Sporadically metastatic Mel57 cells and non-metastatic 530 and 1F6 cells did not show promoter methylation (Figure 4c). Treatment with the demethylation agent 5-Aza-dC restored TIMP3 expression in BLM cells and increased the expression in M14 cells confirming our earlier observations of the MSP (Figure 4d). No changes in gene expression were observed in the other cell lines.

Effect of TIMP3 overexpression in melanoma cells

Next we evaluated the functional consequences of TIMP3 expression on melanoma cell behavior. We overexpressed TIMP3 in the otherwise negative BLM cell line (Figure 5a) and assayed several parameters crucial to tumor growth and metastasis. Enforced TIMP3 expression did not alter the growth properties of BLM cells, as evaluated by the colony formation assay (Figure 5b). However, we found a significant decrease in the ability to resist anoikis (Figure 5c). Interestingly, TIMP3 overexpression significantly impaired the migratory capacity (Figure 5d) and invasive capacity of the highly motile BLM cells (Figure 5e).

Effect of TIMP3 knockdown in melanoma cells

Further, stable knockdown of TIMP3 in 1F6 cells was achieved by lentiviral transduction of short hairpin RNA (shRNA) vectors (Figure 6a). No differences in cellular proliferation were observed upon TIMP3 silencing (Figure 6b). However, a significant increase in anoikis resistance (Figure 6c), cell migration (Figure 6d) and cell invasion (Figure 6e) were observed.

DISCUSSION

Neoplastic transformation and the acquisition of an invasive phenotype is the result of several molecular aberrations, including the activation of oncogenes and the loss or inactivation of tumor suppressor genes[182]. The metastatic cascade in melanoma is a highly complex, multifactorial, multi-step process that involves breaching of the underlying basement membrane, extracellular matrix remodeling, migration and local invasion, and entry into hematogenous and lymphatic channels, which ultimately results in secondary tumor formation[57]. Although several advances have been made in characterizing the metastatic cascade in melanoma, the molecular determinants regulating this process remain to be elucidated[55,70].

   TIMP3, a member of the TIMP family of endogenous matrix metalloproteinase inhibitors, is a multifunctional protein and exerts several antitumor properties including inhibition of angiogenesis, invasion and tumor growth[114,115,117,127,148]. We and others have

shown that these effects are propagated through MMP-dependent and MMP-independent mechanisms[121,152]. Further, reduced expression of TIMP3 has been observed in several high grade human malignancies[146,153,158] and as such TIMP3 is regarded as a tumor suppressor. In a recent study, we observed reduced TIMP3 expression in a majority of stage III melanoma samples evaluated, indicating that loss of TIMP3 might be an important event in melanoma progression. As the role of TIMP3 in melanoma progression is hitherto unknown, we evaluated protein expression in matched stage I/II, stage III and stage IV samples from melanoma patients. Immunohistochemical analysis revealed inter- and intratumoral heterogeneity in protein expression. Based on our scoring criteria, we observed that there was a general trend of reduction in protein expression with increasing tumor stage. The median TIMP3 score reduced from stage I/II, to stage III and stage IV, suggesting that loss of TIMP3 might be an important event in melanoma progression. Evaluation of the clinical impact of the loss of TIMP3 expression in our data set however, did not reveal any significant differences between 5-year DFS or OS.

In several tumors, the loss of TIMP3 expression has been attributed to epigenetic regulatory events such as promoter hypermethylation[125,143,144]. MSP analysis of stage III and stage IV samples revealed promoter methylation of TIMP3 in only 2 of the 33 patients, indicating that this epigenetic regulation is a low frequency event in melanoma. These results are in accordance with a previous study[128] and our recent study, where promoter methylation mediated gene silencing was observed in only 18% of the tested melanoma samples. Although our recent study indicated that this epigenetic regulation impacted clinical outcome, survival analysis based on promoter methylation status could not be performed in the current study due to the low number of patients. Recent studies have also suggested alternate modes of expression regulation, such as the post-transcriptional regulation by miRNAs[159], and these mechanisms are currently being investigated.

Furthermore, to obtain mechanistic insights and evaluate functional consequences of TIMP3 expression on the behavioral biology of melanoma, we used a well described panel of melanoma cell lines which vary in their metastatic competence in nude mice. We observed an inverse correlation between TIMP3 protein expression and the reported metastatic potential of the melanoma cell lines. Through gene modulation experiments, we were able to demonstrate that TIMP3 regulates several phenotypic traits of melanoma cells which are crucial to the metastatic cascade, including the resistance to anoikis, cell migration and cell invasion. Taken together, our data indicates that TIMP3 is a negative regulator of the metastatic cascade of melanoma. Current studies are therefore aimed at elucidating the underlying mechanisms responsible for these observations.

7

ACKNOWLEDGEMENTS

SECTION III

Sprouting angiogenic events

CHAPTER 8

High resolution *in vivo* and *ex vivo* imaging of vascular sprouting events using the eNOS-Tag-GFP transgenic mouse

Asha M. Das, Rien van Haperen, Ann L.B. Seynhaeve, Cindy E. Vermeulen,
Joost A.P Rens, Alexander M.M. Eggermont, Rini de Crom, Timo L.M. ten Hagen

INTRODUCTION

The manipulation, inhibition and destruction of the tumor-associated vasculature are intensely pursued avenues in cancer research. To obtain regulatory insights and ascertain effects of treatment, it is imperative to incorporate *in vivo* models which enable real-time observation of the tumor vasculature. An elegant approach is the skin-fold window model, which allows non-invasive and serial observations[210-213]. In this model a flap of skin is held between two frames, which hold glass windows for imaging. In conjunction with intravital microscopy, processes such as tumor growth and angiogenesis can be followed real-time. Intravital microscopy can be further strengthened by the use of transgenic cells or mice, which express specific fluorescent markers.

A major technological advance in the spatiotemporal investigation of *in vivo* processes was the introduction of fluorescent protein tags like Green Fluorescent Protein (GFP)[214,215]. Image analysis with GFP fusion proteins, alone or in combination with spectral variants of GFP, is immensely valuable since it can provide novel insights into behavioural and organizational aspects of biochemical processes[216]. After GFP, an abundance of fluorescent proteins and molecules have been developed ranging from the blue spectrum to the near infrared which allows deeper imaging in tissues[217]. Intercrossing mice with expression patterns of fluorescent proteins further improved the tools to investigate cellular processes *in vivo*.

The skin-fold window model in conjunction with fluorescently labeled tumor cells has been used for the examination of early events during tumor formation[218], and for monitoring the effect of anti-angiogenic therapy on tumor cell migration[219]. However, detailed examination of angiogenesis and vascular effects, especially early processes involving microcapillaries, by non-invasive imaging of GFP labeled tumors, remains difficult due to the inability to positively identify blood vessels. In the skin-fold window model blood vessels can be defined as columns of red blood cells in bright-field view, or can be highlighted by the injection of fluorescent blood markers. However, early non-conducting sprouts, non-functional or disintegrated vessels, or vessels in dark tissue (e.g. melanoma tumors) are difficult to identify. To address these issues, we generated a transgenic mouse which expresses high and consistent levels of GFP in endothelial cells. The eNOS-Tag-GFP transgenic mouse model described herein is used to visualize endothelial cells in various settings and stages of development, including tumor neovascularization and sprouting. The ability to image endothelial cells at high resolution, both *in vivo* as well as *ex vivo*, enables us to study these cells in their natural context, longitudinally and without the need for external interference. This aids in monitoring the kinetics of vascular development, including the identification of early vascular sprouts, and enables discrimination between non-functional and functional vessels.

8

MATERIALS AND METHODS

eNOS-Tag-GFP transgenic mice

A DNA fragment containing a 6.3kb promoter sequence (including a localization signal) and 123bp of the first exon of the human eNOS gene, to ensure protein expression, were isolated from a homemade human genomic cosmid library. This sequence was fused in frame with GFP cDNA with polyA tail. A solution of 1-2 µg/ml of DNA was used for microinjection of fertilized oocytes from FVB/n donor mice and transplanted into the oviducts of pseudopregnent B10xCBA mice. Founder mice and offspring were genotyped by PCR on DNA isolated from tail biopsies. Mice were backcrossed to C57BL/6 for more than 20 generations. All animal experiments were performed in compliance with institutional (Erasmus Medical Center, Rotterdam, NL) and national guidelines.

Cell lines and generation of subcutaneous tumors

Tissue culture reagents, unless otherwise specified, were obtained from Biowhittaker (Walkersville, MD). Murine melanoma B16-BL6 cells, murine fibrosarcoma BFS-1 cells and murine Lewis lung carcinoma LLC cells were maintained in Dulbecco's Modified Eagle Medium (DMEM) with glutamine, supplemented with 10% fetal calf serum (FCS), and subcultured when confluent. Tumors generated from cultured murine melanoma B16-BL6 cells were used for implantation in the skinfold window model as described later. Tumors were induced in donor C57BL/6 mice (Harlan-CPB) by subcutaneous inoculation of 1×10^6 tumor cells in PBS in the flank. Alternatively, for immunohistochemical stainings, tumors were generated in eNOS-Tag-GFP transgenic mice by subcutaneous inoculation of 1×10^6 tumor cells in PBS in the flank. At tumor volumes of 250-300 mm^3, tumors were excised and snap frozen in liquid nitrogen. All experiments with mice were approved by the committee on Animal Research of the Erasmus MC (Rotterdam, NL).

Histology and immunostaining

eNOS-Tag-GFP embryos were harvested at 8.5, 10.5 and 12.5 dpc (days post coitum). To visualize GFP expression, embryos were fixed directly with 4% PFA (paraformaldehyde) and imaged. Alternatively, immunohistochemistry was performed on frozen sections of organs (liver, spleen, heart, thymus, lung) or tumors (B16/BL6, BFS-1, LLC) from eNOS-Tag-GFP mice. After sacrificing the mice, organs or tumors were excised, snap frozen in liquid nitrogen, cut into 5 µm sections and stored at −20°C until the staining procedure. Sections were thawed for 30 min at R.T. and fixed with 4% PFA for 10 min, followed by three rinses with PBS/0.05% Tween-20. Sections were permeabilized with PBS/0.1% Triton X-100 for 10 min at R.T. and aspecific binding sites were blocked with 10% donkey serum/1% BSA/0.1% Triton X-100 in PBS for 30 min at R.T. Primary antibodies were diluted in 1% BSA in PBS and incubated overnight at 4°C. Secondary antibody incuba-

tions were performed for 1 h at R.T. Between all steps of the staining procedure, the slides were washed three times, for two min each, with PBS/0.05% Tween-20. Primary antibodies used were rat anti-mouse CD31 (monoclonal, BD Pharmingen, 1:100) and rabbit anti-GFP (polyclonal, Abcam, 1:100). Secondary antibodies used were donkey anti-rat Alexa Fluor 594 and donkey anti-rabbit Alexa Fluor 488 (monoclonal, Molecular Probes, 1:500). The stained organ and tumor sections were mounted with Fluoromount-G (Southern Biotech, Birmingham, AL) and images were acquired using a Zeiss LSM 510 Meta confocal microscope.

Preparation of window chambers and tumor implantation

The preparation of the dorsal skin-fold chamber is an adaptation from previously described procedures[210,218,220,221]. At tumor volumes of 180-200 mm^3, tumor tissue was excised under sterile conditions, dissected into small pieces in sterile physiological solution, and directly used for implantation in the window chamber. We used home-made synthetic polyoxymethylene frames which are relatively light and small. A true visible field of 11 mm for this mouse skin-fold window chamber was established. The complete window consists of few parts such as collar, spacers, retaining ring and frame. Mice were anesthetized with a subcutaneous injection of 150 μl of a 1:1:2 (v:v) mixture of Ketamine (Alfasan, Woerden, NL), Xylazine (Bayer AG, Leverkussen, FRG) and physiologic salt solution. Hair was removed from the back and the midline was marked. On one side of the skin-flap, the frame of the window was outlined and a 12 mm diameter flap of skin was dissected away, leaving the fascia and opposing skin. The skin-fold on the back of mice was sandwiched between the two frames, fixed with two light metal bolts and sutures. On both sides, the windows were closed with a 12 mm diameter microscopic cover glass (0.13-0.16 mm thick) held in place with a retaining metal ring. This thickness of the cover glass, in combination with the flat construction of the frame, allows the use of objectives with relatively high magnification and numerical aperture. Before closing of the surgical site a small piece of tumor (0.1 mm^3) was transplanted in the fascia using a micro-surgical microscope. Hereto a small pocket was created in which the tumor piece was placed. After implantation of the tumor tissue the mice were individually housed in an incubation room with an ambient temperature of 32°C and a humidity of 50%. The tumor was allowed to develop for 10 to 14 days.

Preparation and characterization of long circulating liposomes

To visualize the functionality of the tumor associated vasculature in the skin fold window, long circulating liposomes of circa 100 nm labeled with Rhodamine were used as blood marker. Empty liposomes were prepared by the lipid film hydration and extrusion method, as described[222]. Total phospholipid content was determined using the phosphate assay[223].

8

Fluorescence intravital microscopy

Animals bearing the skinfold chamber were anesthetized with the inhalation anesthetic isoflurane (Nicholas Piramal, London, UK), placed on a thermal mattress maintained at 37°C and fixed to the stage of a microscope. Observations of the tumor vasculature was made with a Zeiss LSM 510 META confocal microscope. Scans were made with an argon laser (488 nm) and GFP filter setting (BP 500-530 nm). Vessel perfusion and functionality was visualized by imaging long circulating Rhodamine labeled liposomes described above. Tumor bearing mice were injected with 1 μmol liposomes, via the tail vein, 30 min before imaging. Circulating liposomes were visualized with a He-Ne laser (543 nm) and Rhodamine filter setting (BP 560-615 nm).

Retina angiogenesis assays

To analyze retinal vasculature development in the eNOS-Tag-GFP transgenic mice, eyes were isolated from pups at postnatal days P3, 6, 9, 12, 16 and 20. Whole eyes were fixed for 30 min at RT with 4% PFA. After several washes in PBS, the retinas were dissected as previously described[224], and flat mounted on glass slides with Fluoromount-G. Additionally, pharmacological inhibition of Notch signaling was tested, using the γ-secretase inhibitor DAPT, in postnatal retinas of littermate pups[225]. Pups were injected i.p. with 0.2 mg/g DAPT (Calbiochem) in a 1:4 mixture of ethanol and peanut oil on P5 and P6. Control pups received vehicle treatments.

Aortic ring assay

Aortic ring assays and subsequent immunofluorescence stainings were performed according to the protocol described by Baker et al.[226], with minor modifications. Aortic rings were dissected from 7 week old eNOS-Tag-GFP transgenic mice and serum starved overnight in Opti-MEM medium supplemented with 1% P/S at 37°C. The following day, aortic rings were embedded in a 1 mg/mL collagen matrix (Collagen Type 1, rat tail, Millipore) on ice, followed by the addition of 30 ng/mL recombinant mouse VEGF 164 (R&D Systems Europe, Abingdon, UK) in Opti-MEM medium. Treatment with Opti-MEM alone was used as a negative control. All treatments were supplemented with 2.5% FBS and 1% P/S. Growth medium was replenished on days 3, 5 and 7 and sprout formation from rings was imaged on day 3, and days 6-9. For immunofluorescence staining experiments, rings were fixed on day 9 with 4% PFA.

RESULTS AND DISCUSSION

Since the recognition of angiogenesis as a crucial step in tumor development and progression, much effort has been put in unraveling this process[227]. The dependence of tumor growth on neovascularization has initiated antiangiogenic therapy, which has had its

successes independently and in combination with radiation or chemotherapy[39,228]. Unfortunately, antiangiogenic therapy is still far from optimal, due to a lack of understanding of tumor pathophysiology and the kinetics of tumor vascular development. Various physical barriers need to be overcome, in addition to clearance by the immune system and lymphatics, and intravital microscopy delivers much needed insight into these processes[211].

Endothelial nitric oxide synthase (eNOS) is part of an important family of signaling molecules, including inducible NOS (iNOS) and neural NOS (nNOS), involved in processes ranging from maintaining homeostasis to destruction of invading microorganisms[229,230]. The endothelial isoform, eNOS, was first isolated and characterized from endothelial cells[231,232], while later studies demonstrated expression by various other cell types. For maintenance of homeostasis low levels of eNOS are constitutively produced, which is tightly regulated, while production of eNOS is affected by flow or through calcium dependent receptor signaling[233].

The universal and constitutive expression of eNOS by endothelial cells provides an attractive possibility to identify these cells and characterize their role in vascular development. Previously, a transgenic mouse expressing eNOS-GFP fusion protein was generated (eNOS-GFPtg)[234], where the entire human eNOS gene was fused in frame with GFP cDNA. Although GFP expression was restricted to the endothelial vessel lining, transgenic mice exhibited increased eNOS enzymatic activity and elevated NO levels due to eNOS overexpression. Further, both mean aortic pressure and pulmonary artery pressure were reduced in transgenic mice. Therefore, in this study we generated a transgenic mouse where GFP was inserted in frame with the eNOS promoter and 123 bp of the first codon which was necessary for GFP expression (Figure 1a). Immunohistochemical analysis of harvested mouse embryos revealed that GFP expression was visible through all stages of development (Figure 1b) and was restricted to the endothelial vessel lining (Figure 1c). Further, immunohistochemical analysis of organs from adult transgenic mice also showed GFP expression co-localizing with the vessel marker, CD31 (Figure 2).

Further, to ascertain the effect of transgene expression on xenograft growth, we compared the growth rate of B16, BFS-1 and LLC mouse tumor cells injected in C57BL/6 mice and eNOS-Tag-GFP mice. Xenografts exhibited similar growth rates in both mouse strains suggesting that GFP expression did not alter tumor development (Figure 3a and data not shown). Tumor induced vasculature was visualized by staining for vessel coverage (CD31) and we observed a clear overlap with GFP expression (Figure 3b). Immunohistochemical analysis also revealed the presence of young non-quiescent vessels (determined by CD105 staining) in the tumor sections, which showed co-localization with GFP (data not shown).

To visualize real-time kinetics of tumor induced vasculature development, we implanted a piece of the B16 tumor in the skin-fold window of transgenic mice (Figure 4a). This tumor expresses high levels of melanin resulting in a very dark, almost black tumor,

8

a
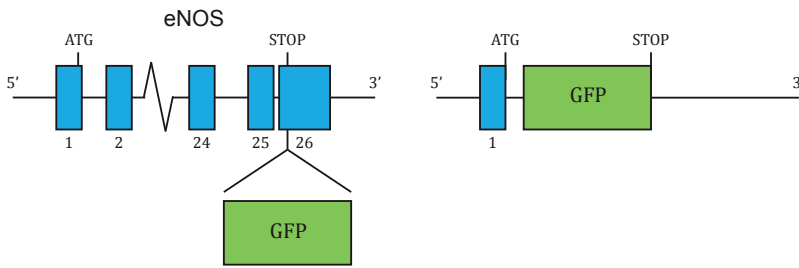
b
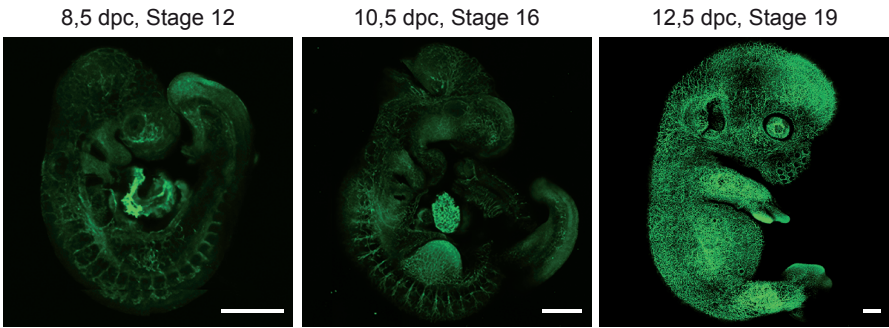
c
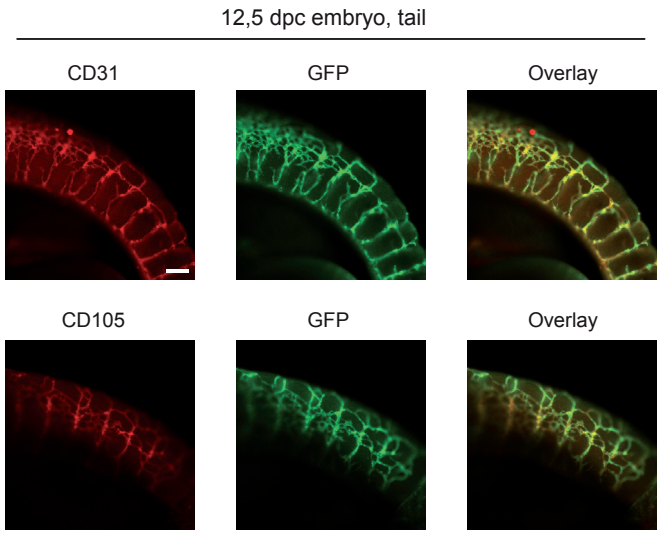
Figure 1. eNOS-Tag-GFP transgenic mice. (**a**) Comparative schematics of the eNOS-GFPtg construct and the eNOS-Tag-GFP construct. The latter consists of the eNOS promoter which contains the localization signal, 123 bp of the first eNOS codon and the Green Fluorescent Protein (GFP) cloned in frame. (**b**) Detection of GFP expression in various stages of embryonic development of the eNOS-Tag-GFP mouse. Scale bars, 500 μm. (**c**) Immunohistochemical staining of a 12.5 dpc eNOS-Tag-GFP embryo showing colocalization of GFP and CD31. Scale bar, 100 μm.

	Liver	Spleen	Heart	Thymus	Lung
GFP					
CD31					
Overlay					
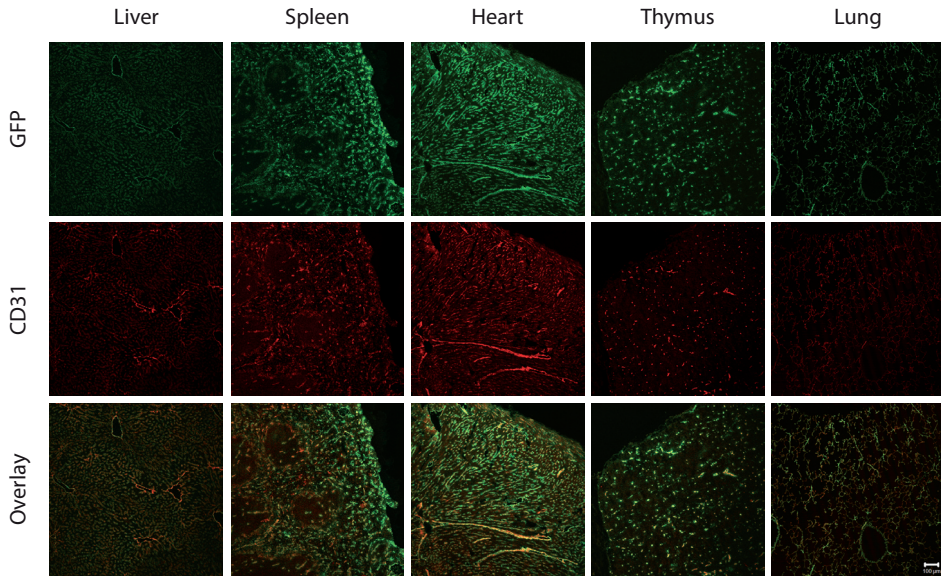
Figure 2. GFP distibution in transgenic mice. Snap-frozen organs of the transgenic mice were subjected to immunohistochemical stainings using the vessel marker CD31 and an anti-GFP antibody. Scale bar, 100 µm.

and identification of blood vessels by trans-illumination is difficult already at a small tumor size. The tumors were allowed to grow to a diameter of 2.5 mm at which time point intravital microscopy was commenced and continued to a tumor diameter of 8 mm. The expression of GFP by the endothelial cells allowed visualization of the endothelial lining of the vessels in the tumor. We observed the presence of small sprouts protruding into the tumor early after tumor implantation (day 7, 8). By day 10, long thin endothelial cell extensions into the tumor were observed. By day 14, a dense and fully developed vascular bed was present throughout the tumor. Signs of central necrosis were absent at all stages. Real-time imaging of the sprouting angiogenic front showed advancing and retracting sprouts, indicative of the role of the microenvironment in providing guidance cues (Figure 4b).

In addition to vessel presence, vessel functionality is paramount to angiogenesis, as the lack of functionality adversely affects drug distribution and drug delivery[235]. The functionality of tumor vasculature is heterogeneous and dynamic, resulting in regrowth after antiangiogenic or conventional treatment. During all stages of the vascular development we observed regions, which are poorly or not vascularized. At an early stage the center of the small nodule is not perfused, limiting penetration at that time point. At a later stage the solid tumor seems highly vascularized throughout. Injection of Rhodamine labeled liposomes indicated a perfused vascular front (Figure 4c) and the presence of large non-functional vessels towards the tumor periphery (data not shown). These ob-

servations indicate that previously functional vessels can become non-functional, which has a strong impact on nutrient and oxygen delivery and tumor cell survival, as well as on the potential of therapy targeting the tumor-associated vasculature. Additionally, high resolution imaging also provides insights into the spatiotemporal regulation of sprouting events (Figure 4d). During *in vivo* sprouting events, endothelial cells extend actin-rich filopodia to probe the surrounding environment and obtain guidance cues which further regulate sprout formation and vascular patterning[236]. An interesting observation was the presence of single endothelial cells in the tumor center (Figure 4e). As single endothelial cells and sprouting was observed in areas which were previously a-vascular, these cells therefore are not a result of vessel degradation. We hypothesize that these cells contribute to vascular bed formation.

a
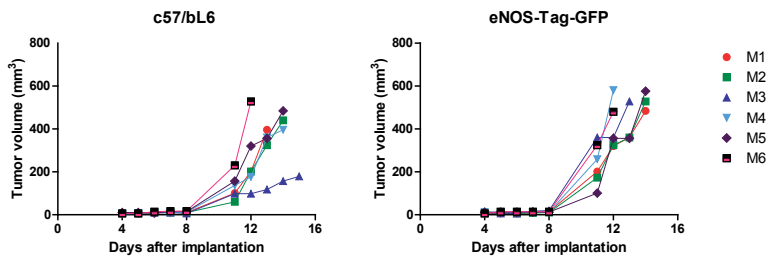
b
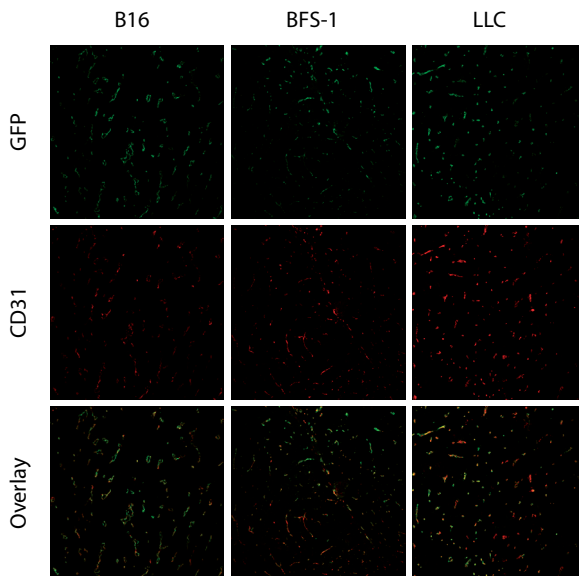
Figure 3. Xenograft growth. (**a**) Comparison of xenograft growth with subcutaneously injected B16-BL6 cells in C57Bl6 mice and transgenic mice. (**b**) Immunohistochemical analysis of vessel coverage (CD31) and GFP expression in frozen tumor sections. Scale bar, 100 µm.
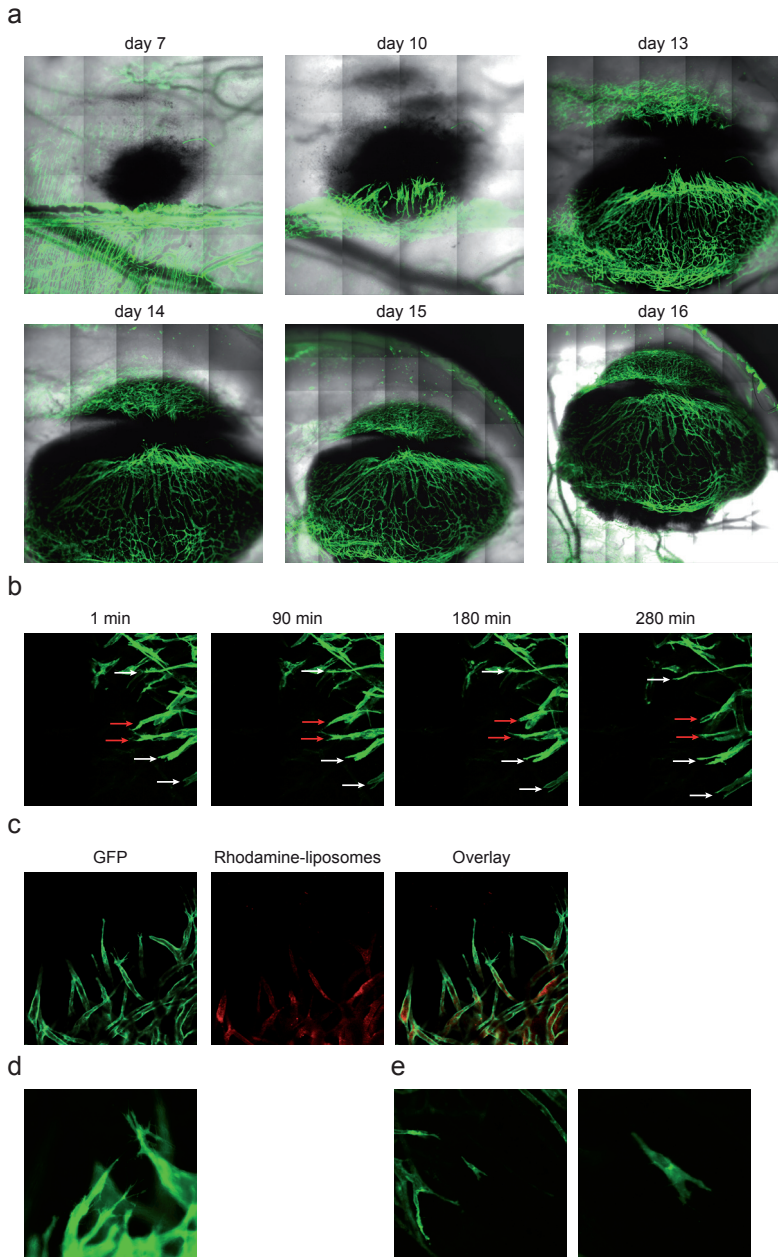
Figure 4. Intravital imaging. (**a**) eNOS-Tag-GFP mouse bearing the skinfold chamber containing a B16 melanoma tumor (black). Longitudinal imaging shows the initiation of the angiogenic front (green) and subsequent tumor vascularization. (**b**) Live intravital imaging of the dynamic angiogenic front shows movement of endothelial sprouts. Red arrows indicate receding sprouts and white arrows indicate advancing sprouts. (**c**) Vessel perfusion and functionality was evaluated by injecting Rhodamine-labeled liposomes. Depicted are the vessels (green), the liposomes (red), and the overlay image. (**d**) *In vivo* visualization of tip cells and filopodia. (**e**) Identification of single endothelial cells in the tumor center.

In addition to providing mechanistic insights into tumor related angiogenic events, the eNOS-Tag-GFP transgenic mouse provides an ideal platform to evaluate physiological events such as the development of the retinal vasculature. Analysis of retinas of post-natal pups reveal the branching and morphogenesis of the retinal plexus without the requirement of additional staining procedures (Figure 5a). Moreover, pharmacologi-
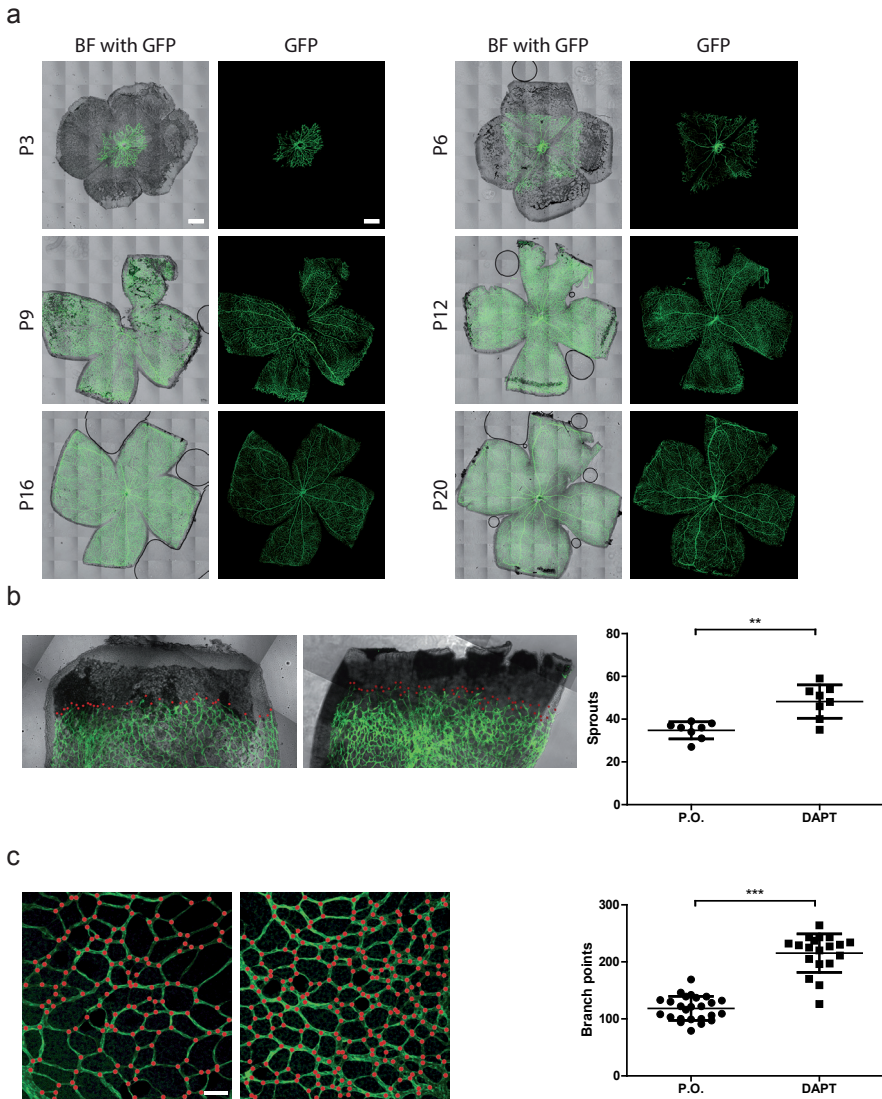
Figure 5. Retinal vasculature development. (**a**) Isolated retinas at postnatal days, P3, 6, 9, 12, 16 and 20, showing GFP expression. Scale bar, 500 μm. (**b,c**) Pharmacological inhibition of Notch signaling was achieved by treatment with DAPT. (**b**) Quantification of sprouts and (**c**) branch points in fixed, mounted retinas. P.O., peanut oil. Scale bars, 50 μm.

cal inhibition of Notch signaling showed an increase in both sprouting and branching in the retinas of transgenic mice (Figure 5b, c). Additionally, *ex vivo* aortic ring assays performed with aortas isolated from transgenic mice showed stable expression of GFP in the vasculature (Figure 6). This enables the study and screening of angiogenic modulators and inhibitors. Further, interactions between various cell types can also be visualized using this assay, although without the proper context of the body or for instance blood flow.
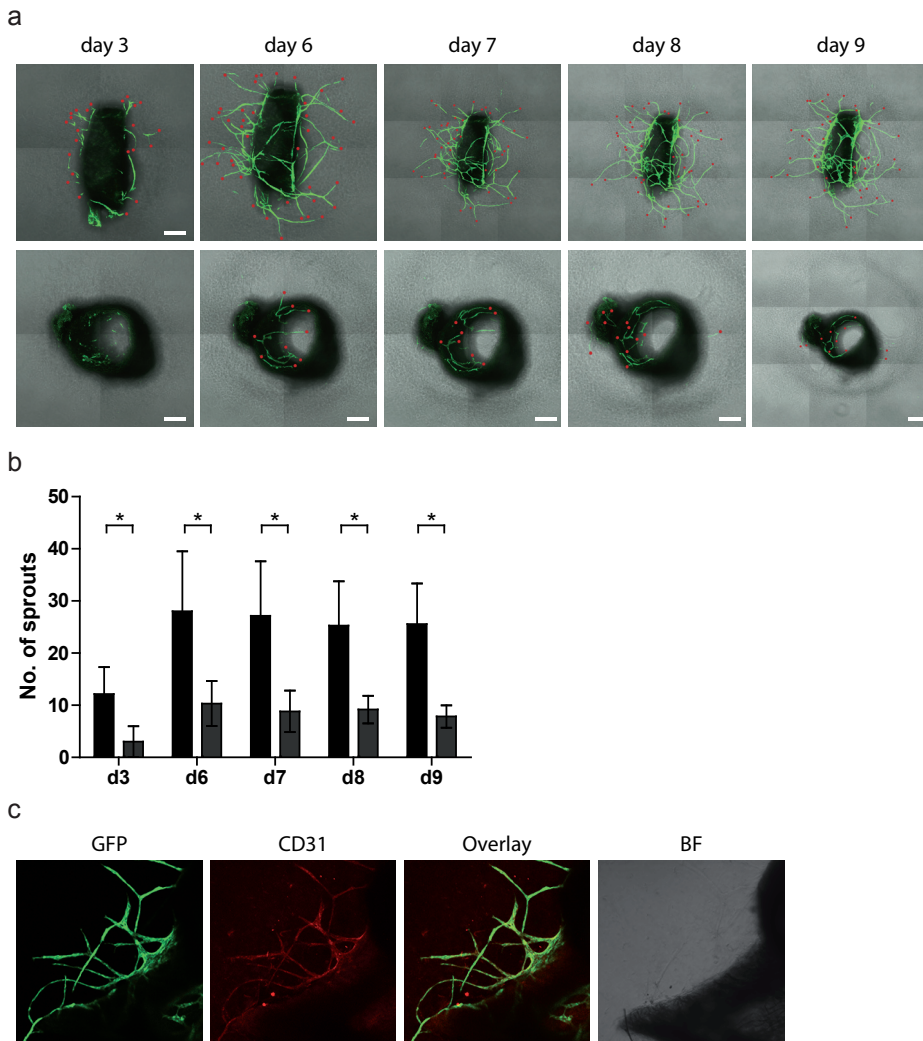
Figure 6. Aortic ring assay. Aortic rings from eNOS-Tag-GFP mice were embedded in collagen and imaged on the indicated days. (**a**) Angiogenic response upon treatment with Opti-MEM with 30 ng/mL recombinant mouse VEGF or Opti-MEM alone as control. Scale bars, 200 μm. (**b**) Quantification of angiogenic sprouts. (**c**) Immunofluorescence staining of fixed aortic rings shows colocalization of CD31 with GFP.

Taken together, our data indicates that the eNOS-Tag-GFP mouse is a useful model to study the dynamic behavioral aspects of endothelial cells during the angiogenic process. These studies provide insight into the behavior of endothelial cells and the formation of a vascular network *in vivo*, which is essential for the development and assessment of anti-angiogenic therapy. Real-time kinetics of endothelial cells during vascular development can be investigated efficiently by combining the eNOS-Tag-GFP transgenic mice with high resolution intravital imaging. Additionally, the retina angiogenesis assay and aortic ring assays can be used to evaluate effects of anti-angiogenic molecules. This model can therefore be used to analyze sub- and intracellular mechanisms *in vivo*, including leukocyte/endothelial cell interaction, vessel growth and destruction, endothelial cell migration, and vascular mimicry and mosaicism.

CHAPTER 9

General discussion

GENERAL DISCUSSION

Malignant melanoma- where we were, are, and heading

Melanoma represents a significant health burden with an increasing rate of incidence and high resistance to therapeutic intervention[2]. Traditional therapeutic approaches have consistently failed to improve the long-term prognosis of this disease and the lack of effective curative options led to advanced stage melanoma being designated a 'graveyard of pharmaceutical development'[25,237,238]. However, in the past decade unprecedented strides have been made in understanding the molecular etiology and behavioral biology of melanomas, which have been successfully translated into clinical practice and tremendously improved the standard of care[1,208,239].

Historically, melanoma research has predominantly been focused on the neoplastic cell. A plethora of evidence now indicates that melanoma tumorigenesis is a concerted effort between neoplastic cells and the host microenvironment. This is furthered by multiple genetic lesions and deregulations in critical regulatory networks which impact the course of disease and other crucial aspects, such as responsiveness to therapy and the acquisition of drug resistance. An elegant study recently demonstrated how BRAF-mutant melanoma cells develop a tolerance to BRAF inhibition by activating melanoma-associated fibroblasts. This inadvertent hyperactivation of the host stroma leads to extensive matrix remodeling, which provides the melanoma cells with stimulatory signals enabling survival and resistance[240]. These and other recent observations clearly indicate that the host microenvironment is not just a passive bystander, but an active participant in the neoplastic process, and that such reciprocal signaling networks arbitrate multiple aspects of melanoma aggressiveness.

In light of these findings, several modifications have been made to the classical view of melanoma progression and disease biology. Continued deciphering of the melanoma landscape illustrates the complexity of pathogenesis, and the multiple factors which govern it. Several biological mechanisms such as genetic and epigenetic alterations, tumor heterogeneity, tumor-host microenvironment cross-talk, parallel progression models, tumor dormancy and organ-specific metastasis are therefore the focus of current research endeavors[25,55,70].

The work described in this thesis aimed to obtain novel mechanistic insights into melanoma biology. Two fundamental cascades crucial to the growth and progression of melanomas, the angiogenic and metastatic cascades, were studied. A combination of cell-based assays, gene expression analysis, gene modulation experiments, animal models and imaging techniques were used to link the phenotypic traits of melanoma cells with the genetic modulators responsible for the biological behavior. Furthermore, novel models which enable characterization of biological processes are described. These results, and their implications thereof, are further discussed.

9

The angiogenic landscape of melanoma- not only a VEGF story

The progression of most solid tumors from a benign to a malignant state is accompanied by an 'angiogenic switch'[241,242]. This cardinal pathophysiological hallmark of tumor development refers to the increase in proangiogenic ligands produced by the tumor cells and the tumor microenvironment, with a concomitant decrease in angiogenic inhibitors. These tumor-associated modulators facilitate the enhanced proliferative, survival and migratory responses exhibited by endothelial cells, culminating in unregulated and unimpeded angiogenesis[102]. Targeting angiogenesis is therefore a rational approach, as it is one of the rate-limiting steps of tumor growth.

Melanomas are in general highly angiogenic tumors. The degree of angiogenesis in melanoma has been shown to correlate with tumor grade, risk of recurrence and metastatic potential[50]. Additionally, several proangiogenic modulators like VEGF, bFGF, PDFG and IL-8 are frequently overexpressed in melanomas[243]. Among the angiogenic ligands, VEGF has been the most investigated. Elevated levels of VEGF and its receptors have been detected in the sera of melanoma patients and shown to correlate with poor clinical outcome[47-49]. Further, a large tissue microarray study reported increased expression of VEGF, VEGF-R1, VEGF-R2 and VEGF-R3 in melanomas as compared to benign nevi[44]. Additionally, several preclinical studies targeting the VEGF-VEGFR signaling axis have demonstrated inhibition of tumor growth and metastasis in human melanoma xenograft models[244]. These observations led to the therapeutic implementation of a large variety of anti-angiogenic approaches including antisense and antibody-mediated ligand and receptor neutralization, receptor signaling inhibition using soluble decoy traps (VEGF-trap) and small molecule receptor tyrosine kinase inhibitors (TKI) to target signaling pathways. Clinically however, antiangiogenic approaches have only yielded modest benefits, and although well tolerated, antiangiogenic treatments either as monotherapy or in combination with chemotherapy have thus far failed to improve survival rates in melanoma patients[43,78].

Given the experimental and theoretical evidence of the pivotal role of angiogenesis in melanoma, we postulated that there might be yet undiscovered and uncharacterized modulators regulating the angiogenic cascade. To test this hypothesis we examined a well described panel of melanoma cell lines which differ in their degree of aggressiveness and production of known proangiogenic molecules[83,88]. We evaluated the angiogenic potential of the melanoma cell lines by testing their ability to promote endothelial cell (EC) survival under severe hypoxic conditions (Chapter 2). We observed that all melanoma conditioned media (MCM) were capable of sustaining long-term EC survival by preventing apoptotic cell death, while this effect was not observed with conditioned media derived from melanocytes or other tumor cell lines (breast and pancreatic). These data suggest that the production of this pro-survival molecule or molecules is an acquired and unique feature of melanoma development. Strikingly, size fractionation of the MCM indicated

the localization of the survival promoting factor in the < 1 kDa range, which further excludes known proangiogenic modulators implicated in melanoma pathogenesis such as VEGF and bFGF. Global changes in gene expression and pathway analysis indicated the activation of critical signaling pathways involved in EC survival, upon treatment with MCMs. The small molecule MCM fraction was able to induce a pronounced activation of AKT and ERK-1/2 signaling in ECs, and inhibition of signal transduction with specific pathway inhibitors resulted in apoptotic cell death. Moreover, reduced expression of downstream effectors of apoptosis such as p38 MAPK and active caspases was also observed in the MCM treated samples.

These results describe a novel and unique feature of melanoma biology and provides a clear indication that much remains to be learned of the angiogenic effectors of this disease. Initial attempts at characterizing the melanoma-specific factor suggest that it might be a lipid or lipophilic molecule. Larger studies are required to verify the specificity of the observed pro-survival effect as a feature unique to melanoma. Further, the application of high throughput techniques such as mass spectrometry will enable the elucidation and characterization of these molecules. Our results also provide possible clues for the development of new therapies, which focus on targeting the capacity of melanoma cells to enable the survival of its stromal partners.

TIMP3 regulates multiple aspects of melanoma progression

Several tumor related processes including neovasculature initiation and metastatic dissemination require the breaching of the underlying basement membrane and invasion into the extracellular matrix (ECM)[131]. Remodeling and turnover of the ECM is mediated by tightly regulated reciprocal interactions between matrix degrading enzymes, the matrix metalloproteinases (MMPs) and their natural inhibitors, the tissue inhibitor of matrix metalloproteinases (TIMPs). The TIMP family consists of four homologous proteins, TIMPs 1 through 4, which regulate a range of physiological processes including cell proliferation, migration, invasion and apoptosis[124]. Recent evidence indicates that these functions are mediated by both MMP-dependent and MMP-independent mechanisms[245].

Among the TIMP family, TIMP3 has been reported to be unique in that it is insoluble and tightly sequestered to the matrix[118]. We were able to detect high levels of TIMP3 in the conditioned medium generated from melanoma cell lines which endogenously expressed TIMP3 (Chapter 3). Further, enforced expression of TIMP3 in otherwise negative melanoma cell lines, also showed accumulation of secreted TIMP3 in the conditioned medium. These results suggest paracrine modes of TIMP3 signaling in melanoma. We also observed a differential expression in secreted levels of TIMP3 among the melanoma cell lines, with expression inversely correlating to tumor aggressiveness. Through evaluation of the ability of the MCM to promote directional EC migration, a process critical to tumor-associated neovasculature formation, and subsequent size fractionation

9

experiments, we were able to identify TIMP3 as an inhibitor of the angiogenic cascade in melanoma. These results were also verified *in vivo*, where TIMP3 expression reduced tumor growth and vascular coverage in melanoma xenograft models. The inhibitory effect of TIMP3 on the angiogenic cascade has been reported to be mediated by MMP inhibition as well as through the inhibition of VEGF-VEGFR2 signaling[121]. Our results indicate that in melanoma TIMP3 mediated angiogenesis inhibition is, at least in part, regulated through MMP-independent mechanisms.

An important observation of this study was the striking reduction in tumor infiltrating macrophages upon enforced expression of TIMP3. In melanoma, the presence of infiltrating macrophages has been shown to correlate with angiogenesis, disease progression and poor clinical outcome[51-53,129]. Further, studies in breast and pancreatic xenograft tumors have shown a reduction in tumor infiltrating macrophages upon inhibition of the VEGF-VEGFR2 signaling axis[138,139]. Thus while the exact role of TIMP3 in this regard remains to be elucidated, it is tempting to speculate that TIMP3 inhibits macrophage infiltration by binding to VEGFR2 and inhibiting ligand-receptor signaling.

To determine the clinical relevance of these observations, we examined TIMP3 expression and correlation to vascular coverage and macrophage infiltration in a cohort of melanoma positive stage III lymph node samples (Chapter 4). We observed a significant inverse correlation between TIMP3 expression and mean vessel density (visualized by CD31 staining) in melanoma biopsies. Corroborating previous observations[51,52], we also detected a significant positive association between mean vessel density and macrophage infiltration in melanomas. However, in our dataset, no significant association was observed between TIMP3 expression and infiltrating macrophages. A possible explanation for this could be the marker chosen to detect the presence of tumor-associated macrophages. The pan monocyte-macrophage marker, CD68K, used in our study does not discriminate between pro-inflammatory and anti-inflammatory macrophage subsets. Thus further studies are required to ascertain the association between TIMP3 expression and the presence of tumor promoting macrophage populations in melanoma.

TIMP3 has been ascribed a tumor suppressor role in several human malignancies[140-142] and loss of expression has been attributed to epigenetic regulatory events such as gene promoter hypermethylation[125,143-145] and allelic loss of heterozygosity[146,147]. Analysis of the methylation status of TIMP3 in our dataset revealed it to be a low frequency event in melanomas (18% of analyzed samples). These data are in accordance with a previous study reporting low frequency of methylation associated TIMP3 silencing in melanoma cell lines and tumor biopsies[128]. Interestingly however, despite the low frequency detected, this epigenetic modulation seemed to impact outcome. Analysis of clinical associations revealed that patients with methylated TIMP3 experience significantly shorter overall survival (OS) and disease-free survival (DFS). Thus while our data suggests that promoter methylation of TIMP3 in melanoma could have value as a prognostic marker,

these results need to be validated in a larger cohort on account of the limited number of samples used in our study.

Immunohistochemical analysis of TIMP3 expression in the lymph node biopsies dataset also revealed low expression of TIMP3 in the majority of the samples. These observations are in line with the reduced expression of TIMP3 reported in other advanced stage tumors[146,153,158]. Therefore we hypothesized that the loss of TIMP3 might be an important event in melanoma progression and secondary tumor formation. To this end we used a valuable set of matched stage I/II, stage III and stage IV samples from melanoma patients and analyzed changes in TIMP3 expression during melanoma progression from primary to disseminated disease (Chapter 7). We observed a decrease in the median TIMP3 immunohistochemistry score with disease progression, suggesting that loss of TIMP3 is an important event in melanoma pathogenesis. Methylation specific PCR analysis indicated promoter hypermethylation in only 2 of the 34 samples analyzed. These results further verify that TIMP3 methylation is a low frequency event in melanoma. Recent studies have reported alternate modes of TIMP3 expression regulation, such as the post-transcriptional regulation by miRNAs[159,246-248]. Due to sample limitations, these aspects could not be verified in our study. Further studies are therefore required to investigate alternative modes of TIMP3 expression regulation. We also assessed the functional aspects of the loss of TIMP3 expression on the metastatic potential of melanomas. Using melanoma cell lines, we observed that TIMP3 inhibits the migratory and invasive capacity of melanomas. Taken together, these studies indicate that TIMP3 exerts a tumor suppressor role in melanoma pathogenesis and regulates multiple aspects of disease biology.

Delineating effectors of melanoma metastasis

Metastatic dissemination to regional and visceral sites is responsible for the majority of melanoma-related mortalities. In melanoma, the identification of core mediators essential to the initiation and propagation of the metastatic phenotype is challenging due to the high mutational load[184] and considerable disease heterogeneity[185]. Therefore there is an urgent need to define molecular determinants and signaling pathways which predict the biological manifestation of this complex and multifactorial process. As the acquisition of a motile and invasive phenotype is one of the hallmarks of melanoma progression, we investigated the migratory potential of a panel of melanoma cell lines, with known metastatic propensities[87] (Chapter 6). We observed a clear correlation between the migratory and metastatic competence of the melanoma cell lines. Through correlation analysis of the migratory phenotype with the genetic make-up of these cells, we identified WNT5A as a dominant regulator of this phenotype. Through functional gene modulation assays, we were able to demonstrate that WNT5A regulates the migratory and invasive potential of melanoma cells. These data are in accordance with a previous study where WNT5A was reported to regulate melanoma cell motility[200]. Interestingly,

9

although WNT5A has been reported to modulate cell proliferation in melanoma[206], we did not observe differences in cell growth either upon enforced expression or gene knockdown. Further, WNT5A knockdown did not alter *in vivo* xenograft growth rates. Strikingly, longitudinal imaging in an experimental metastasis model showed that the formation of lung metastasis was dramatically delayed or inhibited. Conversely, over-expression of WNT5A in the otherwise negative and non-metastatic cell line resulted in the formation of lung metastases. Interestingly, we also observed an increase in the *in vivo* growth rate of these tumors. The observed differences of *in vitro* and *in vivo* growth might be attributed to the stromal microenvironment, and requires further investigation. Collectively, our results indicate that WNT5A is an important effector of the metastatic cascade in melanoma. A recent study reported upregulation of WNT5A in a subset of BRAF resistant melanomas[206], implicating WNT5A in the acquisition of drug resistance. Thus obtaining further insights into the signaling cascade might offer avenues for therapeutic management. This study also highlights that biological profiling of tumors, i.e. characterizing phenotypic traits to identify genetic modulators of disease biology, is a powerful approach.

Novel tools

In addition to obtaining novel insights into biological phenomenon, there is a need for the development of novel tools which enable quantitative and standardized assessment of biological processes. This thesis describes the development and application of such tools to characterize several biological parameters.

Cell migration

Cell migration is elemental to the regulation of a wide variety of physiological and pathological processes[160] and has been traditionally evaluated using the wound-healing or scratch assay[164,165]. While cost-efficient and relatively simple to perform, several aspects crucial to the regulation of the migratory process, including the effect of matrix coatings and cell-cell interactions, are obscured in the scratch assay. To address these issues, we developed the 'ring barrier-based migration assay', which enables the quantitative determination of several parameters of cell migration (Chapter 5). This assay continues to provide useful and quantitative data in determining migratory parameters in a range of biological contexts, including tumor development and metastasis[171,187,209].

Intravital imaging

Obtaining insights into the regulation of the angiogenic cascade is critical to the implementation of antiangiogenic approaches. Chapter 8 introduces the eNOS-Tag-GFP transgenic mouse model which aids in the visualization of endothelial cell behavior during neovasculature initiation in physiological and pathological contexts. In combination with

high resolution intravital microscopy, this model enables the real-time and longitudinal *in vivo* monitoring of the kinetics of tumor vascular development.

Digital microscopy

In this thesis, the use of digital microscopy and automated analysis has been shown to be very valuable to quantitatively determine vessel density and tumor associated macrophages (Chapter 4). For instance, in melanoma the prognostic value of neovascularization remains unsettled and the reason for discrepant results might be attributed to the use of non-standardized scoring methodologies such as the 'hot-spot' method[244]. The use of virtual microscopy in conjunction with image analysis software enables quantitative and high throughput analysis of such parameters, and minimizes bias and inter-observer discrepancies.

CONCLUDING REMARKS

Melanoma has long been regarded as one of the most indecipherable and treatment-resistant of all human cancers. Multiple therapeutic strategies have dismally indicated the impressive versatility and resistance exhibited by melanomas. Fortunately, there has been a dramatic change in the outlook for patients over the last few years. Several breakthrough advances have been made in characterizing melanoma biology, and implementation of the same in a clinical setting. Elucidating and defining the role of core mediators of tumor biology is therefore crucial to identify potential targets susceptible to therapeutic intervention and for the development of new treatment rationales.

In this thesis, novel mechanistic insights into melanoma biology were obtained. We identified the capacity of melanoma-derived small molecules to promote long-term survival of endothelial cells under severe hypoxic conditions. This observation excludes known proangiogenic molecules which have been the focus of anti-angiogenic therapies and sets the stage for the identification of novel regulators with therapeutic potential. Moreover, we identified TIMP3 as a dominant negative regulator of melanoma development. We were able to validate the inhibitory role of TIMP3 in melanoma angiogenesis and further extend this observation to clinical samples from melanoma patients. We showed that promoter methylation mediated TIMP3 silencing impacts clinical outcome in melanoma. We also evaluated the implications of the tumor suppressor role of TIMP3 in melanoma metastasis, using matched samples from melanoma patients. We observed a decrease in expression with disease progression and further showed that TIMP3 expression inhibits melanoma cell migration and invasion.

To characterize core mediators of the metastatic cascade of melanomas, we determined the migratory profile of melanoma cell lines and performed correlation analysis to identify potential genetic modulators. We identified WNT5A as a dominant regulator of the

9

metastatic cascade in melanoma and further showed that WNT5A inhibition decreased the migratory and metastatic potential of melanoma cells. Additionally, this thesis also describes novel tools to quantitatively characterize several biological processes. The ring barrier-based migration assay enables the quantitative assessment of several parameters of cell migration. The eNOS-Tag-GFP mouse model provides a platform for the *in vivo* and *ex vivo* study of early angiogenic events in physiological and pathological conditions.

Collectively, the results presented in this thesis identify crucial pathophysiological determinants of melanoma. These insights and tools may further guide the discovery of novel regulators of melanoma biology and result in the implementation of new treatment rationales for therapeutic benefit.

REFERENCES

1   Schadendorf, D. & Hauschild, A. Melanoma in 2013: Melanoma--the run of success continues. *Nat Rev Clin Oncol* **11**, 75-76 (2014).

2   Eggermont, A. M., Spatz, A. & Robert, C. Cutaneous melanoma. *Lancet* **383**, 816-827 (2014).

3   Rigel, D. S. & Carucci, J. A. Malignant melanoma: prevention, early detection, and treatment in the 21st century. *CA Cancer J Clin* **50**, 215-236 (2000).

4   Balch, C. M. *et al.* Final version of 2009 AJCC melanoma staging and classification. *J Clin Oncol* **27**, 6199-6206 (2009).

5   Tsao, H., Atkins, M. B. & Sober, A. J. Management of cutaneous melanoma. *N Engl J Med* **351**, 998-1012 (2004).

6   Marquez-Rodas, I., Martin Algarra, S., Aviles Izquierdo, J. A., Custodio Cabello, S. & Martin, M. A new era in the treatment of melanoma: from biology to clinical practice. *Clin Transl Oncol* **13**, 787-792 (2011).

7   Thompson, J. F. *et al.* Prognostic significance of mitotic rate in localized primary cutaneous melanoma: an analysis of patients in the multi-institutional American Joint Committee on Cancer melanoma staging database. *J Clin Oncol* **29**, 2199-2205 (2011).

8   Eggermont, A. M. & Gore, M. Randomized adjuvant therapy trials in melanoma: surgical and systemic. *Semin Oncol* **34**, 509-515 (2007).

9   Morton, D. L. *et al.* Sentinel-node biopsy or nodal observation in melanoma. *N Engl J Med* **355**, 1307-1317 (2006).

10   van Akkooi, A. C. *et al.* Sentinel node tumor burden according to the Rotterdam criteria is the most important prognostic factor for survival in melanoma patients: a multicenter study in 388 patients with positive sentinel nodes. *Ann Surg* **248**, 949-955 (2008).

11   van der Ploeg, A. P. *et al.* Prognosis in patients with sentinel node-positive melanoma is accurately defined by the combined Rotterdam tumor load and Dewar topography criteria. *J Clin Oncol* **29**, 2206-2214 (2011).

12   Pawlik, T. M., Ross, M. I., Thompson, J. F., Eggermont, A. M. & Gershenwald, J. E. The risk of in-transit melanoma metastasis depends on tumor biology and not the surgical approach to regional lymph nodes. *J Clin Oncol* **23**, 4588-4590 (2005).

13   Testori, A. *et al.* Surgery and radiotherapy in the treatment of cutaneous melanoma. *Ann Oncol* **20 Suppl 6**, vi22-29 (2009).

14   Garbe, C., Eigentler, T. K., Keilholz, U., Hauschild, A. & Kirkwood, J. M. Systematic review of medical treatment in melanoma: current status and future prospects. *The oncologist* **16**, 5-24 (2011).

15   Chapman, P. B. *et al.* Phase III multicenter randomized trial of the Dartmouth regimen versus dacarbazine in patients with metastatic melanoma. *J Clin Oncol* **17**, 2745-2751 (1999).

16   Quirbt, I. *et al.* Temozolomide for the treatment of metastatic melanoma. *Curr Oncol* **14**, 27-33 (2007).

17   Avril, M. F. *et al.* Fotemustine compared with dacarbazine in patients with disseminated malignant melanoma: a phase III study. *J Clin Oncol* **22**, 1118-1125 (2004).

18   Atkins, M. B. *et al.* High-dose recombinant interleukin 2 therapy for patients with metastatic melanoma: analysis of 270 patients treated between 1985 and 1993. *J Clin Oncol* **17**, 2105-2116 (1999).

19   Kirkwood, J. M. *et al.* Interferon alfa-2b adjuvant therapy of high-risk resected cutaneous melanoma: the Eastern Cooperative Oncology Group Trial EST 1684. *J Clin Oncol* **14**, 7-17 (1996).

20   Bhatia, S., Tykodi, S. S. & Thompson, J. A. Treatment of metastatic melanoma: an overview. *Oncology (Williston Park, N.Y.)* **23**, 488-496 (2009).

21   Hodi, F. S. *et al.* Improved survival with ipilimumab in patients with metastatic melanoma. *N Engl J Med* **363**, 711-723 (2010).

22   Robert, C. *et al.* Ipilimumab plus dacarbazine for previously untreated metastatic melanoma. *N Engl J Med* **364**, 2517-2526 (2011).

23   Robert, C. *et al.* Nivolumab in Previously Untreated Melanoma without BRAF Mutation. *N Engl J Med* **372**, 320-330 (2015).

24   Robert, C. *et al.* Pembrolizumab versus Ipilimumab in Advanced Melanoma. *N Engl J Med* **372**, 2521-2532 (2015).

25   Schadendorf, D. *et al.* Melanoma. 15003, doi:10.1038/nrdp.2015.3 (2015).

26   Chapman, P. B. *et al.* Improved survival with vemurafenib in melanoma with BRAF V600E mutation. *N Engl J Med* **364**, 2507-2516 (2011).

27   Hauschild, A. *et al.* Dabrafenib in BRAF-mutated metastatic melanoma: a multicentre, open-label, phase 3 randomised controlled trial. *Lancet* **380**, 358-365 (2012).

28   Sosman, J. A. *et al.* Survival in BRAF V600-mutant advanced melanoma treated with vemurafenib. *N Engl J Med* **366**, 707-714 (2012).

29   Flaherty, K. T. *et al.* Combined BRAF and MEK inhibition in melanoma with BRAF V600 mutations. *N Engl J Med* **367**, 1694-1703 (2012).

30   Clark, W. H., Jr. *et al.* A study of tumor progression: the precursor lesions of superficial spreading and nodular melanoma. *Hum Pathol* **15**, 1147-1165 (1984).

31   Meier, F. *et al.* Molecular events in melanoma development and progression. *Front Biosci* **3**, D1005-1010 (1998).

32   Herlyn, M. Human melanoma: development and progression. *Cancer Metastasis Rev* **9**, 101-112 (1990).

33   FitzGerald, M. G. *et al.* Prevalence of germ-line mutations in p16, p19ARF, and CDK4 in familial melanoma: analysis of a clinic-based population. *Proc Natl Acad Sci U S A* **93**, 8541-8545 (1996).

34   Goldstein, A. M. *et al.* High-risk melanoma susceptibility genes and pancreatic cancer, neural system tumors, and uveal melanoma across GenoMEL. *Cancer Res* **66**, 9818-9828 (2006).

35   Davies, H. *et al.* Mutations of the BRAF gene in human cancer. *Nature* **417**, 949-954 (2002).

36   Labrousse, A. L., Ntayi, C., Hornebeck, W. & Bernard, P. Stromal reaction in cutaneous melanoma. *Crit Rev Oncol Hematol* **49**, 269-275 (2004).

37   Kalluri, R. Basement membranes: structure, assembly and role in tumour angiogenesis. *Nat Rev Cancer* **3**, 422-433 (2003).

38   Carmeliet, P. Angiogenesis in health and disease. *Nat Med* **9**, 653-660 (2003).

39   Folkman, J. Angiogenesis in cancer, vascular, rheumatoid and other disease. *Nat Med* **1**, 27-31 (1995).

40   Hanahan, D. & Folkman, J. Patterns and emerging mechanisms of the angiogenic switch during tumorigenesis. *Cell* **86**, 353-364 (1996).

41   Basu, B., Biswas, S., Wrigley, J., Sirohi, B. & Corrie, P. Angiogenesis in cutaneous malignant melanoma and potential therapeutic strategies. *Expert Rev Anticancer Ther* **9**, 1583-1598 (2009).

42   Mahabeleshwar, G. H. & Byzova, T. V. Angiogenesis in melanoma. *Semin Oncol* **34**, 555-565 (2007).

43   Zaki, K. A., Basu, B. & Corrie, P. The role of angiogenesis inhibitors in the management of melanoma. *Curr Top Med Chem* **12**, 32-49 (2012).

44   Mehnert, J. M. *et al.* Quantitative expression of VEGF, VEGF-R1, VEGF-R2, and VEGF-R3 in melanoma tissue microarrays. *Hum Pathol* **41**, 375-384 (2010).

45   Reed, J. A., McNutt, N. S. & Albino, A. P. Differential expression of basic fibroblast growth factor (bFGF) in melanocytic lesions demonstrated by in situ hybridization. Implications for tumor progression. *Am J Pathol* **144**, 329-336 (1994).

46 Nurnberg, W., Tobias, D., Otto, F., Henz, B. M. & Schadendorf, D. Expression of interleukin-8 detected by in situ hybridization correlates with worse prognosis in primary cutaneous melanoma. *J Pathol* **189**, 546-551 (1999).

47 Tas, F. *et al.* Circulating serum levels of angiogenic factors and vascular endothelial growth factor receptors 1 and 2 in melanoma patients. *Melanoma Res* **16**, 405-411 (2006).

48 Ugurel, S., Rappl, G., Tilgen, W. & Reinhold, U. Increased serum concentration of angiogenic factors in malignant melanoma patients correlates with tumor progression and survival. *J Clin Oncol* **19**, 577-583 (2001).

49 Mouawad, R., Spano, J. P., Comperat, E., Capron, F. & Khayat, D. Tumoural expression and circulating level of VEGFR-3 (Flt-4) in metastatic melanoma patients: correlation with clinical parameters and outcome. *Eur J Cancer* **45**, 1407-1414 (2009).

50 Kashani-Sabet, M., Sagebiel, R. W., Ferreira, C. M., Nosrati, M. & Miller, J. R., 3rd. Tumor vascularity in the prognostic assessment of primary cutaneous melanoma. *J Clin Oncol* **20**, 1826-1831 (2002).

51 Torisu, H. *et al.* Macrophage infiltration correlates with tumor stage and angiogenesis in human malignant melanoma: possible involvement of TNFalpha and IL-1alpha. *Int J Cancer* **85**, 182-188 (2000).

52 Storr, S. J. *et al.* Objective assessment of blood and lymphatic vessel invasion and association with macrophage infiltration in cutaneous melanoma. *Mod Pathol* **25**, 493-504 (2012).

53 Jensen, T. O. *et al.* Macrophage markers in serum and tumor have prognostic impact in American Joint Committee on Cancer stage I/II melanoma. *J Clin Oncol* **27**, 3330-3337 (2009).

54 Emmett, M. S., Dewing, D. & Pritchard-Jones, R. O. Angiogenesis and melanoma - from basic science to clinical trials. *Am J Cancer Res* **1**, 852-868 (2011).

55 Damsky, W. E., Rosenbaum, L. E. & Bosenberg, M. Decoding melanoma metastasis. *Cancers* **3**, 126-163 (2010).

56 Miller, A. J. & Mihm, M. C., Jr. Melanoma. *N Engl J Med* **355**, 51-65 (2006).

57 Haass, N. K., Smalley, K. S., Li, L. & Herlyn, M. Adhesion, migration and communication in melanocytes and melanoma. *Pigment Cell Res* **18**, 150-159 (2005).

58 Tas, F. Metastatic behavior in melanoma: timing, pattern, survival, and influencing factors. *J Oncol* **2012**, 647-684 (2012).

59 Albelda, S. M. *et al.* Integrin distribution in malignant melanoma: association of the beta 3 subunit with tumor progression. *Cancer Res* **50**, 6757-6764 (1990).

60 Natali, P. G., Nicotra, M. R., Bartolazzi, A., Cavaliere, R. & Bigotti, A. Integrin expression in cutaneous malignant melanoma: association of the alpha 3/beta 1 heterodimer with tumor progression. *Int J Cancer* **54**, 68-72 (1993).

61 Schadendorf, D. *et al.* Tumour progression and metastatic behaviour in vivo correlates with integrin expression on melanocytic tumours. *J Pathol* **170**, 429-434 (1993).

62 Natali, P. G. *et al.* Clinical significance of alpha(v)beta3 integrin and intercellular adhesion molecule-1 expression in cutaneous malignant melanoma lesions. *Cancer Res* **57**, 1554-1560 (1997).

63 Lade-Keller, J. *et al.* E- to N-cadherin switch in melanoma is associated with decreased expression of phosphatase and tensin homolog and cancer progression. *Br J Dermatol* **169**, 618-628 (2013).

64 Hofmann, U. B. *et al.* Expression and activation of matrix metalloproteinase-2 (MMP-2) and its colocalization with membrane-type 1 matrix metalloproteinase (MT1-MMP) correlate with melanoma progression. *J Pathol* **191**, 245-256 (2000).

65 Hofmann, U. B. *et al.* Matrix metalloproteinases in human melanoma cell lines and xenografts: increased expression of activated matrix metalloproteinase-2 (MMP-2) correlates with melanoma progression. *Br J Cancer* **81**, 774-782 (1999).

66   MacDougall, J. R., Bani, M. R., Lin, Y., Muschel, R. J. & Kerbel, R. S. 'Proteolytic switching': opposite patterns of regulation of gelatinase B and its inhibitor TIMP-1 during human melanoma progression and consequences of gelatinase B overexpression. *Br J Cancer* **80**, 504-512 (1999).

67   Dai, D. L., Martinka, M. & Li, G. Prognostic significance of activated Akt expression in melanoma: a clinicopathologic study of 292 cases. *J Clin Oncol* **23**, 1473-1482 (2005).

68   Wan, P. T. *et al.* Mechanism of activation of the RAF-ERK signaling pathway by oncogenic mutations of B-RAF. *Cell* **116**, 855-867 (2004).

69   Cohen, C. *et al.* Mitogen-actived protein kinase activation is an early event in melanoma progression. *Clin Cancer Res* **8**, 3728-3733 (2002).

70   Damsky, W. E., Theodosakis, N. & Bosenberg, M. Melanoma metastasis: new concepts and evolving paradigms. *Oncogene* **33**, 2413-2422 (2014).

71   Bennett, D. C. How to make a melanoma: what do we know of the primary clonal events? *Pigment Cell Melanoma Res* **21**, 27-38 (2008).

72   Cummins, D. L. *et al.* Cutaneous malignant melanoma. *Mayo Clinic proceedings* **81**, 500-507 (2006).

73   Hamid, O., Boasberg, P. D., Rosenthal, K. & O'Day, S. J. Systemic treatment of metastatic melanoma: new approaches. *J Surg Oncol* **104**, 425-429 (2011).

74   Robert, C. *et al.* Improved overall survival in melanoma with combined dabrafenib and trametinib. *N Engl J Med* **372**, 30-39 (2015).

75   Carvajal, R. D. *et al.* KIT as a therapeutic target in metastatic melanoma. *JAMA* **305**, 2327-2334 (2011).

76   Robert, C. *et al.* Nivolumab in previously untreated melanoma without BRAF mutation. *N Engl J Med* **372**, 320-330 (2015).

77   Larkin, J. *et al.* Combined Nivolumab and Ipilimumab or Monotherapy in Untreated Melanoma. *N Engl J Med* **373**, 23-34 (2015).

78   Nikolaou, V., Stratigos, A., Bafaloukos, D. & Katsambas, A. Antiangiogenic and antiapoptotic treatment in advanced melanoma. *Clin Dermatol* **31**, 257-263 (2013).

79   Liao, D. & Johnson, R. S. Hypoxia: a key regulator of angiogenesis in cancer. *Cancer Metastasis Rev* **26**, 281-290 (2007).

80   Rofstad, E. K. *et al.* Hypoxia promotes lymph node metastasis in human melanoma xenografts by up-regulating the urokinase-type plasminogen activator receptor. *Cancer Res* **62**, 1847-1853 (2002).

81   Rofstad, E. K. & Halsor, E. F. Hypoxia-associated spontaneous pulmonary metastasis in human melanoma xenografts: involvement of microvascular hot spots induced in hypoxic foci by interleukin 8. *Br J Cancer* **86**, 301-308 (2002).

82   Matsushita, H. *et al.* Hypoxia-induced endothelial apoptosis through nuclear factor-kappaB (NF-kappaB)-mediated bcl-2 suppression: in vivo evidence of the importance of NF-kappaB in endothelial cell regulation. *Circ Res* **86**, 974-981 (2000).

83   Westphal, J. R. *et al.* Vascular density in melanoma xenografts correlates with vascular permeability factor expression but not with metastatic potential. *Br J Cancer* **76**, 561-570 (1997).

84   Sviderskaya, E. V. *et al.* p16/cyclin-dependent kinase inhibitor 2A deficiency in human melanocyte senescence, apoptosis, and immortalization: possible implications for melanoma progression. *J Natl Cancer Inst* **95**, 723-732 (2003).

85   Jaffe, E. A., Nachman, R. L., Becker, C. G. & Minick, C. R. Culture of human endothelial cells derived from umbilical veins. Identification by morphologic and immunologic criteria. *J Clin Invest* **52**, 2745-2756 (1973).

86   Crop, M. J. *et al.* Inflammatory conditions affect gene expression and function of human adipose tissue-derived mesenchymal stem cells. *Clin Exp Immunol* **162**, 474-486 (2010).

87 Van Muijen, G. N. *et al.* Antigen expression of metastasizing and non-metastasizing human melanoma cells xenografted into nude mice. *Clin Exp Metastasis* **9**, 259-272 (1991).

88 Westphal, J. R. *et al.* Angiogenic balance in human melanoma: expression of VEGF, bFGF, IL-8, PDGF and angiostatin in relation to vascular density of xenografts in vivo. *Int J Cancer* **86**, 768-776 (2000).

89 Ezhilarasan, R., Mohanam, I., Govindarajan, K. & Mohanam, S. Glioma cells suppress hypoxia-induced endothelial cell apoptosis and promote the angiogenic process. *Int J Oncol* **30**, 701-707 (2007).

90 Lazar-Molnar, E., Hegyesi, H., Toth, S. & Falus, A. Autocrine and paracrine regulation by cytokines and growth factors in melanoma. *Cytokine* **12**, 547-554 (2000).

91 Streit, M. & Detmar, M. Angiogenesis, lymphangiogenesis, and melanoma metastasis. *Oncogene* **22**, 3172-3179 (2003).

92 Potgens, A. J., Westphal, H. R., de Waal, R. M. & Ruiter, D. J. The role of vascular permeability factor and basic fibroblast growth factor in tumor angiogenesis. *Biol Chem Hoppe Seyler* **376**, 57-70 (1995).

93 Neve, R. M. *et al.* A collection of breast cancer cell lines for the study of functionally distinct cancer subtypes. *Cancer Cell* **10**, 515-527 (2006).

94 Deer, E. L. *et al.* Phenotype and genotype of pancreatic cancer cell lines. *Pancreas* **39**, 425-435 (2010).

95 Shalini, S., Dorstyn, L., Dawar, S. & Kumar, S. Old, new and emerging functions of caspases. *Cell Death Differ* **22**, 526-539 (2015).

96 Wang, Y. & Becker, D. Antisense targeting of basic fibroblast growth factor and fibroblast growth factor receptor-1 in human melanomas blocks intratumoral angiogenesis and tumor growth. *Nat Med* **3**, 887-893 (1997).

97 Graeven, U. *et al.* Modulation of angiogenesis and tumorigenicity of human melanocytic cells by vascular endothelial growth factor and basic fibroblast growth factor. *Cancer Res* **61**, 7282-7290 (2001).

98 Benjamin, L. E., Golijanin, D., Itin, A., Pode, D. & Keshet, E. Selective ablation of immature blood vessels in established human tumors follows vascular endothelial growth factor withdrawal. *J Clin Invest* **103**, 159-165, doi:10.1172/JCI5028 (1999).

99 Benjamin, L. E. & Keshet, E. Conditional switching of vascular endothelial growth factor (VEGF) expression in tumors: induction of endothelial cell shedding and regression of hemangioblastoma-like vessels by VEGF withdrawal. *Proc Natl Acad Sci U S A* **94**, 8761-8766 (1997).

100 Liu, W., Davis, D. W., Ramirez, K., McConkey, D. J. & Ellis, L. M. Endothelial cell apoptosis is inhibited by a soluble factor secreted by human colon cancer cells. *Int J Cancer* **92**, 26-30 (2001).

101 Folkman, J. Seminars in Medicine of the Beth Israel Hospital, Boston. Clinical applications of research on angiogenesis. *N Engl J Med* **333**, 1757-1763 (1995).

102 Bergers, G. & Benjamin, L. E. Tumorigenesis and the angiogenic switch. *Nat Rev Cancer* **3**, 401-410 (2003).

103 Pankov, R. *et al.* A Rac switch regulates random versus directionally persistent cell migration. *J Cell Biol* **170**, 793-802 (2005).

104 Petrie, R. J., Doyle, A. D. & Yamada, K. M. Random versus directionally persistent cell migration. *Nat Rev Mol Cell Biol* **10**, 538-549 (2009).

105 Chung, C. Y., Lee, S., Briscoe, C., Ellsworth, C. & Firtel, R. A. Role of Rac in controlling the actin cytoskeleton and chemotaxis in motile cells. *Proc Natl Acad Sci U S A* **97**, 5225-5230 (2000).

106 Sasaki, A. T., Chun, C., Takeda, K. & Firtel, R. A. Localized Ras signaling at the leading edge regulates PI3K, cell polarity, and directional cell movement. *J Cell Biol* **167**, 505-518 (2004).

107 Funamoto, S., Meili, R., Lee, S., Parry, L. & Firtel, R. A. Spatial and temporal regulation of 3-phosphoinositides by PI 3-kinase and PTEN mediates chemotaxis. *Cell* **109**, 611-623 (2002).

108 Fink, R. D. & Trinkaus, J. P. Fundulus deep cells: directional migration in response to epithelial wounding. *Dev Biol* **129**, 179-190 (1988).

109 Chirco, R., Liu, X. W., Jung, K. K. & Kim, H. R. Novel functions of TIMPs in cell signaling. *Cancer Metastasis Rev* **25**, 99-113 (2006).

110 Bertaux, B., Hornebeck, W., Eisen, A. Z. & Dubertret, L. Growth stimulation of human keratinocytes by tissue inhibitor of metalloproteinases. *J Invest Dermatol* **97**, 679-685 (1991).

111 Hayakawa, T., Yamashita, K., Ohuchi, E. & Shinagawa, A. Cell growth-promoting activity of tissue inhibitor of metalloproteinases-2 (TIMP-2). *J Cell Sci* **107 (Pt 9)**, 2373-2379 (1994).

112 Nagase, H. Cell surface activation of progelatinase A (proMMP-2) and cell migration. *Cell Res* **8**, 179-186 (1998).

113 Ma, D. H., Chen, J. I., Zhang, F., Hwang, D. G. & Chen, J. K. Inhibition of fibroblast-induced angiogenic phenotype of cultured endothelial cells by the overexpression of tissue inhibitor of metalloproteinase (TIMP)-3. *J Biomed Sci* **10**, 526-534 (2003).

114 Baker, A. H., George, S. J., Zaltsman, A. B., Murphy, G. & Newby, A. C. Inhibition of invasion and induction of apoptotic cell death of cancer cell lines by overexpression of TIMP-3. *Br J Cancer* **79**, 1347-1355 (1999).

115 Ahonen, M., Baker, A. H. & Kahari, V. M. Adenovirus-mediated gene delivery of tissue inhibitor of metalloproteinases-3 inhibits invasion and induces apoptosis in melanoma cells. *Cancer Res* **58**, 2310-2315 (1998).

116 Baker, A. H., Zaltsman, A. B., George, S. J. & Newby, A. C. Divergent effects of tissue inhibitor of metalloproteinase-1, -2, or -3 overexpression on rat vascular smooth muscle cell invasion, proliferation, and death in vitro. TIMP-3 promotes apoptosis. *J Clin Invest* **101**, 1478-1487 (1998).

117 Spurbeck, W. W., Ng, C. Y., Strom, T. S., Vanin, E. F. & Davidoff, A. M. Enforced expression of tissue inhibitor of matrix metalloproteinase-3 affects functional capillary morphogenesis and inhibits tumor growth in a murine tumor model. *Blood* **100**, 3361-3368 (2002).

118 Leco, K. J., Khokha, R., Pavloff, N., Hawkes, S. P. & Edwards, D. R. Tissue inhibitor of metalloproteinases-3 (TIMP-3) is an extracellular matrix-associated protein with a distinctive pattern of expression in mouse cells and tissues. *J Biol Chem* **269**, 9352-9360 (1994).

119 Apte, S. S., Olsen, B. R. & Murphy, G. The gene structure of tissue inhibitor of metalloproteinases (TIMP)-3 and its inhibitory activities define the distinct TIMP gene family. *J Biol Chem* **270**, 14313-14318 (1995).

120 Anand-Apte, B. *et al.* A review of tissue inhibitor of metalloproteinases-3 (TIMP-3) and experimental analysis of its effect on primary tumor growth. *Biochem Cell Biol* **74**, 853-862 (1996).

121 Qi, J. H. *et al.* A novel function for tissue inhibitor of metalloproteinases-3 (TIMP3): inhibition of angiogenesis by blockage of VEGF binding to VEGF receptor-2. *Nat Med* **9**, 407-415 (2003).

122 Anand-Apte, B. *et al.* Inhibition of angiogenesis by tissue inhibitor of metalloproteinase-3. *Invest Ophthalmol Vis Sci* **38**, 817-823 (1997).

123 van Horssen, R., Galjart, N., Rens, J. A., Eggermont, A. M. & ten Hagen, T. L. Differential effects of matrix and growth factors on endothelial and fibroblast motility: application of a modified cell migration assay. *J Cell Biochem* **99**, 1536-1552 (2006).

124 Lambert, E., Dasse, E., Haye, B. & Petitfrere, E. TIMPs as multifacial proteins. *Crit Rev Oncol Hematol* **49**, 187-198 (2004).

125 Bachman, K. E. *et al.* Methylation-associated silencing of the tissue inhibitor of metalloproteinase-3 gene suggest a suppressor role in kidney, brain, and other human cancers. *Cancer Res* **59**, 798-802 (1999).

126 Wild, A. *et al.* Frequent methylation-associated silencing of the tissue inhibitor of metalloproteinase-3 gene in pancreatic endocrine tumors. *J Clin Endocrinol Metab* **88**, 1367-1373 (2003).

127 Anania, M. C. *et al.* TIMP3 regulates migration, invasion and in vivo tumorigenicity of thyroid tumor cells. *Oncogene* **30**, 3011-3023 (2011).

128 Liu, S., Ren, S., Howell, P., Fodstad, O. & Riker, A. I. Identification of novel epigenetically modified genes in human melanoma via promoter methylation gene profiling. *Pigment Cell Melanoma Res* **21**, 545-558 (2008).

129 Varney, M. L., Johansson, S. L. & Singh, R. K. Tumour-associated macrophage infiltration, neovascularization and aggressiveness in malignant melanoma: role of monocyte chemotactic protein-1 and vascular endothelial growth factor-A. *Melanoma Res* **15**, 417-425 (2005).

130 van der Laak, J. A. *et al.* An improved procedure to quantify tumour vascularity using true colour image analysis. Comparison with the manual hot-spot procedure in a human melanoma xenograft model. *J Pathol* **184**, 136-143 (1998).

131 Fassina, G. *et al.* Tissue inhibitors of metalloproteases: regulation and biological activities. *Clin Exp Metastasis* **18**, 111-120 (2000).

132 De Becker, A. *et al.* Migration of culture-expanded human mesenchymal stem cells through bone marrow endothelium is regulated by matrix metalloproteinase-2 and tissue inhibitor of metalloproteinase-3. *Haematologica* **92**, 440-449 (2007).

133 Gialeli, C., Theocharis, A. D. & Karamanos, N. K. Roles of matrix metalloproteinases in cancer progression and their pharmacological targeting. *Febs J* **278**, 16-27 (2011).

134 Qi, J. H. *et al.* Tissue inhibitor of metalloproteinases-3 peptides inhibit angiogenesis and choroidal neovascularization in mice. *PLoS One* **8**, e55667 (2013).

135 Stetler-Stevenson, W. G. Tissue inhibitors of metalloproteinases in cell signaling: metalloproteinase-independent biological activities. *Sci Signal* **1**, re6 (2008).

136 Fernandez, C. A., Butterfield, C., Jackson, G. & Moses, M. A. Structural and functional uncoupling of the enzymatic and angiogenic inhibitory activities of tissue inhibitor of metalloproteinase-2 (TIMP-2): loop 6 is a novel angiogenesis inhibitor. *J Biol Chem* **278**, 40989-40995 (2003).

137 Seo, D. W. *et al.* TIMP-2 mediated inhibition of angiogenesis: an MMP-independent mechanism. *Cell* **114**, 171-180 (2003).

138 Roland, C. L. *et al.* Inhibition of vascular endothelial growth factor reduces angiogenesis and modulates immune cell infiltration of orthotopic breast cancer xenografts. *Mol Cancer Ther* **8**, 1761-1771 (2009).

139 Dineen, S. P. *et al.* Vascular endothelial growth factor receptor 2 mediates macrophage infiltration into orthotopic pancreatic tumors in mice. *Cancer Res* **68**, 4340-4346 (2008).

140 Helleman, J. *et al.* Association of an extracellular matrix gene cluster with breast cancer prognosis and endocrine therapy response. *Clin Cancer Res* **14**, 5555-5564 (2008).

141 Hilska, M. *et al.* Prognostic significance of matrix metalloproteinases-1, -2, -7 and -13 and tissue inhibitors of metalloproteinases-1, -2, -3 and -4 in colorectal cancer. *Int J Cancer* **121**, 714-723 (2007).

142 Riddick, A. C. *et al.* Identification of degradome components associated with prostate cancer progression by expression analysis of human prostatic tissues. *Br J Cancer* **92**, 2171-2180 (2005).

143 Barski, D., Wolter, M., Reifenberger, G. & Riemenschneider, M. J. Hypermethylation and transcriptional downregulation of the TIMP3 gene is associated with allelic loss on 22q12.3 and malignancy in meningiomas. *Brain Pathol* **20**, 623-631 (2010).

144 Hu, S. *et al.* Association of aberrant methylation of tumor suppressor genes with tumor aggressiveness and BRAF mutation in papillary thyroid cancer. *Int J Cancer* **119**, 2322-2329 (2006).

145 Zochbauer-Muller, S. *et al.* Aberrant promoter methylation of multiple genes in non-small cell lung cancers. *Cancer Res* **61**, 249-255 (2001).

146 Masson, D. *et al.* Loss of expression of TIMP3 in clear cell renal cell carcinoma. *Eur J Cancer* **46**, 1430-1437 (2010).

147 Nakamura, M. *et al.* Frequent LOH on 22q12.3 and TIMP-3 inactivation occur in the progression to secondary glioblastomas. *Lab Invest* **85**, 165-175 (2005).

148 Bian, J. *et al.* Suppression of in vivo tumor growth and induction of suspension cell death by tissue inhibitor of metalloproteinases (TIMP)-3. *Carcinogenesis* **17**, 1805-1811 (1996).

149 Han, X., Zhang, H., Jia, M., Han, G. & Jiang, W. Expression of TIMP-3 gene by construction of a eukaryotic cell expression vector and its role in reduction of metastasis in a human breast cancer cell line. *Cell Mol Immunol* **1**, 308-310 (2004).

150 Mahller, Y. Y. *et al.* Tissue inhibitor of metalloproteinase-3 via oncolytic herpesvirus inhibits tumor growth and vascular progenitors. *Cancer Res* **68**, 1170-1179 (2008).

151 Mansfield, A. S. & Markovic, S. N. Inhibition of angiogenesis for the treatment of metastatic melanoma. *Curr Oncol Rep* **15**, 492-499 (2013).

152 Das, A. M. *et al.* Differential TIMP3 expression affects tumor progression and angiogenesis in melanomas through regulation of directionally persistent endothelial cell migration. *Angiogenesis* **17**, 163-177 (2014).

153 Guan, Z., Zhang, J., Song, S. & Dai, D. Promoter methylation and expression of TIMP3 gene in gastric cancer. *Diagn Pathol* **8**, 110 (2013).

154 Zheng, P. P., van der Weiden, M. & Kros, J. M. Fast tracking of co-localization of multiple markers by using the nanozoomer slide scanner and NDPViewer. *J Cell Physiol* **229**, 967-973 (2014).

155 Balch, C. M., Gershenwald, J. E., Soong, S. J. & Thompson, J. F. Update on the melanoma staging system: the importance of sentinel node staging and primary tumor mitotic rate. *J Surg Oncol* **104**, 379-385 (2011).

156 van der Ploeg, A. P. *et al.* The prognostic significance of sentinel node tumour burden in melanoma patients: an international, multicenter study of 1539 sentinel node-positive melanoma patients. *Eur J Cancer* **50**, 111-120 (2014).

157 Bingle, L., Brown, N. J. & Lewis, C. E. The role of tumour-associated macrophages in tumour progression: implications for new anticancer therapies. *J Pathol* **196**, 254-265 (2002).

158 Catasus, L., Pons, C., Munoz, J., Espinosa, I. & Prat, J. Promoter hypermethylation contributes to TIMP3 down-regulation in high stage endometrioid endometrial carcinomas. *Histopathology* **62**, 632-641 (2013).

159 Martin del Campo, S. E. *et al.* MiR-21 enhances melanoma invasiveness via inhibition of tissue inhibitor of metalloproteinases 3 expression: in vivo effects of MiR-21 inhibitor. *PLoS One* **10**, e0115919 (2015).

160 Lauffenburger, D. A. & Horwitz, A. F. Cell migration: a physically integrated molecular process. *Cell* **84**, 359-369 (1996).

161 Horwitz, A. R. & Parsons, J. T. Cell migration--movin' on. *Science* **286**, 1102-1103 (1999).

162 Ridley, A. J. *et al.* Cell migration: integrating signals from front to back. *Science* **302**, 1704-1709 (2003).

163 Trinkaus, J. P. Directional cell movement during early development of the teleost Blennius pholis: I. Formation of epithelial cell clusters and their pattern and mechanism of movement. *J Exp Zool* **245**, 157-186 (1988).

164 Cory, G. Scratch-wound assay. *Methods Mol Biol* **769**, 25-30 (2011).

165 Liang, C. C., Park, A. Y. & Guan, J. L. In vitro scratch assay: a convenient and inexpensive method for analysis of cell migration in vitro. *Nat Protoc* **2**, 329-333 (2007).

166 Qiang, L. *et al.* Regulation of cell proliferation and migration by p62 through stabilization of Twist1. *Proc Natl Acad Sci U S A* **111**, 9241-9246 (2014).

167 Varani, J., Orr, W. & Ward, P. A. A comparison of the migration patterns of normal and malignant cells in two assay systems. *Am J Pathol* **90**, 159-172 (1978).

168 Pratt, B. M., Harris, A. S., Morrow, J. S. & Madri, J. A. Mechanisms of cytoskeletal regulation. Modulation of aortic endothelial cell spectrin by the extracellular matrix. *Am J Pathol* **117**, 349-354 (1984).

169 Ohtaka, K., Watanabe, S., Iwazaki, R., Hirose, M. & Sato, N. Role of extracellular matrix on colonic cancer cell migration and proliferation. *Biochem Biophys Res Commun* **220**, 346-352 (1996).

170 Van Horssen, R. & ten Hagen, T. L. Crossing barriers: the new dimension of 2D cell migration assays. *J Cell Physiol* **226**, 288-290 (2011).

171 Bakker, E. R. *et al.* Wnt5a promotes human colon cancer cell migration and invasion but does not augment intestinal tumorigenesis in Apc1638N mice. *Carcinogenesis* **34**, 2629-2638 (2013).

172 Cheng, C. *et al.* PDGF-induced migration of vascular smooth muscle cells is inhibited by heme oxygen-ase-1 via VEGFR2 upregulation and subsequent assembly of inactive VEGFR2/PDGFRbeta heterodimers. *Arterioscler Thromb Vasc Biol* **32**, 1289-1298 (2012).

173 van Horssen, R. *et al.* E-cadherin promotor methylation and mutation are inversely related to motility capacity of breast cancer cells. *Breast Cancer Res Treat* **136**, 365-377 (2012).

174 Drabek, K. *et al.* Role of CLASP2 in microtubule stabilization and the regulation of persistent motility. *Curr Biol* **16**, 2259-2264 (2006).

175 van Horssen, R. *et al.* Modulation of cell motility by spatial repositioning of enzymatic ATP/ADP exchange capacity. *J Biol Chem* **284**, 1620-1627 (2009).

176 Kuiper, J. W. *et al.* Local ATP generation by brain-type creatine kinase (CK-B) facilitates cell motility. *PLoS One* **4**, e5030 (2009).

177 Gorelik, R. & Gautreau, A. Quantitative and unbiased analysis of directional persistence in cell migration. *Nat Protoc* **9**, 1931-1943 (2014).

178 Deforet, M. *et al.* Automated velocity mapping of migrating cell populations (AVeMap). *Nat Methods* **9**, 1081-1083 (2012).

179 Zaritsky, A. *et al.* Cell motility dynamics: a novel segmentation algorithm to quantify multi-cellular bright field microscopy images. *PLoS One* **6**, e27593 (2011).

180 Huth, J. *et al.* Significantly improved precision of cell migration analysis in time-lapse video microscopy through use of a fully automated tracking system. *BMC cell biology* **11**, 24 (2010).

181 Valastyan, S. & Weinberg, R. A. Tumor metastasis: molecular insights and evolving paradigms. *Cell* **147**, 275-292 (2011).

182 Gupta, G. P. & Massague, J. Cancer metastasis: building a framework. *Cell* **127**, 679-695 (2006).

183 Hodis, E. *et al.* A landscape of driver mutations in melanoma. *Cell* **150**, 251-263 (2012).

184 Mar, V. J. *et al.* BRAF/NRAS wild-type melanomas have a high mutation load correlating with histologic and molecular signatures of UV damage. *Cancer Res* **19**, 4589-4598 (2013).

185 Anaka, M. *et al.* Intratumoral genetic heterogeneity in metastatic melanoma is accompanied by variation in malignant behaviors. *BMC medical genomics* **6**, 40, doi:10.1186/1755-8794-6-40 (2013).

186 Das, A. M., Eggermont, A. M. & Ten Hagen, T. L. A ring barrier-based migration assay to assess cell migration in vitro. *Nat Protoc* **10**, 904-915 (2015).

187 Hoekstra, E. *et al.* Low molecular weight protein tyrosine phosphatase (LMWPTP) upregulation mediates malignant potential in colorectal cancer. *Oncotarget* **6**, 8300-8312 (2015).

188 Gaggioli, C. & Sahai, E. Melanoma invasion - current knowledge and future directions. *Pigment Cell Res* **20**, 161-172 (2007).

189 Weeraratna, A. T. A Wnt-er wonderland--the complexity of Wnt signaling in melanoma. *Cancer Metasta-sis Rev* **24**, 237-250 (2005).

190 Da Forno, P. D. *et al.* WNT5A expression increases during melanoma progression and correlates with outcome. *Clin Cancer Res* **14**, 5825-5832 (2008).

191 Kurayoshi, M. *et al.* Expression of Wnt-5a is correlated with aggressiveness of gastric cancer by stimulating cell migration and invasion. *Cancer Res* **66**, 10439-10448 (2006).

192 Yamamoto, H. *et al.* Laminin gamma2 mediates Wnt5a-induced invasion of gastric cancer cells. *Gastroen-terology* **137**, 242-252, 252 e241-246 (2009).

193 Yamamoto, H. *et al.* Wnt5a signaling is involved in the aggressiveness of prostate cancer and expression of metalloproteinase. *Oncogene* **29**, 2036-2046 (2010).

194 Pukrop, T. *et al.* Wnt 5a signaling is critical for macrophage-induced invasion of breast cancer cell lines. *Proc Natl Acad Sci U S A* **103**, 5454-5459 (2006).

195 Huang, C. L. *et al.* Wnt5a expression is associated with the tumor proliferation and the stromal vascular endothelial growth factor--an expression in non-small-cell lung cancer. *J Clin Oncol* **23**, 8765-8773 (2005).

196 Blanc, E., Roux, G. L., Benard, J. & Raguenez, G. Low expression of Wnt-5a gene is associated with high-risk neuroblastoma. *Oncogene* **24**, 1277-1283 (2005).

197 Liang, H. *et al.* Wnt5a inhibits B cell proliferation and functions as a tumor suppressor in hematopoietic tissue. *Cancer Cell* **4**, 349-360 (2003).

198 Bittner, M. *et al.* Molecular classification of cutaneous malignant melanoma by gene expression profiling. *Nature* **406**, 536-540 (2000).

199 Hoek, K. S. *et al.* Metastatic potential of melanomas defined by specific gene expression profiles with no BRAF signature. *Pigment Cell Res* **19**, 290-302 (2006).

200 Weeraratna, A. T. *et al.* Wnt5a signaling directly affects cell motility and invasion of metastatic melanoma. *Cancer Cell* **1**, 279-288 (2002).

201 Shojima, K. *et al.* Wnt5a promotes cancer cell invasion and proliferation by receptor-mediated endocytosis-dependent and -independent mechanisms, respectively. *Sci Rep* **5**, 8042 (2015).

202 Huang, Y. *et al.* Wnt-5a regulates proliferation in lung cancer cells. *Oncol Rep* **23**, 177-181 (2010).

203 Pulvirenti, T. *et al.* Dishevelled 2 signaling promotes self-renewal and tumorigenicity in human gliomas. *Cancer Res* **71**, 7280-7290 (2011).

204 Ma, G., Yasunaga, J., Fan, J., Yanagawa, S. & Matsuoka, M. HTLV-1 bZIP factor dysregulates the Wnt pathways to support proliferation and migration of adult T-cell leukemia cells. *Oncogene* **32**, 4222-4230 (2013).

205 Chien, A. J. *et al.* Activated Wnt/beta-catenin signaling in melanoma is associated with decreased proliferation in patient tumors and a murine melanoma model. *Proc Natl Acad Sci U S A* **106**, 1193-1198 (2009).

206 Anastas, J. N. *et al.* WNT5A enhances resistance of melanoma cells to targeted BRAF inhibitors. *J Clin Invest* **124**, 2877-2890 (2014).

207 Eggermont, A. M., Maio, M. & Robert, C. Immune checkpoint inhibitors in melanoma provide the cornerstones for curative therapies. *Semin Oncol* **42**, 429-435 (2015).

208 Tsao, H., Chin, L., Garraway, L. A. & Fisher, D. E. Melanoma: from mutations to medicine. *Genes Dev* **26**, 1131-1155 (2012).

209 Hernanda, P. Y. *et al.* SMAD4 exerts a tumor-promoting role in hepatocellular carcinoma. *Oncogene*, doi:10.1038/onc.2014.425 (2014).

210 Huang, Q. *et al.* Noninvasive visualization of tumors in rodent dorsal skin window chambers. *Nat Biotechnol* **17**, 1033-1035 (1999).

211 Jain, R. K., Munn, L. L. & Fukumura, D. Dissecting tumour pathophysiology using intravital microscopy. *Nat Rev Cancer* **2**, 266-276 (2002).

212 Palmer, G. M. *et al.* In vivo optical molecular imaging and analysis in mice using dorsal window chamber models applied to hypoxia, vasculature and fluorescent reporters. *Nat Protoc* **6**, 1355-1366 (2011).

213 Dellian, M., Helmlinger, G., Yuan, F. & Jain, R. K. Fluorescence ratio imaging of interstitial pH in solid tumours: effect of glucose on spatial and temporal gradients. *Br J Cancer* **74**, 1206-1215 (1996).

214 Prasher, D. C. Using GFP to see the light. *Trends Genet* **11**, 320-323 (1995).

215 Chiesa, A. *et al.* Recombinant aequorin and green fluorescent protein as valuable tools in the study of cell signalling. *Biochem J* **355**, 1-12 (2001).

216 Cubitt, A. B. *et al.* Understanding, improving and using green fluorescent proteins. *Trends Biochem Sci* **20**, 448-455 (1995).

217   Day, R. N. & Davidson, M. W. The fluorescent protein palette: tools for cellular imaging. *Chem Soc Rev* **38**, 2887-2921 (2009).

218   Li, C. Y. *et al.* Initial stages of tumor cell-induced angiogenesis: evaluation via skin window chambers in rodent models. *J Natl Cancer Inst* **92**, 143-147 (2000).

219   Read, T. A. *et al.* Intravital microscopy reveals novel antivascular and antitumor effects of endostatin delivered locally by alginate-encapsulated cells. *Cancer Res* **61**, 6830-6837 (2001).

220   Papenfuss, H. D., Gross, J. F., Intaglietta, M. & Treese, F. A. A transparent access chamber for the rat dorsal skin fold. *Microvasc Res* **18**, 311-318 (1979).

221   Leunig, M. *et al.* Angiogenesis, microvascular architecture, microhemodynamics, and interstitial fluid pressure during early growth of human adenocarcinoma LS174T in SCID mice. *Cancer Res* **52**, 6553-6560 (1992).

222   Lasic, D. D. Liposomes from physics to applications. 63-107 (1993).

223   Rouser, G., Fkeischer, S. & Yamamoto, A. Two dimensional then layer chromatographic separation of polar lipids and determination of phospholipids by phosphorus analysis of spots. *Lipids* **5**, 494-496 (1970).

224   Pitulescu, M. E., Schmidt, I., Benedito, R. & Adams, R. H. Inducible gene targeting in the neonatal vasculature and analysis of retinal angiogenesis in mice. *Nat Protoc* **5**, 1518-1534 (2010).

225   Benedito, R. *et al.* Notch-dependent VEGFR3 upregulation allows angiogenesis without VEGF-VEGFR2 signalling. *Nature* **484**, 110-114 (2012).

226   Baker, M. *et al.* Use of the mouse aortic ring assay to study angiogenesis. *Nat Protoc* **7**, 89-104 (2012).

227   Folkman, J. Tumor angiogenesis: therapeutic implications. *N Engl J Med* **285**, 1182-1186 (1971).

228   Griffioen, A. W. & Molema, G. Angiogenesis: potentials for pharmacologic intervention in the treatment of cancer, cardiovascular diseases, and chronic inflammation. *Pharmacol Rev* **52**, 237-268 (2000).

229   Michel, T. & Feron, O. Nitric oxide synthases: which, where, how, and why? *J Clin Invest* **100**, 2146-2152 (1997).

230   Dudzinski, D. M., Igarashi, J., Greif, D. & Michel, T. The regulation and pharmacology of endothelial nitric oxide synthase. *Annu Rev Pharmacol Toxicol* **46**, 235-276 (2006).

231   Pollock, J. S. *et al.* Purification and characterization of particulate endothelium-derived relaxing factor synthase from cultured and native bovine aortic endothelial cells. *Proc Natl Acad Sci U S A* **88**, 10480-10484 (1991).

232   Lamas, S., Marsden, P. A., Li, G. K., Tempst, P. & Michel, T. Endothelial nitric oxide synthase: molecular cloning and characterization of a distinct constitutive enzyme isoform. *Proc Natl Acad Sci U S A* **89**, 6348-6352 (1992).

233   Dimmeler, S. *et al.* Activation of nitric oxide synthase in endothelial cells by Akt-dependent phosphorylation. *Nature* **399**, 601-605 (1999).

234   van Haperen, R. *et al.* Functional expression of endothelial nitric oxide synthase fused to green fluorescent protein in transgenic mice. *Am J Pathol* **163**, 1677-1686 (2003).

235   Stylianopoulos, T. & Jain, R. K. Combining two strategies to improve perfusion and drug delivery in solid tumors. *Proc Natl Acad Sci U S A* **110**, 18632-18637 (2013).

236   Gerhardt, H. *et al.* VEGF guides angiogenic sprouting utilizing endothelial tip cell filopodia. *J Cell Biol* **161**, 1163-1177 (2003).

237   Flaherty, K. T. *et al.* Surrogate endpoints for overall survival in metastatic melanoma: a meta-analysis of randomised controlled trials. *The lancet oncology* **15**, 297-304 (2014).

238   Ives, N. J., Stowe, R. L., Lorigan, P. & Wheatley, K. Chemotherapy compared with biochemotherapy for the treatment of metastatic melanoma: a meta-analysis of 18 trials involving 2,621 patients. *J Clin Oncol* **25**, 5426-5434 (2007).

239 Eggermont, A. M. & Robert, C. Melanoma: smart therapeutic strategies in immuno-oncology. *Nat Rev Clin Oncol* **11**, 181-182 (2014).

240 Hirata, E. *et al.* Intravital imaging reveals how BRAF inhibition generates drug-tolerant microenvironments with high integrin beta1/FAK signaling. *Cancer cell* **27**, 574-588 (2015).

241 Hanahan, D. & Weinberg, R. A. The hallmarks of cancer. *Cell* **100**, 57-70 (2000).

242 Hanahan, D. & Weinberg, R. A. Hallmarks of cancer: the next generation. *Cell* **144**, 646-674 (2011).

243 Rofstad, E. K. & Halsor, E. F. Vascular endothelial growth factor, interleukin 8, platelet-derived endothelial cell growth factor, and basic fibroblast growth factor promote angiogenesis and metastasis in human melanoma xenografts. *Cancer Res* **60**, 4932-4938 (2000).

244 Helfrich, I. & Schadendorf, D. Blood vessel maturation, vascular phenotype and angiogenic potential in malignant melanoma: one step forward for overcoming anti-angiogenic drug resistance? *Mol Oncol* **5**, 137-149 (2011).

245 Murphy, G. Tissue inhibitors of metalloproteinases. *Genome Biol* **12**, 233 (2011).

246 Son, D. J. *et al.* The atypical mechanosensitive microRNA-712 derived from pre-ribosomal RNA induces endothelial inflammation and atherosclerosis. *Nat Commun* **4**, 3000 (2013).

247 Nagao, Y. *et al.* Association of microRNA-21 expression with its targets, PDCD4 and TIMP3, in pancreatic ductal adenocarcinoma. *Mod Pathol* **25**, 112-121 (2012).

248 Song, B. *et al.* MicroRNA-21 regulates breast cancer invasion partly by targeting tissue inhibitor of metalloproteinase 3 expression. *J Exp Clin Cancer Res* **29**, 29 (2010).

Summary, future perspectives

Samenvatting, toekomstperspectief

SUMMARY

Metastatic melanoma accounts for nearly all skin cancer related mortality and has been historically refractive to cytotoxic chemotherapy. While localized disease in early stages can effectively be treated by surgical intervention, late stage or disseminated disease was, until recently, largely untreatable. The advent of the concept of "personalized medicine" led to the development and FDA approval of two new drugs in 2011, ipilimumab (anti-CTLA-4 antibody) and vemurafenib (BRAF inhibitor), for the treatment of metastatic melanoma. More recently, trametenib (MEK inhibitor) and the immune checkpoint inhibitor molecules, nivolumab and pembrolizumab (both anti-PD1 antibodies), have been approved for exceptional activity and a clear impact on overall survival. These are the first drugs in decades to demonstrate a clinical benefit in patients. Despite the recent successes, there is still room for much improvement. Several challenges such as transient responses, adverse immune reactions and the acquisition of drug resistance remain to be addressed. The development of a stable curative therapeutic modality for metastatic melanoma will thus require the further understanding of the complex molecular mechanisms driving disease development and progression. This in turn will contribute to the identification of new therapeutic targets and improve the clinical efficacy of current treatment approaches.

In this thesis I have studied some of the fundamental cascades which contribute to melanoma development and a general introduction to these topics is presented in **Chapter 1**.

Studies described in *Section I* of this thesis are focused on essential steps in the sequence of the angiogenic cascade in melanomas. Melanoma progression and metastatic dissemination is intimately associated with the process of angiogenesis.

In **Chapter 2** we investigated the angiogenic potential of a panel of melanoma cell lines by monitoring survival of endothelial cells (ECs) upon exposure to melanoma conditioned medium (MCM) under restrictive culture conditions. We observed that MCMs specifically promoted long-term EC survival under hypoxia while CM generated from melanocytes, breast and pancreatic tumor cells did not have this effect. Through size fractionation we identified the survival factor to be in the < 1 kDa range. Investigation of global changes in gene expression revealed an increased expression of transcripts involved in cytokine signaling, cell metabolism and cell survival in MCM treated ECs. These findings offer new insights into the angiogenic potential of melanomas and might lead to the discovery of potential new therapeutic targets.

Endothelial cell migration is an essential step in the process of neovascularization. In **Chapter 3** we evaluated the influence of conditioned medium derived from melanoma cells on directional endothelial cell migration. We identified TIMP3 in the MCM as a

negative modulator of melanoma induced endothelial cell migration. Moreover, using gene modulation experiments in xenograft models, we could demonstrate that TIMP3 expression inversely correlated to blood vessel density and macrophage infiltration in melanomas.

In **Chapter 4**, we extended our *in vivo* observations of the influence of TIMP3 expression on mean vessel density and macrophage infiltration to a cohort of stage III melanoma lymph node biopsies. We observed reduced TIMP3 expression in the majority of the cases studied and observed a significant inverse correlation with mean vessel density. No significant associations with macrophage infiltration was observed. Interestingly, we also observed that gene promoter silencing by methylation impacted clinical outcome. Collectively, these findings suggest a tumor suppressor role of TIMP3 in malignant melanomas.

Studies described in *Section II* of this thesis are focused on identifying key regulators of the metastatic cascade of melanomas.

Cell migration is a vital feature of virtually every biological process and is central to the regulation of physiological and pathological events. **Chapter 5** describes the use of a 'ring-barrier' based migration assay to quantitatively deduce several parameters of cell migration *in vitro*. This assay supersedes the traditional scratch or wound healing assay commonly used to evaluate cell migration, as both the cells and matrix are unharmed, and facilitates the study of contribution of matrix substrates, genetic modulations and the effect of small molecule drugs to the migratory process.

In **Chapter 6** we analyzed the migratory and invasive potential of a panel of melanoma cell lines which differed in their degree of aggressiveness and metastatic propensity. We observed a clear correlation between the migratory capacity of the cell lines and the ability to form lung metastases in mice. Correlation analysis of gene expression data identified WNT5A as a determinant of the biological phenotype assayed. In subsequent gene manipulation experiments we were able to show that WNT5A regulates the migratory potential of melanoma cells and in extension, the metastatic propensity.

In **Chapter 7** we evaluated the role of TIMP3 in the metastatic cascade of melanomas. Analysis of protein expression in matched Stage I/II, Stage III and Stage IV samples from melanoma patients revealed the loss of TIMP3 during melanoma progression. Through gene modulation and phenotypic assays, we were able to demonstrate that TIMP3 inhibits the migratory and invasive capacity of melanoma cells.

Section III of this thesis focuses on the use of a transgenic mouse model to study sprouting angiogenic events during neovasculature development.

The induction of new vessels from pre-existing host vessels is essential for tumor growth and progression. **Chapter 8** describes the use of the transgenic eNOS-Tag-GFP

mouse model, where GFP expression is restricted to the endothelial lining of the vasculature, for the *in vivo* and *ex vivo* study of sprouting angiogenic events. Using this platform we provide insights into the behavior of endothelial cells during vascular development in physiological and pathological (tumor) conditions. The use of the dorsal skin flap window chamber in mice, in conjunction with intravital microcopy, enables the real time monitoring of tumor arbitrated angiogenic induction. Together, these tools facilitate the *in vivo* study of a wide range of processes including vascular remodeling, vessel growth and regression, vascular mosaicism, perivascular/endothelial cell interaction and drug delivery.

In summary, this thesis contains novel insights into melanoma biology and provides tools to study key phenotypical traits associated with disease development. **Chapter 9** discusses the significance and implications of these findings and how these findings contribute to our understanding of disease biology and could assist in the development of new therapeutic approaches.

FUTURE PERSPECTIVES

It is an exciting time in the field of melanoma biology as we discover crucial determinants of the pathophysiology of this aggressive disease. Such advances have been made possible by sustained efforts in unraveling the complex molecular mechanisms governing disease development and progression. It would be of immense interest to compound our current knowledge of genomic abnormalities, aberrant cell signaling pathways, contribution of the stromal component, clinical properties and biological phenotype, and translate it into a conceptual leap.

   An important aspect, beyond the scope of this thesis, is tumor heterogeneity. Molecular classification of melanomas reveals it to be a highly heterogeneous, complex neoplasm with subpopulations of tumor cells exhibiting varied molecular and biological phenotypes. Challenges for the future include further identification of key molecular aberrations to predict effective therapeutic regimens, and the optimization of combination therapies to combat drug resistance.

NEDERLANDSE SAMENVATTING

Het uitgezaaide melanoom is resistent voor chemotherapeutica en de oorzaak van vrijwel alle huidkanker gerelateerde mortaliteit. Een lokaal melanoom kan in een vroeg stadium effectief worden behandeld door een chirurgische ingreep, terwijl de ziekte in een later stadium met uitzaaiingen tot voor kort vrijwel onbehandelbaar was. Met de opkomst van persoonsgebonden therapie, zijn recentelijk nieuwe medicijnen ontwikkeld, goedgekeurd door de FDA en de EMEA, en in 2011 op de markt gebracht, te weten ipilimumab (anti-CTLA4) en vemurafenib (BRAF-inhibitor). Daarnaast zijn in 2014 en 2015, trametenib (MEK-inhibitor), pembrolizumab en nivolumab (beide anti-PDL1 antilichamen) toegevoegd voor de behandeling van een uitgezaaid melanoom. Dit zijn de eerste medicijnen in jaren die in de kliniek een effect laten zien bij patiënten. Ondanks deze recente successen blijft verbetering van de behandelingen hard nodig, omdat de huidige moleculgerichte therapieën kortlevend zijn, soms geassocieerd worden met ongunstige immuunreacties en er uiteindelijk resistentie tegen deze medicijnen wordt opgebouwd. Een beter begrip van complexe moleculaire mechanismen ten aanzien van ontwikkeling en progressie van de ziekte zal uiteindelijk bijdragen aan het vaststellen van nieuwe therapeutische doelen en zal het de klinische effectiviteit van huidige behandelingen verbeteren.

In dit proefschrift heb ik enkele fundamentele stadia bestudeerd die bijdragen aan melanoomontwikkeling. Een algemene introductie over deze onderwerpen is gegeven in **Hoofdstuk 1**.

De beschreven studies in *Sectie I* van deze thesis richten zich op de essentiële stappen in het angiogene stadium van een melanoom. Progressie van het melanoom en metastaserende groei zijn nauw geassocieerd met het proces van angiogenesis.

In **Hoofdstuk 2** hebben we het angiogene potentieel onderzocht van een aantal melanoomcellijnen door het bepalen van vitaliteit van endotheelcellen na blootstelling aan medium, afgeleid van melanoomcelkweek, onder verder beperkte kweekcondities. We zagen dat melanoom-afgeleid medium specifiek lange termijn endotheelcel overleving onder hypoxie bewerkstelligd, terwijl medium afgeleid van melanocyten, borst- en pancreaskankercellen dit niet lieten zien. Na scheiding van moleculen op grootte werd een overlevingsfactor geidentificeerd in het < 1 kDa gebied. Onderzoek naar globale veranderingen in de genexpressie, lieten zien dat een verhoogde transcript expressie was betrokken bij cytokinesignalering, celmetabolisme, en celoverleving in met melanoom-afgeleid medium behandelde endotheelcellen. Deze ontdekking biedt een nieuw inzicht in het angiogene potentiaal van het melanoom en kan mogelijk leiden tot de ontdekking van nieuwe therapeutische richtpunten.

Endotheelcelmigratie is een essentiele stap in het proces van neovascularisatie. In **Hoofdstuk 3** hebben we de invloed van een medium afgeleid van melanoomcellen op een

gerichte endotheelcelmigratie geëvalueerd. We hebben TIMP3 in het medium geïdentificeerd als negatieve modulator van melanoom-geïnduceerde endotheelcelmigratie. Daarnaast hebben we gedemonstreerd, met behulp van genmodulatie experimenten in xenotransplantatie tumormodellen, dat TIMP3 expressie omgekeerd is gecorreleerd met bloedvatdichtheid en macrofaaginfiltratie in een melanoom.

In **Hoofdstuk 4** is *in vivo* de invloed van TIMP3-expressie op de gemiddelde bloedvatdichtheid en macrofaaginfiltratie geobserveerd in een cohort van niveau III melanoom gerelateerde lymfeklierbiopten. We hebben gezien dat een verlaagde TIMP3 expressie een omgekeerde correlatie heeft met de gemiddelde bloedvatdichtheid in het merendeel van de bestudeerde gevallen. De associatie met macrofaaginfiltratie is niet significant gebleken. Echter, het is belangwekkend dat ook de inactivatie van de genpromotor door methylatie, invloed heeft op de uitkomst van de ziekte. Samengevat suggereren deze ontdekkingen dat TIMP3 een tumorsuppressorrol heeft in maligne melanomen.

De in *Sectie II* van dit proefschrift beschreven studies richten zich op het identificeren van sleutelregulators van het metastaserende melanoom.

Celmigratie is een vitale eigenschap in vrijwel elk biologisch proces en is onmisbaar voor de regulatie van fysiologische en pathologische voorvallen. **Hoofdstuk 5** beschrijft het gebruik van een ring-barrière-migratietest om verscheidene parameters van celmigratie kwantitatief *in vitro* vast te stellen. De test gaat voorbij aan de traditionele kras- of wondhelingstesten, die normaliter gebruikt worden om celmigratie te bepalen, doordat zowel cel als matrix onbeschadigd blijven, mede omdat het de studie van matrixsubstraten, genmodulatie en kleine moleculaire medicijnen faciliteert tijdens het migratieproces.

In **Hoofdstuk 6** wordt het migratie- en invasiepotentieel geanalyseerd van een aantal melanoomcellijnen die variëren in hun mate van agressiviteit en metastatische capaciteit. We hebben geconstateerd dat er een duidelijke correlatie bestaat tussen de migratiecapaciteit van de cellijnen en het vermogen om longmetastasen te vormen in muizen. Correlatieanalyse van genexpressiedata identificeerde WNT5A als determinant van het vastgestelde biologische fenotype. In hier opvolgende genmanipulatie experimenten, waren we in staat te demonsteren dat WNT5A het migratiepotentieel van melanoomcellen reguleert en in een verlengde daarvan de metastatische capaciteit beïnvloedt.

In **Hoofdstuk 7** hebben we de rol van TIMP3 in het metastatische proces van melanomen geëvalueerd. Eiwitexpressie-analyse van patientmateriaal in verschillende stadia van ontwikkeling laat verlies van TIMP3-expressie zien over tijd als het melanoom zich verder ontwikkeld. Daarnaast hebben we door genmodulatie en fenotypische onderzoeken kunnen aantonen dat TIMP3 de migratie- en invasiecapaciteit van melanoomcellen negatief beïnvloedt.

Sectie III van dit proefschrift richt zich op het gebruik van transgene muizenmodellen voor studie van het proces van angiogeen kiemen tijdens de neovasculaire ontwikkeling.

De inductie van nieuwe vaten uit reeds bestaande (gastheer)vaten, is essentieel voor tumorgroei en -ontwikkeling. **Hoofdstuk 8** beschrijft het gebruik van het transgene eNOS-Tag-GFP muizenmodel, waarin de GFP-expressie beperkt is tot de endotheellaag van de vaten, zodat *in vivo* en *ex vivo* het kiemen of ontspruiten van nieuwe bloedvaten tijdens de angiogenese vastgesteld kan worden. Door gebruik te maken van dit platform leveren we inzicht in het gedrag van endotheelcellen gedurende vasculaire ontwikkeling in fysiologische en pathologische (tumor)condities. Het gebruik van de dorsale 'skinfold window chamber', oftewel huidplooi venster in muizen, in combinatie met intravitale microscopie, maakt het mogelijk om 'real-time' de angiogene inductie in de tumor te volgen. Deze hulpmiddelen maken het mogelijk om *in vivo* een scala aan processen te bestuderen, waaronder vasculaire hervorming, vaatgroei en regressie, vaatmosaïcisme, perivasculaire cel- en endotheelcel-interactie en medicijnafgifte.

Dit proefschrift bevat nieuwe inzichten in de biologie van een melanoom en het levert het inzicht en de instrumenten om sleuteleigenschappen in het fenotype, geassocieerd met de ontwikkeling van deze ziekte te bestuderen. **Hoofdstuk 9** omvat de discussie van dit proefschrift waar de betekenis en implicaties van deze bevindingen uiteen worden gezet en waar wordt besproken op welke wijze deze bevindingen kunnen bijdragen aan het beter begrijpen van ziekte-geassocieerde biologie en aan de ontwikkeling van nieuwe therapeutische stategieën.

TOEKOMSTPERSPECTIEF

Het is een spannende tijd in de melanoombiologie met het ontdekken van cruciale determinanten binnen de pathofysiologie van deze aggressieve ziekte. Dergelijke vorderingen zijn mede mogelijk gemaakt door de gestage inspanning om complexe moleculaire mechanismen, betrokken bij de ziekteontwikkeling en -progressie te ontrafelen. Het zou bijzonder belangwekkend zijn om onze huidige kennis van genomische afwijkingen, abnormale celsignalering, bijdrage van het steunweefsel, klinische eigenschappen en het biologische fenotype, te combineren in een significantie sprong naar voren in het melanoomonderzoek.

Een belangrijk aspect, buiten het bereik van dit proefschrift, is de heterogeniteit van de tumor. Moleculaire classificatie laat zien dat melanomen een zeer heterogeen en complexe maligniteit zijn, met subpopulaties van tumorcellen die een divers moleculair en biologisch fenotype hebben. De identificatie van moleculaire afwijkingen met een sleutelrol in het voorspellen van effectieve therapeutische strategieën en het optimaliseren van combinatietherapieën om medicijnresistentie tegen te gaan, zijn de uitdagingen voor de toekomst.

LIST OF PUBLICATIONS

Association of TIMP3 expression with vessel density, macrophage infiltration and prognosis in human malignant melanoma
Asha M. Das, Senada Koljenović[#], Charlotte M.C. Oude Ophuis[#], Thom van der Klok, Boris Galjart, Alex L. Nigg, Wiggert A. van Cappellen, Vincent Noordhoek Hegt, Winand N.M. Dinjens, Peggy N. Atmodimedjo, Cindy E. Vermeulen, Cornelis Verhoef, Alexander M.M. Eggermont, Timo L.M. ten Hagen
European Journal of Cancer. 2015 *In Press*

A ring barrier-based migration assay to assess cell migration in vitro
Asha M. Das, Alexander M.M. Eggermont, Timo L.M. ten Hagen
Nature Protocols. 2015 June. 10(6):904-915

Low molecular weight protein tyrosine phosphatase (LMWPTP) upregulation mediates malignant potential in colorectal cancer
Elmer Hoekstra, Liudmila L. Kodach, **Asha M. Das**, Roberta R. Ruela-de-Sousa, Carmen V. Ferreira, J.C. Hardwick, Janneke van der Woude C., Maikel P. Peppelenbosch, Timo L.M. ten Hagen, Gwenny M. Fuhler
Oncotarget. 2015 April. 6(10):8300-8312

SMAD4 exerts a tumor-promoting role in hepatocellular carcinoma
Pratika Y. Hernanda[#], Kan Chen[#], **Asha M. Das**[#], Kostandinos Sideras[#], Steven J. A. Bots, Harry L. A. Janssen, Liudmila L. Kodach, Jaap Kwekkeboom, Dave Sprengers, Marco J. Bruno, Herold J. Metselaar, Timo L. M. ten Hagen, Maikel P. Peppelenbosch, Qiuwei Pan.
Oncogene. 2014 December. doi: 10.1038/onc.2014.425

Differential TIMP3 expression affects tumor progression and angiogenesis in melanomas through regulation of directionally persistent endothelial cell migration
Asha M. Das, Ann L.B. Seynhaeve, Joost A.P. Rens, Cindy E. Vermeulen, Gerben A. Koning, Alexander M.M. Eggermont, Timo L.M. ten Hagen
Angiogenesis. 2013 September. 17(1):163-177

Wnt5a promotes human colon cancer cell migration and invasion but does not augment intestinal tumorigenesis
Elvira R. M. Bakker, **Asha M. Das**, Werner Helvensteijn, Patrick F. Franken, Sigrid Swagemakers, Martin A. van der Valk, Timo L. M. ten Hagen, Ernst J. Kuipers, Wendy van Veelen, Ron Smits.
Carcinogenesis. 2013 June. 34(11):2629-2638

[#] these authors contributed equally

Lipid phosphatase SHIP2 functions as oncogene in colorectal cancer by regulating PKB activation

Elmer Hoekstra, <u>**Asha M. Das**</u>, Marcella Willemsen, Marloes Swets, Peter Kuppen, Christien J. van der Woude, Jigisha P. Shah, Timo ten Hagen, John D. Chisholm, William G. Kerr, Maikel P. Peppelenbosch and Gwenny M. Fuhler

Submitted.

PTP1B expression and phosphatase activity are increased in colorectal cancer, leading to a more invasive phenotype and worse patient outcome

Elmer Hoekstra, <u>**Asha M. Das**</u>, Marloes Swets, Janneke van der Woude, Maikel Peppelenbosch, Peter Kuppen, Timo ten Hagen, Gwenny Fuhler

Submitted.

Melanomas prevent endothelial cell death under restrictive culture conditions by signaling through AKT and p38 MAPK/ERK-1/2 cascades

<u>**Asha M. Das**</u>, Mario Pescatori, Cindy E. Vermeulen, Joost A.P. Rens, Ann L.B. Seynhaeve, Gerben A. Koning, Alexander M.M. Eggermont, Timo L.M. ten Hagen

Submitted.

TIMP3 expression decreases during melanoma progression and inhibits melanoma cell migration

<u>**Asha M. Das**</u>, Michiel Bolkestein[#], Thom van der Klok[#], Charlotte M.C. Oude Ophuis[#], Cindy E. Vermeulen, Joost A.P Rens, Winand N.M Dinjens, Peggy N. Atmodimedjo, Cornelis Verhoef, Senada Koljenović, Ron Smits, Timo L.M. ten Hagen, Alexander M.M. Eggermont

Submitted.

Biological profiling of the migratory phenotype of melanoma identifies WNT5A as a metastasis determinant

<u>**Asha M. Das**</u>, Michiel Bolkestein, Mario Pescatori, Joost A.P. Rens, Cindy E. Vermeulen, Alexander M.M. Eggermont, Ron Smits, Timo L.M. ten Hagen

In preparation.

High resolution *in vivo* and *ex vivo* imaging of vascular sprouting events using the eNOS-Tag-GFP transgenic mouse

<u>**Asha M. Das**</u>, Rien van Haperen, Ann L.B. Seynhaeve, Cindy E. Vermeulen, Joost A.P. Rens, Alexander M.M. Eggermont, Rini de Crom, Timo L.M. ten Hagen

In preparation.

[#] these authors contributed equally

PhD PORTFOLIO

Summary of PhD training

Erasmus MC Department:	Department of Surgery
Research School:	Molecular Medicine
PhD period:	2008–2015
Promoter:	Prof. dr. A.M.M. Eggermont
Co-promoter:	Dr. T.L.M. ten Hagen

Courses and training	Year	ECTS
Workshop on InDesign CS5	2015	0.3
In Vivo Imaging: from Molecule to Organism	2011	1.8
Molecular Immunology	2010	3.0
Laboratory Animal Science Art 9	2010	3.0
Animal Imaging Workshop by AMIE: From mouse to man	2009	1.4
Basic Confocal Microscopy	2009	0.3
Molecular Medicine	2008	0.7
Basic and Translational Oncology	2008	1.8
Biomedical Research Techniques	2008	1.5
Molecular Diagnostics	2008	1.0

Oral presentations		
JNI Oncology Lectures	2008–2014	2.0
Annual Science Day of the Department of Surgery	2008–2014	2.0
Weekly Research meeting	2008–2014	2.0
Journal Club	2008–2014	2.0

Attendance to national/international congresses with poster presentation		
Molecular Medicine Day, Rotterdam, the Netherlands	2008–2014	1.5
Kloster-Seeon Tumor Vessel Meeting, Germany	2011	2.0
4th International Meeting on Angiogenesis, Amsterdam, the Netherlands	2011	2.0
AACR, Denver, Colorado, USA	2009	3.0

ACKNOWLEDGEMENTS

As I finally come to the end of my PhD period at the Erasmus MC, I would like to thank everybody who contributed to this thesis. These 7 years have helped me discover the full spectrum of my emotional compass and yet as I look at this completed thesis, I realize how blessed I was to have the support of several wonderful people along the way.

To my promoter, Prof. Alexander Eggermont; dear Lex, thank you for giving me the opportunity to work at LECO. Your patience, guidance and constant support gave me the strength to overcome many a difficult situation. Thank you for always finding the time to answer all my questions, whether you were in New York, Paris or Kazakhstan! You have been a father figure to me during this process and helped me stay on track every time I lost faith. For this and everything else, I will be forever indebted to you!

To my copromoter, Dr. Timo ten Hagen; dear Timo, thank you for giving me the opportunity to work on the melanoma project. You gave me the creative space to grow as a researcher, the freedom to exercise my ideas and the liberty to always do that one extra experiment!

Dr. Gerben Koning, dear Gerben, it has been an absolute honor and privilege knowing you. I fondly remember all the discussions we had, work-wise and otherwise. Your presence in the lab is truly missed.

Cindy, aka CinCin, I am deeply grateful for the companionship and support you have provided over the years. I would have wanted nothing more than to celebrate the completion of this thesis with you. Having you by my side ensured that no new protocol was too difficult to set up! With an open heart and a contagious smile, you always managed to cheer me up in difficult times. I will cherish and hold on to the many memories we created over these years, knowing that they can bring me some small comfort in the face of this overwhelming grief. My life is richer for having known you and you will live on forever in my heart.

Joost, aka YoYo, I cannot thank you enough for all the technical assistance over the years. From blotting to cloning to imaging, you were always there to help me with everything. This project would not have come together without your enthusiasm, support and dedication and I am really going to miss working with you!

Wouter, aka Woutertje, thank you for the company and our many conversations about everything and nothing! Whether it was weekends at the lab or beers at the Wester Paviljoen, I enjoyed all the time we spent together.

Billy, aka Boomie, thank you for the fun and friendship. We started our work in this lab together and it is an appropriate end that we graduate only a day apart!

Mario, thank you for teaching me everything I know about microarrays, fishing and cleaning squid properly! Also, thank you for spoiling me with your culinary expertise!

Reza and Azadeh, I hope I managed to help you guys adjust to Dutch culture and customs and I appreciate that you kept me company in the lab during weekends! You showed me a dedication and understanding that few researchers have mastered.

To all my LECO colleagues, past and present, thank you for the laughs and the memories. It has been a lot of fun working with you and I wish you the very best in all future endeavors.

Dear Ron Smits, thank you for giving me much needed supervision with regards to the many biological pathways I tried to tackle. Thank you for the guidance and always finding the time to accommodate my requests and answer my never-ending questions!

Gert van Cappellen and Alex Nigg, thank you both for all the help with microscopy and image analysis which helped me immensely.

Thijs, it was always comforting to know that there was someone a few doors down, who kept odd working hours just as I did!

To some truly amazing people from the department of Pathology; Senada, Vincent, Thom, Hans, Sharmiela, Riadi, it was an absolute pleasure working with you! Thank you for all the help with stainings and scoring in the last years of my PhD.

Charlotte, thank you for all the help with the clinical projects. I really enjoyed working with you and hope we can work together again!

Benjamin, thanks for being the go-to guy regarding flow cytometry and helping me with all the sorting experiments.

To everyone I have had the pleasure of collaborating with; Elvira, Elmer, Abdullah, it was really enjoyable working with you and I hope we can continue to work together in the future.

The one absolutely positive aspect about being a globe-trotting nomad is that you end up having several families. To all my family-away from-family, thank you for welcoming me into your life and giving me very few reasons to miss home.

To all the awesome people back it Austria, you taught me to appreciate snow, schnapps and schnitzels! Albert, Gerold, Martin (Heitz), Katrin, Aga, thank you for the many beautiful memories.
Martin, for the love and friendship over the years.

Monique and Peter, thank you for the parental wisdom everybody needs, no matter how old they are! Also, thank you for many a warm pumpkin soup and a life-time supply of port wine!

Pri, Martin, Shweta, Maron, you are my closest friends and I hope to celebrate this thesis with you as only you guys know how to best! Thanks for always being there for me!

Nazneen, Jigar, Raj, Subroto, Mukul, thank you for being some of my oldest and dearest friends. I hope we get to spend more time together, be it in India or abroad.

To my paranymphs, Priyanka and Michiel, you have been with me through this whole process, celebrating my victories and dragging me out of my lows! Thank you for the many years of friendship, for standing by me today, and being there for me, always!

To my family, for their unwavering support and unconditional love.
To my grandmother, Ammuma, thank you for ever so patiently listening to my complaints about experiments not working. It's always reassuring to have a wise 84 year-old tell you that the Western blots will work!
To my little brother, Unni, thank you for always looking out for me. Your phone calls and visits kept me grounded and thank you for regularly spoiling me with treats from back home!
Mama, none of this would have been possible without your constant support. I would consider myself blessed if I can be half the woman you are (height-wise too). I do realize that the whole point of having a family reunion is to actually show up- and I intend to do so more frequently!
To the man who made me; Papa, I know you're watching- this one's for you!!

Now that I've spent the better half of my twenties in the (subterranean) labyrinths of the Erasmus MC, with mostly pipettes, mice and a few final year PhD students keeping me company, it is time to reclaim those lost weekends and start having a social life again; as soon as I finish those collaboration experiments, submit that revised manuscript, start my postdoctoral research, write that grant application……

CURRICULUM VITAE

Asha Mooppilmadham Das was born on the 6th of July 1984 in the city of Cochin, Kerala, India. She completed her secondary education at Our Lady Queen of the Missions and Frank Anthony high school in Calcutta, West Bengal, India. In 2005 she completed her Bachelor's degree in Biochemistry, Genetics and Biotechnology and graduated with distinction from the University of Bangalore, Karnataka, India. After this she went to Skövde, Sweden, in 2006 to obtain her Master of Science in Molecular Biology. This comprised of a Master-thesis internship at the Tyrolean Cancer Research Institute in Innsbruck, Austria. After a dissertation about microRNA profiling for colorectal cancer screening, she graduated in 2007 from the University of Skövde. From 2008 till 2015 she performed her PhD research at the department of Surgery at the Erasmus Medical Center, Rotterdam, the Netherlands, investigating key aspects of melanoma biology, including but not limited to, angiogenesis, cell migration, and metastasis. In her research she has used an impressive range of tools, including cell-based assays, intravital imaging, and whole-body computed tomography imaging, in addition to various molecular biology techniques. These skills have led to numerous collaborations and the research presented in this thesis.

"Exactly!" said Deep Thought. "So once you do know what the question actually is, you'll know what the answer means."

– Douglas Adams,
The Hitchhiker's Guide to the Galaxy